Towards Individualised Model-based Monitoring: From Biology to Technology

Tim TAMBUYZER

Supervisors:

Prof. dr. ir. J.M. Aerts (KU Leuven), promoter

Prof. dr. D. Balschun (KU Leuven), co-promotor

Members of the examination committee:

Prof. dr. ir. D. Berckmans (KU Leuven)

Prof. dr. ir. H. Ramon (KU Leuven)

Prof. dr, ir. E. Schrevens (KU Leuven), chairman

Prof. dr. B. Nuttin (KU Leuven)

PD. dr. S. Zenker (University of Bonn, Germany)

Dissertation presented in partial fulfilment of the requirements for the degree of Doctor in Bioscience Engineering

January 2018

Doctoraatsproefschrift nr.1488 aan de faculteit Bio-ingenieurswetenschappen van de KU Leuven

Uitgegeven in eigen beheer, TIM TAMBUYZER, B-3001 HEVERLEE (BELGIUM)

"If there is man, then that is because a technology has made him evolve out of the prehumen."

— Peter Sloterdijk —

(From: Sloterdijk, Peter, "Anthropo-Technology" in New Perspectives Quarterly (2004), p. 43)

Acknowledgements

As a bachelor student, the thought of starting a PhD not even once occurred to me. As it turned out, during my Masters I found that doing research was an undiscovered passion I was about to retain and, one year later, this passion and some luck would allow me to become a PhD candidate at M3-BIORES (KU Leuven). During my PhD I came across many scientific and personal challenges and, without the help of my colleagues, family, friends and partner, it would have been impossible to overcome these obstacles and reach the final phase of this project.

First, I would like to thank my promotor Jean-Marie for the continuous critical and constructive support. Also, for the patience and the long inspirational meetings that were often associated with moments of laughter. In addition, I want to express my gratitude to my co-promotor, Detlef, for introducing me to the field of neuroscience and other less serious matters (i.e. lab football challenge).

I want to thank all my other professors, Daniel, Erik, and Thomas, and the other colleagues that form our team at the lab. All of you contributed to make that place an amazing and fruitful environment.

A huge 'dank' to my parents, Vake en Moeke, for the never-ending motivation and love to push me through to finish writing this thesis. I love you both. Of course, I cannot forget to thank my brothers: Geert, Wim, Jo, Tom, Bart and Koen. Your brotherhood is not always necessarily related with the product of this project, but is pivotal to the person I am today.

Finally, I would like to thank all 'bio-ingenieur' friends, the 'Mothership' friends (independently of which country you all might be in now), the friends from Berlaar, and all other friends that perhaps do not belong to any of these groups, but are nevertheless amazing friends. A special thanks to Jack Brooks for the help and energy to proofread my texts into impeccable English.

Finally, I want to thank my love, Jonatas. You are my personal coach who was always there for me, and for being even more anxious about my deadlines than I was–sorry about it! You made me a better person since the moment I met you and I cannot wait to see what journeys the future holds for us.

Tim Tambuyzer
Leuven, 2018

Summary

Biological systems and their underlying processes (i.e. bio-processes) are continuously exposed to a wide range of perturbations in their micro-environment. Moreover, each individual biological process is unique and will respond in a different way to these perturbations. The two main reasons for this individual diversity are widely accepted: i) differences due to gene effects (i.e. nature) and ii) differences due to environmental effects (i.e. nurture). However, dealing with the inter- and intra-individual variations remains one of the main obstacles in applying engineering approaches to biological processes and, therefore, it is highly challenging to accurately monitor their individual state (e.g. individual response to infection, personalised medicine). The focus of this PhD is on individualised model-based monitoring of biological processes.

The general objective of this PhD was to develop a framework for individualised model-based monitoring for biological processes, as inspired by control engineering concepts. The presented approach addresses four main topics: i) the biological process itself (i.e. bio-process), ii) the process model, iii) model-based features and iv) individualised change detection. To explore the validity of the formulated sub-objectives, six different case studies (cell, embryo, animal, human) were examined: i) Individualised monitoring of activity and body weight in the activity-based anorexia rat model, ii) Individualised model-based monitoring of interleukin-6 for early detection of infection in pigs, iii) Model-based monitoring of heart rate and blood cytokine time series for early detection of infections in critically ill patients, iv) Model-based monitoring of mGluR-dependent synaptic plasticity in hippocampal brain slices of rat, v) Individualised monitoring of hippocampal theta oscillations and individualised electrical stimulation in the mesencephalic reticular formation for

real-time closed-loop suppression of locomotion in rat and vi) Individualised model-based monitoring of chicken embryo status during incubation based on eggshell temperature and micro-environmental air temperature. In case study ii and iii similar methods are applied to obtain a monitor for infection in animals and humans respectively. This example shows how it is possible to make the step from animal to human health engineering.

Overall, this thesis has led to some innovative individualised monitoring applications based on the six specific case studies. Since the case studies are very different, the developed individualised model-based approach could potentially be used in a wide range of application domains (e.g. human health engineering, precision livestock farming, bio-technological processes,...).

The first sub-objective focuses on the biological process: Individual biological processes (individual system structure, individual system dynamics, and individual bio-signals) will be interpreted as the biological equivalents of control engineering components by defining actuator and homeostatic variables for each of the six case studies.

The results of the case studies showed that the involved bio-processes can be considered as the biological equivalents of clever-designed control engineering components such as sensors, actuators, feedback loops and controllers. This allows them to preserve homeostasis and stable internal conditions, to adapt (e.g. learning by brain plasticity) and to grow (e.g. chicken embryo development) in spite of uncertain environmental conditions. When one of the components of a homeostatic control system fails, this can lead to dangerous states (e.g. dysfunction of the control system for energy homeostasis in animals or patients with anorexia nervosa; cfr. case study i).

By starting from the individual details of the biological processes, we could define actuator and homeostatic variables for the different bio-processes of each case study. Therefore, as the first step in the development of an individualised model-based monitoring system for bio-signals, we suggested combining insights from biology and control engineering to interpret measured bio-signals (i.e. developing monitoring systems “from biology to technology”).

The second sub-objective was formulated as: Although biological processes are known to contain many nonlinearities, we will use compact individual linear models (general Box-Jenkins models) for the specific individualised monitoring applications of the case studies (cfr. case studies ii, iii, iv and v). By using these models we aim to obtain a good approximation of the individual bio-process dynamics and/or to uncover information about the underlying mechanisms/state by applying data-based mechanistic modelling approaches (case study iv and vi).

Several examples, spread across the various case studies, confirmed that we can use compact individual linear models (i.e. Box-Jenkins (BJ) models) for monitoring individual non-linear bio-processes. These models allow accurate descriptions of the dynamic, time-varying and individual character of bio-processes. The fact that we can use such compact BJ models to describe such bio-processes is, at first-sight, highly unexpected because bio-processes are, without any exception, very complex (e.g. nonlinearities). However, as mentioned before, bio-processes can be considered robustly controlled engineering systems. In light of this, such systems often show relatively simple responses (expressing the crucial dominant processes that ascertain healthy internal homeostatic or homeodynamic conditions) when exposed to perturbations as illustrated by the bio-processes of the case studies. Consequently, these systems can be modelled successfully using compact models such as BJ models. Moreover, for two case studies (case study iv and vi), links were shown between the models and physiological mechanisms (i.e. data-based modelling of synaptic plasticity; monitoring chicken embryo state during incubation) and therefore the models can be considered as data-based mechanistic models, since they are both data-based and able to give insight in the individual state of the bio-processes.

In the third sub-objective we stated: We will identify generic metrics from the fields of complex systems science, change detection and control engineering that can be used while analysing individual time series. This list of metrics can be used for all individual bio-processes in the design of model-based monitoring applications and will be generated based on the specific case studies (case studies i-vi).

Based on the results, we suggested three different model-based features that can be used to detect individual state changes in bio-processes: model parameter changes, changes in model order and changes in model noise characteristics. In addition, more than 20 other generic metrics from the fields of complex systems science, change detection and control engineering were identified that can be used while analysing individual time series.

Finally, the last sub-objective introduced the use of individual thresholds: By integrating insights from control engineering and change detection, we will develop a general framework for individualised model-based monitoring of biological processes based on individual thresholds. This general approach could potentially be implemented in a wide range of applications and could improve the generally accepted population-based approaches (case study i, ii, v and vi).

Examples from the chapters (cfr. case studies i, ii, iii, v and vi) showed the presence of inter- and intra-individual differences in most monitoring applications, indicating the need for a monitoring approach based on individualised thresholds in order to capture the individual state changes. Methods of online change detection are typically characterised by the use of threshold methods. Here, we combined insights from change detection and control engineering and developed a framework for individualised model-based monitoring with individual thresholds based on the specific case studies. In addition to the general, more traditional change detection methods (e.g. CUSUM algorithms), three possible approaches were proposed: 1) Individual thresholds based on (sub-)population information, 2) Individual thresholds based on universal laws and insights from control engineering, complex systems science and biology and 3) Individual thresholds based on individual serial baseline measurements, which can be considered as the most individualised way.

The way forward in the monitoring of individuals is using serial baseline measurements of normal system behaviour (e.g. healthy state) to detect individual changes (e.g. state of illness such as infection). Such an individualized approach allows us to define individual thresholds (cfr. case studies v and vi) purely based on data generated from the same individual process, which can lead to higher detection accuracies in comparison with population-based methods.

Until now the existence of general frameworks for individualised model-based monitoring of biological processes is limited. In this thesis, each specific case (i.e. animal and human health engineering applications) contributed to the development of such general framework inspired by control engineering concepts. The presented general approach could be used in a broad range of application domains, thus stressing the generic power of the suggested framework for individualized model-based monitoring of bio-processes. All the elements and methods handled in this PhD are summarised in one flow chart for individualised model-based monitoring of biological processes that combines methodologies from the fields of statistics, control engineering, complex systems science and change detection. In the future, population-based threshold approaches should be merged with methods at an individual level so as to optimise the performance of the monitoring systems (e.g. mixed-effect models). Moreover, the list of used methods could be further expanded (e.g. non-linear models, validation methods, etc.). Finally, the individualised model-based monitoring approach could also be integrated in a broader framework, which, additionally, includes methods for defining individualised interventions and individualised control applications (e.g. closed-loop deep brain stimulation systems for reduction of pathological symptoms).

Samenvatting

Biologische systemen en hun onderliggende processen (i.e. bio-processen) worden voortdurend blootgesteld aan een groot aantal verstoringen in hun micro-omgeving. Bovendien is elk individueel biologisch proces uniek en zal het op een andere manier reageren op deze storingen. De belangrijkste twee redenen voor deze individuele diversiteit zijn algemeen bekend: i) verschillen ten gevolge van gen-effecten (i.e. “nature”) en ii) verschillen door omgevingseffecten (i.e. “nurture”). Het omgaan met de inter- en intra-individuele variaties blijft echter een van de belangrijkste obstakels bij het toepassen van modelgebaseerde ingenieurstechnieken op biologische processen en daarom is het zeer uitdagend om de individuele toestand van biologische processen nauwkeurig te volgen (bijvoorbeeld de individuele respons op infectie, gepersonaliseerde geneeskunde). De focus van dit doctoraat ligt op de geïndividualiseerde modelgebaseerde monitoring van biologische processen.

De algemene doelstelling van dit doctoraat was een algemeen kader te ontwikkelen voor geïndividualiseerde modelgebaseerde monitoring van biologische processen, geïnspireerd door ingenieurstechnieken voor controle van dynamische systemen. De voorgestelde benadering heeft betrekking op vier hoofdonderwerpen: i) het biologische proces zelf, ii) het procesmodel, iii) modelgebaseerde kenmerken en iv) geïndividualiseerde veranderingsdetectie. Om de validiteit van de geformuleerde sub-objectieven te onderzoeken, werden zes verschillende casestudies (cel, embryo, dier, mens) verricht: i) Geïndividualiseerd monitoren van activiteit en lichaamsgewicht in het activiteitsgerelateerde anorexia-ratmodel, ii) Geïndividualiseerd en modelgebaseerd monitoren van interleukine-6 voor vroege detectie van infectie bij varkens, iii) Modelgebaseerd monitoren van hartslagfrequentie en cytokinetijdreeksen voor vroege detectie van infecties bij

kritisch zieke patiënten, iv) Modelgebaseerd monitoren van mGluR-afhankelijke synaptische plasticiteit in hippocampale hersensneden van de rat, v) Geïndividualiseerd monitoren van hippocampale theta-oscillaties en geïndividualiseerde elektrische stimulatie in de mesencefalic reticular formation voor real-time closed-loop onderdrukking van voortbeweging van de rat en vi) Geïndividualiseerd en modelgebaseerd monitoren van de status van kippenembryo's tijdens incubatie op basis van eierschaaltemperatuur en micro-omgevings-temperatuur. In casestudies ii en iii worden vergelijkbare methoden toegepast om een monitor voor infectie bij dieren en mensen te ontwikkelen. Dit voorbeeld laat zien hoe het mogelijk is om de overstap te maken van animal naar human health engineering. Over het algemeen heeft dit doctoraat geleid tot verschillende innovatieve geïndividualiseerde monitoringtoepassingen op basis van de zes specifieke casestudies. Aangezien de topics van de casestudies heel uiteenlopend zijn, zou de ontwikkelde geïndividualiseerde modelgebaseerde aanpak mogelijk kunnen worden gebruikt in een brede waaier van toepassingsdomeinen (bijvoorbeeld human health engineering, precisie veeteelt, biotechnologische processen, ...).

Het eerste sub-objectief van dit doctoraat is gericht op het biologisch proces: Individuele biologische processen (individuele systeemstructuur, individuele systeemdynamica, individuele bio-signalen) worden geïnterpreteerd als de biologische equivalenten van componenten uit het domein van controle engineering. Dit zal verwezenlijkt worden via het definiëren van actuator- en homeostatische variabelen voor elk van de zes casestudies.
Uit de resultaten van de casestudies bleek dat de betrokken bio-processen kunnen worden beschouwd als de biologische equivalenten van slimme engineerings-componenten zoals sensoren, actuatoren, feedbacklussen en controllers. Dit stelt hen in staat om homeostase en stabiele interne condities te behouden, om te adapteren (bijv. Nieuwe dingen aanleren door hersenplasticiteit) en te groeien (bijv. Embryo ontwikkeling bij kippen) ondanks onzekere condities in de (micro-)omgeving. Wanneer één van de componenten van een homeostatisch controlesysteem faalt, kan

dit leiden tot gevaarlijke toestanden (bijv. Dysfunctie van het controlesysteem voor energiehomeostase bij dieren of patiënten met anorexia nervosa).
Door te starten vanuit de individuele details van de biologische processen, kunnen we actuator- en homeostatische variabelen definiëren voor de verschillende bio-processen van elke casestudy. Daarom suggereerden we op basis van de resultaten dat de ontwikkeling van een geïndividualiseerd modelgebaseerd monitorings-systeem voor bio-processen initieel zou moeten starten met de combinatie van inzichten uit biologie en inzichten vanuit ingenieurstechnieken voor controle van dynamische systemen. (i.e. het ontwikkelen van monitoring systemen "van biologie naar technologie").

Het tweede sub-objectief werd geformuleerd als volgt: Hoewel het bekend is dat biologische processen veel niet-lineariteiten bevatten, zullen we compacte individuele lineaire modellen (algemene Box-Jenkins-modellen) gebruiken voor de specifieke geïndividualiseerde monitoringstoepassingen van de casestudies (zie casestudies ii, iii, iv en v). Door deze modellen te gebruiken, proberen we een goede benadering te verkrijgen van de individuele bio-procesdynamiek en/of informatie over de onderliggende mechanismen/toestand bloot te leggen door data-gebaseerde mechanistische modelleringstechnieken toe te passen (casestudy iv en vi).
De voorbeelden, verspreid over de verschillende casestudies, bevestigden dat we compacte individuele lineaire modellen (i.e. BJ modellen) kunnen gebruiken om individuele niet-lineaire bio-processen op te volgen. De modellen waren in staat nauwkeurige beschrijvingen te maken van het dynamische, tijdvariabele en individuele karakter van bio-processen. Het feit dat we dergelijke compacte BJ-modellen kunnen gebruiken om bio-processen te beschrijven is op het eerste gezicht zeer onverwacht, omdat bio-processen zonder twijfel zeer complex zijn (bijv. o.w.v. niet-lineariteiten). Echter, zoals eerder vermeld, kunnen bio-processen worden beschouwd als robuuste gecontroleerde systemen. Daarom reageren dergelijke systemen vaak op een relatief eenvoudige manier op verstoringen (waarbij vaak de effecten tot uiting komen van slechts een beperkt aantal cruciale dominante processen, die zorgen voor gezonde interne homeostatische of homeodynamische condities). Dit werd geïllustreerd voor de verschillende bio-processen van de

casestudies. Bijgevolg kunnen deze systemen succesvol gemodelleerd worden met behulp van compacte modellen zoals BJ-modellen. Bovendien werden in twee casestudies links getoond tussen de modellen en fysiologische mechanismen (bijv. Data-gebaseerde modellering van synaptische plasticiteit, ontwikkelingsstatus van kippenembryo's tijdens de incubatie) en daarom kunnen de modellen beschouwd worden als data-gebaseerde mechanistische modellen. Zij zijn immers zowel data-gebaseerd als in staat inzicht te kunnen geven over de individuele staat van de bio-processen.

In het derde sub-objectief hebben we verklaard: We zullen generische technieken identificeren vanuit het domein van complexe systemen, change detection en control engineering, die kunnen worden gebruikt bij het analyseren van individuele tijdreeksen. Deze lijst van technieken kan worden gebruikt voor alle individuele bio-processen in het ontwerp van modelgebaseerde monitoringstoepassingen en zal worden gegenereerd op basis van de specifieke casestudies (casestudies i-vi).
Op basis van de resultaten werden drie verschillende modelgebaseerde variabelen voorgesteld, die kunnen worden gebruikt om individuele toestandsveranderingen in bio-processen te detecteren: i) veranderingen in modelparameters, ii) veranderingen in modelorde en iii) veranderingen in modelruiskarakteristieken. Daarnaast zijn er op basis van de specifieke geïndividualiseerde modelgebaseerde monitorings-toepassingen van dit doctoraat meer dan 20 andere generische methodes geïdentificeerd vanuit het domein van complexe systeemwetenschappen, change detection en controle engineering, die kunnen gebruikt worden voor tijdreeksanalyses.

Ten slotte introduceerde het laatste sub-objectief het gebruik van individuele drempelwaarden: Door inzichten uit controle engineering en change detection te integreren, zullen we een algemeen kader ontwikkelen voor geïndividualiseerde modelgebaseerde monitoring van biologische processen op basis van individuele drempelwaardes. Deze algemene benadering kan mogelijk worden geïmplementeerd in een breed scala van toepassingen en zou de algemeen aanvaarde populatie-gebaseerde benaderingen kunnen verbeteren (casestudies i, ii, v en vi).

Voorbeelden uit de hoofdstukken (cfr. casestudies i, ii, iii, v and vi) toonden de aanwezigheid aan van inter- en intra-individuele verschillen in de meeste monitoringstoepassingen en bevestigden op die manier de nood aan geïndividualiseerde monitoring met individuele drempelwaardes om een toestandsverandering te detecteren. Methoden uit het domein van change detection worden typisch gekenmerkt door het gebruik van drempelwaardes. Hier combineerden we inzichten uit change detection en controle engineering en ontwikkelden we een algemeen framework voor geïndividualiseerde modelgebaseerde monitoring met individuele drempelwaardes op basis van de specifieke casestudies. Naast de algemene, meer traditionele methodes uit het domein van change detection (bijv. CUSUM-algoritmes) werden drie mogelijke benaderingen voorgesteld: 1) Individuele drempelwaardes op basis van (sub-)populatie informatie, 2) Individuele drempelwaardes gebaseerd op universele wetten en inzichten van control engineering, complexe systemen en biologie en 3) individuele drempelwaardes gebaseerd op individuele seriële referentiemetingen. Deze laatste kan beschouwd worden als de meest geïndividualiseerde methode.
Het is daarom dat monitoren van individuen optimaal gezien gebruik maakt van seriële 'baseline'-metingen van normaal systeemgedrag (bijv. gezonde toestand) om individuele veranderingen te detecteren (bijv. ziekte zoals infectie). Een dergelijke geïndividualiseerde aanpak stelt ons in staat om individuele drempelwaardes te definiëren (zie casestudies v en vi), wat kan leiden tot hogere detectienauwkeurigheden in vergelijking met populatie-gebaseerde methoden.

Tot op heden is het bestaan van algemene kaders voor geïndividualiseerde modelgebaseerde monitoring van biologische processen beperkt. In dit doctoraat heeft elk specifiek geval (dat wil zeggen monitoringstoepassingen voor zowel dier als mens) bijgedragen tot de ontwikkeling van een dergelijk algemeen kader, geïnspireerd door concepten van controle engineering. In het algemeen zou de voorgestelde aanpak kunnen worden gebruikt in uiteenlopende toepassingsdomeinen, waardoor de generische waarde van het voorgestelde kader duidelijk wordt. Alle elementen en methoden die in dit doctoraat werden behandeld, werden samengevat in een flowchart voor geïndividualiseerd modelgebaseerd

monitoren van biologische processen. De flowchart combineert methodologieën van statistiek, control engineering, het domein dat complexe systemen bestudeert en het domein van change detection. In de toekomst moeten populatie-gebaseerde methodes worden samengevoegd met meer geïndividualiseerde methoden om de prestaties van de monitoringssystemen te optimaliseren (e.g. mixed-effect models). Bovendien kan de lijst van gebruikte methoden verder worden uitgebreid (bijv. niet-lineaire modellen, validatiemethodes, etc.). Tenslotte kan de geïndividualiseerde modelgebaseerde benadering voor het monitoren van biologische processen ook geïntegreerd worden in een bredere context, die methoden omvat voor het definiëren van geïndividualiseerde interventies en geïndividualiseerde controle toepassingen (bijv. controle systemen voor diepe hersenstimulatie ter vermindering van pathologische symptomen).

Table of Contents

List of acronyms and symbols

ABA
Activity-based anorexia

AIC
Akaike information criterion

AMP
custom amplifier

AN
anorexia nervosa

AR(1) model
First order autoregressive model

ARD
Arduino Uno board

BJ
Box-Jenkins

BMI
Body Mass Index

CI
Confidence intervals

CITD
Complex, individual, time-varying, dynamic

CUSUM
Cumulative sum

DAR
Dynamic auto-regression

DAQ
Data acquisition card

DBS
Deep brain stimulation

Dmax
Deviation maximum method

ERK1/2
Extracellular signal-regulated kinase

EWS
Early warning signs

FAA
Food Anticipatory Activity

HS
High responders

HR
Heart rate

ICU
Intensive Care Unit

IFN
interferon gamma

IL-1b
interleukin-1 beta

IL-2
interleukin-2

IL-4
interleukin-4

IL-5
interleukin-5

Il-6
interleukin-6

IL-10
interleukin-10

IL-12
interleukin-12

IL-13
inter-leukin-13

IRW
Random Walk Model

LFP
Local field potential

PI3K
Phosphatidylinositol 3-kinase

PLF
Precision livestock farming

MOC
Mechanism operated cell

mRt
Mesencephalic reticular formation

MS
Medium responder

NS
Non-responders

NVR
Noise Variance Ratio

R_T^2
Coefficient of determination

ROC AUC
Area under the receiver operating characteristic curve

RWA
Running wheel activity

SE
Standard error

SISO
Single-input, single-output

SSG
Steady state gain

STEP
Striatal-enriched tyrosine phosphatase

Stim
Stimulator

Tair
Micro-environmental air temperature

Tegg
Eggshell temperature

TC
Time constant

Tmax
Maximum body temperature

TNFa
Tumor necrosis factor-alpha

TNR
True negative rate

TPR
True positive rate

Uconc
Blood urea concentration

WBC
White blood cell count

YIC
Young identification criterion

List of figures

Part 3 General discussion

List of tables

Part 3 General discussion

Part 1

Introduction and objectives

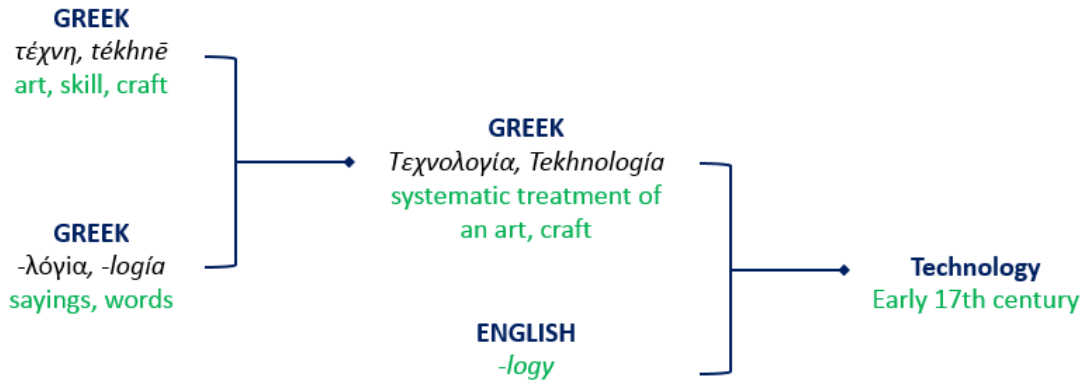

Scheme representing the etymology of the word "Technology"
(Based on: Liddell, H. G. (1894). A Greek-English Lexicon. Harper & brothers).

1.1 MONITORING SIGNALS FROM BIOLOGICAL PROCESSES

The focus of this PhD is on the monitoring of signals from biological systems (cells, animals, humans,…) and their underlying biological processes. Whereas measuring can be defined as quantifying the (bio)signal of a biological process in a physical way (e.g. using sensors), monitoring refers to the observation and assessment of such measurements of a (biological) process, over a longer time, in order to effectively manage it. In this PhD dissertation, we pay particular attention to model-based monitoring applications, which, with the application of models, are used to extract relevant features of the measured data for monitoring purposes. From a more technical perspective, monitoring can be defined as checking measured variables or model-based features of process variables with regard to tolerances, whereas alarms are generated for the operator (Isermann, 2005). Indeed, the first monitoring systems were mainly designed for the automation of (electromechanical or physical) industrial processes (Basseville and Nikiforov, 1993). However, most features of (living) biological processes diverge strongly from those of industrial processes. Biological processes are Complex, Individually different, Time-varying and Dynamic processes (CITD; Quanten et al., 2006). Essentially, therefore, it is challenging to develop monitoring systems for bio-processes.

Secondly, we place emphasis on the most essential difference between industrial and biological processes—the individual character of organisms—for such individual differences make it difficult to develop treatments for diseases, for example. Figure 1.1 shows visual representations of the percentages of the patient population for which a particular drug is, on average, ineffective. It's clear that many of these drugs are only effective for a specific subpopulation of patients. This figure indicates, in a very convincing way, how individually different living organisms (e.g. patients) are from one another. As Lesko (2007) says:

"The elusive dream is to eventually have a treatment custom matched for you, as a patient, based on your individual genetic profile, demographics, and environmental factors. The imminent reality is that we are not there yet."

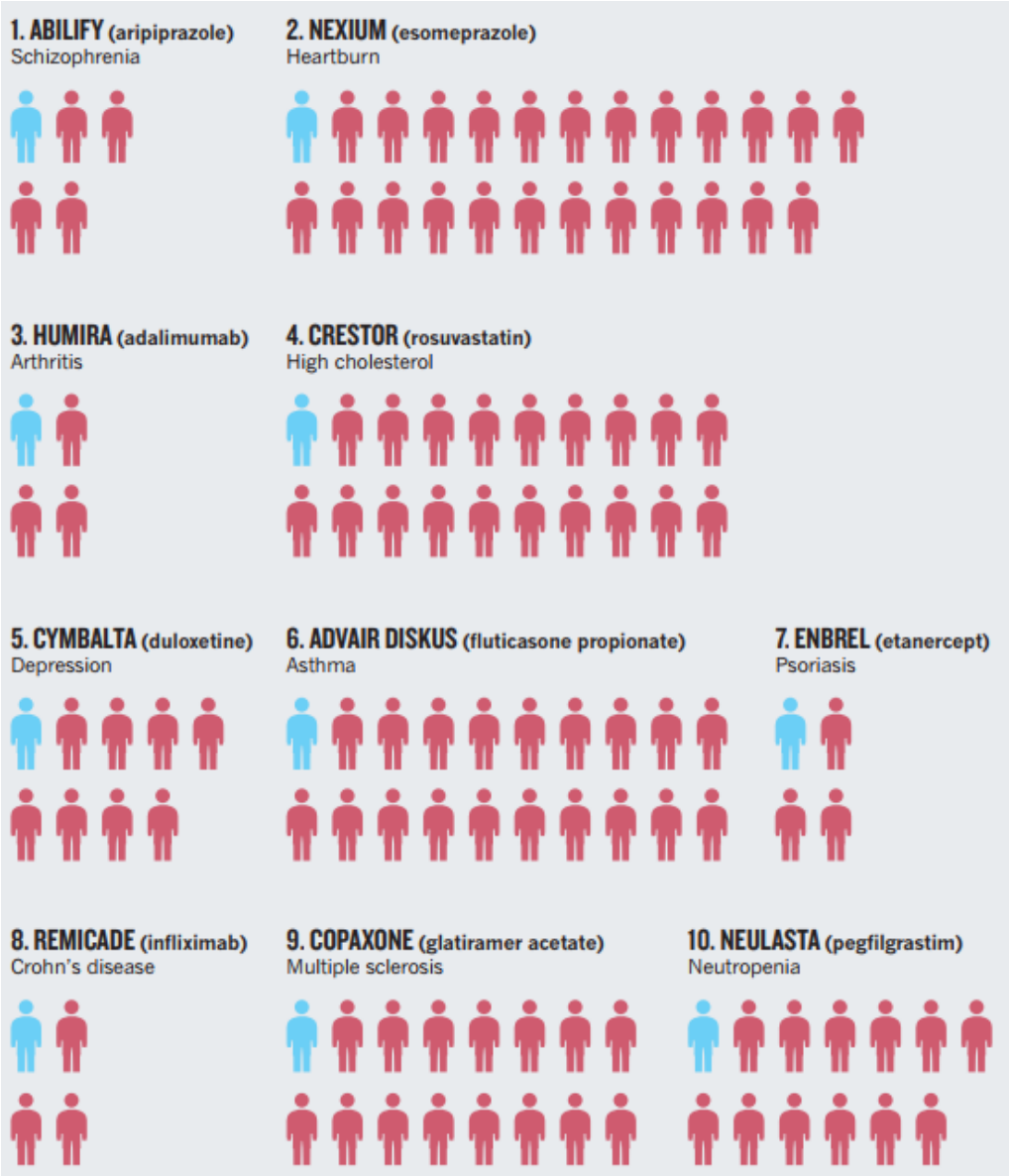

Figure 1.1 Overview of top ten highest-grossing drugs in the United States with visual representation of patient group for which the drugs are ineffective. Every person in blue represents someone for whom the drugs do help. However, these drugs fail to improve the conditions related with the specific illness for 75% up to 94% of the patients (red) (Adapted from: Schork, 2015).

Finally, we elaborate on the extent to which individualised monitoring of biological processes can be applied. As part of this framework, we define the following important terms: living systems, bio-processes, bio-signals and homeostasis; describe the recent advances in the monitoring of such bio-processes; and, subsequently, discuss why organisms are individually different and how we could obtain an individualized monitoring approach.

1.2 DEFINITIONS: LIVING SYSTEMS, BIO-PROCESSES, BIO-SIGNALS AND HOMEOSTASIS?

1.2.1 Living systems

For the optimal development of a monitor of a biological system, it is crucial to comprehend the main characteristics of the system (e.g. system architecture, system inputs and outputs, system dynamics, system limits,…; see e.g. Kitano, 2002). Therefore, it is essential to start from the available knowledge of the specific system. Evidently, biological systems are associated with the concept of life. To better understand the main properties of a living system, we must first define living systems in a more general way. Represented in BOX 1.1 are two possible definitions, from both a biological and thermodynamic point of view, for describing a living system.

1.2.2 Bio-processes and Bio-signals

Biological processes (i.e. bio-processes) can be described as all transformations (e.g. chemical reactions) that exist in biological systems and involve the consumption, alteration, production and/or constitution of entities (Mossio et al., 2016). To quantify the state of a particular biological process, one should find its relevant biological signals so they can be measured directly or indirectly by sensors. Most biological processes are manifested in the form of biochemical, electrical or physical signals (i.e. bio-signals). These bio-signals contain a lot of information and can be an

indication for the mental or physical (health) status of the organism (such as positive/negative stress, depression, fever, infection, general fitness, fatigue,…) and the occurrence/s of specific events within the organism (e.g. myocardial infarction of the heart, action potential of a neuron, falling asleep, decision making in the brain, movements,…).

1.2.3 From homeostasis to homeodynamics

Biological systems are in a state of permanent flux, continuously exchanging mass, energy and information with their environment (Walleczek, 2000). The human body, for example, is not only continuously measuring its environment, but also assessing the internal state of the sub-components for the preservation of healthy conditions. The sensory systems measure the state of the local environment, and sensors located near the body systems measure the internal state. At organism scale (or level), the central nervous system acts as controller of the many body systems. Based on sensory inputs, it calculates optimal actuator settings to preserve homeostasis. As mentioned in BOX 1.1, this is one of the key properties of a living system. Homeostasis was first described by Cannon (1932) as:

"The coordinated physiological processes which maintain most of the steady states in the organism are so complex and so peculiar to living beings—involving, as they may, the brain and nerves, the heart, lungs, kidneys, and spleen, all working cooperatively—that I have suggested a special designation for these states, homeostasis. The word does not imply something set and immobile, a stagnation. It means a condition—a condition which may vary, but which is relatively constant (Cannon, 1932)."

A widely familiar, unambiguous homeostatic variable is body temperature, which is relatively constant between 36.5°C - 37.5°C. Through neural control, blood vessels are forced into vasoconstriction or vasodilation (muscles in vessels as actuator), which directly influences the exchange of heat between the body and its environment.

BOX 1.1 Definitions of living systems:

What makes a system 'alive'? This is a central open question in the field of biology. Today, there is still no universally accepted definition of a living system (Macklem and Seely, 2010). Typically, a list of characteristics is proposed, which are shared by all living organisms. Raven et al. (2005) listed the following fundamental characteristics:

- **Cellular organization**: Living systems are composed of one or more cells.
- **Order**: Molecules in living systems are highly ordered in specific complex structures.
- **Sensitivity**: Response to environmental stimuli
- **Growth, development and reproduction:** Living systems are able to grow, develop and reproduce.
- **Energy utilization**: Living systems require to capture and use energy
- **Evolutionary adaptation**: Living systems evolve adaptations to unique situations in their surroundings.
- **Homeostasis:** Living systems maintain relatively constant internal conditions

This unique combination of properties could be defined as life from a biological point of view (for more details see Raven et al., 2005).

From a thermodynamic point of view, living organisms are **dissipative systems** or, in other words, open thermodynamic systems relatively far from equilibrium which are continuously perturbed by changes in the micro-environment (Prigogine, 1978). Based on their distance from equilibrium and complexity, we can order open thermodynamic systems. Living systems, which are neither linear nor chaotic, are considered as complex systems. In a more complete thermodynamic definition (Macklem and Seely , 2010), a living system could be described as "a self-contained, self-regulating, self-organizing, self-reproducing, interconnected, **open thermodynamic network** of component parts which performs work, existing in a complex regime which combines stability and adaptability in the phase transition between order and chaos, as a plant, animal, fungus, or microbe."

Other researchers claim that the definition of homeostasis is incomplete: "Instead of 'homeostasis', the term 'homeodynamics' may be a more accurate definition that captures the nonlinear regulatory principles governing the dynamical stability of a living system (Walleczek, 2000)." This means that the body not only maintains a constancy among homeostatic variables, but also tries to ascertain system stability for itself and all of its sub-systems. The body's failure to control dynamical stability in its subsystems can lead to dangerous states (illness). For example, a failure of the endocrine response to an infection can lead to sepsis, or a failure of the neuro-endocrine response to an overload of stress and/or a lack of sleep can lead to psychosis.

1.3 RECENT ADVANCES OF MONITORING BIOLOGICAL PROCESSES

In the previous section, we described a number of key concepts relating to biological systems and their underlying bio-processes. To assess the state of a biological process, one can measure the relevant variables to quantify the homeostasis and/or homeodynamics of the body or of the specific subsystem. For example, by measuring body temperature one can determine whether someone has a fever or not. By measuring the heart rate dynamics one can quantify someone's fitness. Today, there are already several monitoring systems which try to determine the state of living organisms or bio-processes. The field of bio-process monitoring is making progress in different application domains. This section gives an overview of important recent advances in this field.

1.3.1 Precision livestock farming (PLF)

Nowadays, people are more worried than ever about food safety and quality, sustainable animal farming, animal welfare and the environmental impact of livestock production. As a reverberation of these concerns, there is a growing demand for automated systems that allow monitoring of multiple variables during the entire production process (Berckmans, 2006). However, the field of monitoring

within PLF is still in its infancy (see also Wathes, 2009). Compared to other industrial fields, monitoring in livestock production is still relatively undeveloped. This can be explained by the fact that animals are biological and, therefore, individually different— a factor which complicates the development of such systems (Frost, 1997). However, due to the latest emerging technologies, such monitoring systems are becoming an increasingly vital part of the production process (Berckmans, 2006). Table 1.1 gives examples of current applications of PLF. There are many recent studies available on the development of such systems for cows (Viazzi et al., 2013; Schlageter-Tello et al., 2014; Van Hertem et al. 2014), pigs (Oczak et al., 2013; Kashiha et al., 2014; Kashiha et al., 2014; Vandermeulen et al., 2015), chickens (Exadaktylos et al., 2011; Kashiha et al., 2013; Romanini et al., 2013; Aydin et al., 2014; Youssef et al., 2014), horses (Jansen et al., 2008; Exadaktylos et al., 2013; Nuyts et al., 2013) and fish (Viazzi et al., 2014).

1.3.2 Human health

In the field of human health monitoring, there are predominantly three general types of states of interest to be monitored: mental states, physical states and disease states. Most studies focus on the monitoring of disease states in patients: in hospitals, monitoring systems are omnipresent. Figure 1.2 gives an overview of the general elements in a patient monitoring system (Mora et al, 1993). In intensive care units, patients are surrounded by multiple devices for monitoring vital signs (Imhoff, 2006). Continuous measurement of patient variables, such as heart rate and rhythm, respiratory rate, blood pressure, blood-oxygen saturation, and many other variables has become a common feature of the care of critically ill patients (Gardner et al., 2001). Thus, as Bravi (2014) points out: “The future in ICU monitoring is therefore to translate ‘raw information’ into scores to support clinical decision” (Bravi, 2014).

Table 1.1 Examples of current applications of PLF (adapted from Banhazi, 2012).

Technology /Tools
Improved egg incubators via synchronisation of hatching (e.g. Exadaktylos et al., 2011; Romanini et al., 2013; Youssef et al., 2014)
Monitoring systems for broiler houses (e.g. Kashiha et al., 2013; Aydin et al., 2014;)
Intelligent ventilation control in livestock buildings
Weight estimation of pigs via machine vision tools (e.g. Kashiha et al., 2014) Monitoring pig locomotion (e.g. Kashiha et al., 2014)
Dairy management to maximise profit
Improving profitability via precision feeding for pigs Monitoring aggressive behaviours of pigs (e.g. Oczak et al., 2013
Sensor placement robot for pigs
Cattle monitoring system (e.g. Viazzi et al., 2013; Schlageter-Tello et al., 2014; Van Hertem et al., 2014)
Udder health and hygiene monitoring in dairy cattle
Automated egg counting and identification
Improved thermal control for pigs via machine vision
Cough recognition in pigs (e.g. Vandermeulen et al., 2015)
Automated fish sizing and sortings (e.g. Viazzi et al., 2014)

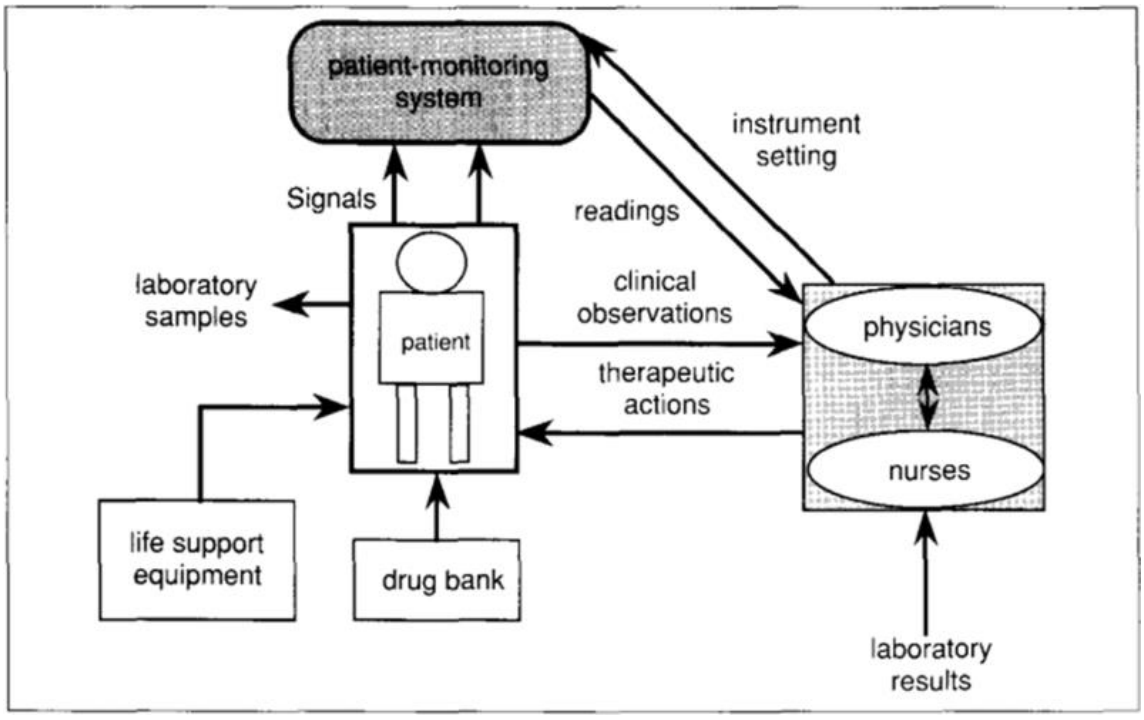

Figure 1.2 Patient monitoring and management environment elements (Mora et al, 1993).

However, Bravi also remarks: “To date there are only few systems that embodied these principles.” Two of the few of Bravi’s referenced systems are Visensia™ and Hero™ (Bravi, 2014). The Visensia monitoring system calculates a score based on a combination of heart rate, respiratory rate, blood pressure, temperature, and oxygen saturation. This score is then used to detect deteriorations in the patient’s state (Tarassenko, 2005). The HERO monitoring system uses heart rate variability measures to predict neonatal sepsis (Moorman, 2011; Fairchild, 2012; Bravi, 2014).
However, patient monitoring can also be extended to cover patients off-site (outside of medical institutions) for the detection of unexpected life-threatening conditions or to efficiently record routine, but required, data (Fotiadis et al.,2006; e.g. glucose monitors).

The use of systems for the monitoring of physical states can be most accessibly observed in sport. Over the last 30 years, heart rate monitors (HRMs) have become a commonplace training aid in a variety of sports (Achten et al.,2003). Additionally, accelerometers have been widely accepted as useful, as have practical sensors in wearable technology, which measure and assess physical activity. Activity monitors or accelerometers can objectively capture body movement and provide information on the total amount, intensity, duration and frequency of physical activities performed (Plasqui et al., 2013; Mukhopadhyay, 2015).

A limited number of studies can also be found concerning the monitoring of mental states of humans (e.g. Smets et al., 2013; Torous et al., 2014). Examples of mental states could be mental stress (e.g. Salahuddin et al., 2007; Choi et al, 2012), depression (e.g. Doryab et al., 2014; Manning et al., 2015; ; Topalovic et al., 2017), psychosis-related diseases (e.g. Tait et al., 2002; Yung et al., 2014), etc.

1.3.3 Bio-technological processes

Biotechnological processes include a wide range of sectors, from pharmaceutical, agro-food and beverage production to bioreactors and to wastewater and bio-waste treatment (Lourenco et al., 2012). In this field, current monitoring (and control) systems are lagging behind compared with other engineering fields. There are two main reasons for this: i) living organisms are complex (e.g. due to their individual characteristics), ii) an absence of cheap and reliable sensors that can be used for real-time monitoring (van Impe et al., 2013).
That said, recently, an increasing number of examples can be found on the development of monitoring systems for bioreactors (Komives et al. 2003; Junker et al., 2006; Baradez et al., 2011; Kresnowati et al., 2011; Lourenço et al., 2012; Csaszar et al., 2014; Lambrechts et al., 2014), wastewater monitoring (Bourgeois et al., 2001; Vanrolleghem et al., 2003), bio-chemical batch processes (Vanlaer, 2013; Van den Kerkhof et al., 2012) and the pharmaceutical industry (Ündey et al., 2010).

1.4 THE NEED FOR INDIVIDUALISED MONITORING OF BIOLOGICAL PROCESSES

Thus far, we have defined biological processes and briefly listed recent advances in the field of monitoring biological processes. However, as stressed in the opening section (1.1), one of the main difficulties in monitoring biological processes is in dealing with individual differences. In this section, we will address why organisms are individually different and, thereafter, discuss the main characteristics of an individualized monitoring system compared with population-based monitoring systems.

1.4.1 Origin of individual differences

There are different scales by which individual living systems can be defined (figure 1.3 and BOX 1.2). However, independent of scales, we deem each biological individual as unique. Individual variation is a necessary characteristic of a living organism for evolutionary adaptation to new environmental conditions (BOX I.3). There are two main reasons for this individual diversity: i) differences due to gene effects (nature) and ii) differences due to environmental effects (nurture). Inherited influences include variations in DNA sequence, which are transmitted from generation to generation over an evolutionary time scale. Every individual (except for identical twins) has a unique genome, and, although a pair of genomes are approximately 99.9 % identical, there exists millions of differences among the 3.2 billion base pairs. Thus, a substantial proportion of our individual differences are determined by our genetic profile. That said, our genetic profile alone does not comprehensively account for all the differences between individuals. Figure 1.4 shows the average grey matter difference in the brains of identical twins. Their brains are presumed to contain an identical genome (Thompson et al., 2001), but despite this, substantial individual differences in the quantity of grey matter are found in each region of the cortex. This can be explained by the fact that the brain has the ability to change structure and function based on experiences (i.e. environmental effects), a function known as brain plasticity.

Environmental effects occur over developmental and physiological time scales, and the related anatomical brain changes cause individual behavioural differences in subjects (Kolb et al., 1998).

BOX 1.2 Biological individuals.

In an organism-centred view, there are three different kinds of biological individuals (Wilson et al., 2014):

- Organisms (e.g. humans, pigs, rats, chickens)
- Parts of organisms (e.g. cardiovascular system, cells, organs)
- Groups of organisms (e.g. group of fireflies, schooling fishes, flock of birds)

Thus, cells, organs and tissues are also individual biological systems (Figure 3.3). DNA can also be considered as individual, as suggested by Dawkins (i.e. the "selfish gene"; Dawkins 1976), whereas the body is only the survival machine of the genome. On the other hand, in some cases we can also consider a group of individuals as an individual system which exhibits typical group behaviour. For example, a group a fireflies is known to flash light in synchrony (Figure B.1.2; Strogatz, 1994) .

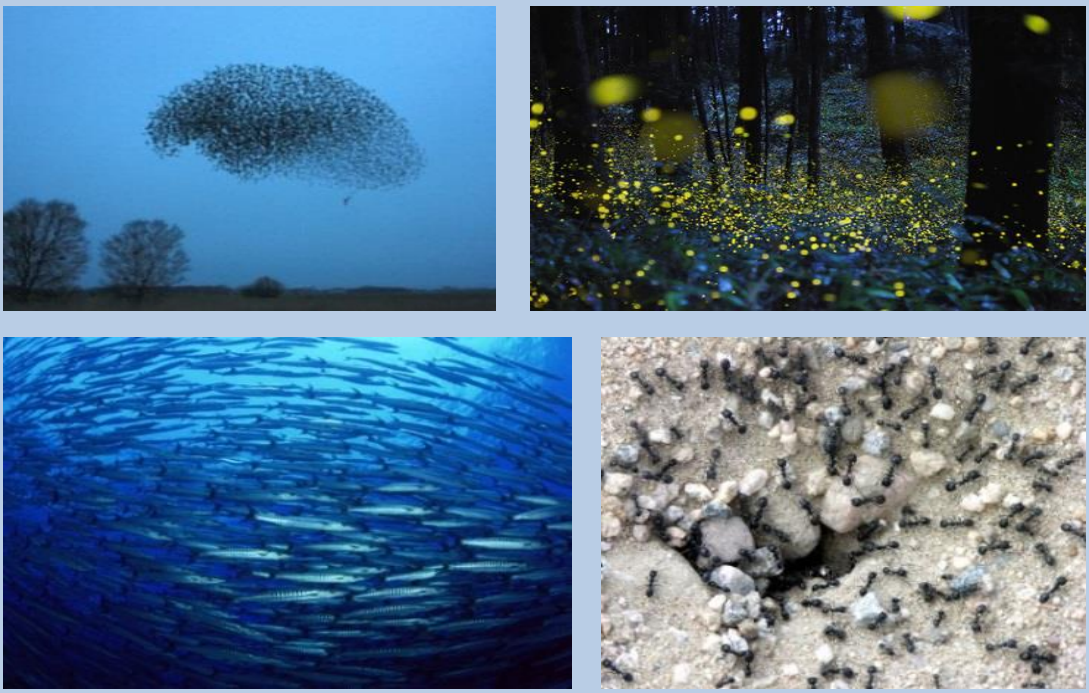

Figure B.1.2. Groups of animals often show cooperating behaviour which exceeds the organism level. Top right: group of fireflies; top left: flock of birds; bottom right: group of ants; bottom left: schooling fish.

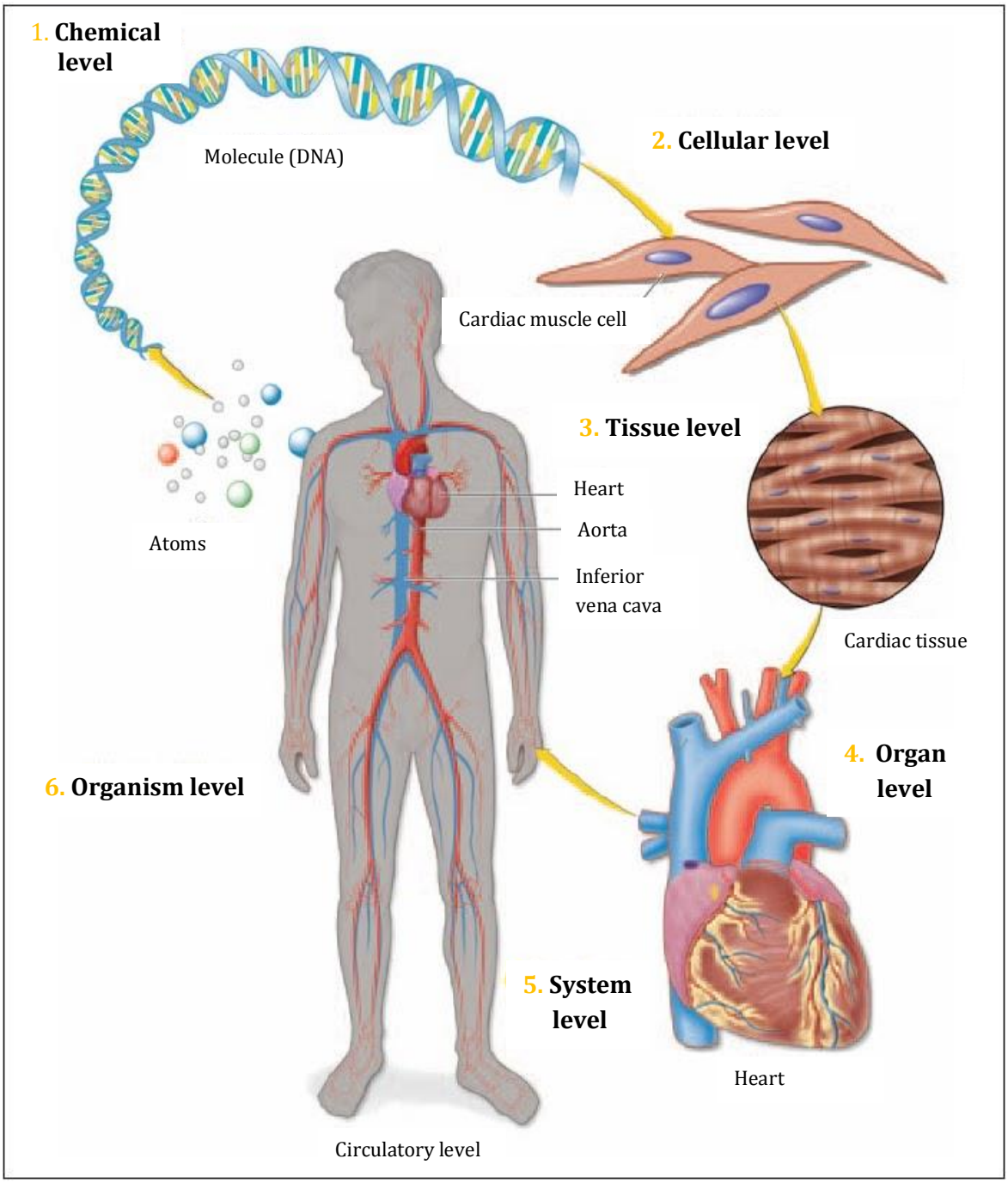

Figure 1.3. The human body at different spatial levels (From: Premkumar, 2004).

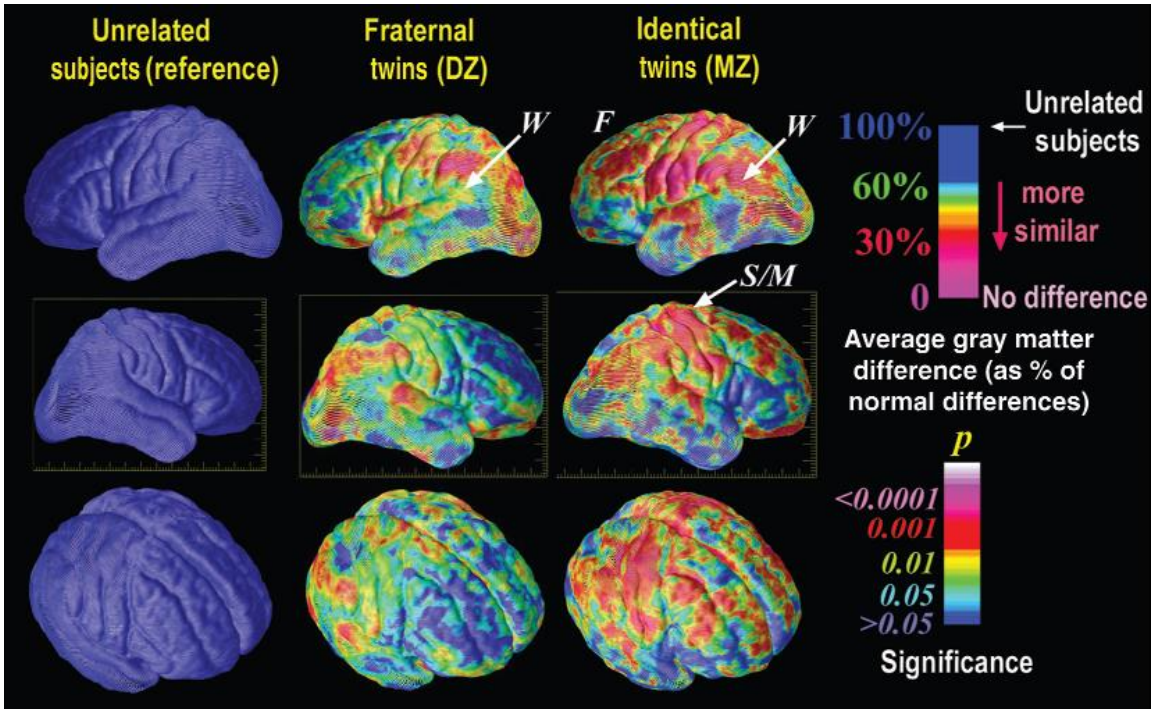

Figure 1.4 Depicted are the differences in the volume of grey matter in each cortical region of 10 identical (monozygotic or MZ) and 10 fraternal (dizygotic or DZ) twin pairs. The results are compared with the average differences that would be found in pairs of unrelated individuals. The colours of the three-dimensional brain maps represent the percentage reduction in intra-pair variance for each region of the cortex (For more details: see Thompson et al., 2001).

BOX 1.3 Individual variation for evolutionary adaptation

"I cannot doubt that during millions of generations individuals of a species will be occasionally born with some slight variation, profitable to some part of their economy. Such individuals will have a better chance of surviving, and of propagating their new and slightly different structure; and the modification may be slowly increased by the accumulative action of natural selection to any profitable extent" (Darwin, 1858; Figure B.1.3).

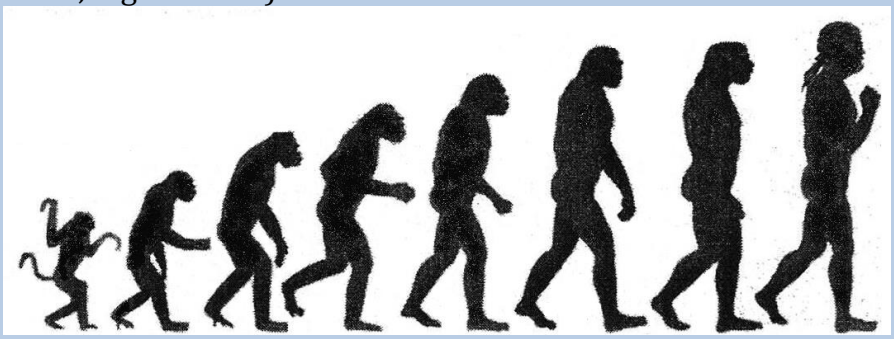

Figure B.1.3 Drawing representing human evolution

1.4.2 Individualised vs population-based monitoring

To detect changes of events and states in biological processes, monitoring systems typically use thresholds—which characterise the changes. In some cases, threshold methods are used in combination with probabilistic approaches to deal, for example, with uncertainty of the bio-process state (Attia, 2003; Zenker et al., 2007; Meyfroidt et al., 2011).

Many examples of thresholds can be found in living organisms. However, in developing monitoring systems for living organisms, it is not sufficient to assess—based on population rules—thresholds relating to specific states or events, and therein lies the problem. Every living organism, organ and cell is unique, and each has its own individual thresholds.

1.4.2.1 Individual and population thresholds

The various methods by which we can determine individual thresholds are a focal point of this PhD. A well-known example of a population-based threshold is body temperature, which can indicate the presence of fever. As previously mentioned, body temperature is a homeostatic variable which should be more or less constant within a range. If someone's body temperature is to exceed 37.5 degrees Celsius, we know they have a fever.

We can also look to the action potential of a firing brain cell to observe another cellular-scale threshold (figure 1.5). Once the membrane potential exceeds a certain value, it will reach a point of no return and the neuron will start to fire (Hodgkin & Huxley, 1952). The resting potential at the axon hillock of a neuron is +/- –70 millivolts (mV). The threshold potential is +/- –55 mV. Typically, synaptic inputs lead to the depolarisation or hyperpolarisation of the neuronal membrane. Action potentials are triggered when the depolarization increases and brings the membrane potential up to the threshold value.

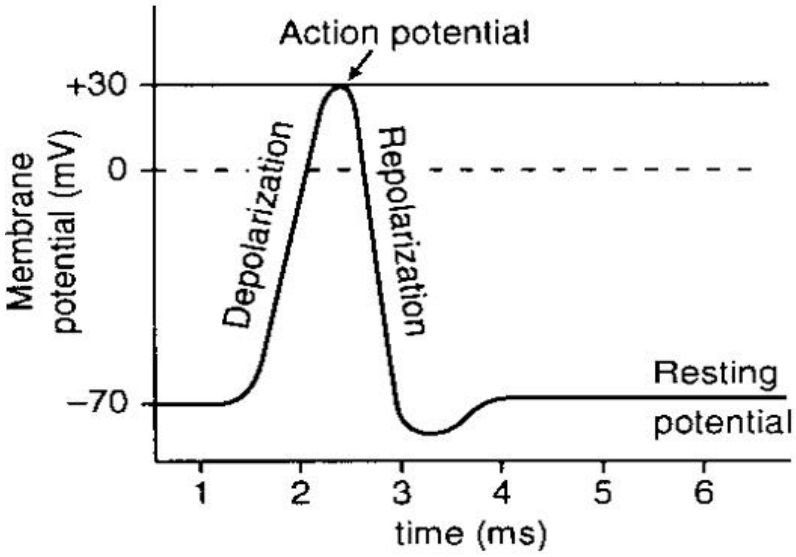

Figure 1.5 Illustration of an action potential after exceeding the threshold potential (Retrieved from: Psychlopedia, 2017).

There are also examples of well-known individual thresholds, such as the pain threshold of individuals, which can vary enormously. Figure 1.6 indicates that the average pain threshold is lower in women than it is in men. However, both histograms are very broad, demonstrating that there is a lot of individual variation with regards to pain thresholds. Let's consider the lactate threshold, another sound example of an individual threshold, for good measure. The lactate threshold can be considered a measure of the physical fitness of athletes. It is defined as the exercise intensity at which lactate starts to accumulate in the blood. Often, this lactate threshold is defined with a fixed population-based threshold such as 2 or 4 mmol/L (Gavin et al., 2013). However, such fixed markers of the lactate threshold disregard individual lactate variability during rest and exercise. Therefore, several methods are necessary for determining the lactate threshold (i.e. onset of exponential accumulation of lactate in the blood) in an individualized way (e.g. deviation maximum (Dmax) method; Cheng et al., 1992).

In addition, also in many other applications the use of individualised thresholds for identifying changes of the biological processes may be designated (e.g general health status: Schork and Goetz, 2017).

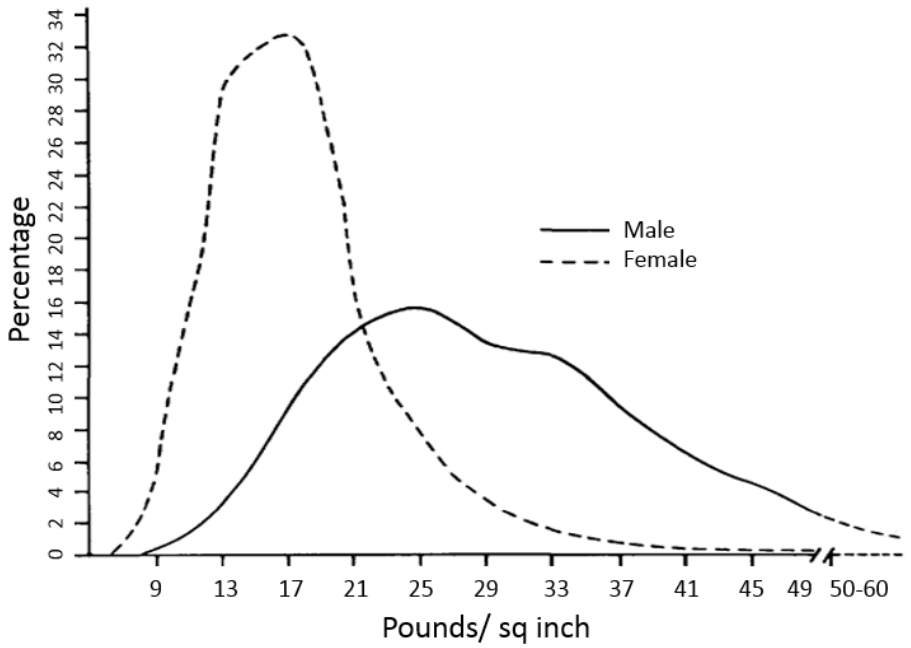

Figure 1.6 Pain tolerance distributions in men and women (Woodrow et al., 1972).

1.4.2.2 Individualised model-based monitoring: schematic representation

What the various examples in this section have shown is that the bio-signals of different individuals might contain significant individual differences. Such variation of bio-signals at both group and individual level is schematically represented in figure 1.7. To illustrate, when measuring the value of a bio-signal at time point X, for a range of different individuals, we get an idea of the inter-individual differences of the bio-signal. In other words, we garner an understanding of the distribution of the particular bio-signal at population level, which can be characterized by a mean: μ, and a variance: σ^2. That said, most bio-signals vary over time in a way that is unique in each individual and subject to the individual properties of the biological process (history of perturbations, architecture, etc.). Therefore, each bio-signal of an individual *n* must be characterised by its own mean, μ_n, and variance, σ^2_n. Because of such intra-individual differences, a biological system often responds differently to two similar perturbations. In accordance with the latter, some individuals show values that are above a population-based threshold and others have bio-signal fluctuations over time that may be biologically meaningful despite not reaching the population threshold (Schork and Goetz, 2017).

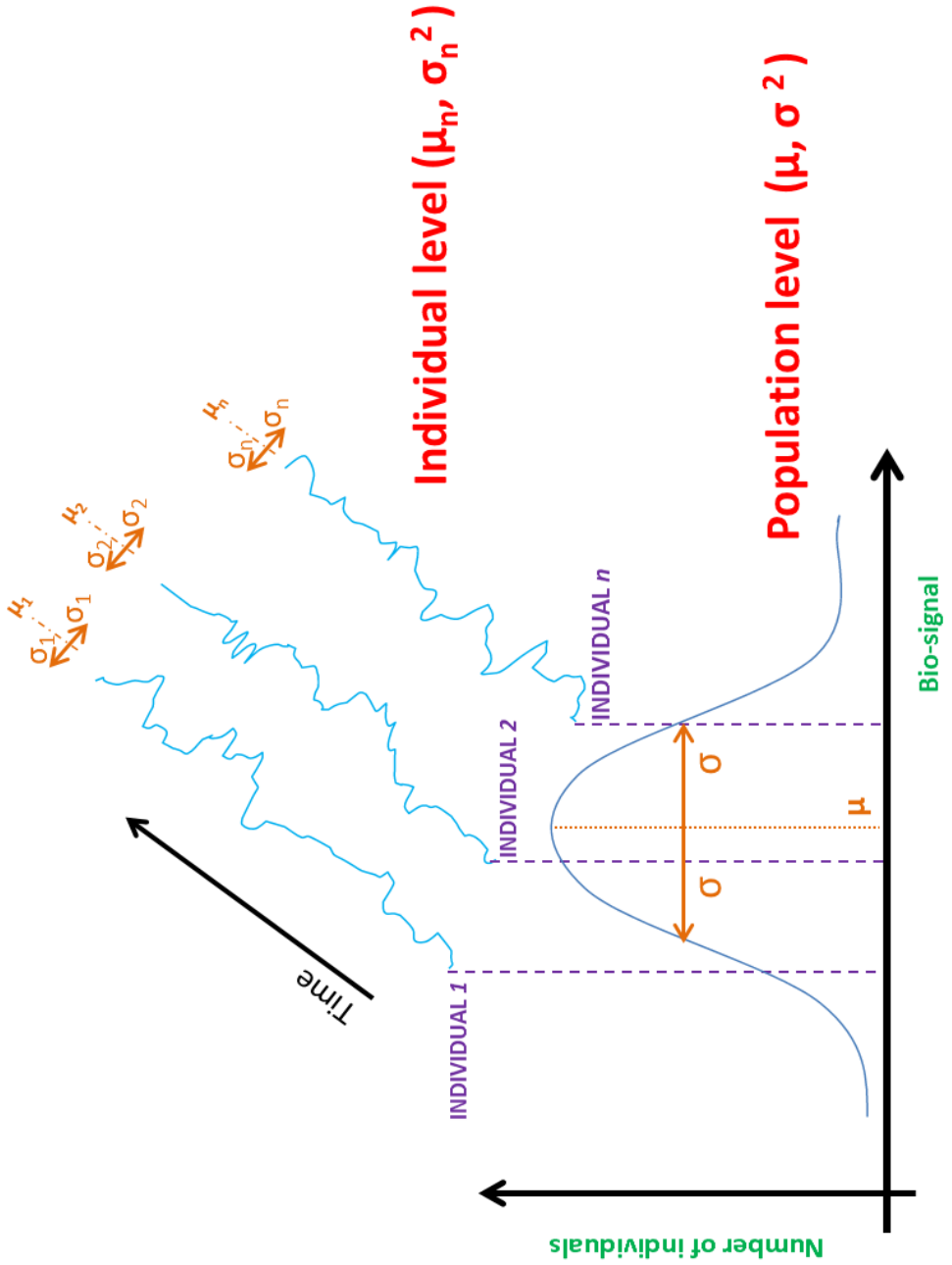

Figure 1.7 Visual representation of individual and group variations of bio- signals over time (see e.g. Berckmans and Aerts, 2015).

Nowadays, individualised monitoring gets most attention in the field of personalised medicine. However, personalised medicine also faces various practical problems inhibiting the common use of individualised approaches (e.g. lack of appropriate disease biomarkers, additional costs, slow implementation of the newest health-monitoring devices, the need for a cultural shift on many levels even beyond the

hospital setting such as regulatory agencies and pharmaceutical companies, etc.) (Schork, 2015). Nevertheless, individualised approaches and the use of personal thresholds to guide inferences about health status changes have been shown to be useful in an increasing number of monitoring studies for medical applications (e.g. Tait et al., 2002; Van Loon et al., 2009; Drescher et al., 2013; Schork and Goetz, 2017). In addition, the use of individualised approaches has also been useful for other human health applications (e.g. Quanten et al., 2006) and animal health applications (e.g. Romanini et al., 2013; Viazzi et al., 2013; Kashiha et al., 2014).

For each individualised monitoring application, accurate and detailed bio-process (e.g. patient) information should be collected as frequent as possible and over a sufficiently long time (Schork, 2015). However, to reveal the potential of such datasets, there is need for more frameworks in data analysis, in modelling and in interpretation of such complex, individual, time-varying, dynamic processes (Quanten et al. 2006; Colijn et al., 2017). In this PhD, we propose a model-based framework for the development of a monitor for bio-signals in individuals. The general model-based framework for monitoring bio-processes has been applied for a long time at M3-BIORES (e.g. Aerts et al., 2003; Berckmans, 2006), but in this PhD we focus on how to individualise this approach with individual threshold approaches. The Figure 1.8 illustrates a general scheme of the proposed individualised monitoring approach based on individual thresholds. As shown, the applied approach focuses on model-based monitoring of individual biological processes. Such individual biological processes can be characterised by an interaction between input and output variables. An input variable can be seen as a controllable variable which perturbs the considered process (i.e. environmental variable). An output variable, on the other hand, is used to quantify the specific response (i.e. bio-signal) to the applied input. Moreover, bio-processes are continuously subject to a wide range of uncontrollable perturbations in their (internal and external) micro-environment (e.g. temperature, medications, social contact etc.). By use of a process model, and in applying specific model features—such as model parameters, model noise and/or model structure—relations between measured input and output variables of the individual bio-process can be captured. In comparing the model

features with features under baseline conditions (e.g. normal system behaviour), individual changes in features can be detected. Subsequently, the detected changes of such model features can be considered in relation to changes in system states (e.g. healthy vs ill). Features can be selected on group level, but should ideally be individually selected for the individual bio-process. Based on individual thresholds on these individual (or group) features, such state changes can be detected in an automated way and the operator (e.g. doctor in a hospital) can be informed.

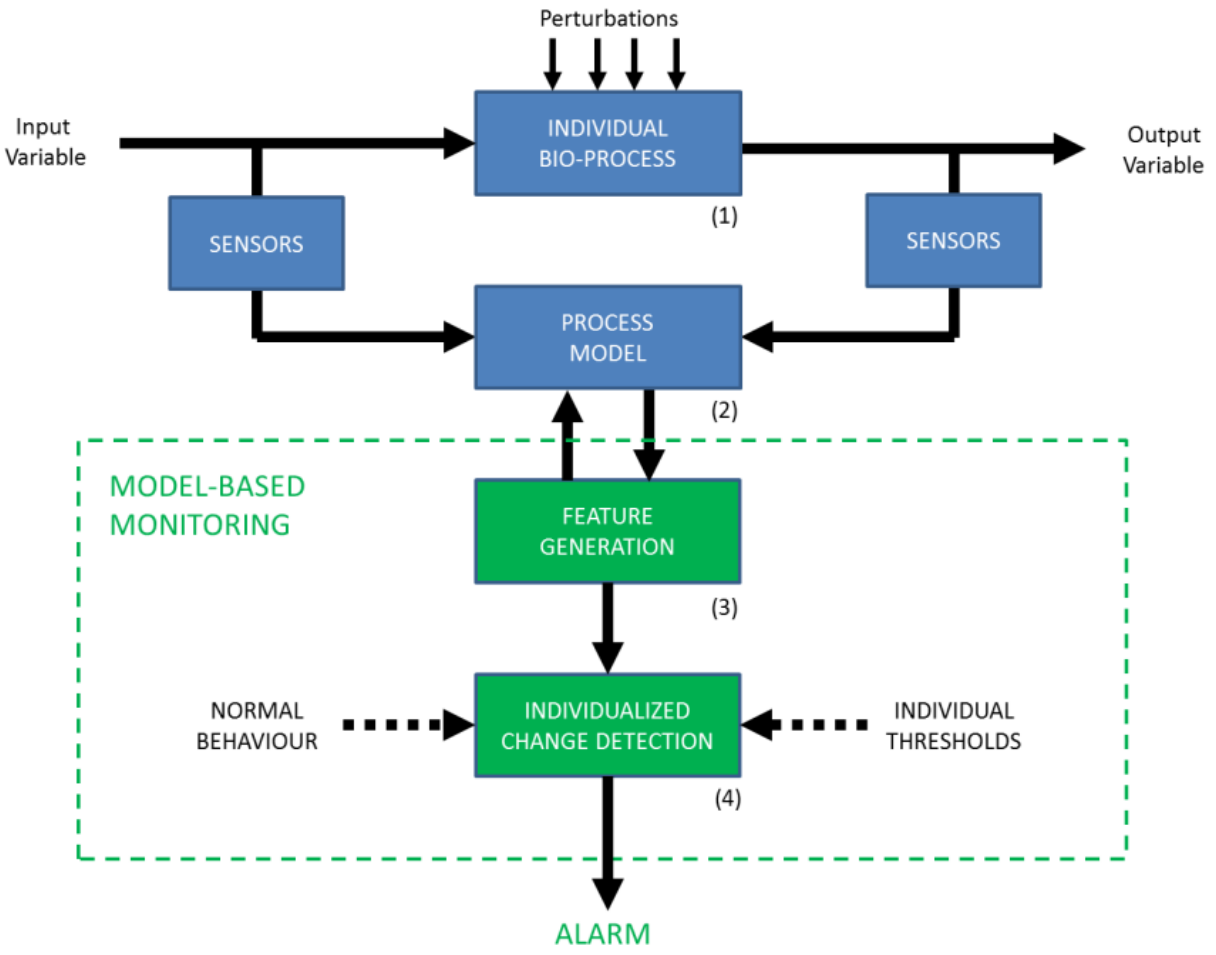

Figure 1.8 Introducing the use of individual thresholds in the general scheme of data-based mechanistic modelling for individuals (for more details on the general scheme: see Berckmans and Aerts, 2015). There are four main blocks: (1) bio-process, (2) process model, (3) model-based features, (4) individual change detection. The green dashed line emphasises how models can be used to monitor biological processes based on individual thresholds.

1.5 OBJECTIVES AND HYPOTHESES

The **general objective** of this PhD thesis was to develop an individualised model-based monitoring framework for biological processes, as inspired by control engineering concepts. The general concept of this objective was examined in six different case-studies (cell, embryo, animal, human; see Part II; Chapter I to VI). In every chapter we will get one step closer to unravelling key elements for an individualised model-based monitoring approach. Each case study corresponds with one case-specific hypothesis. Therefore, all case-specific hypotheses of the chapters will be elucidated at the beginning of each chapter. An overview of all specific hypotheses is given in section 1.6.

The complexity and amount of methods used to obtain an individualised model-based monitoring approach increases from Chapter I to Chapter VI. In each successive chapter more elements of the general framework (Figure 1.8) will be addressed in line with the general objective of this PhD. Therefore, all chapters will be discussed in Part III starting from the four general blocks of figure 1.8. In addition to the general objective formulated above, each block corresponds with one general sub-objective (SO):

- **SO1: The biological process**

  Individual biological processes (individual system structure, individual system dynamics, individual bio-signals) will be interpreted as the biological equivalents of control engineering components by defining actuator and homeostatic variables for each of the six case studies (Chapter I-VI).

- **SO2: The process model**

  Although biological processes are known to contain many nonlinearities, we will use compact individual linear models (general Box-Jenkins models) for the specific individualised monitoring applications of the case studies (Chapter II, III, IV and VI). By using these models we aim to obtain a good approximation of the individual bio-process dynamics and/or to uncover information about the underlying mechanisms/state by applying data-based mechanistic modelling approaches (Chapter IV and VI).

- **SO3: Model-based features**

  We will identify generic metrics from the fields of complex systems science, change detection and control engineering that can be used while analysing individual time series. This list of metrics can be used for all individual bio-processes in the design of model-based monitoring applications and will be generated based on the specific case studies (Chapter I-VI).

- **SO4: Individualised change detection**

  By integrating insights from control engineering and change detection, we will develop a general framework for individualised model-based monitoring of biological processes based on individual thresholds. This general approach could potentially be implemented in a wide range of applications and could improve the generally accepted population-based approaches (Chapter I, II, V and VI).

1.6 SPECIFIC HYPOTHESES FOR THE SIX CASE STUDIES

Individualised monitoring of activity and body weight in the activity-based anorexia rat model (Chapter I)

Hypothesis I: The activity-based anorexia (ABA) rat model is characterised by many inter- and intra-individual differences. Therefore, we hypothesise that a time series-based monitoring approach, as opposed to other approaches focusing on more spread static measurements, can aid to obtain more individual information. Such time-series approach can be used to identify the key factors leading to the inter-individual differences and to determine individualised dynamic thresholds capturing time-varying aspects leading to the intra-individual differences.

Individualised model-based monitoring of interleukin-6 for early detection of infection in pigs (Chapter II)

Hypothesis II: Model-based time series analyses of interleukin-6 (IL-6) at the individual level offers a method in detecting infection with pleuropneumonia in individual pigs. Based on individual IL-6 baseline measurements, we can reveal individual changes of IL-6 dynamics (i.e. IL-6 fluctuations patterns) that can be used as early warning signs

for objective individualised early-warning monitoring of sepsis and inflammation processes in individual pigs.

Model-based monitoring of heart rate and blood cytokine time series for early detection of infections in critically ill patients (Chapter III)

Hypothesis III: We can apply 20 different generic metrics from the field of complex systems science, change detection, and control engineering, while analysing individual heart rate and blood cytokine time series for monitoring of infection in ICU patients. These generic metrics can be used for all individuals in order to distinguish infected from non-infected ICU patients. Afterwards, machine learning techniques (i.e. logistic regression, bootstrapping, and decision tree analysis) can be used for selection of metrics and determination of multivariate monitoring thresholds for detection of infection at ICU.

Model-based monitoring of mGluR-dependent synaptic plasticity in hippocampal brain slices of rats (Chapter IV)

Hypothesis IV: Long-term synaptic modifications play a key role in the plasticity of behaviour, learning, and memory. Reverse engineering using data-based input-output linear transfer function (TF) models, can be used to quantify dynamics and gain more insight in the underlying physiological processes of drug-induced synaptic plasticity responses in the hippocampus of rodents. Thus, it is possible to obtain data-based mechanistic models for monitoring of synaptic plasticity responses in hippocampal brain slices of rodents.

Individualised monitoring of hippocampal theta oscillations and individualised electrical stimulation in the mesencephalic reticular formation for real-time closed-loop suppression of locomotion in rat (Chapter V)

Hypothesis V: Control of the central nervous system by deep brain stimulation (DBS) is a promising example of how control engineering concepts can be applied to adapt (pathological) behaviour of organisms. We hypothesise that it is possible to develop a real-time individualised closed-loop DBS system for suppression of locomotion of rats. The input source of the system is real-time recorded local field potentials (LFPs) from the hippocampus, which are highly related to locomotion. The output electrical stimulation is delivered in the mesencephalic reticular formation (mRt), which induces freezing. Based on baseline measurements, effective individual thresholds for

monitoring the hippocampal LFPs and optimal individual stimulation parameters can be determined.

Individualised model-based monitoring of chicken embryo status during incubation based on eggshell temperature and micro-environmental air temperature (chapter VI)

Hypothesis VI: We hypothesise that we can develop a non-invasive individualised model-based monitoring approach which is able to detect or even predict online the individual progress of embryo development during the incubation of chicken eggs based on egg shell temperature and micro-environmental air temperature. By using a linear data-based mechanistic modelling approach, we can monitor five different stages of embryo development and gain insight in the individual embryo status.

1.7 MAIN STRUCTURE OF THIS THESIS

As indicated in **Part 1**, there is need for methodologies in data collection, data analysis, in modelling and in interpretation of complex, individual, time-varying, dynamic processes that can be used for individualised monitoring (e.g. Quanten et al. 2006; Schork, 2015; Colijn et al., 2017). Despite all inter- and intra-individual differences, such methods should ideally be working for all individuals. This thesis has led to some innovative individualised monitoring applications based on the six specific case studies of **Part 2** (i.e. Chapters I-VI; cell – embryo – animal – human).

Each chapter in Part 2 highlights specific aspects in the process of designing an individualised model-based monitoring application based on combining available biological information with control engineering concepts. **Table 1.2** shows how the complexity and amount of methods used to obtain an individualised model-based monitoring approach increases from chapter I to VI.

In **Chapter I,** individualised monitoring is obtained by determining dynamic thresholds for simple features based on raw variables (i.e. rat activity and body weight) quantifying the bio-process (i.e. activity-based anorexia rat model).

Thus, Chapter I indicated how raw variables could be used for individualised monitoring (**Table 1.2**). However, **Chapter II** shows how compact linear models can be used to extract more individual information of the specific bio-process dynamics (i.e. infection responses of pigs). Moreover, also by using baseline measurements of only one process variable (i.e. interleukin-6) a more individualised approach was obtained.

Whereas Chapter II focuses mainly on a limited amount of model-based bio-signal features, in **Chapter III** 20 specific bio-signal features are determined by applying generic metrics on the process variables (i.e. heart rate and blood cytokine times series; **Table 1.2**). Afterwards, multivariate analysis methods were applied to define multivariate thresholds that could be used for model-based monitoring of the bio-process (i.e. infection monitoring of ICU patients).

In Chapters II and III, model-features were determined by applying compact linear models to single variables. On the contrary, the model-based monitoring application of **Chapter IV** (i.e. mGluR-dependent synaptic plasticity in rat brain slices) is based on data-based mechanistic modelling of input-output variables (**Table 1.2)**. The results of this chapter show how such models could be used to gain physiological insight in highly nonlinear biological processes.

Although each of the previous emphasised different important aspects to obtain individualised monitoring applications, the thresholds were calculated on (sub)population level. **Chapter V** illustrates how individual thresholds can be obtained by using individual serial baseline measurements of the relevant bio-process variables (i.e. hippocampal theta oscillations in rat brain). In addition, individual intervention parameters (i.e. electrical stimulation in mRt) were acquired making it possible to individually control the biological system (i.e. closed-loop deep brain stimulation for locomotion control).

Chapter I to V address some elements of the general block diagram for individualised model-based monitoring (Figure 1.8). Finally, **Chapter VI** tackles all blocks of the general diagram (i.e. individualised model-based monitoring of chicken embryo status). Besides the use of data-based mechanistic models with physiological insight, individual baselines, individual thresholds, also individual predictions were obtained (**Table 1.2)**. Moreover, whereas the previous chapters described specific

monitoring approaches for detecting only one specific state change of the biological process, here we developed an approach for monitoring five different specific state changes (embryo development) of the bio-process.

Until now the existence of general frameworks for individualised model-based monitoring of biological processes are limited (e.g. Colijn et al, 2017). In this thesis, each specific case (i.e. animal and human health engineering applications) contributed to the development of such general framework inspired by control engineering concepts (see discussion, **Part 3**, and conclusions, **Part 4**).

Table 1.2. Schematic overview of the six different individualised model-based monitoring applications (Chapter I-VI). The complexity and amount of methods used to obtain an individualised model-based monitoring approach increases from Chapter I to Chapter VI (blue parts in table).

	BIO-PROCESS	MODEL	FEATURE	INDIVIDUALISED CHANGE DETECTION
Chapter I:	**Raw measured variables**	(No model)	4 raw signal features	**Dynamic thresholds (for sub-populations)**
Chapter II:	One measured variables	**Individual linear model**	3 signal features	**Individual baseline, (Population) thresholds**
Chapter III:	Many measured variables	Individual linear model	**20 generic signal features**	**Multivariate thresholds (for population)**
Chapter IV:	Input-output variables	Individual linear data-based mechanistic model	3 model-based features	**Physiological insight, (Population) threshold**
Chapter V:	Input-output variables	Individual frequency analysis	Individual frequency-based features	**Individual baselines, Individual thresholds, Individual control**
Chapter VI:	Input-output variables	Individual linear data-based mechanistic model	1 model-based feature	**Physiological insight, Individual baselines, Individual thresholds, Individual predictions**

Part 2

Chapters

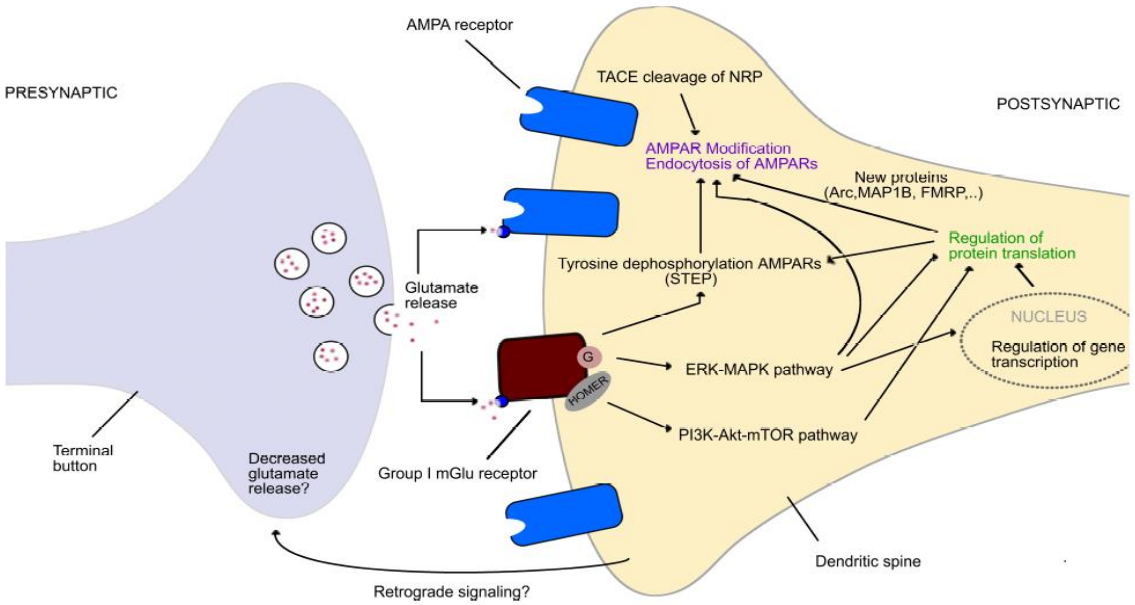

Illustration based on the case study of chapter IV.

Simplified overview of mechanisms involved in mGLuR-dependent LTD made based on two comprehensive review articles: Gladding et al., 2009 and Lüscher and Hüber, 2010.

CHAPTER I

Rethinking Food Anticipatory Activity in the Activity-Based Anorexia Rat Model

Adapted from: Wu, H., Van Kuyck, K., Tambuyzer, T., Luyten, L., Aerts, J. M., & Nuttin, B. (2014). Rethinking food anticipatory activity in the activity-based anorexia rat model. *Scientific reports*, *4*.

BROADER PERSPECTIVE

According to figure 1.8, this chapter focuses mainly on the first block of the general scheme which is **"The individual bio-process"**. The chapter describes the behaviour of individual rats, which are conditioned according to the Activity-Based Anorexia (ABA) rat model. Questions that arise automatically are: What do we know of the specific biological process (link to Hypothesis 1 in Part 1)? Which variables should be measured? How frequent and for how long should these variables be measured? The main **measurable variables** are selected based on **available biological knowledge** of previous studies: body weight, food intake and running wheel activity (RWA). All variables were measured at the level of individual rats and therefore, the **spatial level** of interest can be considered as the whole organism by itself. Whereas most studies focus primarily on the running activity prior to the scheduled feeding of the animals (Food Anticipatory Activity or FAA), this study also investigated activities during other periods and their correlations with body weight. This was possible since RWA was monitored continuously and body weight/food intake were measured daily resulting in three **time series** for each individual rat.

After a decade of experience with the ABA model, it was expected to find significant **inter-individual** differences (environmental effects and gene effects; e.g. susceptibility to ABA) and **intra-individual differences** (major component: disease progress during conditioning period), which could confirm the need for **individualised monitoring approaches**.

1. ABSTRACT

When a rat is on a limited fixed-time food schedule with full access to a running wheel (activity-based anorexia model, ABA), its activity level will increase hours prior to the feeding period. This activity, called food-anticipatory activity (FAA), is a hypothesized parallel to the hyperactivity symptom in human anorexia nervosa. To investigate in depth the characteristics of FAA, we retrospectively analysed the level of FAA and activities during other periods in ABA rats. To our surprise, rats with the most body weight loss have the lowest level of FAA, which contradicts the previously established link between FAA and the severity of ABA symptoms. On the contrary, our study shows that postprandial activities are more directly related to weight loss. We conclude that FAA alone may not be sufficient to reflect model severity, and activities during other periods may be of potential value in studies using ABA model.

2. INTRODUCTION

Routtenberg and Kuznesof first described the relationship between an increase in running activity and a decrease in food intake in rats in 1967. They discovered that when rats were on a restricted feeding schedule (1 hour per day in their experiment) and had free access to a running wheel, their food intake was significantly lower than in control rats, which were on the same feeding schedule but without access to a running wheel. This discrepancy between increased running activity and decreased food intake caused substantial body weight loss, and if rats were not removed from the experimental setup timely, they would eventually die of starvation. This model, later named the activity-based anorexia (ABA) model, is one of the most widely used animal models for the study of anorexia nervosa (AN)(Gutierrez, 2013).

AN is a serious psychiatric disorder most prevalent in adolescent and young females (Bulik et al., 2006). It is multifactorial, the etiology behind is complicated to say the least, and it includes various clinical symptoms, but two of the most noticeable physiological manifestations are self-induced pathological body weight loss and

excessive exercising, and the ABA model exhibits both of these features (Epling et al. 1983; Gutierrez, 2013). Unlike other psychiatric disorders in which specific psychiatric evaluations are the main measures of disease progress (e.g. the Yale–Brown Obsessive Compulsive Scale for obsessive-compulsive disorder), the Body Mass Index (body mass (kg) divided by the square of height (m)) is viewed as the main clinical indicator of disease progress and treatment efficacy (Epling et al., 1983; Gutierrez, 2013). Correspondingly, the rat's body weight is the key measure in the ABA model, but besides body weight, the running wheel activity (RWA, or hyperactivity, quantified in number of wheel rotations) is another important measure to assess in this animal model of AN.

The excessive running activity causes calorie depletion in rats, and the logical idea behind treating rats in the ABA model is: if one could reduce running activity, rats could conserve energy better, which may lead to body weight increase and higher survival rate. Moreover, animal and clinical studies have indicated that the hyper-activity in anorectic patients is more than a method to lose weight; it may be a core element and a psychological drive involved in the evolution of the disease (Gutierrez, 2013). The hyperactivity in the ABA model peaks 2–3 hours before the scheduled feeding (Mistlberger, 1994). This specific peak in running activity prior to the scheduled feeding, called food-anticipatory activity (FAA), is an important feature of the ABA model. The FAA peak increases over time as rats are re-exposed to scheduled feeding, and it is generally argued that it is an indicator of disease progress and treatment effect besides body weight and survival rate: a decrease in FAA is often interpreted as a sign related to an improvement of the anorectic state, though not always correlated with body weight increase and higher survival rate (Lambert & Porter, 1992; Hillebrand et al., 2005; Atchley & Eckel, 2006; Verhagen et al., 2009; Klenotich et al;, 2012).

After a decade of experience with the ABA model, we have observed considerable inter-subject variability. Using the exact same ABA protocol, different rats exhibit different levels of susceptibility to the model. In other words, after 10 consecutive days of whole-day access to a running wheel and scheduled food restriction, the

weight loss varies in a relatively wide range. Given this variability and the variability in FAA - a complex circadian behaviour - we speculated that characteristics of FAA (e.g. level and pattern) may be correlated with the extent of body weight loss.

Based on a general consensus in previous studies (decrease in FAA indicates positive effect of treatment)(Lambert & Porter, 1992; Hillebrand et al., 2005; Atchley & Eckel, 2006; Verhagen et al., 2009; Klenotich et al;, 2012), our main hypothesis is as follows: the higher the amount of FAA a rat demonstrates, the more likely it will lose substantial body weight in the ABA model. We further hypothesize that certain characteristics of FAA could be used as a prognostic indicator, which could predict the percentage of body weight loss in the ABA model. In this study, we investigated the characteristics of FAA and activities during other periods, and their correlations with body weight in 56 ABA rats.

3. MATERIALS AND METHODS

56 female Wistar rats were included in our study. The body weight of each rat upon arrival was 200–250 g. All rats were housed individually on a 12:12 hour light:dark cycle (light onset=07:00) and ambient temperature was maintained at +/-20 degrees Celsius. Rats were given one week of acclimatization (food and water ad libitum) in a standard home cage, prior to the start of the ABA procedure. The research projects were approved by the university ethics committee for laboratory experimentation (project numbers: 045/2006 and 046/2007), and were in accordance with the Belgian and European laws, guidelines and policies for animal experimentation, housing and care (Belgian Royal Decree of 29 May 2013 and European Directive 2010/63/EU on the protection of animals used for scientific purposes of 20 October 2010).

Starting on Day 0, each rat was introduced in/moved to an individual ABA cage (36 x 36 cm; custom-made) with a running wheel (35 cm in diameter, one rotation corresponds to a distance of approximately 110 cm; Campden Instruments, Loughborough, UK) at 11AM after baseline body weight was measured. Water was

available ad libitum in the cage, but each rat was under food restriction: 50 g of food was introduced at 9:30AM and the remainders removed at 11AM, starting from Day 1 for a period of 10 consecutive days (1.5 hours of food access per day). Food intake and body weight of each rat were measured daily at 11AM after the feeding period ended. If body weight dropped below 70% of baseline, the rat would be removed from the model for ethics reasons and experiments ended prematurely in these rats. Running wheel activity (RWA) was monitored in LabView 7.0 (National Instruments, Austin, TX, USA) via position registration of an electro-magnetic rotary encoder (TWK- Elektronik GmbH, Dusseldorf, Germany) attached to the running wheel. After 10 consecutive days, all rats were removed from the ABA model.

The daily RWA was divided into 4 periods: FAA (2.5 hours, from 7:00AM to 9:30AM), feeding activity (FA, 1.5 hours, from 9:30AM to 11AM), postprandial activity (PPA, 8 hours, from 11AM to 7PM), and nocturnal activity (NA, 12 hours, from 7PM to 7AM next day).

Based on the percentage of baseline body weight at the end of the experiment, rats were categorized into three different groups: highly susceptible to ABA (HS, body weight reached below 70% of baseline within 10 days), moderately susceptible to ABA (MS, body weight between 70% and 85% of baseline after 10 days), and not susceptible to ABA (NS, body weight above 85% of baseline after 10 days) (85% and 70% of baseline body weight were predefined values based on previous studies) (Pierce & Epling, 1994; Hebebrand et al., 2000; Luyten et al., 2009).

An independent Mann-Whitney U Test (U test) or one-way analysis of variance (ANOVA) and post-hoc Tukey-Kramer test was performed to investigate the difference between groups. To explore the relationships between body weight loss and hyperactivity, Pearson correlation coefficients (total percentage body weight loss and average daily RWA) were calculated. To test how well RWA during different periods could distinguish between two diagnostic groups (non-responders (NS group) and responders (MS and HS groups)), the area under the receiver operating characteristic curve (ROC AUC) was calculated and compared. All statistical analyses were performed using Statistica (StatSoft, Oklahoma, U.S.A.), significance level $p < 0.05$.

4. RESULTS

Based upon their final percentage body weight (last day of ABA procedure), rats were categorized into 3 groups: NS: 88.80 +/-0.75% (mean +/- standard error of the mean), n=13; MS: 81.07 +/-0.55%, n= 26; HS: 66.91 +/- 0.87%, n=17.

The evolution of daily RWA is plotted in figure I.1A. Rats suffering from the highest percentage weight loss (HS group) manifested the highest level of RWA, which resonates the hypothesis that hyperactivity is playing a major role in pathological weight loss in this model. There was a decrease in daily RWA after day 8 in the HS group, probably related to the increasing weakness of rats nearing the 70% criterion and early dropouts of the more hyperactive rats. On average, the RWA increased by four-fold after 10 days in the ABA model (from 1025 on day 1 (n= 56) to 4221 on day 10 (n=45), U test, $p<0.01$). Figure I.1B shows the change in RWA during different periods. Despite food restriction, there was a clear trend of increase in FAA, PPA, and NA over time (day 1 compared to day 10, U test, $p<0.01$ for all parameters), in alignment with previous findings. Figure I.1C indicates the change in food intake over time. The average daily food intake in the HS group (8.06 +/- 0.27 g) was significantly lower than in the MS (9.94 +/- 0.23 g) and NS groups (12.16 +/- 0.32 g) (ANOVA, $p < 0.01$, post-hoc: HS:MS, $p< 0.01$, HS:NS, $p <0.01$, MS:NS, $p <0.01$).

Figure I.2 shows the average 10-day RWA evolution of NS, MS, and HS groups. FAA peaks (red arrows) formed distinctively in all three groups of rats at similar levels. Secondary peaks (orange arrows) were present between FAA, spanning from PPA to NA, but they were the lowest and the narrowest in the NS group by visual inspection, becoming higher and wider in the MS group, and reached maximal height and width in the HS group (peak surpassing level of FAA starting on day 5 in the HS group).

Comparison of RWA of different groups during different periods is made in figure I.3. FAA, PPA and NA in all three groups were increasing consistently during the first 8 days. FAA in the HS group was not significantly different from FAA in the MS and the NS group (ANOVA). However, PPA was significantly higher in the HS group on

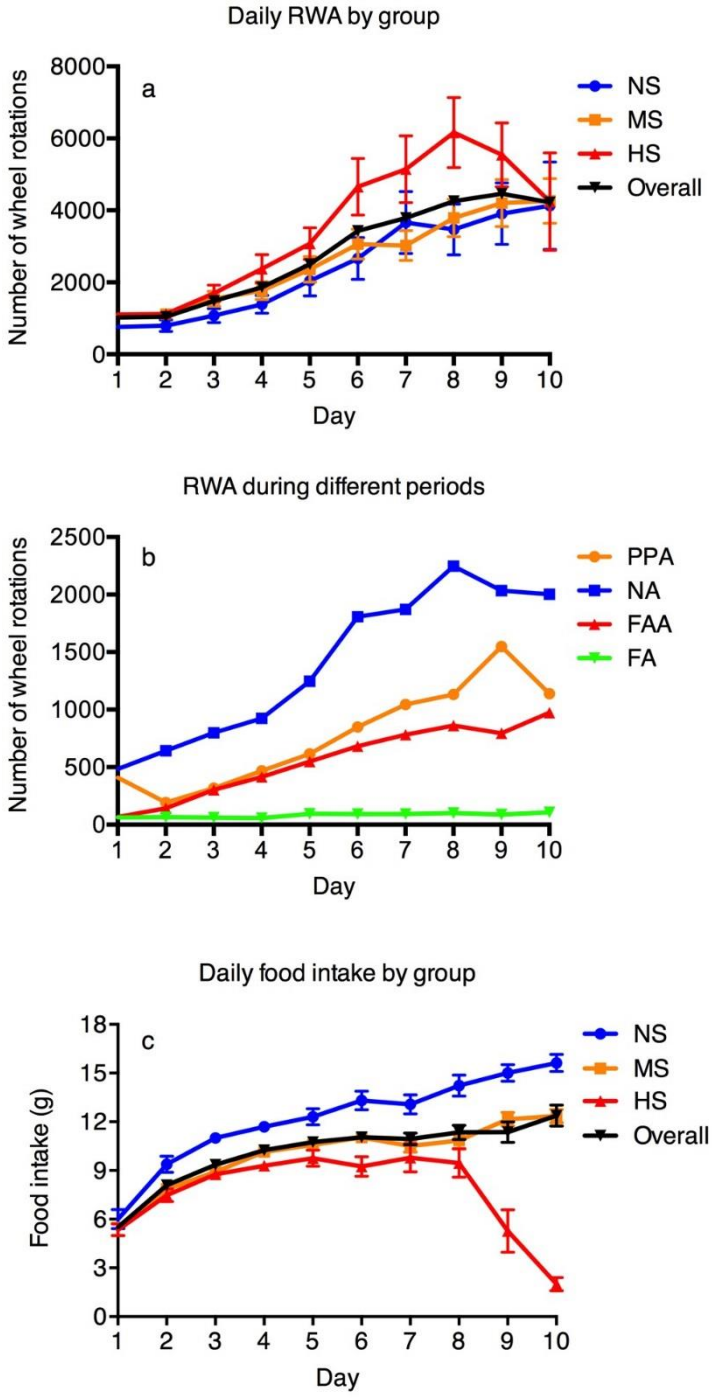

Figure I.1. Evolution of RWA of different groups (1a) and during different periods of time (1b), and evolution of food intake (1c). (1a): Increases in daily RWA were observed in all three groups of rats (most noticeable in the HS group). Daily RWA started to decline in the HS group after day 8, probably related to the increasing weakness of rats nearing the 70% criterion, and early dropouts of the more hyperactive rats. (1b): RWA of all rats during different periods of time, showing a trend of increase in FAA, PPA and NA over time. (1c): Daily food intake was highest in the NS group and lowest in the HS group in general, which confirmed insufficient food intake as a factor of body weight loss in this model. The average daily food intake in HS group (8.06 6 0.27 g) was significantly lower than in the MS (9.94 6 0.23 g) and NS groups (12.16 6 0.32 g). RWA: running wheel activity, NS: non-susceptible group, MS: moderately-susceptible group, HS: highly-susceptible group, PPA: postprandial activity, NA: nocturnal activity, FAA: food anticipatory activity, FA: feeding activity.

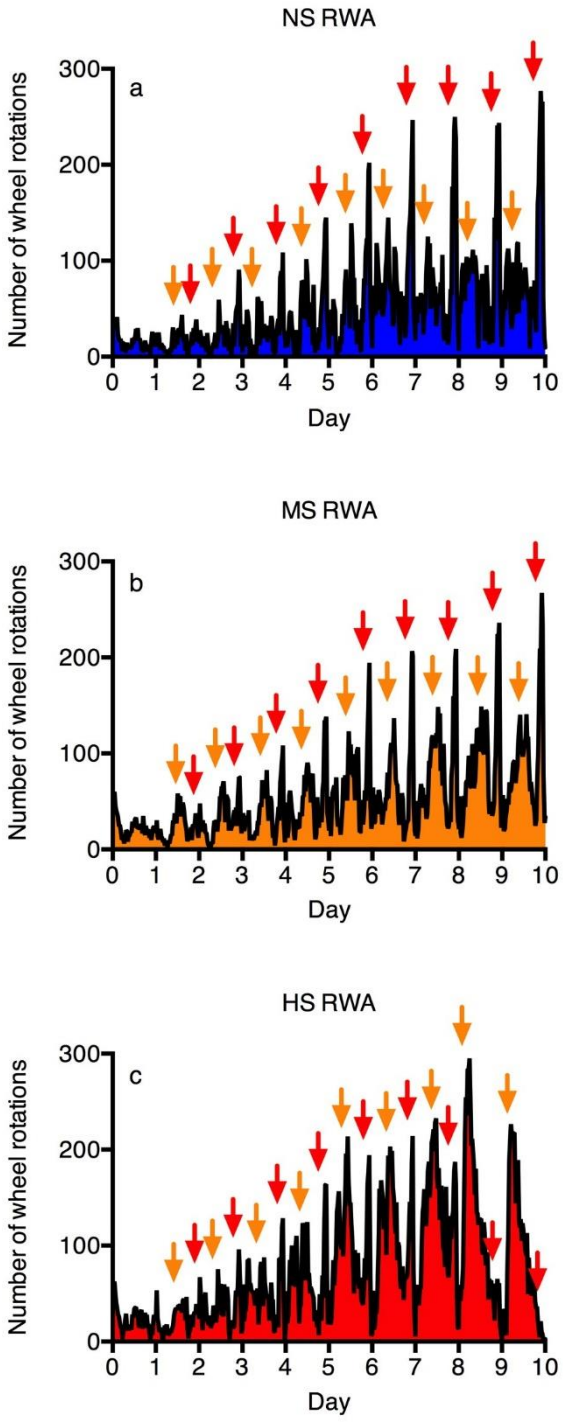

Figure I.2. Evolution of number of wheel rotations over time in the NS (a), MS (b), and HS (c) groups indicates peaks in RWA, which correspond to FAA; indicates peaks in RWA, which span from PPA and NA. The level of PPA-NA peaks was the lowest in the NS group (a), becoming more distinct in the MS group (b), and reached its maximum height and width in the HS group, surpassing the FAA peaks starting on day 5 (c). RWA: running wheel activity, NS: non-susceptible group, MS: moderately-susceptible group, HS: highly-susceptible group, PPA: postprandial activity, NA: nocturnal activity, FAA: food anticipatory activity.

day 3, 4, 5, 6, 8 and 9 compared to the two other groups (ANOVA: day 3, 5, 6, 9: $p < 0.01$, post-hoc, HS:MS and HS:NS, $p<0.01$; day 4: $p<0.01$, post-hoc, HS:MS, $p<0.01$, HS:NS, $p<0.05$; day 8: $p<0.05$; post-hoc, HS:MS, $p<0.01$). NA was also significantly higher in the HS group on day 7 and 8 (ANOVA: day 7, $p<0.01$; post-hoc, HS:NS, $p<0.05$, HS:MS, $p<0.01$, day 8, $p<0.01$; post-hoc, HS:NS, $p<0.01$, HS:MS, $p=0.01$). FA

was significantly lower in the HS group on day 9 and 10 (ANOVA, day 9, $p<0.05$, post-hoc, HS:MS, $p<0.01$; day 10, $p<0.05$, post-hoc, HS: MS and HS:NS, $p<0.01$). Individual RWA of each rat from each group was plotted to illustrate the distribution of raw data, and despite deviations, its general impression further confirms our results based on group averages.

The daily averages of running wheel activity during different periods in relation to total percentage body weight loss were plotted in figure I.4. Pearson correlation of FAA, PPA, NA, and FA were -0.27 ($p<0.05$), 0.49 ($p<0.001$), 0.35 ($p<0.01$), and -0.07 ($p>0.1$), respectively.

The changes in ROC AUC values of PPA and FAA are shown in figure I.5. ROC AUC of PPA was significantly higher ($p<0.01$) than that of FAA on day 5, indicating better predicting value in the PPA in terms of distinguishing the responders (MS and HS) from the non- responders (NS) group. ROC AUC of FA and NA were not significantly higher than that of FAA, and were not shown in this figure.

Since early dropouts may induce bias in the HS group, we made a direct between-group comparison of FAA, PPA, NA and FA based on the rats data on the first day, the second last day, and the last day of the ABA procedure (for instance, if a rat was dropped out on day 8, day 8 would be the last day, and day 7 would be the second last day for this rat) (figure I.6). The results were similar to the findings in figure I.3. The mean FAA values were the lowest in the HS group compared to NS and MS, on the second last day (not significant, ANOVA, $p>0.1$) and the last day in the ABA cage (ANOVA, $p<0.01$, post-hoc: HS lower than both MS and NS ($p<0.01$)) (figure I.6A). On the contrary, the mean PPA values in the HS group were the highest among all three groups (ANOVA: second last day, $p<0.05$, post-hoc: HS significantly higher than MS ($p<0.05$) but not NS; last day, $p<0.01$, post-hoc: HS significantly higher than both MS and NS ($p<0.01$) (figure I.6B). NA was significantly higher in the HS group than the rest on the second last day ($p<0.01$), but not significantly different on the last day (figure I.6C); FA was significantly lower ($p<0.01$) in the HS group than the MS group on the last day on the last day of conditioning (figure I.6D).

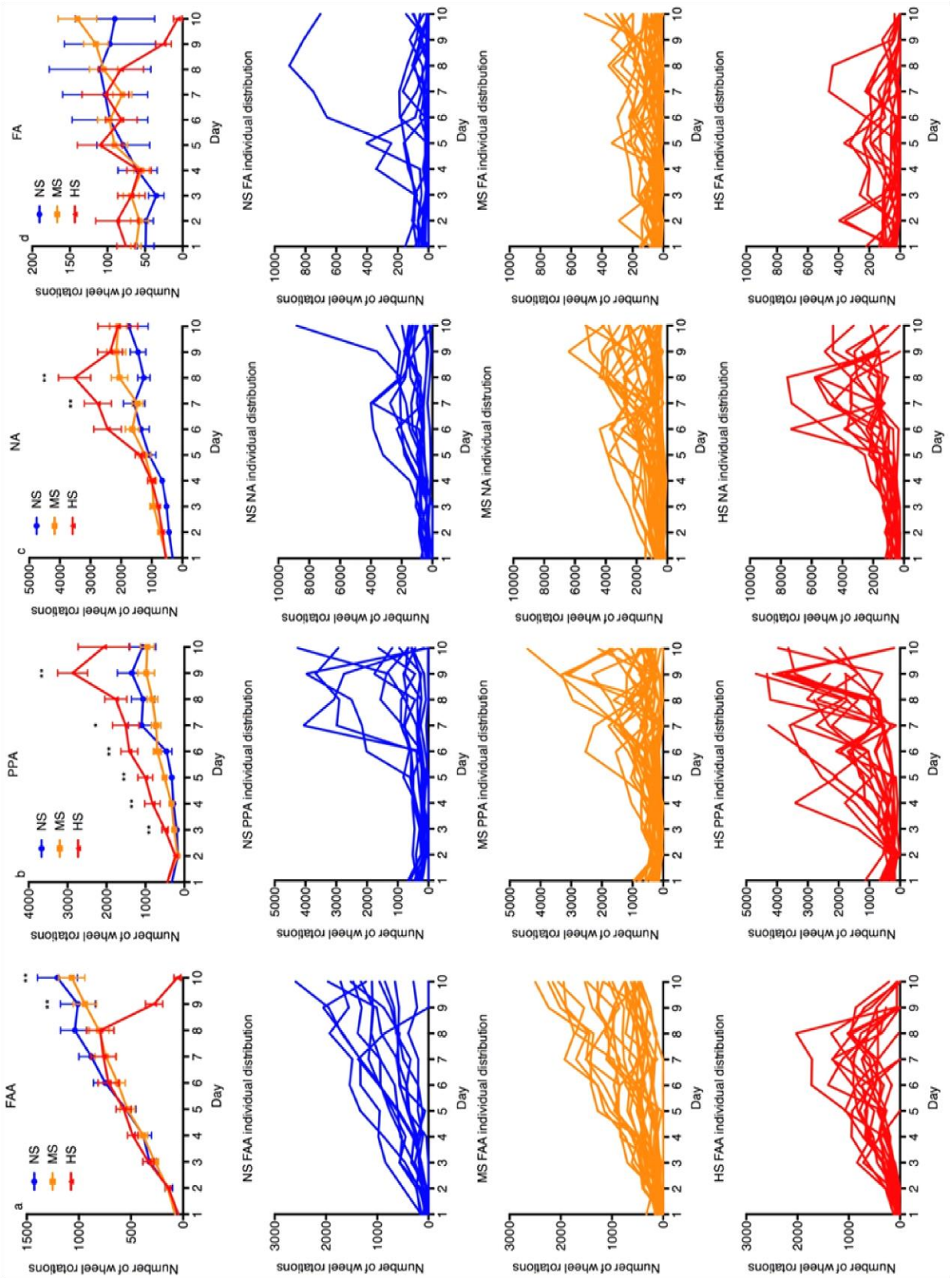
a
FAA
NS
MS
HS
Number of wheel rotations
Day
NS FAA individual distribution
MS FAA individual distribution
HS FAA individual distribution
b
PPA
NS PPA individual distribution
MS PPA individual distribution
HS PPA individual distribution
c
NA
NS NA individual distribution
MS NA individual distrution
HS NA individual distribution
d
FA
NS FA individual distribution
MS FA individual distribution
HS FA individual distribution

Figure I.3. Comparison of FAA, PPA, NA and FA between NS, MS, and HS groups (mean 6 standard error of the mean in the top graph and individual raw data of each group (spaghetti graph) in the bottom three graphs). (a): Increases in FAA were shown in all three groups in the first 8 days of the ABA procedure (difference of sample mean not significant), but FAA was significantly lower in the HS group than the rest on day 9 and 10. (b): PPA in the HS group was significantly higher than the rest on day 3, 4, 5, 6, 8 and 9. (c): NA was significantly higher in the HS group on day 7 and day 8. (d): Change of FA over time was less clear, though it was significantly lower in the HS group on day 9 (than the MS group) and day 10 (than both the MS and the HS groups.). NS: non-susceptible group, MS: moderately-susceptible group, HS: highly-susceptible group, PPA: postprandial activity, NA: nocturnal activity, FAA: food anticipatory activity; *: p , 0.05, **: p , 0.01 (analysis of variance, Tukey's post-hoc tests).

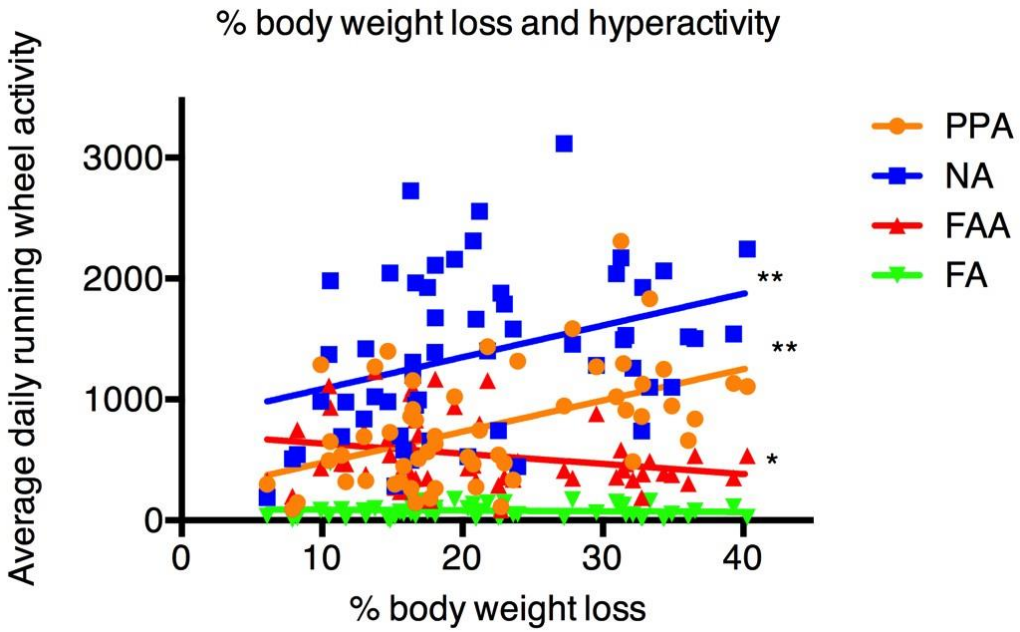

Figure I.4. Total percentage body weight loss in relation to average daily running wheel activity during different periods (individual data with linear regression line). Pearson correlation of FAA, PPA, NA, and FA were -0.27 ($p<0.05$), 0.49 ($p<0.001$), 0.35 ($p<0.01$), and -0.07 ($p<0.1$), respectively. PPA: postprandial activity, NA: nocturnal activity, FAA: food anticipatory activity, FA: feeding activity; *: $p<0.05$, **: $p<0.01$.

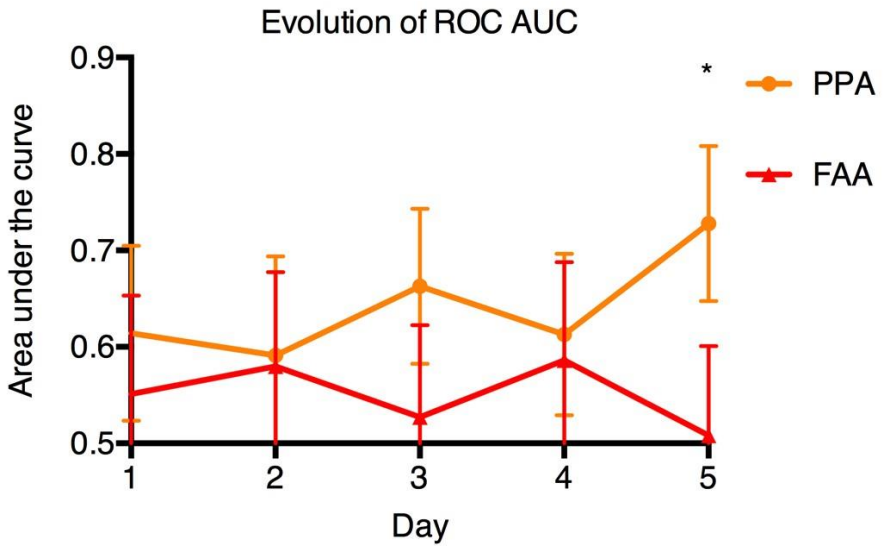

Figure I.5. Change in ROC AUC of PPA and FAA over time. The PPA ROC AUC were higher than the FAA ROC AUC in the first five days in the ABA model (significant on day 5, * 5 p , 0.01). ROC AUC: the area under the receiver operating characteristic curve, FAA: food anticipatory activity, PPA: postprandial activity.

Figure I.7 illustrates the compositions of RWA across different groups. The percentage of FAA increased and stabilized in the NS (day 1: 9%, day 5: 27%, day 10: 29%) and the MS groups (day 1: 7%, day 5: 22%, day 10: 25%), but started to decrease in the HS group after day 5 (day 1: 4%, day 5: 19%, day 10: 1%). Percentage of PPA, on the other hand, was increasing in the HS group, constituting 49% of the total daily RWA on day 10 (26% and 22% in the NS and the MS groups, respectively).

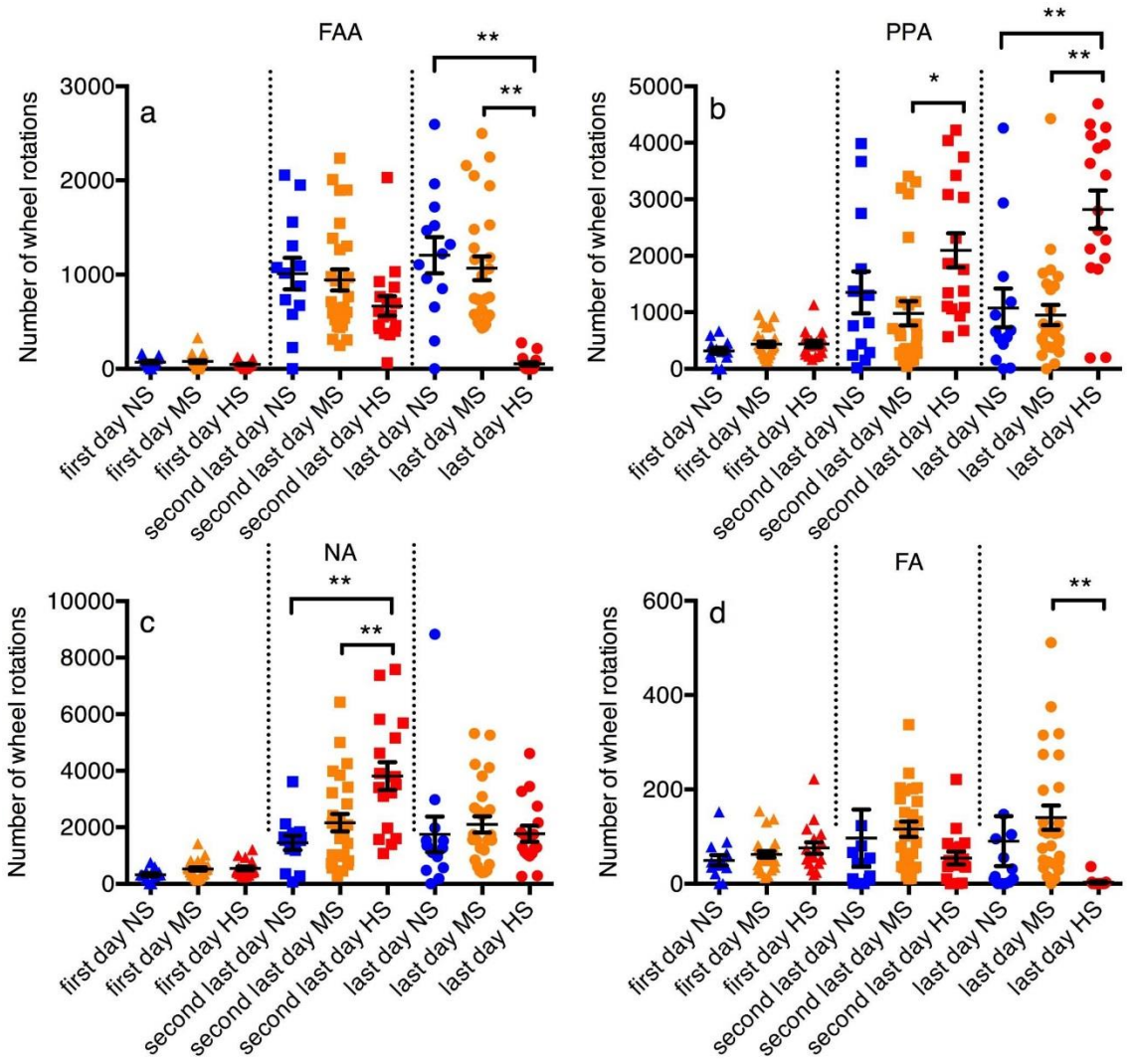

Figure I.6. Comparison of FAA, PPA, NA and FA between groups on different days (in terms of before dropout). (a): FAA was lower in the HS group than the rest on the second last and the last day in the ABA cage/model (significant on the last day ($p<0.01$)). (b): PPA was higher in the HS group than the rest on the second last and the last day in the ABA cage (second last day: HS significantly higher than MS ($p<0.05$) but not NS; last day: HS significantly higher than both MS and NS ($p<0.01$). (c): NA was higher in the HS group on the second last day than the NS group and the MS group ($p<0.01$), and was not the highest in the HS group on the last day (sample mean difference insignificant). (d): FA was the lowest in the HS group on the last day in the ABA cage (significantly lower than the MS group, $p<0.01$). For more detailed graphical representation of the overall data, two data points were not shown (but included in the statistical analysis) in figure I.5D (one in second last day of NS and one in last day of NS, valued 814 and 704, respectively). NS: non-susceptible group, MS: moderately-susceptible group, HS: highly-susceptible group, PPA: postprandial activity, NA: nocturnal activity, FAA: food anticipatory activity, FA: feeding activity; *: $p<0.05$, **: $p<0.01$ (analysis of variance, Tukey's post-hoc tests).

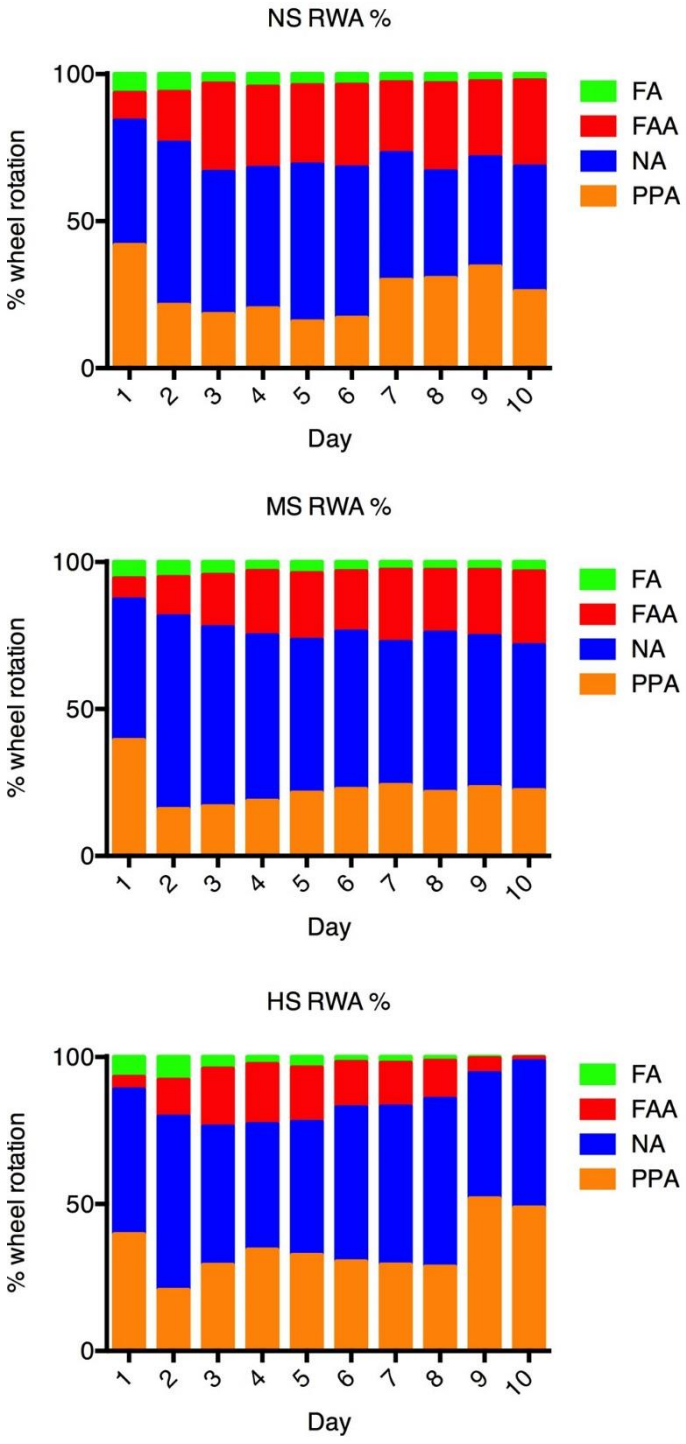

Figure I.7. Composition of daily running wheel activities of different groups of rats. The percentage of FAA increased and stabilized at approximately one quarter of daily running wheel activities in the NS and the MS groups. Despite the decreasing trend of FAA percentage in the HS group (day 5: 19%, day 10: 1%), PPA was showing a clear increase, accounting for 49% of daily running wheel activity on day 10, nearly double of the PPA percentages in the NS (26%) and the MS groups (22%) on the same day.

5. DISCUSSION

To our knowledge, this paper is the first to relate percentage body weight loss and different RWA (FAA, PPA, NA and FA) in a relatively large cohort of 56 ABA rats. The original aim was to find a predictor among RWA during different periods, which may prognosticate percentage of body weight loss in advance. Total daily RWA was higher in the HS group, supporting the previously described correlation between body weight loss and hyperactivity (Adan et al., 2011). We were expecting FAA, a behavioural phenomenon frequently used to evaluate hyperactivity in the ABA model, to be directly proportional to, and the most discriminating predictor of percentage body weight loss (Verhagen et al., 2009). However, our results did not support this.

Though rats in the HS group were manifesting the most severe and rapid degree of percentage body weight loss, FAA in the HS group was not significantly higher than FAA in the other two groups throughout the entire ABA procedure. There was even a sharp drop of FAA in the HS group on the last two days. One may argue that this was caused by emaciation, but this cannot explain why PPA remains at a relatively high level among the same group of rats on the same days (figure I.3 and I.6). Similar to FAA, PPA was increasing over time in all rats undergoing restricted feeding, but unlike FAA, PPA in the HS group was increasing at a faster speed than those in the MS and the NS group, showing significantly higher RWA during this period of time than rats with less percentage body weight loss. Pearson correlations between total percentage body weight loss and average daily RWA during different periods showed a surprisingly negative correlation (-0.27, $p < 0.05$) between percentage body weight loss and FAA (figure I.4). We believed this negative correlation was partially caused by bias (e.g. FAA decreased in rats with most body weight loss because of energy depletion, total percentage body weight loss versus average daily RWA of each individual rat was a rough estimation of the relation between weight loss and hyperactivity). Nonetheless, Pearson correlations between total percentage body weight loss and PPA and NA remained positive (0.49 and 0.35, respectively, $p < 0.01$ in both cases). ROC AUC analysis reconfirmed its superior predicting capacity

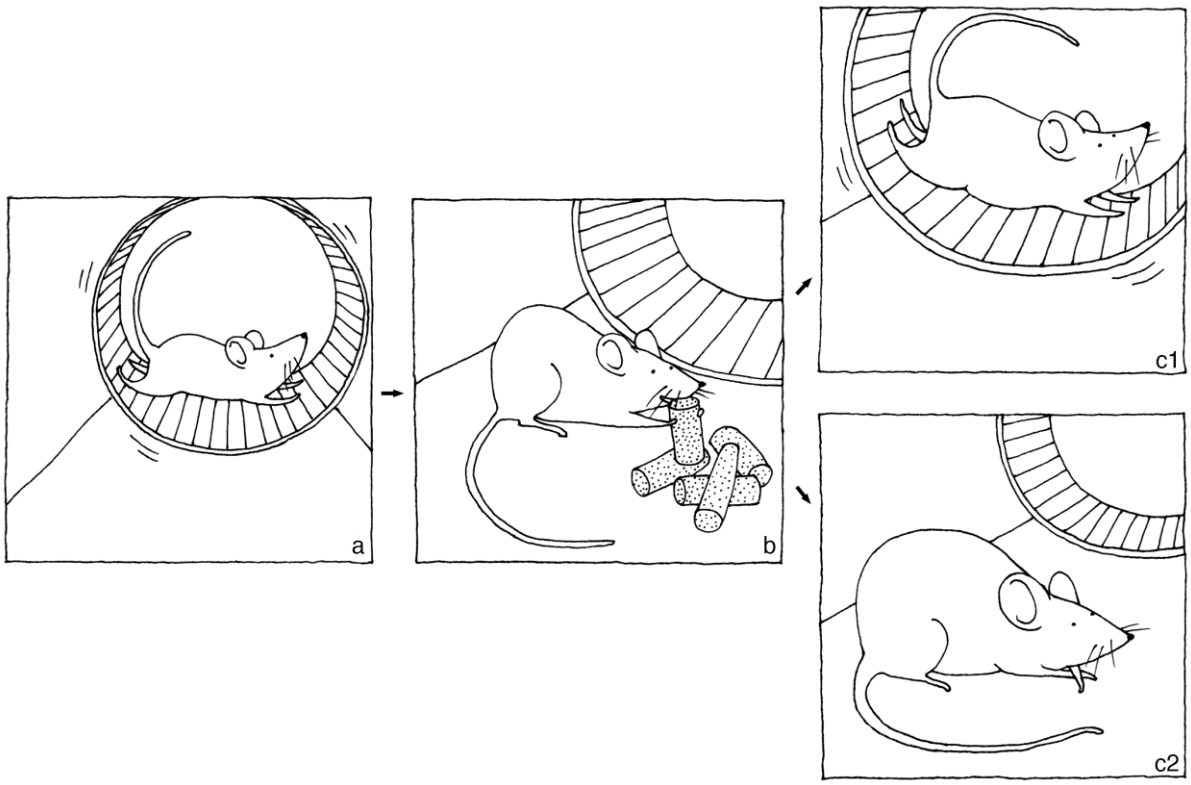

Figure I.8. Change in body weight in relation to individual pre- and postprandial hyperactivity in rats in the activity-based anorexia (ABA) model. (a): Rats in the ABA model (scheduled feeding and access to running wheel) manifest hyperactivity 2–3 hours prior to feeding (food anticipatory activity). This is a general phenomenon. (b): Scheduled feeding. (c1): Rats with a tendency to run more after the feeding period (higher postprandial activity) are subjected to severe weight loss in the ABA model. (c2): Rats running less after the feeding period (lower postprandial activity) are less likely to lose a substantial amount of body weight. Drawing by Stephany Peiyen Hsiao.

on body weight loss over FAA. A drop in daily RWA occurred on day 9 in the HS group, and while FAA, NA, and FA were all decreasing, PPA was the only RWA component that was still elevated (figure I.2 and I.3). Figure I.6 further refutes the possibility that this result was due to distortion of raw data during dropouts: PPA on the last day in the ABA cage (the day before dropout) in the HS group remained significantly higher than the other groups, but FAA was significantly lower in the HS group than the rest. These results challenge the present theory that decreased FAA implied symptom improvement in the rat ABA model.

We concluded the following based on our experimental results: 1) rats in the NS group (refractory, or able to maintain above 85% body weight, after 10 days in the ABA model) did not run significantly less than rats in the HS group (rats suffering from the most severe level of body weight loss) 2.5 hours before feeding (FAA); 2) rats in the HS group ran more than rats in the NS group during the 8-hour period after feeding (PPA); 3) body weight loss in rats in the ABA model was more directly proportional to raises in PPA, or failure to ''rest'' after scheduled feeding. If excessive RWA was related to body weight loss, we discovered that it was not FAA but PPA (or NA) that was playing a vital role in the weight loss in the ABA model; FAA was a more ''common'' behavioural phenomenon, exhibited by most rats under scheduled feeding, whereas PPA was a more ''distinctive'' feature, causing higher percentage weight loss if postprandial hyperactivity was manifested. Figure I.8 summarizes our conclusions.

Numerous studies have been conducted to unravel the underlying mechanisms of FAA (Adan et al., 2011). Leptin and ghrelin, for example, are hormones believed to have certain influences on FAA. While manipulations of these hormones in animal models proved their effects on FAA and RWA in general, PPA was excluded from assessment. Moreover, psychopharmacological studies aiming at relieving hyper-activity in the ABA model rarely take PPA into account.

Both insufficient food intake and increase in RWA contribute to drastic weight loss in the ABA model. Our observation that PPA, not FAA, is the key RWA reflecting body weight loss, contradicts previous theories. FAA increased in virtually all rats undergoing food restriction, and it remains a main feature of hyperactivity in this rodent model of anorexia nervosa. But whether it is the key factor leading to individual differences in terms of body weight loss, and whether decreased FAA indicates symptom alleviation in this animal model of anorexia nervosa, seems debatable at this moment. Our analysis on RWA data suggests PPA to be more positively correlated to percentage body weight loss than FAA. It may be worthwhile in future studies with the ABA model to include PPA and RWA during other periods in addition to FAA as a behavioural measure, during investigation of underlying mechanism and/or treatment of hyperactivity.

6. REFERENCES

1. Adan, R. A. et al. Neurobiology driving hyperactivity in activity-based anorexia. Curr Top Behav Neurosci 6, 229–50 (2011).

2. Atchley, D. P. & Eckel, L. A. Treatment with 8-OH-DPAT attenuates the weight loss associated with activity-based anorexia in female rats. Pharmacol Biochem Behav 83, 547–53 (2006).

3. Bulik, C. M. et al. Prevalence, heritability, and prospective risk factors for anorexia nervosa. Arch Gen Psychiatry 63, 305–12 (2006).

4. Bulik, C. M., Berkman, N. D., Brownley, K. A., Sedway, J. A. & Lohr, K. N. Anorexia nervosa treatment: a systematic review of randomized controlled trials. Int J Eat Disord 40, 310–20 (2007).

5. Epling, W. F., Pierce, W. D. & Stefan, L. A Theory of Activity-Based Anorexia. International Journal of Eating Disorders 3, 27–46 (1983).

6. Gutierrez, E. A rat in the labyrinth of anorexia nervosa: Contributions of the activity-based anorexia rodent model to the understanding of anorexia nervosa. Int J Eat Disord 46, 289–301 (2013).

7. Hebebrand, J., Wehmeier, P. M. & Remschmidt, H. Weight criteria for diagnosis of anorexia nervosa. Am J Psychiatry 157, 1024 (2000).

8. Hillebrand, J. J., van Elburg, A. A., Kas, M. J., van Engeland, H. & Adan, R. A. Olanzapine reduces physical activity in rats exposed to activity-based anorexia: possible implications for treatment of anorexia nervosa? Biol Psychiatry 58, 651–7 (2005).

9. Klenotich, S. J. et al. Olanzapine, but not fluoxetine, treatment increases survival in activity-based anorexia in mice. Neuropsychopharmacology 37, 1620–31 (2012).

10. Lambert, K. G. & Porter, J. H. Pimozide mitigates excessive running in the activity- stress paradigm. Physiol Behav 52, 299–304 (1992).

11. Luyten, L. et al. The effects of electrical stimulation or an electrolytic lesion in the mediodorsal thalamus of the rat on survival, body weight, food intake and running activity in the activity-based anorexia model. Brain Res Bull 79, 116–22 (2009).

12. Mistlberger, R. E. Circadian Food-Anticipatory Activity - Formal Models and Physiological-Mechanisms. Neuroscience and Biobehavioral Reviews 18, 171–195 (1994).

13. Pierce, W. D. & Epling, W. F. Activity Anorexia - an Interplay between Basic And Applied Behavior Analysis. Behavior Analyst 17, 7–23 (1994).

14. Strober, M., Freeman, R. & Morrell, W. The long-term course of severe anorexia nervosa in adolescents: survival analysis of recovery, relapse, and outcome predictors over 10–15 years in a prospective study. Int J Eat Disord 22, 339–60 (1997).

15. Routtenberg, A. & Kuznesof, A. W. Self-starvation of rats living in activity wheels on a restricted feeding schedule. J Comp Physiol Psychol 64, 414–21 (1967).

16. Verhagen, L. A., Luijendijk, M. C., Hillebrand, J. J. & Adan, R. A. Dopamine antagonism inhibits anorectic behavior in an animal model for anorexia nervosa. Eur Neuropsychopharmacol 19, 153–60 (2009).

GENERAL CONCLUSIONS

Individual biological process:

This chapter interpreted the **individual biological process** itself, mainly referring to the first hypothesis of this PhD dissertation. Starting from **available biological knowledge** (selection of measurable variables, spatial and temporal aspects, …; see Hypothesis 1 in part I), we could define the experimental setup and hypotheses specific for this case study. The study showed the added value of using complete **time series**, which enable the researcher to obtain more individual information per animal and to differentiate between different time periods relative to the scheduled moments of feeding. The study indicated that activities during periods other than FAA may be of potential value in studies using ABA model.

Interpreting this case study from a **control engineering perspective**, we can consider anorexia nervosa is a dysfunction of the control system for energy homeostasis in the body. Hereby, food intake could be defined as **actuator variable** and body weight as **homeostatic variable**.

Individualised change detection:

Considerable **inter-individual differences** were shown in the raw data plots (figure I.3). Since also **intra-individual differences** were expected due to the disease progress, **dynamic ROC curves** were used to calculate thresholds values for distinguishing between responders and non-responders (rats not susceptible to ABA) and AUC values for each day of the ABA conditioning period. By specifying the AUC for different days of the conditioning period, the discriminatory power could be improved (figure I.5).

To conclude, by monitoring measurable variables related to the ABA model, we could determine a significant amount of individual variation. These findings suggest the need for **individualised monitoring** approaches and also raises the question: how could we obtain such individualised approach?

CHAPTER II

Interleukin-6 dynamics as a basis for an early-warning monitor for sepsis and inflammation in individual pigs

Adapted from: Tambuyzer, T., De Waele, T., Chiers, K., Berckmans, D., Goddeeris, B. M., & Aerts, J. M. (2014). Interleukin-6 dynamics as a basis for an early-warning monitor for sepsis and inflammation in individual pigs. *Research in veterinary science*, *96*(3), 460-463.

BROADER PERSPECTIVE

Whereas the previous chapter focused mainly on the **individual bio-process**, this chapter presents a first approach for individualised monitoring including the three other blocks of the general scheme: **process model, feature extraction and individualised change detection.** Based on blood cytokine measurements of pigs, we aimed to quantify the cytokine response dynamics and reveal critical information to monitor the infection status of individual pigs.

In this study, the **temporal scale** of the blood sampling (time series, sampling interval, experiment duration, dynamics) was based on practical feasibility of the experiments and major requirements for the dynamic analysis to minimize information loss in the measured cytokine responses. Again the whole animal (i.e. immune system) is considered as **spatial level of interest**, since we focus on the infection state of the pigs.

Based on the previous chapter but also other studies (e.g. Introduction), it was hypothesised that an **individualised monitoring** approach would improve the classification results (infection vs no infection) compared with a population-based approach. However, the main question is still: How can we obtain an individualised approach (link to Hypothesis 4 in Part 1)? Ideally, we could calculate **individual indicators of change** representing the quantification of cytokine time series that could be used as **early warning signs** for critical changes in the individual infection status.

1. ABSTRACT

Static interleukin-6 (IL-6) levels of pigs contain considerable individual differences, which obstruct the practical use of IL-6 for disease monitoring purposes. It was hypothesised that interleukin-6 (IL-6) dynamics could be used to quantify these individual differences and carries critical information of the individual pig infection status. Time series of IL-6 responses in 25 pigs were analysed before and after infection by *Actinobacillus pleuropneumoniae*. The results indicated that amplitude increases of IL-6 fluctuations of individual pigs rather than static IL-6 values should be used as indicator of the infection state. This study shows the added value for IL-6 time series analyses of individual pigs. These results are a first step towards the development of objective individualised methods for monitoring and early detection of sepsis and inflammation processes in pigs by integrating animal response dynamics.

2. INTRODUCTION

IL-6 is often suggested as a key player in the immune response to infection (Borghetti et al., 2009; Kopf et al., 1994). It is well established that the expressions of IL-6 are up-regulated in inflammatory responses to microbial infections. However, previous studies show considerable individual variations in static blood concentrations of IL-6 (Hulten et al., 2003) and other acute phase proteins (Heegaard et al., 2011) in response to infection, which complicate the use of these biomarkers for real-time health monitoring purposes.

Many complex biological processes are involved in sepsis and inflammation (Cinel and Opal, 2009), making it a challenging task to quantify infection and inflammation processes in real-time. In a recent study (Scheffer et al., 2009), an approach was presented to detect sudden changes in complex dynamical systems based on time series data obtained from these systems. These authors suggested the existence of generic early-warning signals in time series which may indicate approaching thresholds for critical changes in complex dynamical systems (Scheffer et al., 20 09).

More specifically, the pattern of fluctuations in detrended time series was proposed as possible indicator of sudden dynamical transitions. Therefore, we hypothesised that changes of IL-6 fluctuation patterns contain critical information related with the infection state of individual pigs. Accordingly, we aimed at applying data-based modelling methods to quantify the dynamic properties (slow trends and fast fluctuations) of interleukin-6 time series in individual pigs before and after infection by Actinobacillus pleuropneumoniae as a first step in developing an early warning monitor for sepsis and inflammation processes. Based on earlier work, it might be expected that the dynamics of biomarkers are related with disease outcome and well-being (e.g. Jansen et al., 2009; Van Loon et al., 2010).

3. MATERIALS AND METHODS

Experiments were approved by the ethical commission of Ghent University (EC2009/029–30/03/2009). Thirty early-weaned outbred pigs were obtained from Rattlerow Seghers Holding N.V. (Lokeren, Belgium). The pigs were catheterised three days before infection. At challenge, 25 animals were endobronchially inoculated with 1 × 107 CFU *A. pleuropneumoniae* (biotype 1-serotype 9 strain, no. 13261; Van Overbeke et al., 2001) under anaesthesia (Table II.1, dataset 1 and 2). Five pigs received sterile medium and were used as control group (Table II.1, dataset 3). Pigs of dataset 3 received sterile medium, since, for instance, catheterisation itself can also influence the animal responses. Based on the blood sampling protocol, the 25 infected pigs were divided into two groups, whereas more samples were collected before inoculation with bacteria for the pigs of dataset 2. For the control pig group, the blood samples were collected according to the sampling protocol of dataset 1. For every blood sample the IL-6 value was measured by commercially available ELISA kits (Porcine IL-6 Duoset, R&D Systems), resulting in an IL-6 time series for every pig. In addition, all pigs were clinically score d by a veterinarian.

Table II.1. Overview of the pig experiments with corresponding blood sampling protocols.

Dataset	Number of pigs	Blood sampling before inoculation with bacteria or with sterile medium (h before inoculation)	Blood sampling starting from moment of inoculation (h after infection)	Infection
1	20	4 samples (-72, -48, -24, -2)	≥ 8 samples (0, 2, 4, …, until max. 76 hours after infection for surviving pigs)	Yes
2	5	12 samples (-32,-30, -28, -26, -24, -22, -20, -18, -8, -6, -4, -2)	≥ 8 samples (0, 2, 4, …, until max. 24 hours after infection for surviving pigs)	Yes
3	5	4 samples (-72, -48, -24, -2)	≥ 8 samples (0, 2, 4, …, until max. 76 hours)	No (sterile medium)

For each pig, changes of IL-6 time series characteristics were quantified by means of static blood IL-6 values and IL-6 fluctuation patterns. All calculations were performed in Matlab using the Statistics Toolbox for the statistical comparisons and the Captain Toolbox for the time series analysis (Taylor et al., 2007). To calculate the fluctuation patterns, the IL-6 time series were first standardised and afterwards detrended using an Integrated Random Walk Model (IRW) with Noise Variance Ratio (NVR) of 0.1 (Taylor et al., 2007). For each individual pig, the IL-6 residuals (fast IL-6 dynamics) were determined by subtracting the slow trend from each raw IL-6 time series. According to Scheffer et al. (2009), an increase in the amplitude of fluctuations in the residuals is expected in a time series containing a dynamical transition. Therefore, the obtained residuals of the IL-6 times series were standardised and the area under the cumulative sum function was quantified as measure of changes in the fast IL-6 fluctuation patterns (fast component of IL-6 dynamics; for more details on change detection with the cumulative sum function, see Basseville and Nikiforov, 1993). In a time series with increasing fluctuations, this value is expected to be lower compared to a time series with random fluctuations. Afterwards, these values were rescaled (by the factorial n!, where n is the number of samples in the analysed time window and the factorial of the positive integer n, denoted n!, is the product of all positive integers less than or equal to n) to enable correct comparisons. For dataset 1, data of a short period after inoculation with

bacteria (2 h before until 14 h after inoculation) were used for the development of the IRW-models. For dataset 2, the data generated at the day of catheterisation (14 hours) were compared with the data of the last 14 hours (dead or end experiment for surviving pigs). The area under the ROC curve (AUC) was calculated for each variable in order to determine the discriminating power for distinguishing between infected and non-infected pigs (Delong et al., 1988). When a high AUC was obtained for one of the variables, the optimal thresh- old was calculated with corresponding true positive rate (TPR) and true negative rate (TNR).

4. RESULTS

Figure II.1 (left) shows the boxplot of the static blood IL-6 values at 14 h after inoculation with bacteria for the infected pig group and the control group, which received sterile medium. Since it is expected that IL-6 levels increase in response to the infection, a one-tail two-sample t-test was used for comparison. The IL-6 concentrations of the infected pig group (dataset 1) were not significantly different from the control group (one-tail two-sample t-test: $P > 0.5$; $mean_{Inf} = 5.5$ ng/ ml; $mean_{Con} = 8.8$ ng/ml). This result suggests that it was not possible to use single IL-6 blood values for infection monitoring at pig group level, which was also confirmed by the low AUC value (AUC = 0.54, $SE_{AUC} = 0.19$). Afterwards, individual changes of IL-6 were calculated (difference between the IL-6 value at 14 h after inoculation and the value at 2 h before inoculation of the same pig). No significant difference was found between the infected group and the control group (one-tail Wilcoxon rank sum test: $P = 0.14$; Fig. II.1, right). At individual level, a small improvement of the discriminating power was found (AUC = 0.66, $SE_{AUC} = 0.17$), but both results show that IL-6 increases measured by one or two IL-6 blood values were insufficient for accurate infection monitoring. Therefore, the IL-6 responses were also dynamically analysed based on the measured time series data. For every IL-6 time series, the slow trend was removed using the IRW models (Fig. II.2, top left; Taylor et al., 2007; Scheffer et al., 2009). The obtained residuals of the infected pigs (dataset 1) and the control pigs (dataset 3) are illustrated in Fig. II.2 (top, right). For the infected pigs,

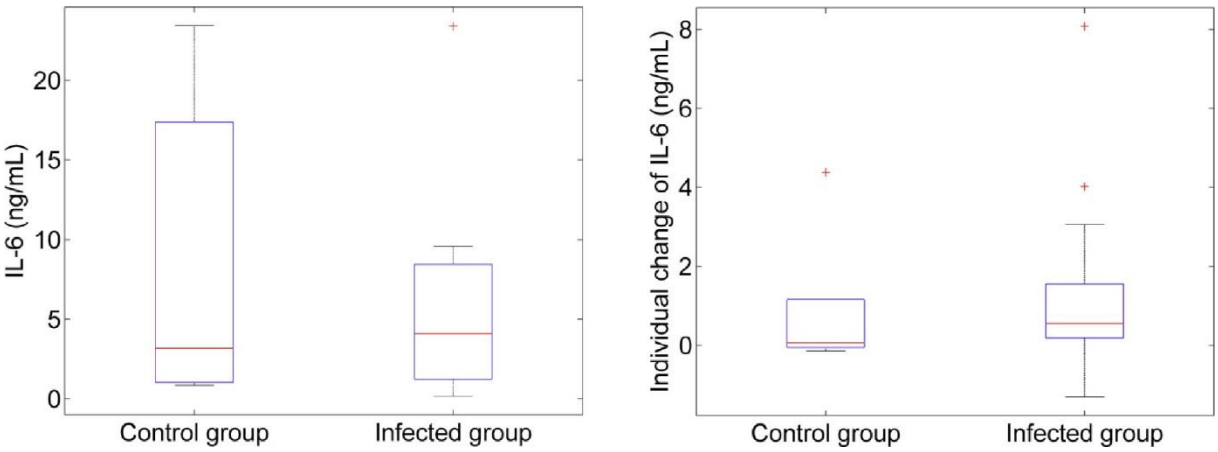

Figure II.1. Comparison of IL-6 concentrations. Boxplots of IL-6 concentrations with the median, interquartile range (box), 1.5 times the interquartile range (whiskers) and outliers (crosses). Left: comparison of infected (dataset 1, n = 20) and control (dataset 3, n = 5) pigs at the pig group level. Right: comparison of individual IL-6 changes from 2 h before to 14 h after inoculation with bacteria or with sterile medium .

the residuals increased starting from 4 to 6 h after inoculation, whereas the residuals of the control pigs behaved like random noise. These results are in line with the study of Scheffer et al. (2009), since they suggested that an increase in the amplitude of fluctuations in the residuals can be an early sign of a dynamical system undergoing a sudden transition. A significant difference was found by comparing this fast fluctuation component of both pig groups (one-tail two-sample t-test: P = 0.001; Fig. II.2, left bottom). In addition, ROC curve analysis showed a high discriminative power for this fast IL-6 component (AUC = 0.88, SE_{AUC} = 0.11). The misclassification error of the corresponding optimal threshold was 2/25 (Th_{opt} = 0.80; TPR = 95%; TNR = 80%), indicating that this variable could be a valuable candidate for infection monitoring. Based on dataset 2, the fast dynamic component could be quantified before and after infection of the same pig, since more blood samples were taken before infection for this pig group. By using the same threshold value (Th_{opt} = 0.80) as was found at the pig group level, only one pig would be misclassified before infection (TNR = 80%) and all pigs would be correctly classified after infection (TPR = 10 0%). The fast dynamic component decreased

significantly for all pigs (one-tail paired t-test: P = 0.001; Fig. II.2, right bottom). For each pig, the shift in the fast fluctuation component was different, stressing the need for individualised infection monitoring.

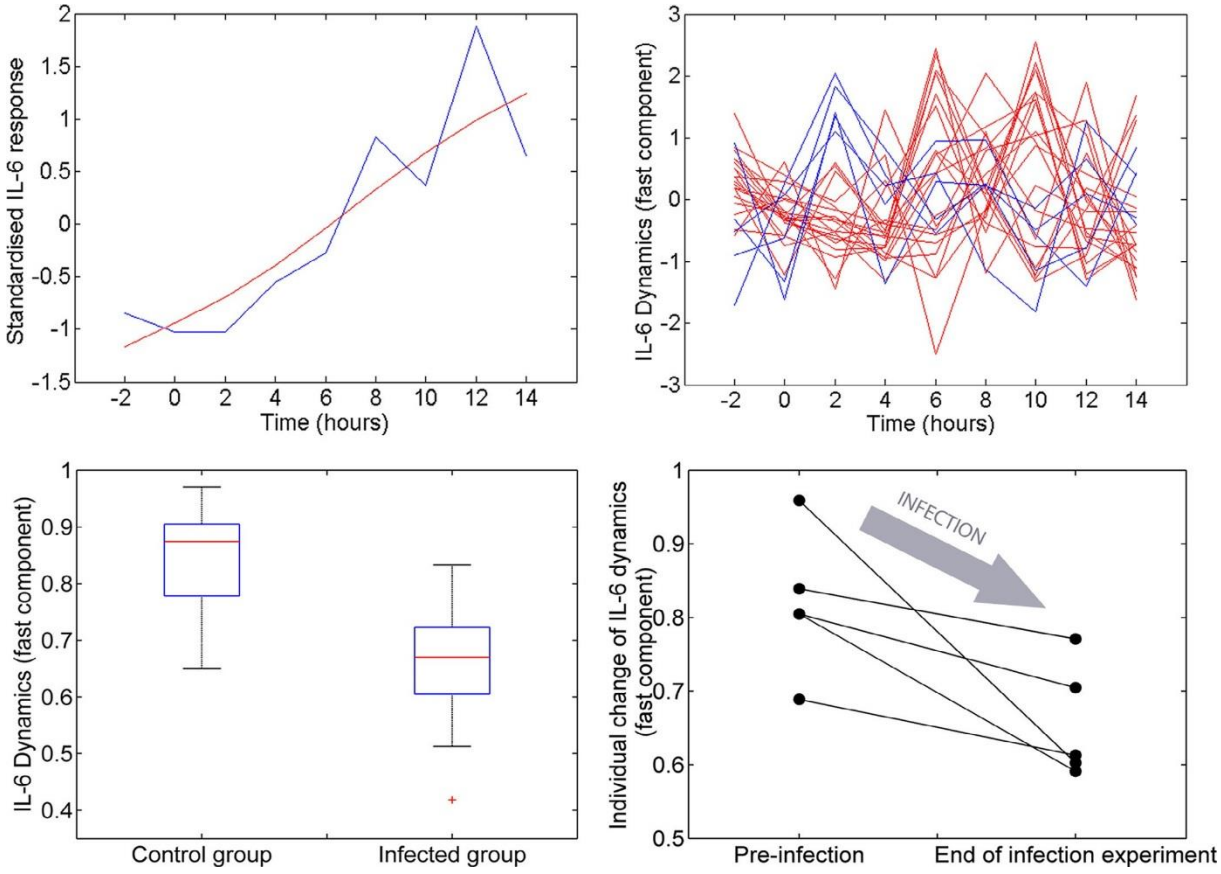

Figure II.2. IL-6 fluctuation patterns. Top left: Example of a standardised IL-6 response (blue) of an infected pig whereas 0 h corresponds to the moment of inoculation. The red curve is the IRW model, which was used to remove the slow trend. Top right: plot of the residual time series after detrending for the infected pigs (red) and the control pigs (blue). Bottom left: Boxplots (median, interquartile range, 1.5 times the interquartile range, outliers) of the quantified IL-6 dynamics (fast fluctuation component) for the control group (dataset 3) and for the infected group (dataset 1). Right: Dataset 2 (n = 5): Individual shifts in IL-6 fluctuation pattern from the pre-infection state (circles) to the state at the end of each experiment. The circle that is connected with two black lines refers to two pigs with the same initial state.

5. DISCUSSION

In outbred animals, IL-6 values of fixed time points after infection show a large individual variation (Fig. II.3; Hulten et al., 2003), as dynamic immune responses are controlled on an individual level. In this study, it was shown that individual changes of fast IL-6 fluctuation patterns reveal critical information about the infection state of the animals (Fig. II.2), whereas no significant differences were found based on the static absolute IL-6 concentrations (Figs. II.1 and II.3). The results indicate the advantages and added value for time series analyses of IL-6 responses for individualised infection monitoring. These results are supported by other studies in which shifts in dynamics are suggested as generic early-warning signals for a changing state in complex biological dynamical systems (e.g. Scheffer et al., 2009; Van Loon et al., 2010). However, as long as there exists no method to measure the IL-6 blood concentrations in a non-invasive and cost-efficient way, this time series approach is not convenient under practical conditions and should be mainly applied in scientific research models. We expect that such time series analyses could contribute to studies which try to define cut-off levels for IL-6 for detecting the infection state (e.g. Celik et al., 2010). In addition, a measure for the pig's well-being could be valuable for other research purposes such as herd health monitoring (Fossum, 1998), vaccine potency testing (Cox et al., 2011), treatment efficacy testing (Hulten et al., 2003) and measuring stress induced by road transport (Piñeiro et al., 2007).

The individual models as developed in our study are a first step towards the development of an objective individualised method for an early detection of sepsis and inflammation in scientific research models. However, in production pigs with a wide genetic variation, great respect has to be paid to the different IL6 responses of different pigs.

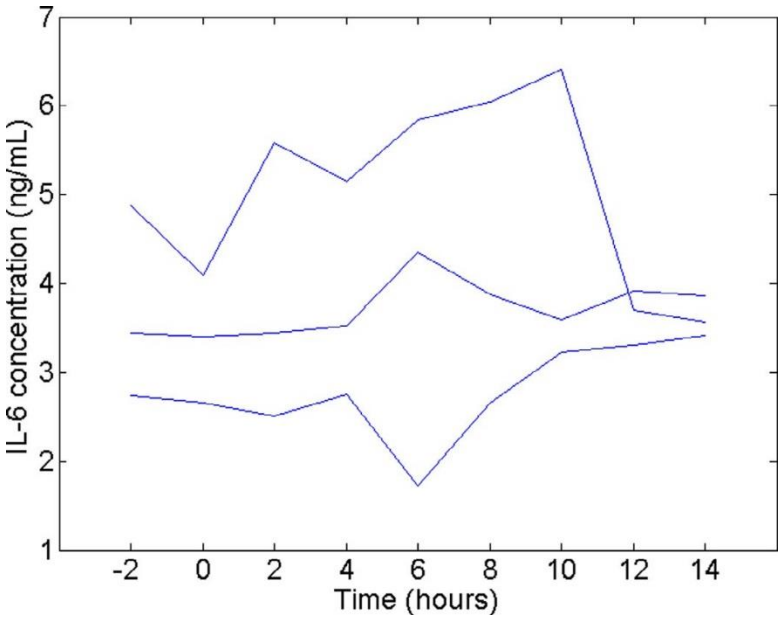

Figure II.3. Individual IL-6 responses. Examples of IL-6 time series (blue) for 3 individual pigs whereas 0 h corresponds to the moment of inoculation with bacteria. Although these 3 pigs have a similar IL-6 concentration at 14 h, the time courses of the IL-6 values are strongly diverging (e.g. each pig reaches its peak value of IL-6 at a different time point).

6. REFERENCES

1. Basseville, M.E., Nikiforov, I.V., 1993. Detection of Abrupt Changes: Theory and Application. Prentice-Hall, Englewood Cliffs, NJ 528 pp.

2. Borghetti, P., Saleri, R., Mocchegiani, E., Corradi, A., Martelli, P., 20 09. Infection, immunity and the neuroendocrine response. Veterinary Immunology and Immunopathology 130, 141–162.

3. Celik, I.H., Demirel, F.G., Uras, N., Oguz, S.S., Erdeve, O., Biyikli, Z., et al., 2010. What are the cut-off levels for IL-6 and CRP in neonatal sepsis? Journal of Clinical Laboratory Analysis 24, 407–412.

4. Cinel, I., Opal, S.M., 2009. Molecular biology of inflammation and sepsis: a primer. Critical Care Medicine 37, 291–304.

5. Cox, S.J., Gubbins, S., Barnett, P.V., 2011. IL-6 production following vaccination in pigs–an additional immune response parameter for assessing FMD vaccine efficacy? Vaccine 29, 4704–4708.

6. Delong, E.R., Delong, D.M., Clarke-Pearson, D.L., 1988. Comparing the areas under two or more correlated receiver operating characteristic curves: a nonparametric approach. Biometrics 44, 837–845.

7. Fossum, C., 1998. Cytokines as markers for infections and their effect on growth performance and well-being in the pig. Domestic Animal Endocrinology 15, 439–444.

8. Heegaard, P.M., Stockmarr, A., Piñeiro, M., Carpintero, R., Lampreave, F., Campbell, F.M., et al., 2011. Optimal combinations of acute phase proteins for detecting infectious disease in pigs. Veterinary Research 42, 50.

9. Hulten, C., Johansson, E., Fossum, C., Wallgren, P., 2003. Interleukin 6, serum amyloid A and haptoglobin as markers of treatment efficacy in pigs experimentally infected with Actinobacillus pleuropneumoniae. Veterinary Microbiology 95, 75–89.

10. Jansen, F., Van der Krogt, J., Van Loon, K., Avezzù, V., Guarino, M., Quanten, S., et al., 2009. Online detection of an emotional response of a horse during physical activity. The Veterinary Journal 181, 38–42.

11. Kopf, M., Baumann, H., Freer, G., Freudenberg, M., Lamers, M., Kishimoto, T., et al., 1994. Impaired immune and acute-phase responses in interleukin-6-deficient mice. Nature 368, 339–342.

12. Piñeiro, M., Piñeiro, C., Carpintero, R., Morales, J., Campbell, F.M., Eckersall, P.D., et al., 2007. Characterisation of the pig acute phase protein response to road transport. The Veterinary Journal 173, 669–674.

13. Scheffer, M., Bascompte, J., Brock, W.A., Brovkin, V., Carpenter, S.R., Dakos, V., et al., 2009. Early-warning signals for critical transitions. Nature 461, 53–59.

14. Taylor, C.J., Pedregal, D.J., Young, P.C., Tych, W., 20 07. Environmental time series analysis and forecasting with the CAPTAIN toolbox. Environmental Modelling & Software 22, 797–814.

15. Van Loon, K., Guiza, F., Meyfroidt, G., Aerts, J.M., Ramon, J., Blockeel, H., et al., 2010. Prediction of clinical conditions after coronary bypass surgery using dynamic data analysis. Journal of Medical Systems 34, 229–239.

16. Van Overbeke, I., Chiers, K., Ducatelle, R., Haesebrouk, F., 2001. Effect of endobronchial challenge with Actinobacillus pleuropneumoniae serotype 9 of pigs vaccinated with a vaccine containing Apx toxins and transferrin-binding proteins. Journal of Veterinary Medicine Series B-Infectious Diseases And Veterinary Public Health 48, 15–20.

GENERAL CONCLUSIONS

Individual biological process:

The **individual biological process** of this case study was part of the immune system in pigs. The measured variable was interleukin-6 which is one of the cytokines, that plays a key role in the infection response.

Concerning the optimal **sampling interval** this study was a special case. The sample frequency should be high enough to prevent information loss of the dynamics of the biomarker responses to infection. However, experiments with long duration and high sample frequency are not feasible in practice, because too much blood would be extracted from the animals possibly inducing unwanted effects on the health status of the pigs. This example confirms again that one should **start from biological insights** of the individual biological structure itself to obtain meaningful and reliable measurements (see Hypothesis 1 in Part 1).

Process model and model-based features:

By applying **model-based methods (Integrated Random Walk Models)**, we were able to quantify the **dynamic properties** of the Il-6 time series. The time series analyses showed significant added value in comparison with analyses based on static absolute Il-6 concentrations (see Hypothesis 3 in Part 1).

Individualised change detection:

The results confirmed other studies suggesting that shifts in dynamics can be considered as **generic early warning signs** for a changing state in complex biological dynamical systems.

Similarly to the previous chapter **ROC-analysis** was used to calculate specific threshold values on the population level.

This study also showed how **serial baseline measurements** of the same individual organism make it possible to detect changes at the individual level.

This study suggested three important elements for obtaining an **individualised monitoring approach** (see Hypothesis 4 in Part 1).**:**

1. Change detection based on (sub-)**population information** (e.g. thresholds from ROC curve analysis).
2. Change detection based **universal laws and insights from control engineering, complex systems science and biology** (e.g. early warning signs for critical transitions).
3. Change detection based on **individual serial baseline measurements.**

CHAPTER III

Heart rate time series characteristics for early detection of infections in critically ill patients

Adapted from: Tambuyzer, T., Guiza, F., Boonen, E., Meersseman, P., Vervenne, H., Hansen, T. K., Bjerre, M., Berckmans, D., Aerts, J.M. & Meyfroidt, G. (2017). Heart rate time series characteristics for early detection of infections in critically ill patients. *Journal of clinical monitoring and computing*, *31*(2), 407-415.

BROADER PERSPECTIVE

Whereas the previous chapter showed a first approach for individualised monitoring of biological processes, this chapter will zoom in on the two middle blocks of the general scheme: **the process model** and **feature extraction**.

Corresponding with Hypothesis 3 of Part 1, we investigate the following question: Can individual model-based features add supplementary information to monitors which would be purely based on measurable variables? More specifically, this chapter studies features derived from heart rate and cytokine time series for early detection of infection in ICU patients.

Since chapter 2 discussed the results of an animal model for infection, some of the techniques of the previous chapter can be translated towards the patient setting of this case study. Similar to the analyses applied in chapter 2, **Integrated Random Walk Models** will be used to differentiate between slow trends and fast dynamics of the bio-signals. In addition to the generic early warning signs applied in Chapter 2, a wide list of other **generic signal features** will be used here for detailed quantification of the measured bio-signals.

By implementing several methods of chapter 2, we make here the **step from animal to human health engineering**.

1. ABSTRACT

It is difficult to make a distinction between inflammation and infection. Therefore, new strategies are required to allow accurate detection of infection. Here, we hypothesize that we can distinguish infected from non-infected ICU patients based on dynamic features of serum cytokine concentrations and heart rate time series. Serum cytokine profiles and heart rate time series of 39 patients were available for this study. The serum concentration of ten cytokines were measured using blood sampled every 10 min between 21:00 and 06:00 hours. Heart rate was recorded every minute. Ten metrics were used to extract features from these time series to obtain an accurate classification of infected patients. The predictive power of the metrics derived from the heart rate time series was investigated using decision tree analysis. Finally, logistic regression methods were used to examine whether classification performance improved with inclusion of features derived from the cytokine time series. The AUC of a decision tree based on two heart rate features was 0.88. The model had good calibration with 0.09 Hosmer–Lemeshow p value. There was no significant additional value of adding static cytokine levels or cytokine time series information to the generated decision tree model. The results suggest that heart rate is a better marker for infection than information captured by cytokine time series when the exact stage of infection is not known. The predictive value of (expensive) biomarkers should always be weighed against the routinely monitored data, and such biomarkers have to demonstrate added value.

2. INTRODUCTION

The risk for a hospital acquired infection for patients admitted to the intensive care unit (ICU) is 5–10 times higher than for other hospital patients (Weber et al., 1999). At the ICU, infection is a common cause of morbidity and mortality (Sax et al., 2013). Infection leads to the release of both inflammatory and anti-inflammatory cytokines (Hotchkiss et al., 2009). An imbalance between both responses can contribute to a potentially lethal course of this condition in critically ill patients (Hotchkiss et al., 2009; Hotchkiss et al., 2010). Early detection of infection could have a major impact

on infection management and disease outcome in acute care settings (Suprin et al., 2000). It is often difficult to differentiate between infection and inflammation as symptoms overlap (Mitaka, 2005). In addition, it is a challenge to diagnose a new infection in a patient with ongoing inflammation (e.g. due to surgery or an earlier infection).

The clinical suspicion of an infection is based on sensitive but non-specific vital signs such as tachycardia, or fever. In addition to tachycardia, several studies proposed that other heart rate characteristics such as signal complexity, signal variability and signal asymmetry could also be used as early markers for infection (Lake et al., 2002; Kovatchev et al. 2003; Griffin et al., 2005; Ahmad et al., 2009). Most of these studies found a satisfactory sensitivity, but a rather low specificity (Lake et al. 2002).

During the last decade many studies focused on the search for accurate laboratory markers of infection. Two potential markers that received much attention are C reactive protein (CRP) and procalcitonin (PCT) (Assicot et al., 1993; Castelli et al., 2004). However, several studies indicate that both parameters can also be increased in non-infectious conditions suggesting the need for other markers which are more specific or for tests which could be used in combination with these parameters.

In this study, we hypothesized that we can differentiate between infected patients and non-infected subjects (patients with inflammation and healthy subjects) based on dynamic features of heart rate and serum cytokine time series. The main objective was to use simple metrics to quantify these time series to obtain an accurate classification of infected patients. First we studied the predictive power of the metrics derived from the heart rate time series, and second whether classification performance improved with inclusion of information derived from static cytokine values or cytokine time series.

3. MATERIALS AND METHODS

3.1 Patients and healthy subjects

A prospective observational study was performed at the surgical and medical intensive care units (ICU) of the University Hospitals Leuven, Belgium. The study was approved by the Institutional Ethical Review Board of the University Hospitals Leuven (ML6625). The clinical trial was registered at the International Standard Randomized Controlled Trial Number Register (ISRCTN49306926). Written informed consent was obtained from the patients' next of kin and from the healthy volunteers.

Consecutive mechanically ventilated adult (age ≥ 18 years) patients, who had an arterial line in place, were eligible for inclusion in the study. In addition, age, gender, and BMI matched healthy volunteers were selected, and were admitted in a room adjacent to the ICU for 1 night, where an arterial line in the left or right radial artery was inserted.

In all subjects, night-time serial blood sampling, over 9 h, from 9 p.m. until 6 a.m. on the next morning, was performed. Undiluted 2 ml arterial blood samples were drawn every 10 min. A blood management protection system (Edwards Lifesciences, Irvine, CA, USA) was used to minimize unnecessary blood waste. Total blood loss per subject did not exceed 110 ml.

Blood was collected in prechilled EDTA tubes that were placed immediately on ice. They were cold-centrifuged, frozen at -20 °C, before they were stored at -80 °C. In the serum of each sample, the concentration of the following 10 cytokines were determined with an immunoassay (Bio-Plex Precision ProTM, BioRad Laboratories, CA, USA): interleukin-1 beta (IL-1b), interleukin-2 (IL-2), interleukin-4 (IL-4), interleukin-5 (IL-5), interleukin-6 (IL-6), interleukin-10 (IL-10), interleukin-12 (IL-12), interleukin-13 (IL-13), interferon gamma (IFNc) and tumor necrosis factor-alpha (TNFa). This immunoassay has a reliable performance as supported by independent studies (e.g. Fu et al., 2009).

During the same period of 9 h, also heart rate measurements were recorded from the patients via surface electrodes and a patient monitor (IntelliVue MX800; Philips , Eindhoven, The Netherlands) and stored with a sampling rate of 1 sample/1 min using a patient data management system (MetaVision ; iMD-Soft , Needham, MA, USA). For the healthy volunteers (N = 5), no heart rate measurements were available.

All patients were scored for infection, by retrospective review of their computerized medical charts, by two independent clinicians (P.M., G.M.). The CDC criteria for infections in the ICU setting were used (Horan et al., 2008). Infection scoring was done in an electronic CRF, in Filemaker Pro (Filemaker, Inc., Santa Clara, CA, USA). Patients were categorized as not-infected when no signs of infection were present, active infection when there were signs of infection, and non-active infection when patients were still treated with antibiotics for an earlier infection, but had no active signs of infection any longer. The volunteers were examined by a medical doctor to confirm that they were healthy and not suffering from infection, at the time of sampling.

3.2 Pre-processing and feature extraction

The hypothesis of this study was that infected patients can be distinguished from non-infected patients based on features of the heart rate and cytokine time series. Therefore, ten different methods were used to derive descriptive features from these time series: mean, variance, minimum, maximum, maximum–minimum, autoregressive coefficient of a first order autoregressive [AR(1)] model, skewness, kurtosis, sample entropy and the cumulative sum (for details on the calculation of the cumulative sum: see Tambuyzer et al., 2014). The selection of these features is supported by other studies, which indicate that such generic features may be used for a detailed quantification of time series in a wide range of fields (e.g. Richman & Moorman, 2000; Dakos et al., 2012)). Most of these metrics are measures for signal complexity (sample entropy), signal variability (variance, kurtosis, cumulative sum,

autoregressive coefficient of AR(1) model) or signal asymmetry (skewness, mean of detrended time series) (Bassevillie & Nikiforov, 1993; Richman et al, 2000; Aboy et al. 2007; Dakos et al., 2012). The same ten features were calculated for the detrended time series. Each time series was first standardised (subtraction of mean and divided by standard deviation) and afterwards detrended using an integrated random walk model (IRW) with noise variance ratio (NVR) of 0.001 for the heart rate time series and a NVR of 0.01 for the cytokine time series (CAPTAIN toolbox in Matlab; Taylor et al., 2006). In this study, these detrended time series are also called the fast dynamics of the time series, because by subtracting the IRW model form the original data, the slow trend was removed.

3.3 Feature selection and classification models

Decision tree analysis was applied to determine appropriate classification models for infection based on these features (Statistics Toolbox in Matlab). First, a decision tree model was developed based only on the features of the heart rate time series (i.e. heart rate model or HR model). To obtain a robust HR model, a bootstrapping procedure (n = 1000 bootstrap samples) was used for the selection of the heart rate based features (Steyerberg, 2008). For each bootstrap sample, a new pruned decision tree was calculated resulting in a total of 1000 decision trees. Afterwards, the frequency of features selected as tree nodes across bootstrap replicas was used to rank them for predictive performance. Features with the highest count were selected for the final decision tree model. Afterwards, receiver operating characteristic (ROC) analysis was used to evaluate the performance of a diagnostic test based on this final decision tree model. The area under the ROC curve (AUC) was calculated to quantify the discriminatory power of the HR model (Fan et al., 2006). Since bootstrapping provides accurate and unbiased estimates of model performance in small datasets, bootstrapping (based on 1000 bootstrap samples) was used to calculate confidence intervals for the used performance metrics (sensitivity, specificity, AUC) (Steyerberg, 2008). Hosmer–Lemeshow p value was used to evaluate the model calibration.

After development of the HR model, the discriminatory power of single blood cytokine levels was investigated. Therefore, the AUC values were calculated for four different time points per cytokine: 9:00 p.m., 0:00, 3:00 a.m. and 6:00 a.m. Afterwards, logistic regression (Statistics toolbox in Matlab) was used to investigate whether the HR model could be improved by adding values of single blood cytokine levels or in more practical terms it was tested whether it is clinically relevant to measure blood cytokine levels in addition to available heart rate recordings for obtaining a more accurate classification of infected patients. The HR model was extended with the most significant cytokines ($p < 0.1$). Finally, the added value of features based on the blood cytokine time series was examined. First, the most predictive features of the cytokine time series were selected based on a bootstrap procedure (see bootstrapping procedure described above for feature selection of heart rate based features). Afterwards, again logistic regression (Statistics toolbox in Matlab) was used to investigate whether the HR model could be ameliorated by adding features of the blood cytokine time series.

4. RESULTS

4.1 Patients

39 subjects, of whom serum from the night-time serial blood sampling was available for cytokine quantification, were included in this study [age (mean ± SD): 59 ± 17; BMI (mean ± SD): 26 ± 5; sex: 26 M and 13 F]. According to the CDC criteria, 16 patients were defined as infected and the other 23 subjects were defined as non-infected (see Table III.1). Five of the non-infected subjects were healthy volunteers.

4.2 Classification of patients based on heart rate time series

As described in the methods section, decision trees were calculated based on all the heart rate based features for each of the 1000 bootstrap samples. Two parameters were present in more than 40 % of the calculated trees: the mean of the fast dynamics of the heart rate and the mean of the raw heart rate time series. Therefore, a decision tree was determined for a combination of these two parameters (i.e. the HR model). Figure III.1 shows the scatter plot of the HR model. The sensitivity and

Table III.1. Detailed overview of patient information.

Subject no.	Age	Sex	BMI	ICU survival?	Hospital survival?	Length of stay at ICU (days)	Length of stay at hospital (days)	Day of stay at the ICU at the time of blood profile	Infection at admission ICU?	Infection at day of blood profile?	APACHE II score	Type of infection at the time of blood profile
1	30.0	V	24.2	Yes	Yes	9	9	4	Yes	Yes	42	PL
2[a]	61.4	M	21.8	Yes	Yes	–	–	–	No	No	–	–
3[a]	57.7	M	24.7	Yes	Yes	–	–	–	No	No	–	–
4[a]	55.2	M	22.9	Yes	Yes	–	–	–	No	No	–	–
5	72.6	M	18.7	Yes	Yes	16	32	9	No	Yes	38	PL
6	52.8	V	27.6	Yes	Yes	12	25	7	Yes	Yes	34	BS, PL, GI
7	27.1	M	24.2	Yes	Yes	7	32	4	Yes	Yes	29	SS, BS, PL, GI
8	52.4	M	19.6	No	No	10	10	6	Yes	No	46	–
9	85.9	M	23.4	Yes	No	15	60	5	Yes	No	45	–
10	52.7	M	24.9	Yes	Yes	396	424	5	Yes	No	35	–
11	45.8	M	25.7	Yes	Yes	21	33	3	Yes	Yes	32	SS
12	84.4	M	24.1	Yes	Yes	31	53	3	No	No	40	–
13	46.4	M	31.0	Yes	Yes	15	26	4	No	No	32	–
14	48.4	V	27.6	Yes	Yes	12	43	5	No	Yes	39	BS
15	69.1	M	22.9	Yes	No	12	32	3	Yes	No	39	–
16	44.4	V	20.8	Yes	Yes	8	33	2	Yes	No	38	–
17	29.6	V	19.6	Yes	Yes	22	34	2	Yes	Yes	37	GI
18	30.6	M	23.1	Yes	Yes	10	64	2	Yes	Yes	33	BS, CV
19	58.6	M	23.4	Yes	Yes	17	45	5	Yes	No	36	–
20	67.7	M	29.0	Yes	Yes	14	60	3	No	Yes	43	BS
21[a]	53.8	V	26.4	Yes	Yes	–	–	–	No	No	–	–
22[a]	59.0	V	21.8	Yes	Yes	–	–	–	No	No	–	–
23	60.1	V	35.2	Yes	Yes	59	59	4	Yes	No	34	–
24	85.5	M	24.7	Yes	Yes	7	67	3	Yes	No	44	–
25	54.1	M	20.8	Yes	Yes	6	6	1	No	No	34	–
26	79.8	V	31.6	Yes	Yes	17	73	2	Yes	Yes	37	GI
27	78.4	V	25.0	Yes	Yes	8	35	3	Yes	Yes	32	CV
28	35.3	V	30.5	Yes	Yes	10	19	5	No	No	31	–
29	56.4	M	27.8	Yes	Yes	19	27	8	No	No	35	–
30	60.9	M	37.0	Yes	Yes	32	54	7	Yes	Yes	33	PL, GI
31	73.5	M	24.8	Yes	Yes	9	27	1	No	No	36	–
32	78.1	M	27.8	Yes	No	11	30	5	Yes	No	39	–
33	64.6	M	21.0	Yes	Yes	23	131	3	No	No	37	–
34	59.3	M	18.0	Yes	Yes	3	22	1	Yes	Yes	36	PL
35	36.5	V	30.4	Yes	Yes	11	44	2	Yes	Yes	29	PL
36	79.8	V	40.0	Yes	Yes	8	37	1	Yes	Yes	41	PL
37	88.3	M	34.4	Yes	Yes	26	50	4	No	Yes	37	PL
38	60.5	M	24.9	No	No	17	17	2	No	No	32	–
39	54.9	M	25.1	No	No	16	16	5	Yes	No	38	–

[a] Healthy control group; [b] PL= Pneumonia or other lower respiratory tract infection; GI = Gastrointestinal infection; CV= Cardiovascular syst. infection; BS = Bloodstream infection; SS = Surgical site infection

specificity of the HR model were 88 % (95 % confidence interval of bootstrap samples: [0.69–1.00]) and 88 % (95 % confidence interval based on bootstrap samples: [0.68–1.00]), respectively. The corresponding AUC was 0.88 (95 % confidence interval based on bootstrap samples: (0.77–1.00)]. The model had good calibration with 0.09 Hosmer–Lemeshow p value.

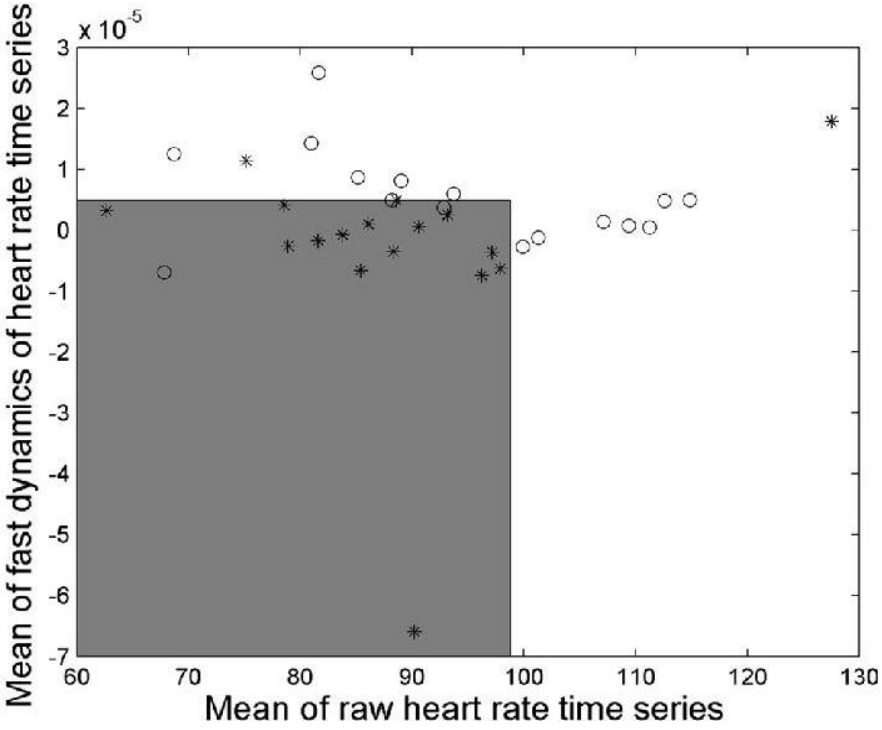

Figure III.1. Scatter plot of results for the HR model (a decision tree based on mean of the raw heart rate and the mean of the high frequent heart rate component). Circles represent the infected patients, whereas stars indicate non-infected patients. All stars/circles within the white area will be classified by the decision tree model as infected. Stars/ circles within the grey area will be classified as non-infected.

4.3 Added value of static blood cytokine levels

First, the discriminatory power of single blood cytokine levels was assessed. Therefore, the AUC values were calculated for four different time points per cytokine: 9:00 p.m., 0:00, 3:00 a.m. and 6:00 a.m. All the AUC values are listed in Table III.2. None of the cytokines has an AUC value which is significantly higher than 0.5, showing very weak discriminatory power for classification of infected patients based on single cytokines. Afterwards, we tested whether the accuracy of the decision tree based on the two heart rate parameters could be improved by adding single cytokine blood level values. In a multivariate logistic regression model for infection, in addition to the two selected heart rate features, four cytokines had a p value below 0.1: IL-1b, IL-4, IL-10 and IL-12. Bootstrapping was applied to quantify the added value of a decision tree based on all these features (four cytokines + two heart rate features) compared with the HR model (the tree based on only the two heart rate parameters). Therefore, we calculated for each bootstrap sample, the AUC value of a tree based on only the two heart rate measures (AUC_{HR}) and the AUC value of a tree based on the two heart rate measures with the four selected cytokines ($AUC_{HR+cyto}$). The difference between both AUC values (AUC_{HR} - $AUC_{HR+cyto}$) was calculated for all bootstrap samples. The 95 % confidence interval based on the differences for all bootstrap samples is [-0.0881 to 0.0883]. Zero is part of this interval showing that there is no significant additional value of adding the cytokines to the generated decision tree model.

Table III.2. Overview of AUC values with bootstrapped confidence intervals (CI) for all cytokines at four different time points: 9:00 p.m., 0:00, 3:00 a.m. and 6:00 a.m.

Time	9:00 p.m.		0:00		3:00 a.m.		6:00 a.m.	
	AUC	CI	AUC	CI	AUC	CI	AUC	CI
IL-1b	0.54	[0.35–0.72]	0.57	[0.33–0.70]	0.52	[0.32–0.71]	0.49	[0.31–0.70]
IL-2	0.52	[0.34–0.72]	0.54	[0.35–0.74]	0.48	[0.30–0.67]	0.58	[0.32–0.72]
IL-4	0.64	[0.40–0.77]	0.58	[0.40–0.77]	0.49	[0.31–0.69]	0.55	[0.32–0.70]
IL-5	0.52	[0.33–0.71]	0.52	[0.32–0.73]	0.54	[0.34–0.73]	0.59	[0.40–0.78]
IL-6	0.49	[0.30–0.70]	0.47	[0.28–0.67]	0.44	[0.26–0.64]	0.44	[0.25–0.64]
IL-10	0.48	[0.29–0.67]	0.48	[0.27–0.69]	0.51	[0.31–0.69]	0.61	[0.35–0.74]
IL-12	0.58	[0.40–0.77]	0.58	[0.40–0.76]	0.50	[0.31–0.70]	0.54	[0.33–0.72]
IL-13	0.58	[0.33–0.70]	0.53	[0.35–0.73]	0.58	[0.39–0.78]	0.51	[0.32–0.71]
IFNg	0.52	[0.32–0.71]	0.55	[0.37–0.74]	0.49	[0.30–0.69]	0.52	[0.33–0.70]
TNFa	0.54	[0.36–0.74]	0.64	[0.41–0.78]	0.54	[0.32–0.70]	0.59	[0.33–0.72]

4.4 Added value of blood cytokine time series

In comparison with the single blood cytokine levels, more detailed information can be obtained by quantification of the complete blood cytokine time series. Figures showing the median time series of all subjects for each cytokine with the corresponding lower detection limit of the used immunoassay are given in Online Resource 1. To investigate the added value of using blood cytokine time series, all the metrics as described in the methods section were calculated based on these time series. Again bootstrapping was used to find the most predictive features. Five parameters were present in more than 10 % of the 1000 calculated trees: the minimum of IL-1B of the raw time series, the sample entropy of IL-2 of the raw time series, the cumulative sum of IL-2 of the detrended time series, the cumulative sum of IL-10 of the detrended time series and the cumulative sum of IL-12 of the detrended time series. The AUC values of these features are summarized in Table III.3. The cumulative sum of the detrended time series was the marker with the highest discriminatory power (AUC [0.70 for IL-10, IL-2 and IL-12). This is a marker for amplitude increases in time series fluctuations (Tambuyzer et al., 2014). However, logistic regression showed that none of these five markers had a significant added value, when they were added to the heart rate model ($p < 0.1$ for all five features). This result confirmed that the decision tree based on the heart rate time series could not be improved by information of the cytokine time series.

Table III.3. Overview of AUC values with bootstrapped confidence intervals (CI) for the selected feature based on the cytokine time series.

Feature of the cytokine time series	AUC	CI
The minimum of IL-1B of the raw time series	0.63	[0.44–0.82]
The sample entropy of IL-2 of the raw time series	0.59	[0.39–0.79]
The cumulative sum of IL-2 of the detrended time series	0.76	[0.60–0.93]
The cumulative sum of IL-10 of the detrended time series	0.72	[0.53–0.90]
The cumulative sum of IL-12 of the detrended time series	0.71	[0.52–0.91]

5. DISCUSSION

In this study we investigated the discriminatory power of information captured by cytokine and heart rate time series to distinguish infected ICU patients from non-infected ICU patients and/or healthy control subjects. We found that among the ICU patients, heart rate was a better marker for infection than information captured by the cytokine time series. Heart rate characteristics appeared to be non-specific but sensitive markers for infection. Based on the bootstrap procedure, two features were selected for the decision tree model: the mean of the raw heart rate signal and the mean of the fast dynamics of the heart rate time series. Infected patients revealed higher values for both parameters (Fig. III.2). The mean of the detrended heart rate time series (or fast dynamics) can be seen as a measure for signal asymmetry. When the fast fluctuations of the time series are symmetrical, this marker is expected to be zero. When this marker is higher than zero, the fast fluctuations tend to higher heart rate values. Figure III.2 shows an example of standardised time series for an infected and a non-infected patient. These plots illustrate that the fast fluctuations are more symmetrical distributed for the non-infected patients. So far, only a limited number of studies quantified asymmetry in physiological signals (Karmakar et al., 2009). This study indicates that this feature deserves more attention in future studies. Interestingly, this decision tree model could not be improved by including information of single cytokine blood levels nor cytokine time series. These results suggest that the determination of cytokine blood levels with a high sample frequency will not lead to a more accurate detection of infection in the ICU setting. This result is unexpected since cytokines are key players in the regulation of the body's response to infection (Cinel & Opal, 2009). However, it is known that cytokine blood levels can also be induced by non-infectious conditions (Turnbull & Rivier, 1999; Opp, 2005; Dimopoulou et al., 2008; Reinhart et al., 2012), which complicates the use of cytokines for infection monitoring purposes. Moreover, depending on the kind of pathogen, the stage of infection and the site of infection the individual responses can be very different (Imanishi, 2000). The results of this study suggest that the predictive value of (expensive) biomarkers

should always be weighed against the routinely monitored data, and such biomarkers have to demonstrate added value.

Several limitations of this study should be noticed. First, a small dataset was used and therefore the obtained results should be confirmed by larger studies. Secondly, short time series were used for which the stage of the infection was not known. This is an inherent limitation of this clinical setting in practice, since the exact onset of infection cannot be measured. Therefore, it was impossible to identify markers related with the start of infection. Longer time series with samples before and after the infection would allow to analyse the initial phase and the different stages of the infection. A third remark is that heart rate can never be a very specific marker, since it is known that heart rate increases in response to a wide range of other stimuli of the body.

Several studies advocate the use of a dynamic system approach, which focuses on the simultaneous dynamic analysis of many parameters and their interactions (Brown et al., 2007; Namas et al., 2012). In this study, we found no added value in the combination of the specific heart rate characteristics (i.e. the mean of the raw heart rate signal and the mean of the fast dynamics of the heart rate time series) and cytokine time series characteristics. In future studies, these parameters should be investigated in combination with dynamic analyses of other markers such as blood temperature, white blood cells, PCT, CRP, etc. Such a dynamic system approach would potentially allow determining the individual dynamic infection state in a more detailed way and could be used to guide interventions for early treatment of infection (e.g. administering antibiotics).

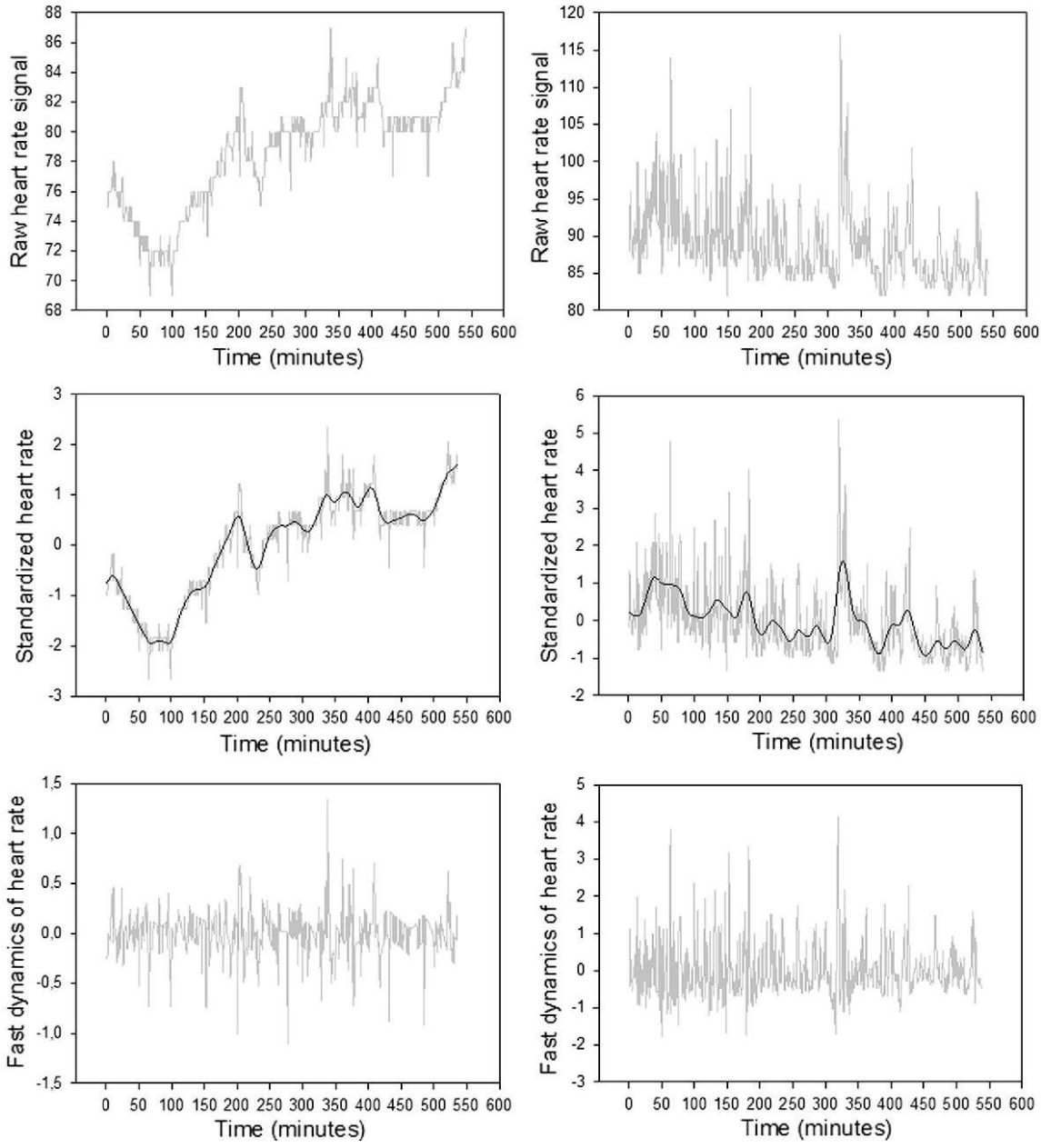

Figure III.2. Raw heart rate signal, standardised heart rate signal and fast dynamics of heart rate signal (i.e. standardized and detrended time series) for an infected (left) and a non-infected (right) patient. In the middle plots, the trend model is represented by a black line

6. REFERENCES

1. Aboy M, Cuesta-Frau D, Austin D, Mico-Tormos P. Character-ization of sample entropy in the context of biomedical signal analysis. In: 29th annual international conference of the IEEE Engineering in Medicine and Biology Society. 2007; p. 5942–5.

2. Ahmad S, Tejuja A, Newman KD, Zarychanski R, Seely AJ. Clinical review: a review and analysis of heart rate variability and the diagnosis and prognosis of infection. Crit Care. 2009;13:232. doi: 10.1186/cc8132.

3. Assicot M, Bohuon C, Gendrel D, Raymond J, Carsin H, Guil-baud J. High serum procalcitonin concentrations in patients with sepsis and infection. Lancet. 1993;341:515–8. doi: 10.1016/0140- 6736(93)90277-N.

4. Basseville ME, Nikiforov IV. Detection of abrupt changes: theory and application. Englewood Cliffs: Prentice Hall; 1993.

5. Brown KL, Cosseau C, Gardy JL, Hancock RE. Complexities of targeting innate immunity to treat infection. Trends Immunol. 2007;28:260–6. doi: 10.1016/j.it.2007.04.005.

6. Castelli GP, Pognani C, Meisner M, Stuani A, Bellomi D, Sgarbi L. Procalcitonin and C-reactive protein during systemic inflam-matory response syndrome, sepsis and organ dysfunction. Crit Care. 2004;8:R234. doi: 10.1186/cc2877.

7. Cinel I, Opal SM. Molecular biology of inflammation and sepsis: a primer*. Crit Care Med. 2009;37:291–304. doi: 10.1097/CCM. 0b013e31819267fb.

8. Dakos V, Carpenter SR, Brock WA, Ellison AM, Guttal V, Ives AR, et al. Methods for detecting early warnings of critical tran-sitions in time series illustrated using simulated ecological data. PLoS One. 2012;7:e41010. doi: 10.1371/journal.pone.0041010.

9. Dimopoulou I, Orfanos S, Kotanidou A, Livaditi O, Giamarellos-Bourboulis E, Athanasiou C, et al. Plasma pro-and anti-inflam-matory cytokine levels and outcome prediction in unselected critically ill patients. Cytokine. 2008;41:263–7. doi: 10.1016/j. cyto.2007.11.019.

10. Fan J, Upadhye S, Worster A. Understanding receiver operating characteristic (ROC) curves. Can J Emerg Med. 2006;8:19–20. doi: 10.1017/S1481803500013336.

11. Fu Q, Zhu J, Van Eyk JE. Comparison of multiplex immunoassay platforms. Clin Chem. 2010;56:314–8. doi: 10.1373/clinchem. 2009.135087.

12. Griffin MP, Lake DE, Bissonette EA, Harrell FE Jr, O'Shea TM, Moorman JR. Heart rate characteristics: novel physiomarkers to predict neonatal infection and death. Pediatrics. 2005;116:1070–4. doi: 10.1542/peds.2004-2461.

13. Horan TC, Andrus M, Dudeck MA. CDC/NHSN surveillance definition of health care-associated infection and criteria for specific types of infections in the acute care setting. Am J Infect Control. 2008;36:309–32. doi: 10.1016/j.ajic.2008.03.002.

14. Hotchkiss RS, Coopersmith CM, McDunn JE, Ferguson TA. The sepsis seesaw: tilting toward immunosuppression. Nat Med. 2009;15(5):496–7. doi: 10.1038/nm0509-496.

15. Hotchkiss RS, Opal SM. Immunotherapy for sepsis: a new approach against an ancient foe. N Engl J Med. 2010;363(1):87. doi: 10.1056/NEJMcibr1004371.

16. Imanishi J. Expression of cytokines in bacterial and viral infections and their biochemical aspects. J Biochem. 2000;2000(127): 525–30. doi: 10.1093/oxfordjournals.jbchem.a022636.

17. Karmakar CK, Khandoker AH, Gubbi J, Palaniswami M. Defining asymmetry in heart rate variability signals using a Poincare´ plot. Physiol Meas. 2009;30:1227. doi: 10.1088/0967- 3334/30/11/007.

18. Kovatchev BP, Farhy LS, Cao H, Griffin MP, Lake DE, Moor-man JR. Sample asymmetry analysis of heart rate characteristics with application to neonatal sepsis and systemic inflammatory response syndrome. Pediatr Res. 2003;54:892–8. doi: 10.1203/01. PDR.0000088074.97781.4F.

19. Lake DE, Richman JS, Griffin MP, Moorman JR. Sample entropy analysis of neonatal heart rate variability. Am J Physiol Regul Integr Comp Physiol. 2002;283:R789–97. doi: 10.1152/ajpregu. 00069.2002.

20. Mitaka C. Clinical laboratory differentiation of infectious versus non-infectious systemic inflammatory response syndrome. Clin Chim Acta. 2005;351(1):17–29. doi: 10.1016/j.cccn.2004.08.018.

21. Namas R, Zamora R, Namas R, An G, Doyle J, Dick TE, et al. Sepsis: something old, something new, and a systems view. J Crit Care. 2012;27:314-e1. doi: 10.1016/j.jcrc.2011.05.025.

22. Opp MR. Cytokines and sleep. Sleep Med Rev. 2005;9:355–64. doi: 10.1016/j.smrv.2005.01.002.

23. Reinhart K, Bauer M, Riedemann NC, Hartog CS. New approaches to sepsis: molecular diagnostics and biomarkers. Clin Microbiol Rev. 2012;25:609–34. doi: 10.1128/CMR. 00016-12.

24. Richman JS, Moorman JR. Physiological time-series analysis using approximate entropy and sample entropy. Am J Physiol Heart Circ Physiol. 2000;278:H2039–49.

25. Sax H, Clack L, Touveneau S, da Liberdade JantaradaF, Pittet D, Zingg W. Implementation of infection control best practice in intensive care units throughout Europe: a mixed-method evaluation study. Implement Sci. 2013;8:24. doi: 10.1186/1748-5908-8-24.

26. Steyerberg EW. Clinical prediction models: a practical approach to development, validation, and updating. New York: Springer; 2008.

27. Suprin E, Camus C, Gacouin A, Le Tulzo Y, Lavoue S, Feuillu A, Thomas R. Procalcitonin: a valuable indicator of infection in a medical ICU? Intens Care Med. 2000;26:1232–8. doi: 10.1007/ s001340000580.

28. Tambuyzer T, De Waele T, Chiers K, Berckmans D, Goddeeris BM, Aerts JM. Interleukin-6 dynamics as a basis for an early-warning monitor for sepsis and inflammation in individual pigs. Res Vet Sci. 2014;96:460–3. doi: 10.1016/j.rvsc.2014.03.014.

29. Taylor CJ, Pedregal DJ, Young PC, Tych W. Environmental time series analysis and forecasting with the captain toolbox. Environ Model Softw. 2006;22:797–814. doi: 10.1016/j.envsoft.2006.03. 002.

30. Turnbull AV, Rivier CL. Regulation of the hypothalamic–pitu-itary–adrenal axis by cytokines: actions and mechanisms of action. Physiol Rev. 1999;79(1):1–71.

31. Weber DJ, Raasch R, Rutala WA. Nosocomial infections in the ICU: the growing importance of antibiotic-resistant pathogens. Chest. 1999;115(Suppl. 1):34S–41S. doi: 10.1378/chest.115.suppl_ 1.34S.

GENERAL CONCLUSIONS

Process models and model-based features:

In this chapter a **compact linear model** was used before the steps of the **feature extraction**. The heart rate model showed that the best results were obtained for a combination of the raw heart rate signal and the fast dynamics of the heart rate time series. Corresponding with Hypothesis 3 of Part 1, this result proves how model-based features can be an added value to monitors which are purely based on measured variables (e.g. **ICU heart rate monitor** only based on raw heart rate signal used in an).

Individualised change detection:

However, the analysis of the cytokine data suggested that the heart rate model could not be improved by including information of cytokine times series. Since cytokine measurements are also much more expensive (and invasive), it is suggested to develop a model-based monitor for infection using only heart rate measurements. However, heart rate characteristics are sensitive, but non-specific markers for infection and should be used in combination with other markers.

Whereas ROC curve analysis was used to calculate the thresholds in the previous chapters, here we used decision tree analysis to obtain **'monitoring thresholds'** for classification based on multiple variables. If more variables are measured, we obtain more individual information of the patient, potentially allowing a more individualised approach. Ideally, future individualised monitors should implement dynamic analyses of different biomarkers for infection and their interactions, which allow the operator to determine the individual dynamic infection state of the patient.

In this study, a list of different **methods for detecting early warning signs** was used inspired by complex systems science. These methods can be added to the approach for **individualised model-based monitoring** discussed at the end of chapter 2.

CHAPTER IV

System identification of mGluR-dependent long-term depression

Adapted from: Tambuyzer, T., Ahmed, T., Taylor, C. J., Berckmans, D., Balschun, D., & Aerts, J. M. (2013). System identification of mGluR-dependent long-term depression. *Neural computation*, *25*(3), 650-670.

BROADER PERSPECTIVE

This chapter will focus on the blocks **process model** and **model-based features** of the general scheme. In contrast to chapter 2 and 3 where compact linear single-output models were used to calculate features based on the model noise (detrended time series or fast dynamics), here **linear input-output models** were applied.

This study focused on the analysis of physiological brain slice recordings of synaptic plasticity responses after the application of a drug. The administration of the drug was used as input variable, whereas the recorded synaptic strength was used as output variable for the model.

Although we believe that building an individualised model-based monitor should start from biological knowledge, we investigated in this chapter whether it is also possible to have a dual interaction where the models can aid to gain new biological insights (i.e. reverse biological engineering).

However, it is known that neural processes contain many nonlinearities. Therefore, we believe that this chapter could give an answer to the main question that arises from Hypothesis 2 of Part 1: Is it possible to use linear models to gain insight in highly **nonlinear biological processes**?

1. ABSTRACT

Recent advances have started to uncover the underlying mechanisms of metabotropic glutamate receptor (mGluR)-dependent long-term depression (LTD). However, it is not completely clear how these mechanisms are linked, and it is believed that several crucial mechanisms remain to be revealed. In this study, we investigated whether system identification (SI) methods can be used to gain insight into the mechanisms of synaptic plasticity. SI methods have been shown to be an objective and powerful approach for describing how sensory neurons encode information about stimuli. However, to our knowledge, it is the first time that SI methods have been applied to electrophysiological brain slice recordings of synaptic plasticity responses. The results indicate that the SI approach is a valuable tool for reverse-engineering of mGluR-LTD responses. We suggest that such SI methods can aid in unravelling the complexities of synaptic function.

2. INTRODUCTION

Synaptic plasticity in general terms is the change in strength of synaptic connections between neurons. Long-term potentiation (LTP) and long-term depression (LTD), two extensively studied forms of synaptic plasticity, are characterized by a persistent increase and decrease of synaptic efficacy, respectively. Long-term synaptic modifications play a key role in the plasticity of behaviour, learning, and memory (Martin, Grimwood, & Morris, 2000; Kandel, 2001; Lamprecht & LeDoux, 2004; Malenka & Bear, 2004; Neves, Cooke, & Bliss, 2008; Richter & Klann, 2009; Collingridge, Peineau, Howland, & Wang, 2010).

This work focuses on metabotropic glutamate receptor (mGluR)- dependent long-term depression. mGluR-LTD initially received less attention than N-methyl-D-aspartic acid receptor (NMDAR)-dependent LTD, but is now the focus of great interest (Bellone, Liischer, & Mameli, 2008). Typically mGluR-dependent LTD is induced in rodent brain slices by paired pulse low-frequency stimulation (PP-LFS) or by application of the group 1 mGluR agonist dihydroxyphenylglycine (DHPG) (Fitzjohn, Kingston, Lodge, & Collingridge, 1999; Kemp, McQueen, Faulkes, & Bashir, 2000; Zho, You, Huang, & Hsu, 2002). During the last decade, multifarious mechanisms have been uncovered to underlie mGluR-LTD. mGluR-LTD was shown to involve endocytosis of AMPA receptor subunits (G1uR -1 and -2), a process that is contingent on tyrosine dephosphorylation and activation of the tyrosine phosphatase striatal-enriched tyrosine phosphatase (STEP) (Moult et al., 2006; Snyder et al., 2001). In contrast to NMDA receptor-dependent LTD, mGluR-LTD does not require postsynaptic increases, LP3-sensitive Ca^{2+} stores, PLC, or PKC activity (Fitzjohn et al., 2001; Kleppisch, Voigt, Allmann, & Offermanns, 2001; Moult et al., 2006; own unpublished data). Among many other mechanisms that have been suggested to be involved (Gladding, Fitzjohn, & Molnar, 2009; Liischer & Huber, 2010), the rapid translation of proteins that regulates AMPA receptor (AMPAR) trafficking such as activity-regulated cytoskeletal associated protein (Arc), microtubule-associated protein lb (MAP1b), and STEP seems to be of central importance (Davidkova & Carroll, 2007; Zhang et al., 2008).

In spite of these advances (reviewed in Massey & Bashir, 2007; Bellone et al., 2008; Collingridge et al., 2010; Liischer & Huber, 2010), it is not completely clear how these mechanisms are linked, and most likely several crucial mechanisms still remain to be revealed. For example, experimental findings supported mGluR-LTD being independent of postsynaptic calcium (Fitzjohn et al., 2001; Kleppisch et al., 2001; Moult et at., 2006), but recent data indicate a role of calcium increases within spines for mGluR-LTD (Holbro, Grunditz, & Oertner, 2009). Furthermore, several studies described that mGluR-LTD is contingent on a rapid protein synthesis (Huber, Kayser, & Bear, 2000;

Karachot, Shirai, Vigot, Yamamori, & Ito, 2000; Mameli, Balland, Lujan, & Luscher, 2007), but others failed to confirm this (Hou et al., 2006; Nosyreva & Huber, 2006; Moult, Collingridge, Fitzjohn, & Bashir, 2008; own data). The reasons for these apparent discrepancies are far from being understood. Notably, many of these studies have emphasized the biological and pathological significance of mGluR-LTD, underlining the importance of further investigations to understand and characterize the mechanisms of mGluR-dependent LTD and their dynamics.

The majority of the models describing long-term synaptic plasticity focus on the NMDAR-dependent forms of LTD and LTP. Moreover, most models are dynamical mechanistic models describing the system based on a priori knowledge of it (Shouval, Bear, & Cooper, 2002; Hardy & Robillard, 2005; Nieus et al., 2006; Graupner & Brunel, 2010; Manninen, Hituri, Kotaleski, Blackwell, & Linne, 2010). In recent years, more and more researchers have been advocating the use of a top-down (data-based) modelling approach in addition to a mechanistic (or bottom-up) approach for improving the knowledge of biological systems (Jarvis, Stauch, Schulz, & Young, 2004; Tomlin & Axelrod, 2005; Tambuyzer, Ahmed, Berckmans, Balschun, & Aerts, 2011). This is particularly useful when not much knowledge about the interactions of the elements involved in the considered biological system is available. Although more and more publications are addressing the topic, the field is still in its infancy, and there is a pressing need for mathematical tools to help understand, quantify, and conceptualize information processing and the dynamic properties of biological systems (Sontag, 2004). The power of the dynamical systems approach to neuroscience, as well as to many other sciences, is that we gain insight into a system without knowing all the details that govern the system evolution (Izhikevich, 2007). System identification (SI) methods have been shown to be an objective and powerful approach for describing how sensory neurons encode information about stimuli (Wu, David, & Gallant, 2006; Pedoto et al., 2010; Kim, Lazar, & Slutskiy, 2011).

The SI approach is not limited to sensory systems (Wu et at, 2006). In this study, we hypothesize that it is possible to uncover the underlying dominant processes of mGluR-LTD by applying mathematical system identification methods. This hypothesis resulted in two main objectives:

1. To quantify the dynamics of LTD responses for different experimental conditions using a discrete-time transfer function (TF) approach. The models describe the relation between the DHPG application (input) and the long-term depression responses (output).
2. To investigate whether system identification methods can be valuable for gaining insight into the mechanisms of synaptic plasticity. Therefore, we examined whether the estimated TF models allowed us to identify and quantify the major subprocesses involved in mGluR dependent long-term depression.

3. MATERIALS AND METHODS

3.1 Animals and Brain Slice Preparation

Wistar rats were killed by cervical dislocation, and the hippocampus was rapidly dissected out into ice-cold (4°C) artificial cerebrospinal fluid (ACSF), oxygen saturated with carbogen (95% 02/5% CO2). ACSF consisted of (in mM) 124 NaCl, 4.9 KO, 24.6 NaHCO3, 1.20, KH2PO4, 2.0 CaC12, 2.0 MgC12, 10.0 glucose, and pH 7.4. Transverse hippocampal slices (400 μm thick) were prepared and placed into a submerged-type chamber, maintained at 33'C with carbogen-saturated ACSF perfused at 2.4 ml/ min by a peristaltic pump. The animals were maintained, and experiments were conducted in accordance with institutional (KU Leuven), state, and government regulations.

3.2 Electrophysiological Recording

Synaptic responses were elicited by stimulation of the Schaffer collateral afferents using a Teflon-coated tungsten electrode. A glass electrode (filled with aCSF, 1-4 MΩ) was used to record the evoked extracellular field excitatory postsynaptic potentials (fEPSPs) in the CA1 region of the hippocampal slices. The slope of the fEPSP curves (mV/ms) was used as an indicator for the synaptic strength as described previously (Balschun et al., 2003). The stimulus intensity (μA) was adjusted to elicit an fEPSP response with a slope 35% of the fEPSP slope maximum, determined by input-output curves.

Column 4 in Table IV.1 shows the different stimulation frequencies used in the experiments. For data sets 1, 2, and 3, a stimulation frequency of 0.0033 Hz was used during the experiments. Supported by the modelling results of these three data sets, a fourth data set was generated with a stimulation frequency of 0.033 Hz (see section 3). For a stimulation frequency of 0.0033 Hz, the stimulating electrode delivered every 5 minutes three stimuli (with 10 s intervals) to the brain slice. These three input stimuli were averaged to obtain one data point (fEPSP) every 5 minutes. For a sampling rate of 0.033 Hz, every generated data point corresponded to a single stimulus. Since the fEPSPs were not averaged for the high-sampled experiments, they were expected to contain more noise compared to the low-sampled experiments.

3.3 Drug Application

After the brain slice preparation and the tuning of the electrode settings, the experiments started. First, there was a period of baseline recording (50 minutes) during which no drug was applied. After the baseline recording, metabotropic (mGluR)-LTD was induced in the rat brain slices by bath application of dihyclroxyphenylglycine (DHPG). For each data set, the drug was applied for different durations (5, 15, and 25 minutes and 2 hours) and in

different concentrations (15 µM, 30 µM) by the peristaltic pump. Table IV.1 gives an overview of the experiments with corresponding experimental conditions.

Table IV.1. Overview of all experiments

Dataset	DHPG concentration (^{1}M)	Duration of DHPG application	Sampling rate	Age rats	Number of repetitions
1	15	5 min	0.0033 Hz	7-8 weeks	4
2	15	15 min	0.0033 Hz	7-8 weeks	32
3	30	25 min	0.0033 Hz	7-8 weeks	10
4	30	2 h	0.033 Hz	10-14 months	9
			Total number of experiments:		55

3.4 Modelling

For the modelling, discrete-time transfer functions (TF) models were used. The models were single-input, single-output (SIS0) models. For this work, brain slices were exposed to a specific DHPG concentration to induce synaptic plasticity in the brain slices. The DHPG concentration (µM) was used as input, and the synaptic strength was the output (measured fEPSP slopes as a percentage of the initial fEPSP slopes before drug application; see Figure IV.1). Every data set (see Table IV.1) consisted of a number of repetitions for the same experimental conditions.

For each data set, the obtained responses (time series of FEPSP slopes) were averaged, and the resulting mean response curves were used to estimate the TF models. A SISO discrete-time TF model can be described by the following general equation (Young, 1984):

$$y_t = \frac{B(z^{-1})}{A(z^{-1})} u_{t-\delta} + \xi_t \,, \tag{3.1}$$

where y_t, is the output (synaptic strength), $u_{t-\delta}$ the input (DHPG concentration), t is the time for discrete time steps, δ is the time delay ($\delta > 0$), and ξ is additive noise, a serially uncorrelated sequence of random variables with variance that accounts for measurement noise, modelling errors, and the effects of unmeasured inputs to the process. Although the details are beyond the scope of this letter, the noise term has been introduced for statistical estimation purposes. The first term on the right-hand side of equation 3.1 is also referred to as x_t, the noise-free output. $A(z^{-1})$ and $B(z^{-1})$ are polynomials of model parameters that can be written as

$$A(z^{-1}) = 1 + a_1 z^{-1} + \ldots + a_n z^{-n}\,, \tag{3.2}$$

$$B(z^{-1}) = b_0 + b_1 z^{-1} + \ldots + b_m z^{-m}\,, \tag{3.3}$$

Every polynomial is a function of z^{-1}, a backward shift operator that is defined as $z^{-1}y_t = y_{t-1}$. Finally, a, and b, are the model parameters. Here, n represents the order of the system. Simplified refined instrumental variable (SRIV) algorithms were used for identifying and estimating the model parameters (Young, 1984). All calculations were performed in Matlab using the Captain Toolbox (Taylor,

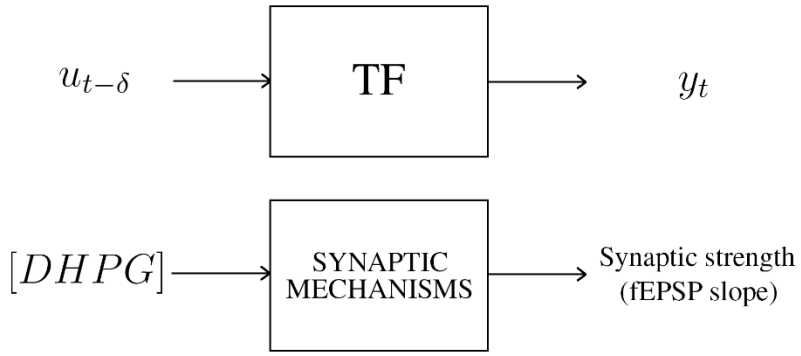

Figure IV.1. Block diagram for single-input, single-output (SISO) discrete-time TF models. (Top) A general diagram with an input, and an output, y_t. (Bottom) The general block diagram applied to the experimental setup of this study.

Pedregal, Young, & Tych, 2007). Different numbers of denominator and numerator parameters (*n* and *m* ranging from 1 to 5) and different time delays (0 to 10) were investigated, resulting in 275 (5 x 5 x 11) model structures. For each of these model structures, TF models were estimated. Three criteria were used to select the best models: values (Young, 1984), the Akaike information criterion (AIC; Akaike, 1974), and the Young identification criterion (YIC; Young, 1984). In addition to these three statistical criteria, each candidate model was evaluated by visual inspection (Ljung, 1987). The three statistical criteria are described below:

$$R_T^2 = 1 - \frac{\hat{\sigma}_e^2}{\sigma_y^2};\ \frac{1}{N}\sum_{t=1}^{t=N}[y_t - \bar{y}]^2\ ;\ \bar{y} = \frac{1}{N}\sum_{t=1}^{t=N}[y_t]^2, \tag{3.4}$$

$$AIC = \log(\sigma_e^2) + 2 - \frac{h}{N}, \tag{3.5}$$

$$YIC = \log\left(\frac{\hat{\sigma}_e^2}{\sigma_y^2}\right) + log_e\{NEVN\}; NEVN = \frac{1}{h}\sum_{i=1}^{i=h}\frac{\hat{\sigma}_e^2\hat{p}_{ii}}{\hat{a}_i^2}\ . \tag{3.6}$$

In these equations, $\hat{\sigma}_e^2$ refers to the variance of the residuals, σ_y^2 is the variance of the output, and h is the number of estimated parameters (i.e., n+m+1) in the parameter vector $\hat{\mathbf{p}}$ (i.e. $\hat{\mathbf{p}} = [a_1, \ldots, a_n, b_0, \ldots, b_m]$). N is the number of samples. $\hat{p}_{ii}$ is the i^{th} diagonal element of the covariance matrix generated by the estimation algorithm, and $\hat{a}_i^2$ is the square of the i^{th} parameter in the $\hat{\mathbf{p}}$ vector.

R_T^2 is a statistical measure for the goodness of fit of the simulation response. *AIC* is partly dependent on the fit of the simulation, but there is also a second component that takes into account the number of parameters, penalizing the *AIC* value for relatively high-order models. The *YIC* criterion is more complex and uses log terms so that improved models are indicated by increasingly negative values. The first term is a relative measure of how well the model explains the data. The second term relates to the conditioning of the instrumental variable cross-product matrix and is a measure of potential overparameterization in the model. In particular $\hat{\sigma}_e^2\hat{p}_{ii}$ in equation 3.6 are the

standard errors of the parameter estimates, with larger standard errors implying poorer YIC values.

Based on the physiological knowledge of the considered system, we might assume that the expected responses will be stable. Therefore, for every model, we also tested whether the poles were inside the unit circle, a requirement for model stability. The TF models were validated by an autocorrelation test for the residuals and a cross-correlation test between the residuals and the inputs (Ljung, 1987).

3.5 Identification and Quantification of Subprocesses

Higher-order TF models (n > 1) can be described as a configuration of first-order models (n = 1), which represent the dynamics of the subsystems. For example, a second-order model can he decomposed into two such first-order TF models corresponding to three important types of coupling: a serial coupling, a parallel coupling, or a feedback coupling (see Figure IV.2). Models with a model order higher than two result in more complex configurations but are not required for the analysis in this letter. Based on such first-order models, the dynamics of the subsystems could be quantified by means of their time constants. The time constant (TC) of a first-order model can be determined as (Young, 1984)

$$TC = \frac{-\Delta t}{\ln(-a_1)} \tag{3.7}$$

where At is the sampling interval and al the denominator parameter. Equation 3.7 is the discrete-time equivalent of the classical continuous-time definition of the time constant for a first-order differential equation. In practical terms, assuming zero initial conditions, it is the time taken for the output to reach 63% of its steady-state value in response to a step input.

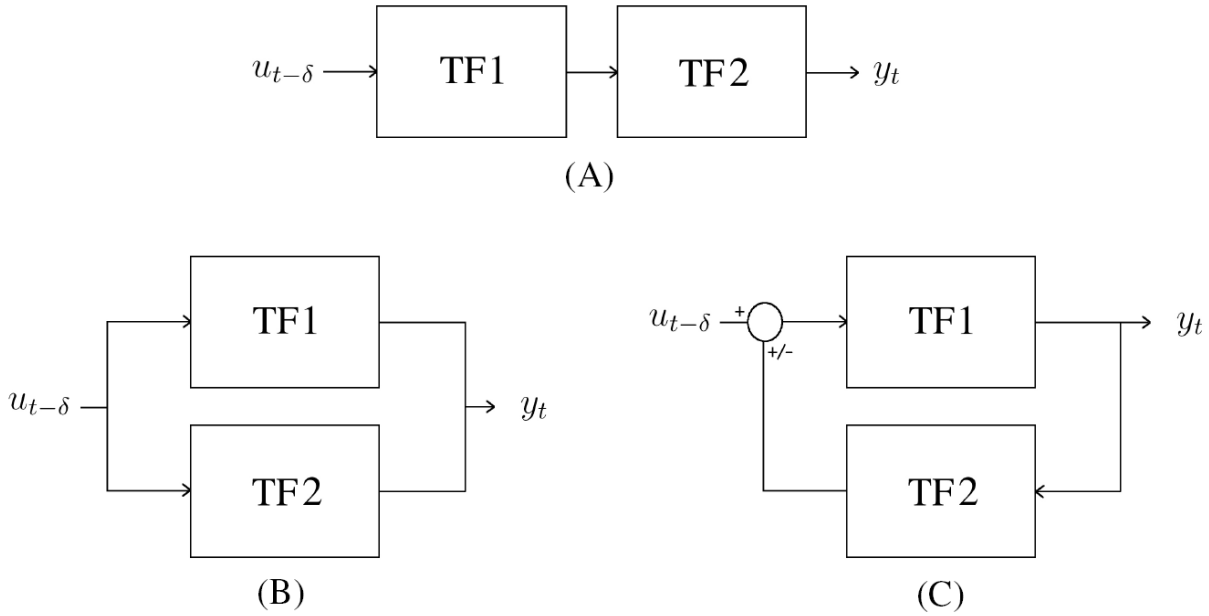

Figure IV.2. Possible configurations of two first-order models. (A) Serial coupling. (B) Parallel coupling. (C) Feedback coupling.

4. RESULTS

4.1 Dynamic Analysis for Different Sampling Rates

TF models were calculated and compared for two sampling rates: 0.0033 Hz and 0.033 Hz (see Table IV.1).

4.1.1 Models for Low Sampling Rate (0.0033 Hz)

For data sets 1, 2, and 3 (see Table IV.1), the sampling rate was 0.0033 Hz, which is frequently used for plasticity experiments (Denayer et al., 2008; Ahmed, Sabanov, D'hooge, & Balschun, 2011; Popkirov & Manahan-Vaughan, 2011). In Figure IV.3, the results of the first- and second-order models are graphically represented for these data sets. Considering the three statistical model selection criteria (*YIC, AIC*, R_T^2), visual inspection of the response, and analysis of the residuals, no better models were obtained for a model order higher than two. First-order models with $n = m = I$ (see Table IV.2) and second-order models with $n = m = 2$ (see Table IV.3) were found.

All first-order models had an R_T^2 higher than 0.81. For the second-order models, the R_T^2 was minimally 0.90, which indicated that the second-order models fit the data more accurately (see Figure IV.3). The best fourth- and fifth-order models were overparameterized, which was shown by higher *YIC* and *AIC* values and was confirmed by visual inspection (see Tables IV.5 and IV.6). Since the *YIC* and *AIC* values showed less consistent results for the third-order models, a more detailed visual examination was required (see Table IV.4). After visual inspection, the third-order models must be excluded as well: data set 1: overparameterization (*AIC, YIC*); data set 2: significant overshoot; data set 3: overparameterization (*AIC*) and model residuals with positive correlation in time.

These results confirm that the models of order 2 account for the data. Interestingly, for all the second-order models, one pole was close to unity, which suggests the presence of a fast initial component and a slow long-term component. The latter indicates that the models approximate an integrator, but not quite since the system is stable. This means the system (nearly) integrated the input effect, and thus, the brief DHPG pulse of 5, 15, or 25 minutes (input; see Figure IV.3) will change the synaptic efficacy (output), and this effect will remain for a long time (hours) after the pulse.

4.1.2 Models for High Sampling Rate (0.033 Hz)

Since discrete measurements of continuous signals cause information loss, it is important to choose an optimal sampling rate. Only for an optimal sampling rate will the model's parameters correctly represent the real underlying system (e.g., mechanisms of mGluR-LTD). The measurement interval between two data points should maximally be half of the value of the time constant (Nyquist-Shannon sampling theorem; Nyquist, 1928). For this reason,

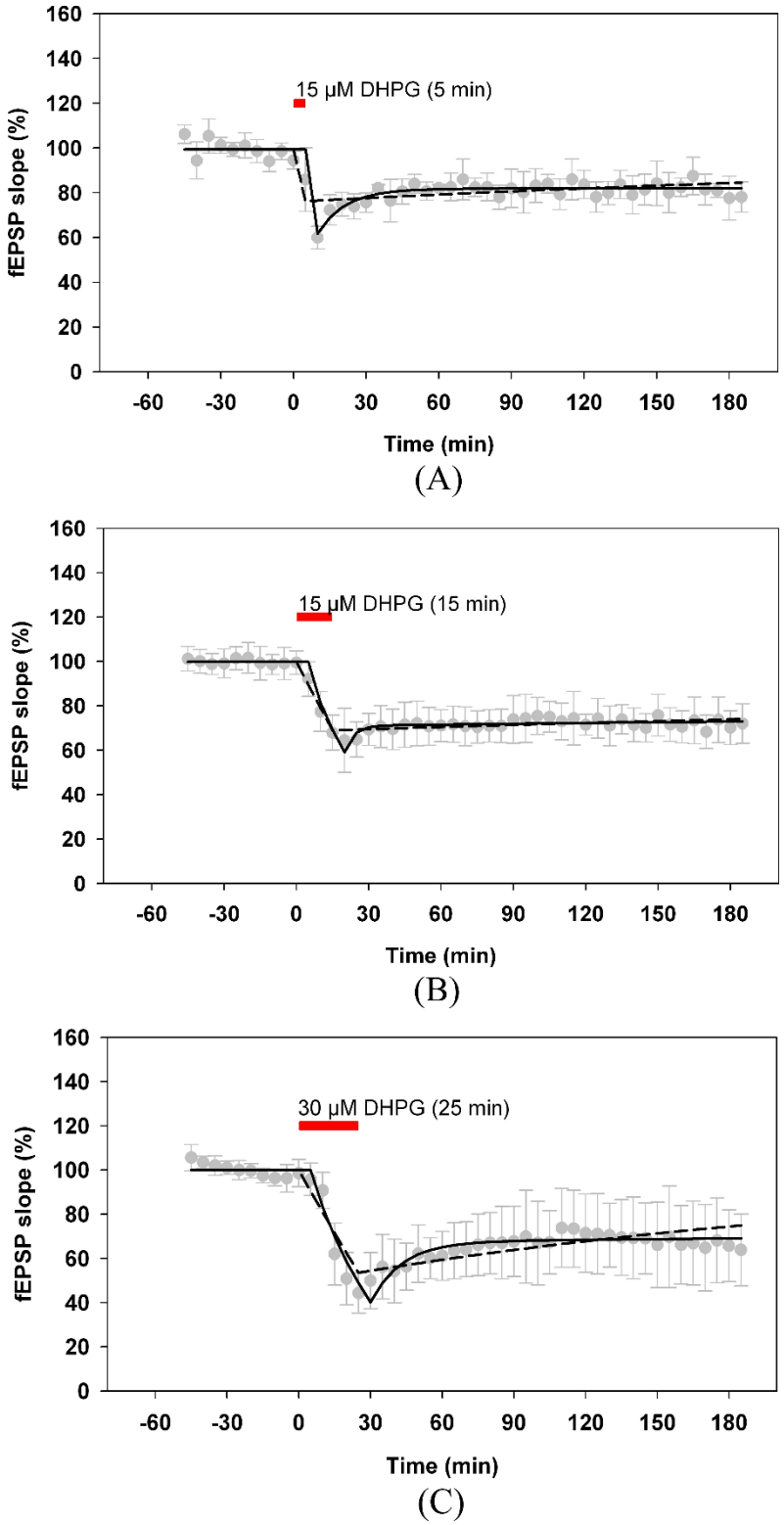

Figure IV.3. Measured mean LTD response curve + / -std (grey) with corresponding best first-order model (dashed line) and best second-order model (solid line) for data sets with sampling frequency of 0.0033 Hz. (A) Data set 1 (5 minutes application of 15 µM DHPG). (B) Data set 2 (15 minutes application of 15 µM DHPG). (C) Data set 3 (25 minutes application of 30 µM DHPG).

additional experiments were carried out with a sampling frequency of 0.033 Hz (see data set 4 in Table IV.1).

For this data set, a first-order model was calculated with an R_T^2 of 0.90 (see Table IV.2 and Figure IV.4). Since the magnitude of the pole is smaller than one, the model is stable. The corresponding time constant was 65 s (see equation 3.7), which strongly suggested the need for a sample rate higher than 0.0033 Hz. Indeed, by applying the Nyquist-Shannon sampling theorem, we find that TC/2 = 65 s/2 = 33s ≈ 30s.

This result supported that the use of a sample frequency of 0.033 Hz (or $1/30$ s^{-1}) was more appropriate for modelling the dynamics of the mGluR-LTD responses. The small TC implies a very fast response of the synaptic mechanisms induced by the mGlu-receptors' activation after exposure to DHPG.

The best third-, fourth-, and fifth-order models were excluded because of overparameterization (*YIC* and *AIC*; see Tables IV.4-6). Therefore, the best higher-order model for the fast sampled data set was once more a second-order model with $n = m = 2$ (see Table IV.3). For this model, the R_T^2- value was 0.89, and the fit was similar to the one of the first-order model (see Figure IV.4). Again, one pole was close to unity, which confirms the previous suggestion of an integrator effect. In addition, the sum of the numerator parameters of the second-order TF model was almost equal to zero ($b_0 + b_1 = -0.0013$; see Table IV.3), which could imply a switch-like effect of the DHPG input on the synaptic efficacy (cf. $t = 0$ in Figure IV.4). This effect can be shown starting from x, the noise-free output of the general TF model equation (see equation 3.1 and Table IV.3):

$$x_t = 1.6023x_{t-1} - 0.6037x_{t-2} - 0.3957u_t + 0.3944u_{t-1} \qquad (4.1)$$

The synapses react especially at the start of the drug application for which $u_t \neq u_{t-1}$ (e.g., for t = 0 in Figure IV.4). When the applied drug concentration is steady, the effect of the drug will saturate, and there will be a neglible effect on the synaptic outputs since $0.3957u_t \approx 0.3944u_{t-1}$ for $u_t = u_{t-1}$.

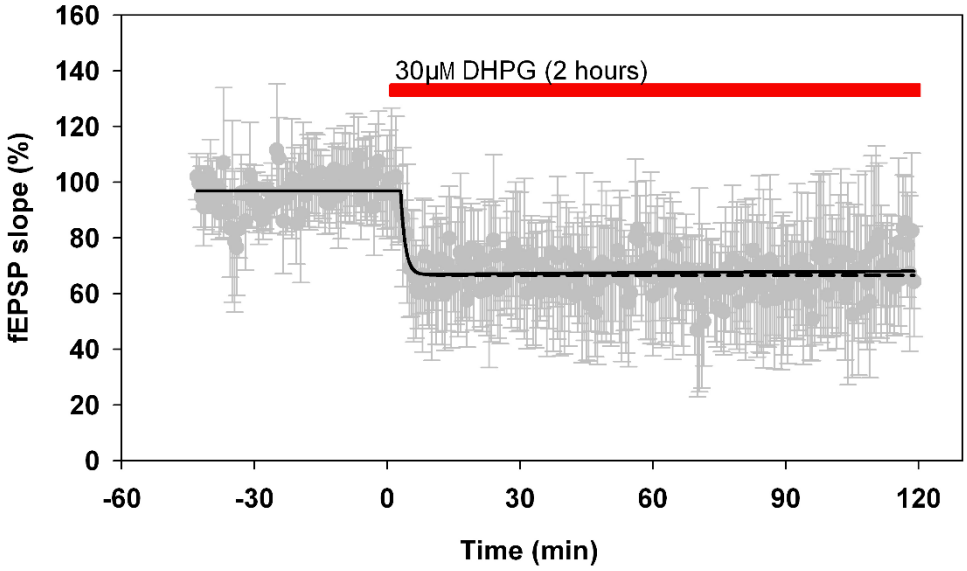

Figure IV.4. Measured mean LTD response curve +/-std (grey) with corresponding best first-order model (dashed line) and best second-order model (solid line) for data set with sampling frequency of 0.033 Hz: data set 4 (2 hours application of 30 μM DHPG).

Table IV.2. Best first order models for mean LTD responses of dataset 1, 2, 3 and 4. For each model, the parameters, a_1 and b_0, with corresponding standard errors, SE, the pole, the time delay, the time constant and the three model selection criteria, YIC, AIC and R_T^2 , are shown.

Dataset	1	2	3	4
a1	-0.9876	-0.9947	-0.9809	-0.6299
SE (a1)	0.0034	0.0012	0.0025	0.0683
b0	-1.5411	-0.6895	-0.3221	-0.3733
SE (b0)	0.0944	0.0159	0.0129	0.0684
Pole 1	0.9876	0.9947	0.9809	0.6299
Time delay	0	0	0	5
YIC	-7.277	-11.168	-8.979	-5.352
AIC	-14.246	-18.391	-15.769	-13.357
RT2	0.82	0.97	0.92	0.90
Time constant	401 min	941 min	259 min	65 sec

Table IV.3. Best second order models for mean LTD responses of dataset 1, 2, 3 and 4. For each model, the parameters, a_i and b_i, with corresponding standard errors, SE, the poles, the time delay and the three model selection criteria, YIC, AIC and R_T^2 , are shown.

Dataset	1	2	3	4
a_1	-1.6460	-1.2649	-1.6797	-1.6023
a_2	0.6462	0.2664	0.6802	0.6037
SE (a_1)	0.0980	0.1526	0.0668	0.0661
SE (a_2)	0.0968	0.1517	0.0657	0.0644
b_0	-2.5036	-1.2348	-0.5586	-0.3957
b_1	2.0891	0.7643	0.4888	0.3944
SE (b_0)	0.1861	0.1016	0.0394	0.0636
SE (b_1)	0.1830	0.0861	0.0300	0.0655
Pole 1	0.9993	0.9979	0.9985	0.9965
Pole 2	0.6467	0.2670	0.6812	0.6058
Time delay	1	1	1	5
YIC	-5.491	-4.461	-7.051	-5.075
AIC	-17.452	-18.559	-19.349	-20.824
R_T^2	0.90	0.97	0.96	0.89

Table IV.4. Best third order models for mean LTD responses of dataset 1, 2, 3 and 4. For each model, the parameters, a_i and b_i, with corresponding standard errors, SE, the poles, the time delay and the three model selection criteria, YIC, AIC and R_T^2 , are shown.

Dataset	1	2	3	4
a_1	-1.6419	-1.6488	-1.6287	-0.4663
$a2$	1.0978	1.0505	1.6518	-0.7413
a_3	-0.4469	-0.3988	-0.9983	0.5155
SE (a_1)	0.1264	0.0992	0.0485	0.1190
SE (a_2)	0.2042	0.1562	0.0754	0.0333
SE (a_3)	0.0916	0.0634	0.0447	0.0965
b_0	-1.2057	-0.5003	-0.4316	-0.3078
SE (b_0)	0.1304	0.0391	0.0229	0.0597
Pole 1	0.9887	0.9961	0.9820	-0.9290
Pole 2	0.3266 + 0.5876i	0.3264 + 0.5421i	0.3234 + 0.9550i	0.6976 + 0.2611i
Pole 3	0.3266 - 0.5876i	0.3264 - 0.5421i	0.3234 - 0.9550i	0.6976 - 0.2611i
Time delay	0	0	1	5
YIC	-4.517	-6.819	-7.798	-4.202
AIC	-15.627	-19.610	-15.983	-13.956
R_T^2	0.88	0.98	0.95	0.90

Table IV.5. Best fourth order models for mean LTD responses of dataset 1, 2, 3 and 4. For each model, the parameters, a_i and b_i, with corresponding standard errors, SE, the poles, the time delay and the three model selection criteria, YIC, AIC and R_T^2 , are shown.

Dataset	1	2	3	4
$a1$	-1.0083	-0.8915	-0.7273	-0.6963
a_2	0.5637	-0.7150	0.1873	0.3348
a_3	-1.2373	1.1301	0.4901	-0.9508
a_4	0.6825	-0.5208	-0.9026	0.6290
$SE\ (a_1)$	0.1305	0.3462	0.9933	0.0963
$SE\ (a_2)$	0.1446	0.7833	1.6126	0.0152
$SE\ (a_3)$	0.1322	0.6521	1.5920	0.0401
$SE\ (a_4)$	0.0953	0.2132	0.9492	0.0813
b_0	-2.5547	-0.6667	-0.4100	-0.3164
$b1$	0.6144	/	-0.4143	/
$b2$	-1.0944	/	/	/
$b3$	2.0306	/	/	/
$SE\ (b_0)$	0.1730	0.1310	0.0981	0.0610
$SE\ (b_1)$	0.3733	/	0.4034	/
$SE\ (b_2)$	0.3892	/	/	/
$SE\ (b_3)$	0.2788	/	/	/
Pole 1	-0.3343 + 0.9466i	-1.0963	-0.9012	-0.4188 + 0.8930i
Pole 2	-0.3343 - 0.9466i	0.9972	0.3234 + 0.9568i	-0.4188 - 0.8930i
Pole 3	0.9993	0.4953 + 0.4807i	0.3234 - 0.9568i	0.7669 + 0.2416i
Pole 4	0.6776	0.4953 - 0.4807i	0.9818	0.7669 - 0.2416i
Time delay	1	0	1	5
YIC	-2.912	-0.626	1.551	-4.845
AIC	-16.121	-16.562	-14.685	-13.751
R^2_T	0.91	0.92	0.95	0.90

Table IV.6. Best fifth order models for mean LTD responses of dataset 1, 2, 3 and 4. For each model, the parameters, a_i and b_i, with corresponding standard errors, SE, the poles, the time delay and the three model selection criteria, YIC, AIC and R_T^2 , are shown.

Dataset	1	2	3	4
$a1$	-1.6929	-1.6448	-2.8434	-2.1691
a_2	1.4738	1.2572	4.2018	2.7489
a_3	-1.3863	-1.0204	-3.9144	-2.5458
$a4$	1.0345	0.6737	2.1179	1.4222
a_5	-0.4212	-0.2635	-0.5550	-0.3166
SE (a_1)	0.0989	0.3856	0.1297	0.3362
SE (a_2)	0.1997	0.9554	0.3402	0.6293
SE (a_3)	0.2200	1.0285	0.4133	0.7053
SE (a_4)	0.1830	0.6094	0.2802	0.6170
SE (a_5)	0.0753	0.1600	0.0824	0.2516
$b0$	-1.2739	-0.5325	-0.1454	-0.1396
SE (b_0)	0.1112	0.0877	0.0165	0.0487
Pole 1	-0.2314 + 0.8360i	-0.2010 + 0.7271i	0.3383 + 0.9512i	0.0979 + 0.9914i
Pole 2	-0.2314 - 0.8360i	-0.2010 - 0.7271i	0.3383 - 0.9512i	0.0979 - 0.9914i
Pole 3	0.9911	0.9973	0.9864	0.7283 + 0.2949i
Pole 4	0.5823 + 0.4751i	0.5247 + 0.4347i	0.5902 + 0.4513i	0.7283 - 0.2949i
Pole 5	0.5823 - 0.4751i	0.5247 - 0.4347i	0.5902 - 0.4513i	0.5167
Time delay	0	0	0	5
YIC	-4.611	-2.554	-5.859	-2.187
AIC	-16.097	-17.239	-18.641	-15.344
R^2_T	0.92	0.95	0.96	0.90

Table IV.6. First order models, TF1 and TF2, obtained after decomposing the second order models for parallel and feedback configuration (see Figure IV.2).

	TF1				TF2			
Configuration	$a1$	$b0$	Pole	Time constant	$a1$	$b0$	Pole	Time constant
Parallel	-0.9965	0.0002	0.9965	24 hrs	-0.6058	-0.3959	0.6058	59.9 sec
Feedback	-0.6058	-0.3958	0.6058	59.8 sec	-0.9967	-0.0006	0.9967	25.2 hrs

4.2 Model-Based Identification of Dominant Subprocesses

Interestingly, since for all data sets consequently, accurate second-order models were found (see Table IV.3), it is suggested that two coupled dominant processes underlie mGluR-LTD. From a mathematical point of view, two possible configurations of first-order models were suggested: a parallel circuit and a feedback circuit (see Figure IV.2). The serial configuration was mathematically impossible for this model structure ($n = m = 2$; see Table IV.3) and could be excluded. The model characteristics of the first-order models for the feedback and parallel solution are shown in Table IV.7. For both configurations, the time constants indicate one slow and one fast subprocess. Future experiments are suggested in which several inhibitors or agonists of specific underlying pathways would be applied in order to further identify the most appropriate configuration and link the identified parameter values of the submodules with specific clusters of physiological pathways obtaining a data-based mechanistic model for mGluR-LTD.

5. DISCUSSION

Synapses are extremely dynamic structures. The effect of a signal transmitted synaptically from one neuron to another can vary enormously, depending on the recent history of activity at either or both sides of the synapse, and such variations can last from milliseconds to months (Abbott & Regehr, 2004). On a timescale of a few minutes, neuronal plasticity is mediated by local protein trafficking, while in order to sustain modifications beyond 2 to 3 hours, changes of gene expression are required (Martin et al., 2000; Groc & Choquet, 2006; Broccard, Pegoraro, Ruaro, Altafini, & Torre, 2009). Recent advances of imaging techniques have made it possible to visualize and quantify synaptic changes on a timescale of months or years. These studies have shown that synapses have many dynamic properties that appear (and disappear) repeatedly over time (Hou et al., 2006; Kondo & Okabe, 2011). Therefore,

dynamical analyses of synaptic plasticity can highly contribute to fully comprehending the underlying synaptic mechanisms.

In many studies, electrophysiological brain slice recordings are used to measure the synaptic strength and analyse the different forms of synaptic plasticity. However, in most studies, the fEPSP recordings are only statically analysed and the fEPSP slopes are compared for only one time point or a limited number of time points after the induction of LTD or LIP. To our knowledge, it is the first time that fEPSP slopes of mGluR-LTD responses are dynamically described using TF models. To quantify the dynamics of the responses, the sampling frequency of the fEPSP recordings has to be high enough (Nyquist, 1928). From the literature, it can be derived that a wide variety of sampling frequencies is used for electrophysiological brain slice recordings ranging from 0.05 Hz (Xu, Chen, Zhang, & Chen, 2010; Li, Kuhn, Wilson, & Lewis, 2007) to 0.0033 Hz (Ahmed et al., 2011; Popkirov & Manahan-Vaughan, 2011) and that there is no consensus about an optimal sampling frequency. The modelling results have shown that a sampling frequency of 0.0033 Hz is not sufficient to completely capture the dynamics. A sampling frequency of 0.033 Hz would be optimal from a mathematical point of view; however, several studies suggest that higher sampling frequencies (e.g., 0.033 Hz) can influence the strength and time course of synaptic plasticity responses (Villarreal, Do, Haddad, & Derrick, 2001; Volianskis & Jensen, 2003). Therefore, it is expected that the optimal sampling frequency has to find a balance between both effects and will lie in the interval between both sampling frequencies.

For all TF models, the sum of the denominator parameters was nearly -1 (see Table IV.3), suggesting an integrator effect. Integration of information across time is a neural computation of critical importance to a variety of higher cognitive brain functions (Goldman, Compte, & Wang, 2009). Interestingly, for all data sets, the same model structure was also found (with $n = m = 2$; see Table IV.3). These second-order models could be decomposed into two first-

order models and suggest that two major subprocesses underlie mGluR-LTD: one slow and one fast subprocess (see Table IV.7). A parallel circuit and a feedback circuit were suggested as candidate configurations of these two subprocesses. The next step is to link the first-order models and the candidate configurations with knowledge of the underlying mechanisms. Recently a number of articles have been published reviewing the mechanisms of mGluR-dependent LTD, including Collingridge et al. (2010) and Lüscher and Huber (2010). Given the multiple signalling cascades that have been reported to be involved in mGluR-LTD, it is difficult to allocate the slow and fast time constants to particular molecular processes. This is complicated by the fact that there is obviously not a single type of mGluR-LTD but rather a family of related forms that differ in the degree to which certain signalling cascades are involved, depending on such parameters as developmental stage, species, strain, brain regions, and measuring conditions, to mention just a few. However, we think that the fast time constants describe the fast processes immediately after induction mediated by activation of the ERK/MAPK pathway and tyrosine dephosphorylation (e.g., of GluR2) with the tyrosine phosphatase striatal-enriched tyrosine phosphatase (STEP) as a main player. This will initiate AMPAR endocytosis and a reduction of surface AMPA receptors, resulting in a net depression of synaptic transmission. We doubt that rapid dendritic protein synthesis is of major importance under our conditions because in pilot experiments, we did not see significant effects when translation inhibitors were bath-applied during the induction of mGluR-LTD. Thus, we predict that the fast time constant does not involve translation-dependent mechanisms. Rather, we anticipate that application of inhibitors of ERK1 /2 or MEK (e.g., SL327), (Ajay & Bhalla, 2004; see Sweatt, 2004, for review) and of tyrosine phosphatases (Gladding et al., 2009) will interfere with the fast time constants. A complementary role for a Rap1-induced activation of p38 mitogen-activated protein kinase (p38 MAPK) in this short time range can be tested with inhibitors such as SB203580 (Huang, You, Wu, & Hsu, 2004; Moult et al., 2008). The slow time constant, in contrast, is likely to reflect structural changes, for example, in spine number and morphology, that were

demonstrated in other models of synaptic plasticity to be protein-synthesis-dependent and to occur on a timescale of hours (Fifkova & Van, 1977; Fukazawa et al., 2003; Lamprecht & LeDoux, 2004; Raymond, 2007). Thus, we expect that long-term application of translation inhibitors will affect the slow time constant.

Many studies show the presence of feedback loops in cellular control systems (Mitrophanov & Groisman, 2008). Moreover, to achieve integrators, typically positive feedback loops are incorporated in neural models (Goldman et al., 2009). Further investigations are required to link the sub- processes with existing a priori knowledge about mechanisms underlying mGluR-LTD and to eliminate unlikely configurations.

Although neural mechanisms are known to contain many nonlinearities, the linear TF models were able to describe the dynamics of the mGluR-responses and uncover information about the underlying mechanisms without knowing all details of this form of LTD (for more detailed explanations on the use of local linear approximations of non-linear processes: see 3.2 The dynamic process model). These modelling results confirm other studies in which discrete-time linear TF models and linear system identification techniques were used for modelling different kinds of brain signals (Liu, Birch, & Allen, 2003; Westwick, Pohlmeyer, Solla, Miller, & Perreault, 2006; Behrend et al., 2009).

Thus, the models can help identify the data structures and algorithms that are used in mammalian cortex to support successive acts of the basic cognitive tasks of memorization, a central open question of computational neuroscience (Valiant, 2005). The discrete-time TF models are interesting to investigate mGlu receptor-dependent LTD because of their computational and conceptional simplicity and since they are able to combine the advantages of a data-based approach (accurate models) with a mechanistic approach (meaningful parameters).

This study suggests that the dynamic data-based modelling approach can be a valuable tool for reverse engineering of mGluR-dependent LTD responses. Moreover, this approach can be extended to other forms of LTD and LTP using other induction protocols as input for the TF models. It is expected that such system identification methods can aid in unravelling the complexities of synaptic function and its role in disease.

6. REFERENCES

1. Abbott, L. F., & Regehr, W. G. (2004). Synaptic computation. Nature, 431,796-803.

2. Ahmed, T., Sabanov, V., D'hooge, R., & Balschun, D. (2011). An N-methyl-d-aspartate-receptor dependent, late-phase long-term depression in middle-aged mice identifies no GluN2-subunit bias. Neuroscience, 185, 27-38.

3. Ajay, S. M., & Bhalla, U. S. (2004). A role for ERKII in synaptic pattern selectivity on the time-scale of minutes. European journal of Neuroscience, 20, 2671-2680.

4. Akaike, H. (1974). A new look at the statistical model identification. IEEE Transactions on Automatic Control, 19, 716-723.

5. Balschun, D., Wolfer, D. P., Gass, P., Mantamadiotis, T., Welzl, H., Schutz, G., et al. (2003). Does cAMP response element-binding protein have a pivotal role in hippocampal synaptic plasticity and hippocampus-dependent memory? Journal of Neuroscience, 23, 6304-6314.

6. Behrend, C. E., Cassim, S. M., Pallone, M. J., Daubenspeck, J. A., Hartov, A., Roberts, D. W., et al. (2009). Toward feedback controlled deep brain stimulation: Dynamics of glutamate release in the subthalamic nucleus in rats. Journal of Neuroscience Methods, 180, 278-289.

7. Bellone, C., Liischer, C., & Mameli, M. (2008). Mechanisms of synaptic depression triggered by metabotropic glutamate receptors. Cellular and Molecular Life Sciences, 65, 2913-2923.

8. Broccard, E, Pegoraro, S., Ruaro, M., Altafini, C., & Torre, V. (2009). Characterization of the time course of changes of the evoked electrical activity in a model of a chemically-induced neuronal plasticity. BMC Research Notes, 1,13.

9. Collingridge, G. L., Peineau, S., Howland, J. G., & Wang, Y. T. (2010). Long-term depression in the CNS. Nature Reviews Neuroscience, 11, 459-473.

10. Davidkova, G., & Carroll, R. C. (2007). Characterization of the role of microtubule-associated protein 1B in metabotropic glutamate receptor-mediated endocytosis of AMPA receptors in hippocampus. Journal of Neuroscience, 27,13273-13278.

11. Denayer, E., Ahmed, T., Brems, H., Van Woerden, G., Borgesius, N. Z., Ca llaerts-Vegh, Z., et al. (2008). Spredl is required for synaptic plasticity and hippocampus- dependent learning. Journal of Neuroscience, 28, 14443-14449.

12. Fifkova, E., & Van, H. A. (1977). Long-lasting morphological changes in dendritic spines of dentate granular cells following stimulation of the entorhinal area. Journal of Neurocytology, 6,211-230.

13. Fitzjohn, S. M., Kingston, A. E., Lodge, D., & Collingridge, G. L. (1999). DHPG- induced LTD in area CAl of juvenile rat hippocampus: Characterisation and sensitivity to novel mGlu receptor antagonists. Neuropharmacology, 38,1577-1583.

14. Fitzjohn, S. M., Palmer, M. J., May, J. E., Neeson, A., Morris, S. A., & Collingridge, G. L. (2001). A characterisation of long-term depression induced by metabotropic glutamate receptor activation in the rat hippocampus in vitro. Journal of Physiology, 537,421-430.

15. Fukazawa, Y., Saitoh, Y., Ozawa, E, Ohta, Y., Mizuno, K., & Inokuchi, K. (2003). Hippocampal LTP is accompanied by enhanced F-actin content within the dendritic spine that is essential for late LTP maintenance in vivo. Neuron, 38,447-460.

16. Cladding, C. M., Collett, V. J., Jia, Z., Bashir, Z. I., Collingridge, G. L., & Molnar, E. (2009). -tyrosine dephosphorylation regulates AMPAR internalisation in mGluR-LTD. Molecular and Cellular Neuroscience, 40, 267-279.

17. Gladding, C. M., Fitzjohn, S. M., & Molnar, E. (2009). Metabotropic glutamate receptor-mediated long-term depression: Molecular mechanisms. Pharmacological Reviews, 61, 395-412.

18. Goldman, M. S., Compte, A., Sr Wang, X. J. (2009). Neural integrator models. Encyclopedia of Neuroscience, 6, 165-178.

19. Graupner, M., & Brunel, N. (2010). Mechanisms of induction and maintenance of spike-timing dependent plasticity in biophysical synapse models. Frontiers in Computational Neuroscience, 4, 136.

20. Groc, L., & Choquet, D. (2006). AMPA and NMDA glutamate receptors trafficking: Multiple roads for reaching and leaving the synapse. Cell and Tissue Research, 326, 423-438.

21. Hardy, S., & Robillard, P. N. (2005). Phenomenological and molecular-level Petrinet modeling and simulation of long-term potentiation. BWSystems, 82, 26-38.

22. Holbro, N., Grunditz, A., & Oertner, T. G. (2009). Differential distribution of endoplasmic reticulum controls metabotropic signaling and plasticity at hippocampal synapses. PNAS, 106,15055-15060.

23. Hou, L., Antion, M. D., Hu, D., Spencer, C. M., Paylor, R., & Klan, E. (2006). Dynamic translational and proteasomal regulation of fragile X mental retardation protein controls mGluR-dependent long-term depression. Neuron, 51, 441-454.

24. Huang, C. C., You, J. L., Wu, M. Y., & Hsu, K. S. (2004). Rapl-induced p38 mitogen-activated protein kinase activation facilitates AMPA receptor trafficking via the GDI.Rab5 complex. Potential role in (S)-3,5-dihydroxyphenylglycene-induced long term depression. Journal of Biological Chemistry, 279, 12286-12292.

25. Huber, K. M., Kayser, M. S., & Bear, M. F. (2000). Role for rapid dendritic protein synthesis in hippocampal mGluR-dependent long-term depression. Science, 288, 1254-1257.

26. Izhikevich, E. M. (2007). Dynamical systems in neuroscience. Cambridge, MA: MIT Press.

27. Jarvis, A. J., Stauch, V. J., Schulz, K., & Young, P. C. (2004). The seasonal temperature dependency of photosynthesis and respiration in two deciduous forests. Global Change Biology, 10, 939-950.

28. Kandel, E. R. (2001). The molecular biology of memory storage: A dialogue between genes and synapses. Science, 294,1030-1038.

29. Karachot, L., Shirai, Y., Vigot, R., Yamamori, T., & Ito, M. (2000). Rapidly turned over protein maintains metabotropic synaptic transmission in Purkinje cells. Neuroreport, 11 , 2903-2906.

30. Kemp, N., McQueen, J., Faulkes, S., & Bashir, Z. I. (2000), Different forms of LTD in the CAl region of the hippocampus: Role of age and stimulus protocol. European journal of Neuroscience, 1,360-366.

31. Kim, A., Lazar, A., & Slutskiy, Y. (2011). System identification of Drosophila olfactory sensory neurons. Journal of Computational Neuroscience, 1, 143-161.

32. Kleppisch, T., Voigt, V., Altmann, R., & Offermanns, S. (2001). G(alpha)q-deficient mice lack metabotropic glutamate receptor-dependent long-term depression but show normal long-term potentiation in the hippocampal CA] region. Journal of Neuroscience, 21, 4943-1948.

33. Kondo, 5., & Okabe, S. (2011). Turnover of synapse and dynamic nature of synaptic molecules in vitro and in vivo. Acta Histochem Cytochem, 44, 9-15.

34. Lamprecht, R., & LeDoux, J. (2004). Structural plasticity and memory. Nature Reviews Neuroscience, 5,45-54.

35. Li, Q., Kuhn, C. M., Wilson, W. A., & Lewis, D. V. (2007). Effects of gamma hydroxybutyric acid on inhibition and excitation in rat neocortex. Neuroscience, 150, 82-92.

36. Liu, Y., Birch, A. A., & Allen, R. (2003). Dynamic cerebra] autoregulation assessment using an ARX model: Comparative study using step response and phase shift analysis. Cell and Tissue Research, 25,647-653.

37. Ljung, L. (1987). System identification: Theory for the user. Englewood Cliffs, NJ: Prentice Hall.

38. Liischer, C., & Huber, K. (2010). Group 1 mGluR-dependent synaptic long-term depression: Mechanisms and implications for circuitry and disease. Neuron, 65, 445-459,

39. Malenka, R. C., & Bear, M. F. (2004). LTP and LTD: An embarrassment of riches. Neuron, 44, 5-21.

40. Mameli, M., Balland, B., Lujan, R., & Liischer, C. (2007). Rapid synthesis and synaptic insertion of GluR2 for mGluR-LTD in the ventral tegmental area. Science, 317, 530-533.

41. Manninen, T., Hituri, K., Kotaleski, J. H., Blackwell, K. T., & Linne, M.-L. (2010). Post-synaptic signal transduction models for long-term potentiation and depression. Frontiers in Conzputational Neuroscience, 4,152.

42. Martin, S. j., Grimwood, P. D., & Morris, R. G. (2000). Synaptic plasticity and memory: An evaluation of the hypothesis. Annual Review of Neuroscience 2000, 23, 649-711.

43. Massey, P. V, & Bashir, Z. L (2007). Long-term depression: Multiple forms and implications for brain function. Trends in Neurosciences, 30, 176-184.

44. Mitrophanov, A. Y., & Groisman, E. A. (2008). Positive feedback in cellular control systems. Bioassays, 30, 542-555.

45. Moult, P. R., Collingridge, G. L., Fitzjohn, S. M., & Bashir, Z. I. (2008). Co-activation of p38 mitogen-activated protein kinase and protein tyrosine phosphatase underlies metabotropic glutamate receptor-dependent long-term depression. Journal of Physiology, 586,2499-2510.

46. Moult, P. R., Cladding, C. M., Sanderson, T. M., Fitzjohn, S. M., Bashir, Z. I., Molnar, E., et al. (2006). Tyrosine phosphatases regulate AMPA receptor trafficking during metabotropic glutamate receptor-mediated Iong-term depression. Journal of Neuroscience, 26, 2544-2554.

47. Neves, G., Cooke, S. E, & Bliss, T.V. F. (2008). Synaptic plasticity, memory and the hippocampus: A neural network approach to causality. Nature Reviews Neuroscience,9, 65-75,

48. Nieus, T., Sala, E., Mapelli, J., Saftenku, E., Rossi, P., & D'Angelo, E. (2006). LTP regulates burst initiation and frequency at mossy fiber-granule cell synapses of rat cerebellum: Experimental observations and theoretical predictions. Journal of Neurophysiology, 95, 686-699.

49. Nosyreva, E. D., & Huber, K. M. (2006). Metabotropic receptor-dependent long-term depression persists in the absence of protein synthesis in the mouse model of fragile X syndrome. journal of Neurophysiology, 95, 3291-3295.

50. Nyquist, H. (1928). Certain topics in telegraph transmission theory. AIEEE Transactions, 47,617-644.

51. Pedoto, G., Santaniello, S., Montgomery, E. B., Gale, J. T., Fiengo, G., Glieimo, L., et al. (2010). System identification of local field potentials under deep brain stimulation in a healthy primate. In Proceedings of the 2010 Annual International Conference of the IEEE: Engineering in Medicine and Biology Society (pp. 4144-4147). Piscataway, NJ: IEEE.

52. Popkirov, S. G., & Manahan-Vaughan, D. (2011). Involvement of the metabotropic glutamate receptor mOuR5 in NMDA receptor-dependent, learning-facilitated long-term depression in CAl synapses. Cerebral Cortex, 21, 501.

53. Raymond, C. R. (2007). LIP forms 1,2 and 3: Different mechanisms for the "long" in long-term potentiation. Trends in Neurosciences, 30,167-175.

54. Richter, J. D., & Klann, E. (2009). Making synaptic plasticity and memory last: Mechanisms of translational regulation. Genes and Development, 23, 1-11.

55. Shouval, H. Z., Bear, M. F., & Cooper, L. N. (2002). A unified model of NMDA receptor-dependent bidirectional synaptic plasticity. PN AS, 99,10831— 10836.

56. Snyder, E. M., Philpot, B. D., Huber, K. M., Dong, X., Fallon, J. R., & Bear, M. F. (2001). internalization of ionotropic glutamate receptors in response to mGluR activation. Nature Neuroscience, 4,1079-1085.

57. Sontag, E. D. (2004). Some new directions in control theory inspired by systems biology. Systems Biology, 1, 9-18.

58. Sweatt, J. D. (2004). Mitogen-activated protein kinases in synaptic plasticity and memory. Current Opinion in Neurobiology, /4,311-317.

59. Tambuyzer, T., Ahmed, T., Berckmans, D., Balschun, D., & Aerts, J. (2011). Reverse engineering of metabotropic glutamate receptor-dependent long-term depression in the hippocampus. EMC Neuroscience 2011, U(Suppl. 1), P1.

60. Taylor, C. J., Ped regal, D. J., Young, P. C., & Tych, W. (2007). Environmental time series analysis and forecasting with the CAPTAIN toolbox. Environmental Modelling and Software, 22, 797-814. http:/ /www.eslancs.ac.uk/cres/captain /

61. Tomlin, C. J., & Axelrod, J. D. (2005). Understanding biology by reverse engineering the control. PNAS, 102, 4219-4220.

62. Valiant, L. G. (2005). Memorization and association on a realistic neural model. Neural Computation, 17,527-555.

63. Villarreal, D. M., Do, V, Haddad, E., & Derrick, B. E. (2001). NMDA receptor an-tagonists sustain LTP and spatial memory: Active processes mediate LIT decay. Nature Neuroscience, 1,48-52.

64. Volianskis, A., & Jensen, M. S. (2003). Transient and sustained types of long-term potentiation in the CAl area of the rat hippocampus. Journal of Physiology, 2, 459-492.

65. Westwick, D. T., Pohlmeyer, E. A., Solla, S. A., Miller, L. E., & Perreault, E. J. (2006). Identification of multiple-input systems with highly coupled inputs: Application to EMG prediction from multiple intracortical electrodes. Neural Computation, 18, 329-355.

66. Wu, M.C.K., David, S. V., & Gallant, J. L. (2006). Complete functional characterization of sensory neurons by system identification. Annual Review of Neuroscience 2006, 477-505.

67. Xu, J. Y., Chen, R., Zhang, J., & Chen, C. (2010). Endocannabinoids differentially modulate synaptic plasticity in rat hippocampal CAl pyramidal neurons. PLoS ONE, 5, e10306.

68. Young, P. C. (1984). Recursive estimation and time-series analysis. Berlin: Springer-Verlag.

69. Zhang, Y., Venkitaramani, D. V., Gladding, C. M., Zhang, Y., Kurup, P., Molnar, E., Collingridge, G. L., et al. (2008). The tyrosine phosphatase STEP mediates AMPA receptor endocytosis after metabotropic glutamate receptor stimulation. Journal of Neuroscience, 28, 10561-10566.

70. Zho, W. M., You, J. L., Huang, C. C., & Hsu, K. S. (2002). The group I metabotropic

71. glutamate receptor agonist (S)-3, 5-dihydroxyphenylglycine induces a novel form of depotentiation in the CAl region of the hippocampus. Journal of Neuroscience, 20, 8838.

GENERAL CONCLUSIONS

Individual biological process:

In this chapter we described electrophysiological brain slice recordings of synaptic plasticity responses to unravel part of the underlying physiological mechanisms.

As shown in this study, it is a challenge to find the optimal sampling frequency for the measurements, since higher **sampling frequencies** can influence the strength and time course of the synaptic plasticity responses. Similarly to chapter 2 and 3, this case suggests that for some biological processes the sampling frequency itself can induce the activation of physiological mechanisms which affect the time course of the measured bio-responses and their underlying processes. In contrast with the other chapter, the biological mechanisms were at cellular level (**spatial scale**). To obtain reliable and clear synaptic plasticity responses, the specific positioning and optimal stimulation parameters of the electrodes are of utmost importance. Therefore, available biological knowledge on the **hippocampal structure** and the cellular connections are essential for accurate experiments.

Process models and model-based features:

Whereas the previous chapters focused mainly on the model noise of single-output models (detrended time series), this study aimed at quantifying the **model structure** and **time constants** of the responses based on the input-output models. Accurate models were obtained and the model structure suggested the presence of two major underlying subprocesses. Based on the estimated times constants, links with existing pathways were suggested. Since the calculated models were data-based and the fact that we could link the models with underlying physiology, the obtained models are **data-based mechanistic models**. Thus, although neural mechanisms are known to contain many **nonlinearities**, the **linear models** were able to describe the dynamics and uncover information about the underlying mechanisms without knowing all details of this form of synaptic plasticity (see hypothesis 3 in Part 1).

Individualised change detection:

In future drug experiments, such models could be used to detect changes in model structures reflecting activation or inhibition of underlying mechanisms. Thus, the results suggest that model structure could be used for **individualised model-based monitoring** of biological processes.

CHAPTER V

Conceptualization and validation of an open-source closed-loop deep brain stimulation system in rat

Adapted from: Wu, H., Ghekiere, H., Beeckmans, D., Tambuyzer, T., Van Kuyck, K., Aerts, J. M., & Nuttin, B. (2015). Conceptualization and validation of an open-source closed-loop deep brain stimulation system in rat. *Scientific reports*, *4*, srep09921.

BROADER PERSPECTIVE

This chapter describes another example of **individualised monitoring**. The main objective was to develop an individualised closed-loop deep brain stimulation system that can suppress locomotion in rats. Theta oscillations in the hippocampus (output variable) are highly related with locomotion, while electrical stimulation in the mesencephalic reticular formation (input variable) induces freezing. Starting from these two biological insights we hypothesised that it is possible to develop a control system for suppression of locomotion in rodents. However, since there are many factors leading to **inter-individual differences** (electrode location, size and shape of brain region, activity of brain cells, animal behaviour, …) an individualised approach is necessary. Other than the previous case studies, this chapter focused on **frequency analysis** instead of time series analysis, but the following steps correspond with the general scheme of the PhD. **Features** (i.e. power spectral densities at specific theta frequencies) will be extracted from the bio-signals and **individualised thresholds** will be calculated based on a fixed period of individual **baseline** measurements (See hypothesis 4 in Part 1).

To conclude, this chapter will present an approach for individualised monitoring of brain signals (i.e. local field potentials) in rodents. In fact, this chapter will go one step further by also implementing the monitoring approach in a control system allowing **individualised interventions** (individual stimulation parameters for deep brain stimulation; link to hypothesis 3 in Part 1).

1. ABSTRACT

Conventional deep brain stimulation (DBS) applies constant electrical stimulation to specific brain regions to treat neurological disorders. Closed-loop DBS with real-time feedback is gaining attention in recent years, after proved more effective than conventional DBS in terms of pathological symptom control clinically.

Here we demonstrate the conceptualization and validation of a closed-loop DBS system using open-source hardware. We used hippocampal theta oscillations as system input, and electrical stimulation in the mesencephalic reticular formation (mRt) as controller output. It is well documented that hippocampal theta oscillations are highly related to locomotion, while electrical stimulation in the mRt induces freezing. We used an Arduino open-source microcontroller between input and output sources. This allowed us to use hippocampal local field potentials (LFPs) to steer electrical stimulation in the mRt. Our results showed that closed-loop DBS significantly suppressed locomotion compared to no stimulation, and required on average only 56% of the stimulation used in open-loop DBS to reach similar effects. The main advantages of open-source hardware include wide selection and availability, high customizability, and affordability. Our open-source closed-loop DBS system is effective, and warrants further research using open-source hardware for closed-loop neuromodulation.

2. INTRODUCTION

Deep brain stimulation (DBS) is a neurosurgical technique in which electrodes are implanted stereotactically in specific parts of the brain, and by applying electric currents, symptoms of various neurological disorders can be controlled. Because it is an invasive neurosurgical treatment with inherent surgical risk, it is mainly used to treat severe and otherwise-refractory diseases. Current clinical applications of DBS include movement disorders (e.g. Parkinson's disease), epilepsy, pain, and psychiatric disorders (e.g. obsessive-compulsive disorder and major depressive disorder).

The conventional DBS system is unidirectional: it delivers electrical stimulation without receiving any neural feedback. Recent technological breakthroughs make it possible to not only stimulate, but also record brain signals from relevant brain regions (Rosin et al., 2011; Little et al., 2013). Based on neural inputs, stimulation can be adjusted in real-time, creating a closed-loop system. Closed-loop DBS has already proved to be more effective than conventional DBS in Parkinsonian symptom in animal research and clinical trials (Rosin et al., 2011; Little et al., 2013). However, the availability of closed-loop DBS systems for research use is rather limited. An ideal closed-loop DBS system for research purposes is robust, reliable, affordable, and easily customizable. The recent emergence of open-source hardware introduced affordable and highly customizable hardware for various applications. Open-source closed-loop multichannel system for single-neuron manipulation has been investigated previously (Newman et al., 2012). Here we describe conceptualization and validation of an open-source closed-loop DBS system for preclinical research purposes.

We used Arduino Uno (manufactured by Smart Projects, Italy), an open-source microcontroller, to control DBS system output (electrical stimulation) based on real-time input (neural signals). The input source is local field potentials (LFPs) from the hippocampus, and the output electrical stimulation is delivered in the mesencephalic reticular formation (mRt) in rats. Theta oscillations in the hippocampus are highly related to locomotion (Kramis et al. 1975), while electrical stimulation in the mRt induces freezing[5]. We hypothesize that our open-source closed-loop DBS system can suppress locomotion by stimulating the mRt based on real-time hippocampal theta power. To test our hypothesis, we measured the level of locomotion in rats under 4 different circumstances: no stimulation (OFF), open-loop stimulation (OL), random stimulation (RANDOM), and closed-loop stimulation (CL).

3. MATERIALS AND METHODS

Study overview. 12 male Wistar rats weighing 200–250 g were used in our study. One twisted bipolar electrode and 2 monopolar electrodes were implanted in the hippocampus and the mRt in each rat, respectively. After one week of recovery, all rats underwent 1 day of baseline measurement followed by 4 days of testing sessions. The level of locomotion of every rat during each testing session was analysed and compared statistically (see text below for more details).

This research project and the experimental protocol were approved by the KU Leuven ethics committee for laboratory experimentation (project number: P093/2012), and was in accordance with the Belgian and European laws, guidelines and policies for animal experimentation, housing and care (Belgian Royal Decree of 29 May 2013 and European Directive 2010/63/EU on the protection of animals use for scientific purposes of 20 October 2010).

Surgical procedures. Rat was anesthetized (Anesketin (0.06 mL/100 g body weight) and Domitor (0.04 mL/100 g body weight)), put on a heating pad with anal probe to keep the body temperature at approximately 37.5°C, and properly fixed in a stereotactic frame. Midline incision and three burr holes were made based on implantation trajectory (1 for hippocampus and 2 for mRt; coordinates of mRt: 5.76 mm posterior to bregma, 3.4 mm lateral to midline, 6 mm deep relative to dura, 14° to sagittal insertion angle; coordinates of hippocampus: 4 mm posterior to bregma, 2.8 mm lateral to midline, 2.7 mm deep relative to dura, 20° to sagittal insertion angle). Three surrounding burr holes were made (1 for reference screw (E363/20, PlasticsOne), 2 for anchoring screws) before 2 monopolar electrodes (E363/8, PlasticsOne) and 1 bipolar electrode (E363/8-2TW, PlasticsOne)

were implanted in the mRt and the hippocampus, respectively. After mounting reference screw and anchoring screws, dental cement was applied and a plastic pedestal (MS363, PlasticsOne) was fixed on top of rat's head, with sockets of implanted electrodes placed inside. Antisedan (0.03 mL/100 g body weight) was administered after operation was completed, and each rat was given one week of recovery.

Experimental setup. The test cage was 34334334 cm. Each rat was placed individually in the test cage for 15 minutes (Slawinska & Kasicki, 1995; Sinnamon, 2005; Chen et al., 2011) each day during baseline and testing sessions. When rat was placed in test cage, the pedestal was connected to a swivel (swivel: SL6C, PlasticsOne; wire: 363-363 (CS), PlasticsOne). LFP was recorded in every rat during baseline and test sessions via a custom filter device (Rossi et al., 2007) to filter out stimulation artifact, a preamplifier (66 dB) to increase signal-to-noise ratio, and a data acquisition card (NI USB-6341, National Instruments, Texas, USA; software environment: MatLab, MathWorks, Natick, MA, USA). Hippocampal LFPs were recorded at 10 kHz. To extract relevant information, two filters were applied: one Butterworth bandpass (1–300 Hz) and one notch (49–51 Hz). An Arduino Uno board was connected between processed input and stimulator output, to steer stimulation based on hippocampal LFPs. A webcam (Logitech HD Webcam Pro C910) was fixed on top of the cage to record behaviour of rat. In total 15 hours of LFPs and videos were recorded.

After one week of recovery from surgery, each rat underwent 1 day of baseline measurement and 4 days of testing period. During baseline measurement, hippo-campal theta threshold and optimal stimulation parameters were determined. During the 4-day testing period, each rat

underwent one of the 4 following intervention each day (random, non-repetitive): no stimulation (OFF), open-loop stimulation (OL), random stimulation (RANDOM) and closed-loop stimulation (CL). During OFF, no electrical stimulation was applied in the mRt; during OL, stimulation was constantly applied in the mRt; during RANDOM, certain percentage (determined during baseline measurement, see text below for details) of ''stimulation-on time'' was applied randomly; during CL, stimulation was applied only when real-time hippocampal theta power exceeded the threshold.

The percentage of movement during each 15-minute test session of each rat was then evaluated by automated video analysis (see text below for more details). We used cresyl violet staining method to examine the three implanted locations (one in right hippocampus, and two in left and right mRt). Rats with misplaced electrodes were excluded from statistical analysis.

Automated video analysis. To perform automated video analysis, an algorithm to detect movement in a video recording of a rat was developed. The two main measurements of automated video analysis were: percentage of movement, and the exact time of movement. The algorithm was based upon a Matlab script developed by Tambuyzer et al. (2012) to measure travelled distance in an experiment with rats on compulsive behavior. This algorithm was used for both baseline measurements and for movement analysis on the video recordings during testing period. In brief, the major steps of video analysis are as follows: each frame of all 15-minute videos (15 frames per second) was first converted to black & white image, and the border of the test cage was automatically detected. A specific grey-scale value was used to separate the rat (white) from background (dark), and the centroid point of

the rat was obtained for each frame. A binary value representing movement (yes/no) between frames was then calculated. Definition of movement: when the total change in centroid position over 3 consecutive frames exceeded 5 pixels (approximately 0.5 cm), the rat was considered to be moving. Lastly, percentage of movement (percentage of time during the recording that the rat spent moving), and the exact time of movement were obtained.

Baseline measurement. Two main goals were achieved during baseline measurement: calculation of hippocampal theta power threshold and optimization of mRt stimulation parameters.

The hippocampal theta power threshold was obtained during baseline measurement, and served as a real-time neurophysiological indicator of locomotion. The rat was placed in the test cage for 15 minutes during baseline measurement.

Hippocampal LFP and behaviour (video) were measured and analysed offline. Percentage of movement and exact moments of movements (time points) were extracted from behavioural measurement based on automated video analysis. Medians and standard deviations of power spectral density at specific theta frequencies (7.8 Hz and 9.8 Hz) were obtained from LFPs (window size: 500 ms, 250 ms overlap). The hippocampal theta power threshold (Threshold) was defined in the following equation:

$$Threshold = Median + threshold\ factor * standard\ deviation$$

A set of threshold factors (0.1–0.5 in 0.05 increment) was tested in both sets of median and standard deviation against behavioural data, and the combination of frequency and threshold factor with the highest accuracy to predict movement was chosen as the hippocampal theta power threshold for a rat. The time delay between the exceeding of threshold value in the LFP data and the actual start of movement seen in the video and vice versa was also taken into account, e.g. if the theta power exceeded threshold value 200 ms before the movement was detected on video, this was still considered a true positive (maximum allowed time delay: 250 ms). Stimulation was switched on for 500 ms once the real-time theta power exceeded Threshold.

Optimization of mRt stimulation parameters was done after LFP and behavioural measurements. Electrical stimulations with different frequencies, pulsewidths, and amplitudes were tested in each rat to achieve maximal freezing without observable side effects (e.g. epileptic behaviours).

After baseline measurements, a set of hippocampal theta power threshold and mRt stimulation parameters in each individual rat was obtained, and would be used in the following testing period.

Besides hippocampal theta power threshold and optimal stimulation parameters, the percentage time of locomotion would be used as the percentage of ‘‘stimulation on’’ time during RANDOM testing, with stimulation applied in random time points without regards to the rat’s behavioural state.

Statistical analysis. The percentages of ‘‘stimulation-on time’’ during RANDOM and CL were compared to examine the level of significance of the difference of sample means (paired t-test). One-way repeated measures

analysis of variance (RM-ANOVA) was used to examine if the main effect of different intervention between groups on percentage of locomotion was significant. We used Statistica (StatSoft Inc., Tulsa, OK, USA) to perform statistical analysis (the level of significance was set at 0.05 for all statistical tests).

4. RESULTS

The overview of hippocampal theta power threshold and mRt stimulation parameters of each individual rat is shown in Table V.1. Figure V.1 is the illustration of two monopolar and one bipolar electrodes implanted in the bilateral mRt and right hippocampus, respectively. In total 7 rats were included in the final analysis (5 dropouts: 4 misplaced electrodes, 1 premature death). The closed-loop hardware scheme is summarized in Figure V.2. Figure V.3 shows examples of hippocampal theta oscillations, and theta threshold during CL. The system delay time (from receiving input to actual output) was tested and estimated to be less than 100 milliseconds.

Stimulation-on time in RANDOM and CL groups. The percentage of ‘‘stimulation-on time’’ during RANDOM and CL test sessions were 43.86 +/- 0.80% and 55.57 +/- 4.56%, respectively (mean +/- standard error of the mean; paired t-test: $p>0.05$).

Effects of Different Stimulation Schemes on Movement. The percentages of movement detected by automated video analysis during the 15-minute test sessions of OFF, OL, RANDOM, and CL were 62.40 +/- 6.28%, 45.73 +/- 5.38%, 67.80 +/- 6.03%, and 44.60 +/- 5.15%, respectively. Mauchly’s test indicated that the assumption of sphericity had not been violated. RM-ANOVA showed that the effect of different interventions on percentage of movement

was significant (p = 0.012). Post hoc pairwise comparisons (with Bonferroni corrections) indicated that the mean difference between OFF and CL was significant (p = 0.042).

Figure V.4 summarizes the percentage of stimulation-on time and effect on movement during each stimulation scheme.

Table V.1. Theta threshold values (logarithmic) and corresponding theta frequencies, and stimulation parameters (amplitudes, band- widths, and frequencies) of each rat during test sessions.

	Theta threshold	Stimulation parameters
Rat 1	–13.61@7.8 Hz	300 uA, 60 us, 130 Hz
Rat 2	–13.20@9.8 Hz	220 uA, 50 us, 130 Hz
Rat 3	–13.19@9.8 Hz	400 uA, 60 us, 130 Hz
Rat 4	–13.19@9.8 Hz	210 uA, 50 us, 130 Hz
Rat 5	–13.70@7.8 Hz	210 uA, 60 us, 130 Hz
Rat 6	–13.64@7.8 Hz	200 uA, 60 us, 130 Hz
Rat 7	–13.30@7.8 Hz	160 uA, 50 us, 130 Hz

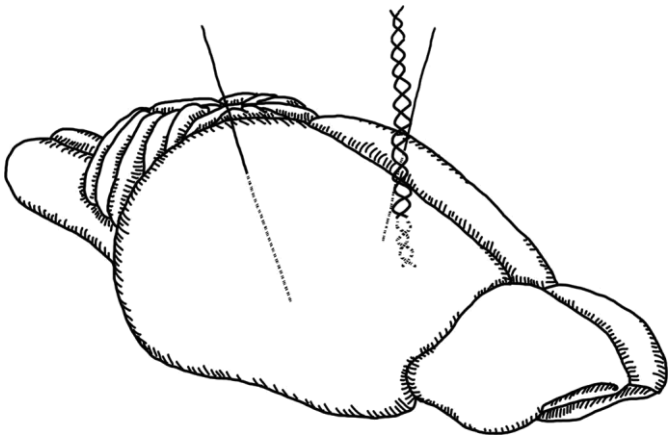

Figure V.1. One bipolar and two monopolar electrodes were implanted in the right hippocampus (recording) and bilateral mesencephalic reticular formation (stimulation), respectively. Drawing by Stephany Pei-Yen Hsiao.

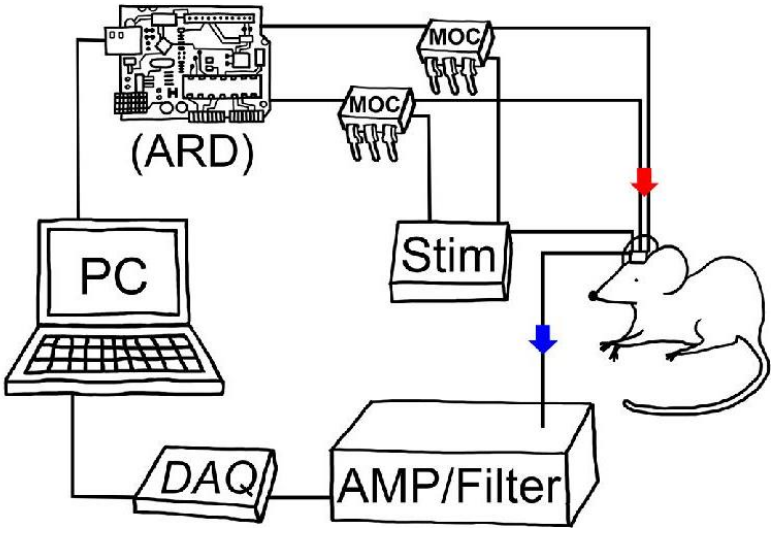

Figure V.2. Schematic illustration of the open source, closed-loop deep brain stimulation system in rats. The blue arrow indicates hippocampal local field potentials, recorded through amplifier, filter and data acquisition device, and analysed in the PC. Based on real-time theta power analysis, electrical stimulation (indicated by the red arrow) sent to the rat brain (mesencephalic reticular formation) is controlled via the Arduino board. AMP: custom amplifier, ARD: Arduino Uno board, DAQ: data acquisition card, MOC: mechanism operated cell, Stim: stimulator. Drawing by Stephany Pei-Yen Hsiao.

5. DISCUSSION

Our results showed that hippocampal-mRt closed-loop DBS significantly reduced locomotion compared to no stimulation. Open-loop mRt DBS also reduced locomotion compared to no stimulation (insignificantly in this study due to small sample size), in alignment with the results from previous study (Robinson, 1978). But with closed-loop DBS, only 55.57% of electrical stimulation was used compared to open-loop DBS to achieve similar effects. Electrical stimulation applied at random interval did not suppress locomotion, indicating that only electrical stimulation in the mRt given at the right moment can effectively suppress locomotion. Figure V.5 summarizes the key steps of our closed-loop DBS.

A dynamic system is a system whose behaviour changes over time, mostly in response to external stimulation/disturbances. A closed-loop system then, refers to a situation in which two or more dynamic systems are interconnected to each other in a cycle, such that each system influences the other and the dynamics of each system are strongly coupled. When there are two systems for instance, the first system influences the second system which in turn influences the first system by giving feedback, this feedback from the second to the first system makes the whole system a closed-loop (Aström & Murray, 2010). Based on the measured output compared to a set of reference values, the error on the system output is measured. When this error reaches a predefined threshold value, the system input is changed by a controller in order to adapt the system output, hence decreasing the error on the output to an acceptable value (Romagnoli & Palazoglu, 2012).

The advantage of a closed-loop control system lies in the fact that feedback control algorithms are designed to acquire the desired performance by altering the inputs immediately once deviations are observed regardless of what caused the disturbance (Marlin & Marlin, 1995). In the case of closed-loop neuromodulation, the central nervous system acts as controller of many body systems at organism scale (e.g. control of movement), and control of the central nervous system by DBS is a promising example of how control theory can be applied to adapt (pathological) behaviour of organisms.

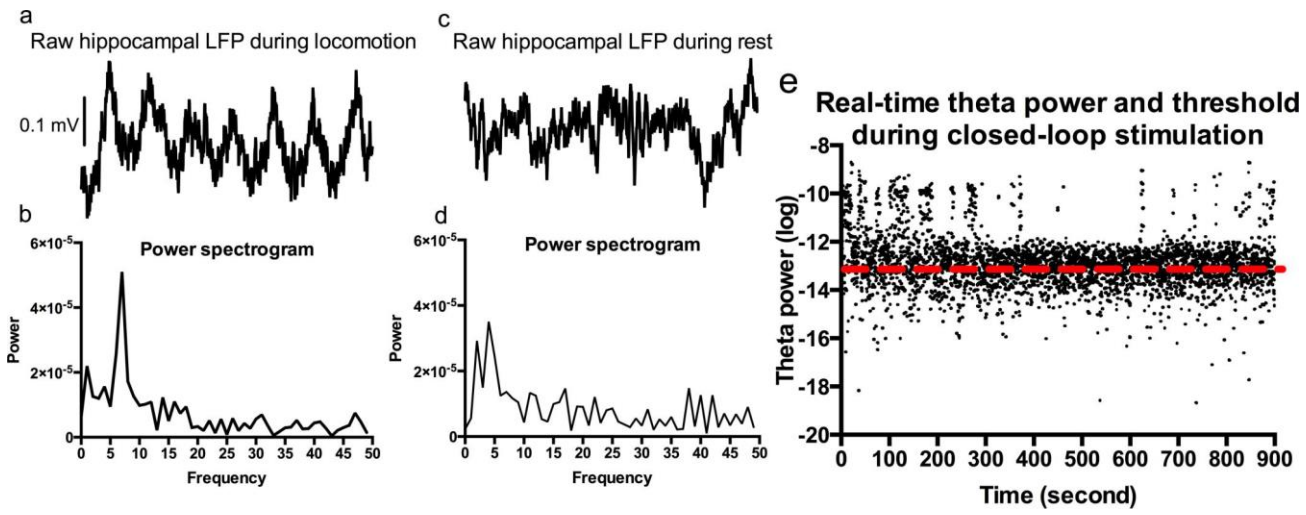

Figure V.3. Measured hippocampal LFPs and theta power during closed-loop stimulation. 3a and b: Rat hippocampal LFP and power spectrogram, showing a clear peak in theta band during locomotion. 3c and d: Hippocampal LFP and power spectrums when the rat was resting. No peak in theta range was observed. 3e: Real-time theta power during closed-loop stimulation. --- indicates the predetermined individual theta threshold. Each black dot represents real-time hippocampal theta power. If theta power exceeded the threshold (black dot above ---), bilateral stimulation in the mesencephalic reticular formation was switched on (until theta power dropped below threshold). LFP: local field potential.

In our study, we have shown that closed-loop DBS is effective in suppressing locomotion with less electrical stimulation used compared to open-loop DBS. This implicates the advantages of less stimulation-induced side effects and more efficient use of energy of closed-loop DBS during clinical application. To the best of our knowledge, this is the first attempt to use hippocampal-LFP-based neuromodulation to manipulate behaviour of rodents. In principle,

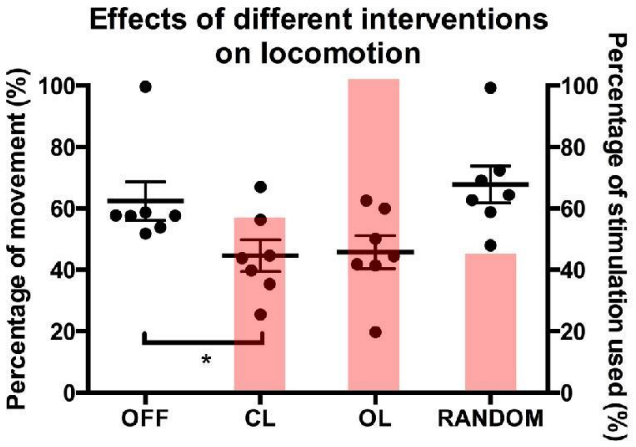

Figure V.4. Effects of OFF, OL, RANDOM, and CL stimulations on locomotion (mean +/- S.E.M., scatter plot), and corresponding percentage of stimulation-on time (mean, red columns). Repeated-measure analysis of variance showed that the main effect of different intervention on percentage of movement detected via automated video analysis was significant ($p = 0.012$). Post hoc pairwise comparisons (Bonferroni correction) indicated that the percentage of movement during CL was significantly lower than during OFF ($p = 0.042$). Percentages of stimulation-on time during RANDOM and CL were 43.86 +/- 0.80% and 55.57 +/- 4.56%, respectively. OFF: no stimulation, OL: open-loop stimulation, RANDOM: randomly-applied, CL: closed-loop. *: $p<0.05$.

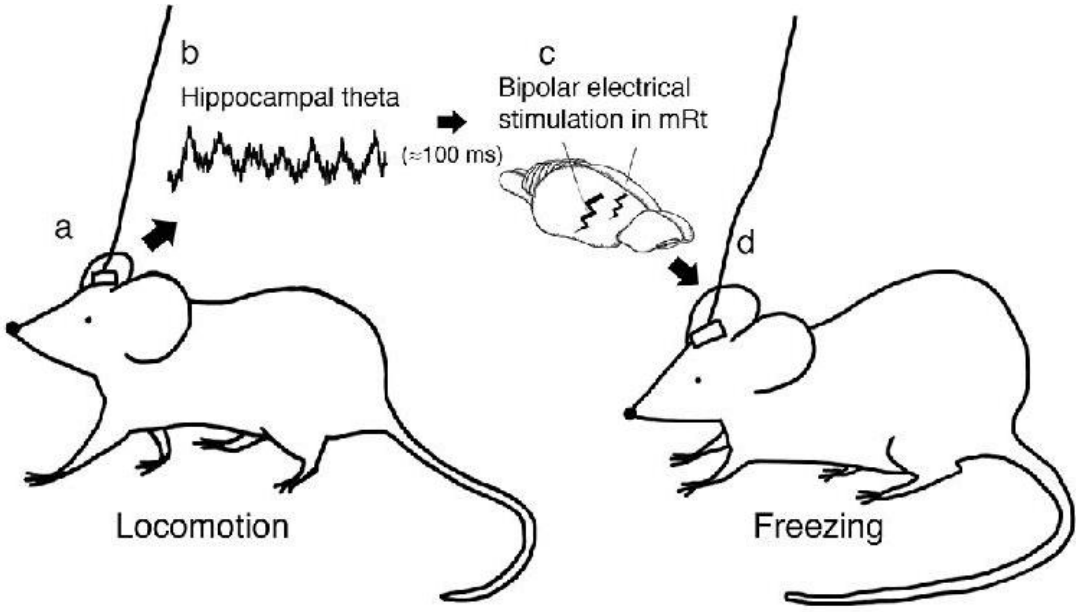

Figure V.5. Graphical illustrations of hippocampal-mRt closed-loop deep brain stimulation. Locomotion (e.g. exploratory walking) in rat (5a) and corresponding hippocampal theta activity (5b, local field potential sample of 1 second), which triggers bipolar electrical stimulation in the mRt (5c), and induces freezing and suppresses locomotion (5d). Drawing by Stephany Pei-Yen Hsiao (5a, c, and d).

we've proven that open-source hardware is capable of effectively intervening neural circuits in a closed-loop fashion. The system delay time (from receiving input to actual output) of less than 100 milliseconds seemed acceptable in our model, and was comparable to other closed-loop neural stimulation systems (Rosin et al., 2011; Little et al., 2013). The main component of the delay came from the processing of the LFP data in Matlab. We also have delay from the Arduino microcontroller (in the order of msec) and the mechanism operated cell (also in the order of msec) for on- and off-switching. The DAQ card is another source of delay, in the range of a few milliseconds maximally. Optimization of hardware (with more powerful chipsets) and software setup (enhanced algorithms) may further reduce delay and improve system efficacy. With our current setup, the open source hardware component is only acting as a controller of output based on input. This is related to limitations of Arduino Uno, but with more advanced open source hardware systems (e.g. open source mini pc and data acquisition system), it is possible to build a complete open source closed-loop neural stimulation system.

The main advantages of open source hardware include wide range of selection and availability, high customizability, and affordability. Our results suggest open source hardware as an effective component for closed-loop DBS system, and warrant future research of closed-loop neural stimulation using open source hardware.

6. REFERENCES

1. Aström, K. J. &Murray, R. M. Feedback systems: an introduction for scientists and engineers (Princeton university press, Princeton, 2010).

2. Chen, C. Y., Yang, C. C., Lin, Y. Y.&Kuo, T. B. Locomotion-induced hippocampal theta is independent of visual information in rats during movement through a pipe. Behav. Brain. Res. 216, 699–704 (2011).

3. Kramis, R., Vanderwolf, C. H. & Bland, B. H. Two types of hippocampal rhythmical slow activity in both the rabbit and the rat: relations to behavior and effects of atropine, diethyl ether, urethane, and pentobarbital. Exp. Neurol. 49, 58–85 (1975).

4. Little, S. et al. Adaptive deep brain stimulation in advanced Parkinson disease. Ann. Neurol. 74, 449–57 (2013).

5. Marlin, T. E. &Marlin, T. Process control: designing processes and control systems for dynamic performance (McGraw-Hill, New York, 1995).

6. Newman, J. P. et al. Closed-Loop, Multichannel Experimentation Using the Open-Source NeuroRighter Electrophysiology Platform. Front Neural Circuits 6, 98 (2012).

7. Robinson, T. E. Electrical stimulation of the brain stem in freely moving rats: I. Effects on behavior. Physiol. Behav. 21, 223–31 (1978).

8. Romagnoli, J. A. & Palazoglu, A. Introduction to process control (CRC Press, Boca Raton, 2012).

9. Rosin, B. et al. Closed-loop deep brain stimulation is superior in ameliorating parkinsonism. Neuron. 72, 370–84 (2011).

10. Rossi, L. et al. An electronic device for artefact suppression in human local field potential recordings during deep brain stimulation. J. Neural. Eng. 4, 96–106 (2007).

11. Sinnamon, H. M. Hippocampal theta activity related to elicitation and inhibition of approach locomotion. Behav. Brain. Res. 160, 236–49 (2005).

12. Slawinska, U. & Kasicki, S. Theta-like rhythm in depth EEG activity of hypothalamic areas during spontaneous or electrically induced locomotion in the rat. Brain. Res. 678, 117–26 (1995).

13. Tambuyzer, T. et al. New criteria for detection of compulsive behaviour in SIP model based on an automated video analysis system. International Journal of Psychophysiology 85, 368 (2012).

GENERAL CONCLUSIONS

Individual biological process:

Starting from biological insights of the process, we were able to develop a control system for suppression of locomotion in rats (Hypothesis 1 in Part 1).

In the case of closed-loop neuromodulation, the central nervous systems acts as controller of many body systems at organisms scale (e.g. control of movement), and control of the central nervous system by DBS is a promising example of how **control engineering concepts** can be applied to adapt (pathological) behaviour of organisms. Since the closed-loop system was effective in suppressing the locomotion, this implicates less stimulation-induced side effects compared with continuous stimulation based on open-loop DBS systems during clinical applications. Often pathological symptoms are not constant and therefore continuous stimulation of the brain with open-loop DBS systems is not the most efficient treatment. Closed-loop systems can adjust to symptoms and may be able to avoid stimulation-induced side effects.

Feature generation:

This chapter showed how we can extract features from biological responses (i.e. theta frequencies) in a way that allows us to effectively manage the biological process (i.e. deep brain stimulation; See hypothesis 3 in Part 1).

Individualised change detection:

Moreover, by using **individual baseline measurements** the control system can be individualised based on individual monitoring thresholds and individualised interventions (Hypothesis 4 in Part 1). As shown by the analyses, the threshold values and stimulation parameters were **individually different** confirming the need for an individualised approach.

CHAPTER VI
Individualised model-based monitoring of chicken embryo status during incubation based on eggshell temperature

Tim Tambuyzer*, Carlos Eduardo Bites Romanini*, et al.
(In preparation for submission)
**Shared first authors*

BROADER PERSPECTIVE

The last chapter of part 2 presents a monitoring application that includes **all blocks of the general scheme** for model-based individualised monitoring of biological processes (see figure 1.8). The main idea of this chapter is to develop an individualised model-based monitoring approach for detection of the different developmental stages of chicken embryos during incubation. Different from the other chapters, here we are not just monitoring a single status (e.g. infection or not), but rather the growth and developmental stages, which is a completely different **temporal level** relative to the lifetime of the organism. The **spatial level** is the full organism: the chicken embryo. Since there is a very clear boundary between the embryo and the surrounding environment (i.e. the eggshell), this case study is ideal for monitoring or control purposes and interpreting the results.

Therefore, in this chapter we will apply most elements of the **individualised model-based monitoring** approach that were used in the previous chapters: bio-process (i.e. chicken embryo), models (i.e. input-output models), feature generation (i.e. model parameters derived metrics) and **individualised change detection based on individual thresholds**. Moreover, in this chapter we even go one step further by also **predicting** future states of the chicken embryos.

1. ABSTRACT

Many incubation variables interact with embryonic development. Often such incubation variables (e.g. eggshell and micro-environmental temperature) have major influences and are associated with, for example, hatchability results and chick quality on group level. However, little is known on the interaction of such variables at individual level (e.g. Romanini et al., 2013). We hypothesise in this study that it is possible to develop an individualised model-based monitoring approach which is able to detect and even predict the individual progress of embryo development during the incubation of chicken eggs based on eggshell temperature (T_{Egg}) and micro-environmental air temperature (T_{Air}). The three main objectives of this study were: i) to quantify the relation between eggshell temperature and the local environmental temperature based on individual first order discrete-time transfer function models. ii) To detect (i.e. monitor) different model-based milestones that can be related with the biological processes of the individual embryo development. iii) To use the individual information obtained by the detected embryo development milestones to make predictions of hatch time.

The results showed that five different milestones in the development of individual broiler embryos can be detected based on dynamic models of the local environment temperature and the individually measured eggshell temperature: i) transition from endothermic to exothermic; ii) plateau phase of embryonic metabolic heat production; iii) the start of pulmonary respiration from the breaking of the internal egg air cell by the beak (internal pipping); iv) the completion of the diffusive respiration via the chorioallantoic membrane with embryos pipping the egg shell externally (external pipping) and; v) the completion of breaking the egg and the emergency from the shell (hatch). In addition, we could make individualised prediction of the hatch day after detection of milestone ii, the plateau phase on embryo heat production (ROC AUC = 0.91). This result can be interpreted as an

early biological sign of the embryo preparing itself in terms of metabolic energy saving to progress towards the hatching phase.

This individualised monitoring approach could be an added value for individualised prediction of hatching and for other experimental designs and studies, where the developmental stage of the embryo is relevant. Moreover, this individualised model-based monitoring approach could also open possibilities in future studies for the development of more precise control systems for synchronised embryo development and uniform hatching.

2. INTRODUCTION

Commercial incubators should capable of providing optimal conditions for embryo development inside the egg by imitating realistic natural conditions and by trying to regulate variables, such as air temperature, air humidity, air speed, gases concentrations, light and egg turning (French 2007, Boleli et al. 2013). Nowadays, a key aspect is the progress from a natural incubation of few eggs in the nest to the large capacities of the latest incubators, which incubate more than a hundred thousand eggs at once. Therefore, spatiotemporal gradients in air temperature, air speed, and 3-dimensional airflow patterns increase significantly (Van Brecht et al., 2003) and thus, the rate of development is modified at the level of individual eggs.

Although an embryo inside an egg seems isolated from the external environment, research recognised the critical role played by heat, gases and water vapour exchanges between an egg and its surrounding microenvironment (Meijerhof, 2000; Hammond et al., 2007; Leksrisompong et al., 2007; Ipek, 2014). T_{Air} is a major influencing variable (Freeman & Vince, 1974; Decuypere & Michels, 1992; Meijerhof, 2009) as it can cause variance in T_{Egg} beyond the optimal range of 37.5 – 37.8 °C and thus affect total incubation length, embryonic metabolic heat production, organ and body sizes, skeletal growth, hatchability results and chick

quality at the day of hatch (Wittow and Tawaza 1991; Decuypere and Mitchels, 1992; Yalcın and Siegel, 2003; Tazawa et al., 2004).

So far, eggshell temperature has been vastly used as a practical measurement of embryo temperature (French, 1997; Lourens et al., 2005; Joseph et al., 2006; Hulet et al., 2007, Molenaar et al., 2010; Walstra et al., 2010; Romanini et al., 2013, Boleli, 2016). It has been demonstrated that eggshell temperature remains low from 0 to 10 days of incubation, since embryonic metabolic heat production is minimal, thus indicating that eggs need to gain heat from external source (Tullett & Deeming, 1987). During the second week of incubation, mainly after 12 to 13 days of incubation, there is an exponential increase in heat production by the embryo related to the growth phase of embryo development (Sotherland et al., 1987; Lourens et al. 2006, 2007). At this stage, internal egg temperature can increase by 1.5 °C above the temperature at the surface of the eggshell (Gualhanone, 2012) and thus heat needs to be lost by the eggs. Around 14 to 16 days of incubation embryonic heat production reaches a plateau phase (French, 2007) as the embryo is saving energy and preparing itself to move towards hatching stages with further increases in T_{Egg} (Sgavioli et al., 2015; De Morita et al., 2016).

In addition to heat, both gas and water vapour exchanges during incubation are also changing in time. The demand for O_2 increases at 10 – 12 days of incubation as a result of increasing embryo metabolism (Hamburger & Hamilton, 1951; Tazawa, 1980; Deeming, 2002; Boleli et al., 2016), resulting in larger exchanges of O_2 and CO_2 with atmospheric air by diffusion through the chorioallantoic membrane (CAM). During the last stages of incubation, embryos begin to clap their beaks and break the internal egg air cell (internal pipping, IP) (Khandoker, 2003). After IP, gases gradually begin to be exchanged via the pulmonary respiratory system (Decuypere & Bruggeman, 2006; Mortola, 2009) until the embryos pip the eggshell externally (external pipping, EP) and subsequently progress towards hatch.

However, individual differences through the course of embryonic development are not sufficiently taken into account. Individual variations due to genetic origin (Chawalibog, 2004), 3-dimensional physical incubation conditions (French, 1997; Nichelmann and Tzschentke, 2002; Van Brecht et al. 2005), egg variables such as size, composition, and shape, eggshell thickness, porosity, heat and water vapour conductance (Boleli, 2003) and pre-incubation conditions (Janke, 2004) may cause deviations from expected results at the level of individual embryos. Therefore, trying to individually monitor and predict the embryo development is a crucial step towards the synchronization of embryo development among eggs and more uniform hatching time among individuals. However, little is known on the interaction of the aforementioned variables at an individual level (e.g. Romanini et al., 2013).

Since T_{Air} and T_{Egg} are major influencing variables during the embryo development, we hypothesise in this study that it is possible to develop an individualised model-based monitoring approach which is able to detect or even predict the individual progress of embryo development based on eggshell temperature and micro-environmental air temperature. The three main objectives of this study were: i) to quantify the relation between eggshell temperature and the local environmental temperature based on individual first order discrete-time transfer function models. ii) To detect different milestones of the individual embryo development based on the calculated models. iii) To use the individual information obtained by detection of the milestones to make predictions of hatch time.

3. MATERIALS AND METHODS

Experiments

Dataset 1

In total, six batches of Ross 308 eggs (600 eggs/batch) were collected from breeders aged between 35 and 57 weeks (Henry Stewart & Co. Ltd., Lincolnshire, United Kingdom). All eggs were incubated and hatched in two small-scale (capacity for 300 eggs each) custom-built 'BioStreamer' incubators (Petersime NV, Zulte, Belgium) using a standard 21-days incubation program. Eggshell temperature was continuously controlled at 37.8 ^{0}C and relative humidity at 60%.

Twenty out of six hundred eggs were randomly picked and individually labelled as 'focal eggs' in each incubation trial to serve as samples for the current study. In total, 120 focal eggs from six repetitions were analysed.

Standard low-cost thermocouples type T sensors were attached to the equator of the shells of the focal egg (Romanini et al., 2013). Another temperature sensor was positioned 1 cm away from each focal egg to record the corresponding micro-environmental air temperature , T_{Air}. The eggshell temperature, T_{Egg} of each focal egg and T_{Air} were recorded every minute throughout the entire incubation.

Out of the 120 focal eggs monitored, the temperature measurement of 54 eggs were included in this study. Remaining focal eggs were detected as infertile (n=15) or did not succeed to hatch because of early (n=3), middle (n=12), or late (n=11) mortality (Tong et al., 2016). Cracked or contaminated eggs (n=15) were excluded from the analyses, as well as eggs with noisy measurements of T_{Egg} or T_{Air} (n=10).

Dataset 2

Supported by the results based on the first dataset, a second dataset was generated with the purpose to further investigate embryonic status during the last phase of the incubation period. The same type of eggs were used. This time, a custom-built small scale incubator model 'GVH 2000' (Petersime NV, Zulte, Belgium) with same

capacity of 300 eggs was used (Van Brecht et al. 2005b). The same standard 21-days incubation program was used; in addition, also the same approach was used for the temperature measurements. The number of focal eggs monitored and hatched was 20. In addition, the status of the embryo was assessed by visual checks during six different time points (see Table VI.1).

Table VI.1. Incubation process times of individual labels based on visual checks.

Number of visual check in chronological order	Incubation process time
1	18 days and 17 hours
2	19 days and 10 hours
3	19 days and 14 hours
4	19 days and 19 hours
5	20 days and 11 hours
6	20 days and 17 hours

During each visual check, all eggs were individually labelled into one of the following four categories as verified by candling method (Crossley and Altimiras, 2000) or direct visual inspection:

i) Pre-internal pipping (pre-IP)

ii) Internal pipping (IP): Internal pipping is when the chick breaks through the air cell inside the egg. Internal pipping cannot be seen from the outside of the egg, but it can be detected by candling an individual egg with a torch.

iii) External pipping (EP): The embryo is completely filling the egg and the beak is poised to start pecking through the shell and to make a hole in the eggshell.

iv) Hatching (H): The chick starts making some regular pipping movements and eventually breaks through the shell circumference until it creates a hole that is large enough to emerge the body completely from the shell.

Modelling

Dynamic data-based models

First order discrete-time transfer function (TF) models were used. The models were single-input, single-output (SISO) models. The micro-environmental air temperature was used as model input, and the eggshell temperature, measured at the equator of the eggs, was used as model output. A first order SISO discrete-time TF model can be described by the following equation (Young, 1984):

$$y_t = \frac{b_0}{1+a_1 z^{-1}} u_{t-\delta} + \xi_t \quad (1)$$

Where y_t is the model output (T_{Egg}), $u_{t-\delta}$ is the model input (T_{Air}), t is the time for discrete time steps, δ is the time delay (δ≥0), and ξ is additive noise, a serially uncorrelated sequence of random variables with variance that accounts for measurement noise, modelling errors, and the effects of unmeasured inputs to the process. b_0 and a_1 are the model parameters. Finally, z^{-1} represents the backward shift operator that is defined as $z^{-1}y_t = y_{t-1}$. All model calculations were performed in Matlab using the Captain Toolbox (Taylor et al., 2007).

Quantification of steady state gain

Based on the model parameters, the steady state gain can be determined to quantify the relation between T_{Air} and T_{Egg} (see equation 2). The steady state gain can be defined as the steady state change of output (i.e. T_{Air}) per unit change of input (i.e. T_{Egg}) (Young, 1984):

$$SSG = \frac{b_0}{1+a_1} \quad (2)$$

Online model identification and moving window approach

A moving window approach was applied with a window length of 120 minutes and a window overlap of 60 minutes. For each window, one first order TF model was calculated. Afterwards, the corresponding SSG could be determined for each window based on the model parameters estimated for each window. Using this moving window approach, a new time series of SSG values was obtained, which was used to detect changes of the relative relation between input and output (T_{Air} and $T_{Egg,}$ respectively).

Statistics

Decision tree analysis was applied to calculate prediction models for the day of hatch based on features of the obtained SSG time series. Afterwards, the Area under the ROC curve (AUC) was calculated to evaluate the discriminatory power of the model-based features (Fan et al., 2006). Linear regression was applied to quantify linear relations between the generated data. Matlab was used for all statistical analyses (i.e. Neural Networks Toolbox and Statistics Toolbox).

4. RESULTS AND DISCUSSION

Detection of the embryo development milestones

The fertile incubated egg, which contains a living organism (chicken embryo), can be considered as Complex, Individually different, Time varying and Dynamic (CITD) systems as introduced by Berckmans et al. (e.g. Quanten et al., 2006). Hence, the dynamic relationship between the eggshell temperature (T_{Egg}) and its surrounding micro-environmental air temperature (T_{Air}) is different from one day to another during the entire incubation cycle of embryo development (Youssef et al. 2014). The dynamic evolution of this relationship is reflected in the time-series of the

calculated steady-state gain (SSG). The analysis of the dynamic variation of the SSG (°C/°C).) could indicate different phases (Milestones, *M*) along the course of embryo development during the 21 days of incubation. The analysis of the dynamic changes in the SSG slope, $S = \frac{d[SSG]}{dt}$, have shown that five milestones could be identified along the SSG time-series of an incubated egg. Figure VI.1 is showing the identified five milestones (i.e., M1, M2, …, M5) for the sampled Egg number 27 in this present study.

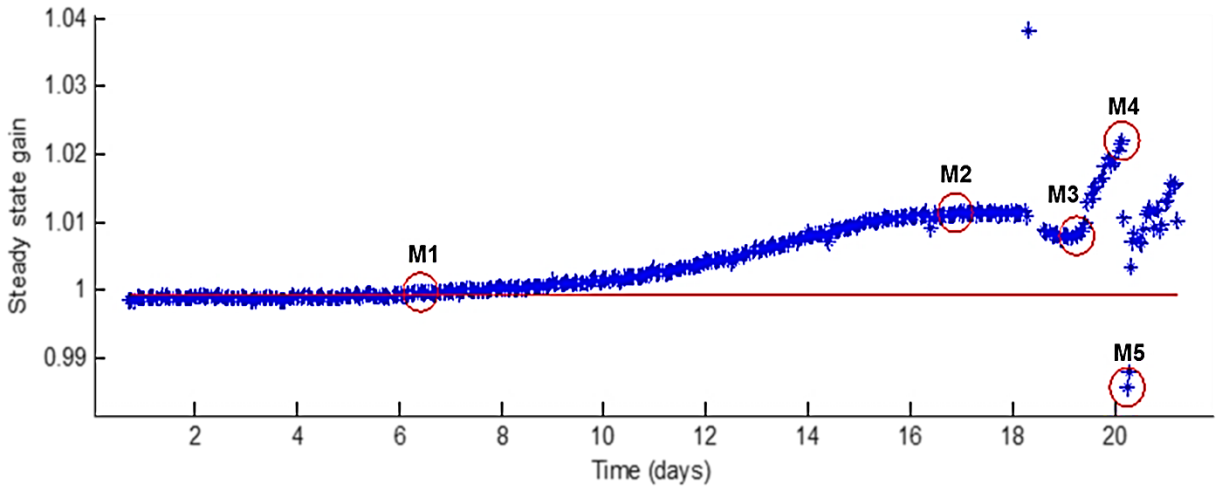

Figure VI.1. Time-series of the calculated steady-state gain (SSG) for sampled Egg number 27, showing the identified five milestones based on the dynamic changes in the SSG signals, which reflect the relationship between T_{Egg} and T_{Air}.

Based on the documented knowledge of the incubation process of chicken eggs and embryos, the five milestones are labelled and defined as follows:

Milestone M1

Heat transfer occurs when there is a temperature difference between two regions or media, and always on the thermal gradient. Eggs present four mechanisms for heat transfer: conduction, radiation, convection, and evaporation (French 1997;

Meijerhof & van Beek 1993). However, in chicken eggs, eggshell temperature remains low (in relation to surrounding air temperature) during the first week of incubation (i.e., until day 6-7 of the incubation period) due to the low metabolic rate (Tazawa et al. 1988; French 1997) and starts to increase in the second week. More specifically, eggshell temperature remains lower than the incubation temperature during the first week, and it is higher than the incubation temperature during the last week of incubation (Sgavioli et al. 2016; French 1997; Hiebert & Noveral 2007). According to the laws of thermodynamics, heat is transferred between the eggs and the incubation environment down a thermal gradient, i.e., always from the warmer to the colder region. Eggs gain or lose heat only when there is a temperature difference (ΔT) between the environment (T_{Air}) and the eggshell (T_{Egg}) until equilibrium is reached. This indicates that eggs incubated under those temperatures need to gain heat in the beginning (i.e. endothermic phase) and to lose it during the last week of incubation (i.e. exothermic phase), respectively. By analysing Figure VI.1, it is noticed that the average SSG values for all eggs is maintained close to 1 ^{o}C/^{o}C during the first 8 days of incubation. Furthermore, starting from incubation day 6 the SSG gains have shown deviation from the mean value (baseline), which is indicating the first milestone (M1) along the embryonic development (see figure VI.1). Milestone M1 is then interpreted as a physical indication of the transition moment in heat flow, at which the incubated eggs starts to lose heat down a thermal gradient ($T_{Egg} > T_{Air}$). An individualized approach is developed to detect this milestone *M1*. First, the mean ($\bar{M}$) and standard deviation (Std) of the SSG were calculated during baseline conditions (first five days of incubation) by knowing that metabolic heat generated by the embryos is insignificant during that period. Afterwards, milestone *M1* was defined as the first SSG value which exceeded the following individual threshold:

$$\bar{M}_{Baseline} + 3.Std_{Baseline} \quad (3)$$

Assuming that the data are normally distributed, this would mean that about 99.7% of the SSG values measured during the first five days of incubation are within 3 standard deviations of the mean measured during baseline.

For most embryos (i.e. 42), milestone M1 was detected between day 7 and day 11 of the incubation period (see figure VI.2; mean $_{M1}$ = 8.2 days, standard deviation$_{M1}$ = 1.7 days).

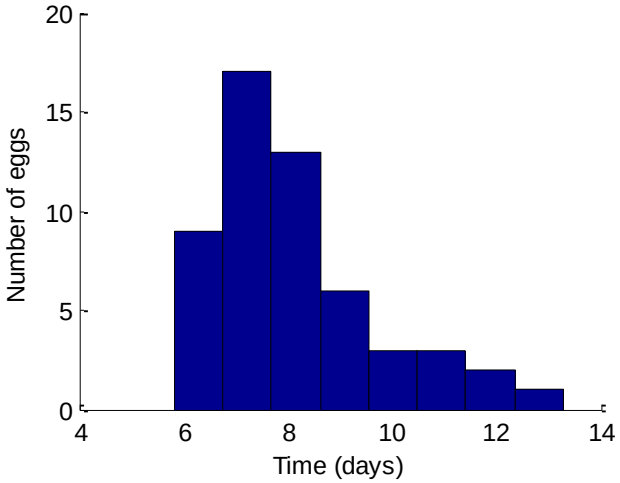

Figure VI.2. The distribution of the detected Milestone M1 over incubation days.

According to the equation of the SSG (equation 3), it would be expected that the SSG is smaller than 1 when the embryo is endothermic (i.e., the difference in T_{Egg} is smaller than the difference in $T_{Air,}$ or, in other words, the egg gains heat). On the other hand, it is expected to be larger than 1 when it is exothermic (i.e., the difference in T_{Egg} is larger than the difference in $T_{Air,}$ or, in other words, the egg dissipates heat). An average SSG of 1 was found (standard deviation = 0.005; see figure VI.3). This finding corresponds with the expected value correlated with the transition from an endothermic status (heat is transferred via convection mode from surrounding air to the egg) to an exothermic status (the metabolic heat generated by the growing embryo is dissipated to the air stream passing through the eggs by forced convection).

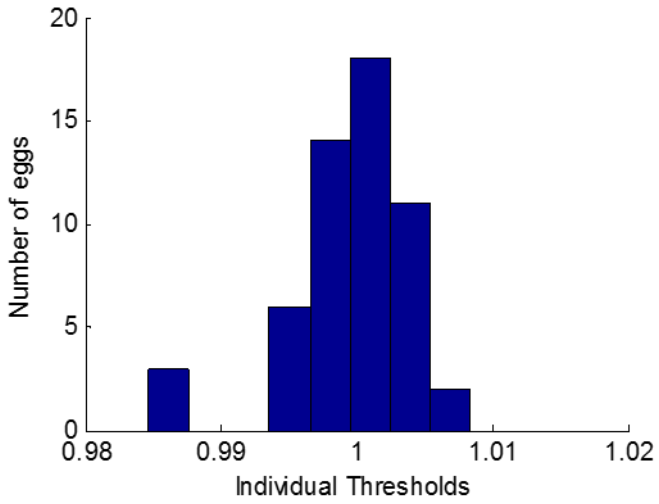

Figure VI.3. The steady-state gain (SSG) threshold distribution for all the examined eggs.

Milestone M2

Based on the changing slope of the SSG signals, along the incubation days, milestone M2, could be detected (see figure VI.4). It is noticed, that after the detected milestone M1, the calculated slope (S) is equal or higher than the slope calculated at the moment of milestone M1. After several days of incubation the slope decreases again and tends to have a stagnation phase. Therefore, an S-shaped curve was detected in the SSG signals between incubation day 8 and 15. Hence, milestone M2 is defined as the first SSG value after incubation day 14 at which the slope value is less than the slope value calculated at M1 (or, in other words: since we expect to see an S-shape, the slope increases starting from M1 and decreases again at the end of the S-shape. Therefore, M2 is defined as the time point where the slope decreases again till the slope value measured at M1).

Based on the aforementioned approach, milestone M2 is detected between day 15 and day 18 of the incubation period (see figure VI.4; mean_{M2} = 16.1 days, standard deviation_{M2} = 0.8 days). This finding corresponds with other studies which indicate that the eggshell temperature increases during the second week as a reflection of

increased embryonic heat production during embryonic growth, and reaches a temperature plateau around incubation day 15 (Nichelmann & Tzschentke 2003; French 1997; Dietz et al., 1998; Boleli et al. 2016). However, only 23 of the 54 sampled eggs showed a clear S-shape of the SSG curve. In future studies, the study design should be optimised by analysing the possible sources of noise in the recorded temperature measurements and by considering other potential embryo measurements (i.e., embryonic motility, vasodilatation and vasoconstrictions activity, heart rate) to have a more accurate mathematical modelling of heat production/dissipation in incubated eggs (Youssef et al., 2014).

Milestone M3

The stagnation phase of the SSG signal ends with an increase of the SSG slope lasting approximately 24 hours (see M3 in figure VI.1), which can be compared with the rise at the end of the heat production plateau phase that occurs when the embryo penetrates the internal air cell with its beak (i.e. IP; Visschedijk 1968).

In order to detect this change in the SSG signals, milestone M3 was defined as the first SSG value for which the slope was greater than 0.0003. The selected threshold value was defined based on visual inspection of the SSG signals of all eggs. Using this method, M3 was detected around day 20 of the incubation period (see figure VI.4; $mean_{M3}$ = 19.3 days, standard deviation $_{M3}$ = 0.3 days) as supported by other studies reporting that internal pipping occurs between incubation day 19 and 20 (Decuypere et al. 2001, Tong et al., 2012; Maatjens et al. 2014; Boleli et al., 2016).

Milestone M4

Milestone M4 corresponds with the moment where the SSG signals show a high peak value (i.e. local maximum) in the final phase of the incubation period (see figure VI.1). The peak was defined as the last SSG value for which the slope was greater than -0.0004. This threshold value was determined based on visual

assessments of the SSG signals. Milestone 4 was detected between incubation days 20 and 21 (see figure VI.4; $mean_{M4}$ = 20.04 days, standard $deviation_{M4}$ = 0.3 days).

This finding is associated with the so-called external pipping (EP), which is also expected around incubation day 20 (e.g. Tong et al., 2012). During EP, the embryo starts tapping the eggshell repeatedly, causing the shell to weaken and eventually break. From the outside of the egg, a small crack or hole in the eggshell can be observed, sometimes with the tip of a beak puncturing through. This is the first time during the incubation period that the chick penetrates the eggshell with its beak as a natural progress towards hatching (Tong et al., 2012). Since the eggshell gains access to atmospheric air at that moment, heat transfer from the egg to the environment is facilitated (Romanini et al. 2015). Therefore, it is expected that external pipping is followed by a drop of the eggshell temperature.

Milestone M5

Milestone M5 was defined as the lowest SSG value after Milestone 4 (see figure VI.1). Based on this detection method, milestone M5 was detected between day 20 and day 21 of the incubation period (see figure VI.4; $mean_{M3}$ = 20.1 days, standard $deviation_{M3}$ = 0.3 days).

As previously discussed, external pipping is soon followed by hatching. Most studies suggest that hatching occurs around day 20-21 (e.g. Tong et al., 2012; Romanini et al., 2013), which corresponds with the detected milestone M5. In order to prepare for the hatching, the embryo starts cutting the eggshell circumference in very small pieces with the egg tooth in regular up-and-down motion gradually creating a neat "zip"-shaped cutting profile while turning around inside the egg. Once approximately ¾ of the shell circumference at the blunt end of the egg has been cut, the embryo pushes itself out of the egg by forcefully stretching its legs causing the last bit of the shell cap to break loose. This allows the embryo to push itself free and to completely emerge itself out of the egg. Since the eggshell

temperature sensors are still attached to the eggshells just after hatching, a sudden temperature drop is expected. There are two main reasons for this drop: i) the embryonic heat source is no longer present since the chick has emerged and ii) any remaining embryonic fluid at the internal eggshell membrane evaporates (Romanini et al., 2013; Romanini et al., 2015).

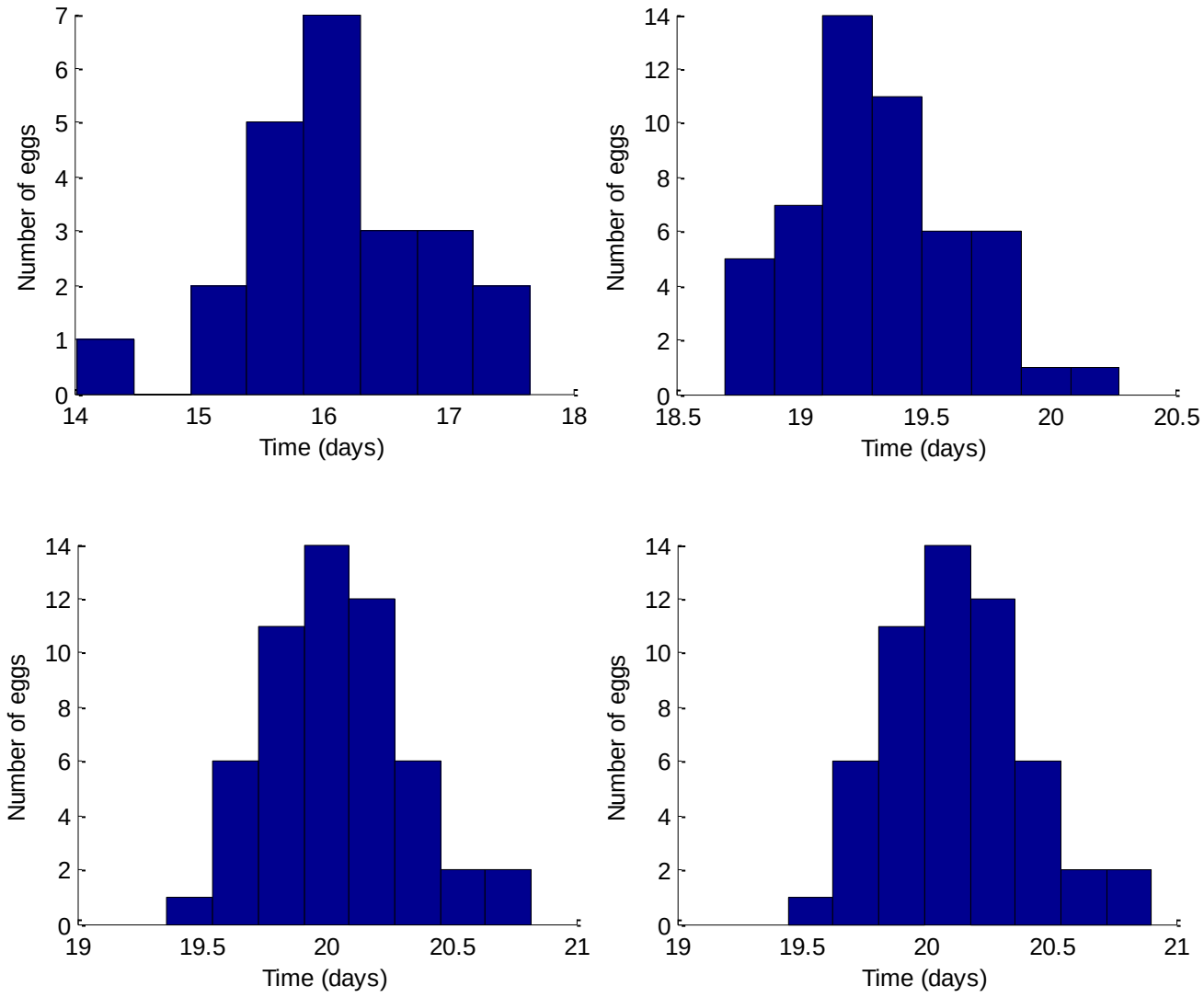

Figure VI.4 The distribution of the detected Milestone M2 (top left), M3 (top right), M4 (bottom left) and M5 (bottom right) over incubation days.

Link between milestones and embryo development based on individual labelling.

The model-based milestones M1 and M2 were linked with the embryo status by comparing them with the timing of developmental stages reported in other studies and by interpreting the parameters of the calculated models. The timing of M1 was correlated with the change in direction of the heat flows during the first period of embryonic growth (i.e. transition from endothermic to exothermic status). The timing of M2 was linked with the timing of the stagnation of embryonic heat production after the second week of incubation (i.e. plateau phase).

Similarly, the model-based milestones M3, M4, and M5 could be related with the main biological transitions reported in literature for the hatching phase: internal pipping, external pipping and hatch. In addition, the onset timings of milestones M3, M4, and M5 were experimentally confirmed by the individual labels obtained for dataset 2 (n=20, see materials and methods).

A number of visual checks at specific times during the hatching process confirmed whether an embryo was internally pipped, externally pipped, or hatched. However, since the incubators had to be opened from time to time to obtain the visual checks and individual labels, there was some extra measurement noise in dataset 2. Therefore, the start of the acute increase of SSG (i.e. milestone M3), the upwards peak of SSG in the final phase of the incubation process (i.e. milestone M4), and the drop of SSG in the final phase of the incubation process (i.e. milestone M5) were determined by manually analysing the SSG signals instead of using fixed threshold values in an automated way.

Afterwards the timing of these milestones could be compared with the corresponding labels. For 12/20 eggs, milestone M3 occurred before internal pipping. For 6/20 eggs, milestone M3 appeared at approximately the same time as internal pipping, and, for 2/20 eggs, it was impossible to detect M3 because of data noise. Vleck et al. (1980) and Hoyt (1987) indicated that there is an increase in heat production just before internal pipping occurs. This could explain why milestone

M3 is often detected before the actual moment of internal pipping, since the determination of M3 is purely based on the start of the acute increase of SSG, which corresponds with an increase in heat production that ultimately triggers IP.

Similarly, milestone 4 occurred after external pipping for 12/20 eggs. For 6/20 eggs, milestone 4 took place at approximately the same time as labelled external pipping and for 2/20 eggs, milestone 4 could not be detected because of noise in the data. Since the chick penetrates the eggshell with its beak during external pipping (Tong et al., 2012 and 2013), it is expected that the drop of the eggshell temperature comes a little after external pipping. Therefore, milestone M4 occurs in most cases after external pipping. The fact that M4 occurs in most cases after external pipping can be explained by elementary principles. Heat from embryo metabolism is no longer completely enclosed by the eggshell and from EP onwards the hole in the eggshell represents an extra pathway of heat loss to the environment beside the natural permeability of eggshell pores.

Lastly, milestone M5 took place after labelled hatching for 11/20 eggs. For 6/20 eggs, milestone 5 occurred at approximately the same time as hatching, and, for 3/20 eggs, milestone 5 could not be found because of noisy data. Since the sudden temperature drop of milestone M5 is caused by the chick completely emerging from the shell, the T_{Egg} drops appear just after hatch.

Thus, T_{Egg} drop during hatching is explained by the fact that existing heat source (e.g. embryo) is supressed (Romanini et al., 2013). Furthermore, the magnitude of T_{Egg} drop is also partially explained by an evaporative cooling effect at the eggshell that, after drying out, reaches an equilibrium with air temperature (i.e. no heat exchange; Romanini et al., 2015).

To conclude, these results confirm the added value of the individualised model-based monitoring approach presented in this study, since strong links between the model-based milestones and the developmental stages of embryos during incubation are found. Revealing individual information of the embryo status by

measuring and modelling air and eggshell temperature continuously may open new horizons on the understanding of energy-related metabolic changes and pathways before hatch (De Oliveira et al., 2008). The developed models can be considered as data-based mechanistic models, since they are both data-based and able to give insight in the embryo status.

Inter-individual differences per milestone

Many studies have emphasized the urgent need for deeper biological understanding of embryo development during the incubation period (Christensen et al., 2007; Leksrisompong et al., 2007; De Oliveira et al., 2008; Ipek and Sozcu, 2016). Individualised non-invasive monitoring of embryo status allows uncovering individual relations between environmental variables (i.e. micro-environmental air temperature) and variables which are more directly related with embryo physiology (i.e. metabolic heat). In fact, eggshell temperature (TEgg) is well known as the most important variable to be controlled during incubation as it impacts directly on the hatchability results, chick quality and post-hatch performance (Ipek and Sozcu, 2016). TEgg depends mainly on the combination of three factors: 1) air temperature around the eggs; 2) the exchange of heat between eggs and its micro-environment; and 3) the time-variable heat production of an incubated embryo (Van Brecht et al., 2005); and will then naturally show a small gradient inside the incubators (Van Brecht et al., 2003).

Moreover, differences in the micro-environment of individual eggs during incubation can also affect the post-hatch status, such as the welfare or gait score of broilers (Ipek and Sozcu, 2016). Revealing such individual relations are not only essential to gain biological understanding, but could also play a vital role in, for example, effective synchronised hatching based on individualised control systems (Tong et al., 2012). In addition, a more uniform embryo development in general

could be an interesting and innovative product development concept for the future of poultry industry (Romanini et al, 2012). Inter-individual differences during embryo development can potentially be quantified based on the individualised monitoring approach used for detecting the five milestones in this study (see previous paragraphs).

Figure VI.5 shows the standard deviations of the timing of each milestone for all individual embryos. Thus, it is can be used as direct measure for their inter-individual differences during embryo development. While the spread of the first milestone is large, the inter-individual differences decrease over time, and the last three milestones show significantly less inter-individual variation suggesting more uniform stages of embryo development during the final period of incubation.

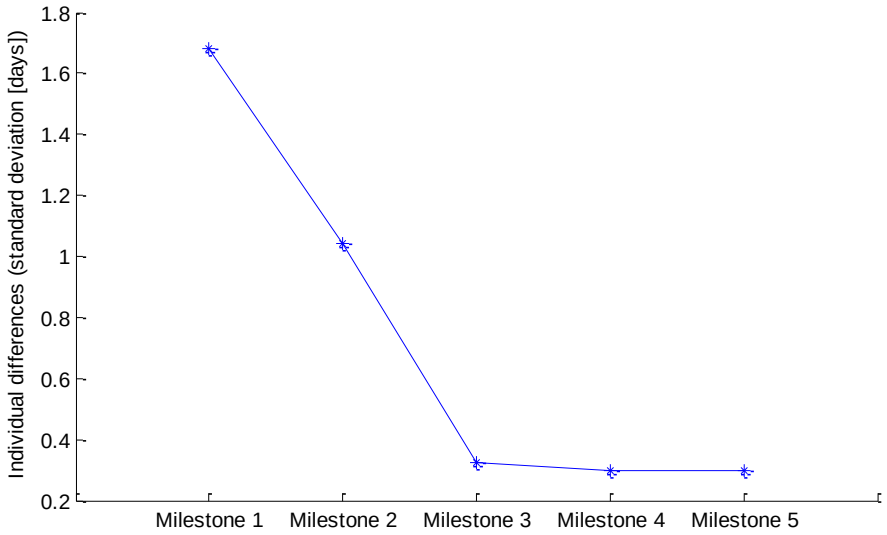

Figure VI.5 The calculated standard deviations of the histograms (see also figure 3 and 5) are shown for each milestone: milestone 1 (i.e. transition from endothermic to exothermic status), milestone 2 (i.e. plateau phase), milestone 3 (i.e. internal pipping), milestone 4 (external pipping) and milestone 5 (i.e. hatch).

This is especially relevant for an improved application of individual stimuli (i.e. temperature, CO2 levels, sound, light, etc.) at the right magnitude and timing according to the developmental stage of the embryo, seen as an attempt to have a more uniform embryos and narrower spread of hatch among individuals (Qin Tong et al., 2015, 2016). Furthermore, adjustments on the incubation profiles can be optimised by taking into consideration the individual embryo development status rather than fixed modifications according to population-based measures of embryo development.

Individualised prediction of hatch time

While monitoring often refers to the detection of the status of the embryo at that specific moment in time, another possible approach would be to predict the status of an embryo based on previously measured individual information (i.e. the onset timing of each measured milestone).

A linear relation was found between milestone M5 and milestone M3 (R^2 = 0.63; p<0.00001) (figure VI.6). These results suggest that we can make a rough prediction of hatch time when milestone M3 (i.e. internal pipping) is detected. On average milestone M3 occurs +/- 20 hours before milestone M5 (mean = 19.7 hours; standard deviation = 4.8 hours). This result is in line with other studies (e.g. Tong et al. 2012), since they also suggest that hatching occurs around 24 hours after internal pipping.

Since the prediction window of the previous relation (i.e. M3 vs M5) is rather small (+/- 20 hours), other properties of the SSG signal during earlier stages of the incubation period were investigated and related with the moment of hatching. Based in the SSG signal properties between the start of incubation and milestone M2, a prediction method with a larger prediction window could be obtained.

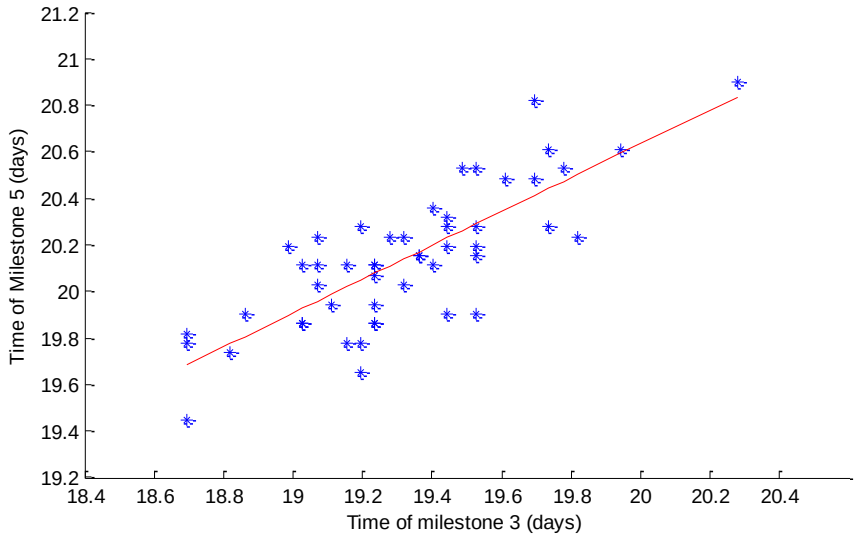

Figure VI.6 Linear relation between timing of milestone 3 (Internal pipping) and milestone 5 (Hatch time).

First, the difference between the SSG at the start of the incubation period and the SSG at milestone 2 was calculated. Since milestone M2 could be detected for 23 sampled eggs of dataset 1 (see Milestone M2), all predictions were only calculated for these eggs. When we try to predict the hatch day (day 20 or day 21; defined based on milestone 5) of the embryos based on this individual SSG difference, accurate classification results are found based on decision tree analysis (figure VI.7). 93% (13/14) of the embryos that hatched at day 21 were correctly classified. In addition, 78% (7/9) of the embryos that hatched at day 20 were correctly classified. For this variable (i.e. value of SSG difference between start of incubation and M2 with best classification results), the area under the ROC curve was 0.91, confirming a high discriminatory power. Thus, these results suggest that we can already make a prediction of hatch day after detection of milestone 2. Obtaining such individual information in advance gives, already early in the process, an idea of the final spread of hatching. Thus, such early individualised predictions could advance synchronisation of hatching (Romanini et al, 2012).

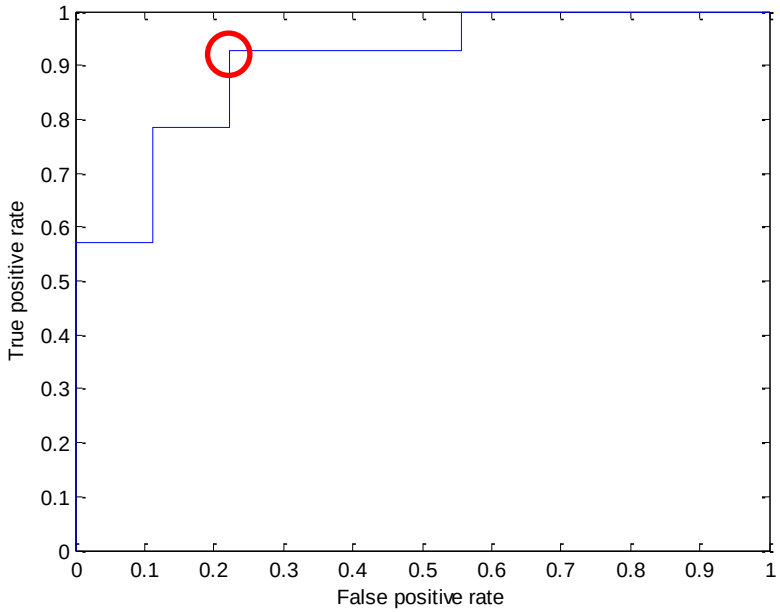

Figure VI.7 ROC curve of hatch day classification based on individual SSG increase between the start of incubation and milestone M2 (AUC = 0.91). The ROC point that corresponds with the optimal classification results is shown by the red circle.

5. CONCLUSIONS

In this study we showed that we can detect, based on dynamic models of the local environment temperature and the individually measured eggshell temperature, five different milestones in the development of individual broiler embryos. Moreover, links were shown with physiological mechanisms and, therefore, the models can be considered as data-based mechanistic models since they are both data-based and able to give insight in the embryo status. This individualised monitoring approach could be an added value for individualised prediction of hatching and for other experimental designs and studies where the developmental stage of the embryo is relevant. Moreover, this individualised model-based monitoring approach could also open possibilities in future studies for the development of more precise control systems for synchronised embryo development and uniform hatching.

6. REFERENCES

1. Boleli, IC, Morita, VS, Matos Jr, JB, Thimotheo, M, & Almeida, VR. (2016). Poultry Egg Incubation: Integrating and Optimizing Production Efficiency. Brazilian Jorunal of Poultry Science, 18(spe), 1-16. https://dx.doi.org/10.1590/1806-9061-2016-0292

2. Chwalibog, A., Tauson, A.-H., Matthiesen, C., Ali, A., Thorhauge, K., Sawosz, E., Thorbek, G., 2004. Oxidation of carbohydrates and fat in newly hatched chickens. J. Anim. Feed Sci. 13, 1–4.

3. Chwalibog, A., Tauson, A.H., Ali, A., Matthiesen, C., Thorhauge, K., Thorbek, G., 2007. Gas exchange, heat production and oxidation of fat in chicken embryos from a fast or slow growing line. Comp. Biochem. Physiol. - A Mol. Integr. Physiol. 146, 305–309. doi:10.1016/j.cbpa.2006.10.035

4. Crossley, D., & Altimiras, J. (2000). Ontogeny of cholinergic and adrenergic cardiovascular regulation in the domestic chicken (Gallus gallus). *American Journal of Physiology-Regulatory, Integrative and Comparative Physiology*, *279*(3), R1091-R1098.

5. De Morita, V.S., De Almeida, V.R., Junior, J.B.M., Vicentini, T.I., Van Brand, H. Den, Boleli, I.C., 2016. Incubation temperature during fetal development influences morphophysiological characteristics and preferred ambient temperature of chicken hatchlings. PLoS One 11. doi:10.1371/journal.pone.0154928

6. DE OLIVEIRA, J.E., UNI, Z., FERKET, P.R., 2008. Important metabolic pathways in poultry embryos prior to hatch. Worlds. Poult. Sci. J. 64, 488–499.

doi:10.1017/S0043933908000160

7. Decuypere, E., Michels, H., 1992. Incubation-Temperature as a Management Tool - a Review. Worlds Poult. Sci. J. 48, 28–38. doi:Doi 10.1079/Wps19920004

8. Deeming, D.C., 2002. Avian incubation. Behaviour, environment, and evolution. Oxford Ornithol. Ser. 119, 421. doi:10.1126/science.186.4159.107

9. Dietz, M.W., van Kampen, M., van Griensven, M.J., van Mourik, S., 1998. Daily energy budgets of avian embryos: the paradox of the plateau phase in egg metabolic rate. Physiol. Zool. 71, 147–56.

10. French, N.A., 1997. Modeling incubation temperature: the effects of incubator design, embryonic development, and egg size. Poult. Sci. 76, 124–133. doi:10.1093/ps/76.1.12.

11. Gualhanone, a, Furlan, R., Fernandez-Alarcon, M., Macari, M., 2012. Effect of breeder age on eggshell thickness, surface temperature, hatchability and chick weigh. Rev. Bras. Ciência Avícola 14, 09–14. doi:10.1590/S1516-635X2012000100002

12. Hammond, C.L., Simbi, B.H., Stickland, N.C., 2007. In ovo temperature manipulation influences embryonic motility and growth of limb tissues in the chick (Gallus gallus). J. Exp. Biol. 210, 2667–2675. doi:10.1242/jeb.005751

13. Hoyt, D. F. 1987. A new model of avian embryonic metabolism. J. Exp. Zool. Suppl. 1:127–138.

14. Hulet, R., Gladys, G., Hill, D., Meijerhof, R., El-Shiekh#, T., 2007. PRODUCTION, MODELING, AND EDUCATION Influence of Egg Shell Embryonic Incubation Temperature and Broiler Breeder Flock Age on Posthatch Growth Performance and Carcass Characteristics. Poult. Sci. 86, 408–412. doi:10.1093/ps/86.2.408

15. Ipek, A., Sahan, U., Baycan, S.C., Sozcu, A., 2014. The effects of different eggshell temperatures on embryonic development, hatchability, chick quality, and first-week broiler performance. Am. Hist. Rev. 119, 464–472. doi:10.1093/ahr/119.2.464

16. Ipek, A., Sozcu, A., 2016. The effects of eggshell temperature fluctuations during incubation on welfare status and gait score of broilers. Poult. Sci. 1–8. doi:10.3382/ps/pew056

17. Janke, O., Tzschentke, B., Boerjan, M., 2004. Comparative Investigations of Heat Production and Body Temperature in Embryos of Modern Chicken Breeds. Avian Poult. Biol. Rev. 15, 191–196. doi:10.3184/147020604783637868

18. Joseph, N.S., Lourens, A., Moran, E.T., 2006. The effects of suboptimal eggshell temperature during incubation on broiler chick quality, live performance, and further processing yield. Poult. Sci. 85, 932–8. doi:10.1093/ps/85.5.932

19. Khandoker, A.H., Dzialowski, E.M., Burggren, W.W., Tazawa, H., 2003. Cardiac rhythms of late pre-pipped and pipped chick embryos exposed to altered oxygen environments, in: Comparative Biochemistry and Physiology - A Molecular and Integrative Physiology. pp. 289–299. doi:10.1016/S1095-

6433(03)00171-5

20. Leksrisompong, N., Romero-Sanchez, H., Plumstead, P.W., Brannan, K.E., Brake, J., 2007. Broiler Incubation. 1. Effect of Elevated Temperature During Late Incubation on Body Weight and Organs of Chicks. Poult. Sci. 86, 2685–2691. doi:10.3382/ps.2007-00170

21. Leksrisompong, N., Romero-Sanchez, H., Plumstead, P.W., Brannan, K.E., Yahav, S., Brake, J., 2009. Broiler incubation. 2. Interaction of incubation and brooding temperatures on broiler chick feed consumption and growth. Poult. Sci. 88, 1321–1329. doi:10.3382/ps.2008-00412

22. Lourens, A., Molenaar, R., van den Brand, H., Heetkamp, M.J.W., Meijerhof, R., Kemp, B., 2006. Effect of Egg Size on Heat Production and the Transition of Energy From Egg to Hatchling. Poult. Sci. 85, 770–776. doi:10.1093/ps/85.4.770

23. Lourens, A., van den Brand, H., Heetkamp, M.J.W., Meijerhof, R., Kemp, B., 2007. Effects of Eggshell Temperature and Oxygen Concentration on Embryo Growth and Metabolism During Incubation. Poult. Sci. 86, 2194–2199. doi:10.1093/ps/86.10.2194

24. Lourens, A., van den Brand, H., Meijerhof, R., Kemp, B., 2005. Effect of eggshell temperature during incubation on embryo development, hatchability, and posthatch development. Poult. Sci. 84, 914–920. doi:10.1093/ps/84.6.914

25. Lourens, a., Molenaar, R., van den Brand, H., Heetkamp, M.J.W., Meijerhof, R., Kemp, B., 2006. Effect of Egg Size on Heat Production and the Transition of

Energy From Egg to Hatchling. Poult. Sci. 85, 770–776. doi:10.1093/ps/85.4.770

26. Meijerhof, R., van Beek, G., 1993. Mathematical Modelling of Temperature and Moisture Loss of Hatching Eggs. J. Theor. Biol. 165, 27–41. doi:10.1006/jtbi.1993.1175

27. Molenaar, R., Reijrink, I., Meijerhof, R., Van den Brand, H., 2010. Meeting embryonic requirements of broilers throughout incubation: a review. Rev. Bras. Ciência Avícola 12, 137–148. doi:10.1590/S1516-635X2010000300001

28. Moran Jr, E. T. (2007). Nutrition of the developing embryo and hatchling. *Poultry Science*, *86*(5), 1043-1049.

29. Mortola, J.P., 2009. Gas exchange in avian embryos and hatchlings. Comp. Biochem. Physiol. - A Mol. Integr. Physiol. doi:10.1016/j.cbpa.2009.02.041

30. Nichelmann, M., Tzschentke, B., 2002. Ontogeny of thermoregulation in precocial birds. Comp. Biochem. Physiol. - A Mol. Integr. Physiol. 131, 751–763. doi:10.1016/S1095-6433(02)00013-2

31. Romanini, C.E.B., Exadaktylos, V., Hong, S.W., Tong, Q., McGonnell, I., Demmers, T.G.M., Bergoug, H., Guinebretière, M., Eterradossi, N., Roulston, N., Verhelst, R., Bahr, C., Berckmans, D., 2015. An insight into the heat and mass transfer mechanisms of eggshells hatching broiler chicks and its effects to the hatcher environment. J. Therm. Biol. 48, 69–76. doi:10.1016/j.jtherbio.2014.12.004

32. Romanini, C.E.B., Exadaktylos, V., Tong, Q., McGonnel, I., Demmers, T.G.M., Bergoug, H., Eterradossi, N., Roulston, N., Garain, P., Bahr, C., Berckmans, D., 2013. Monitoring the hatch time of individual chicken embryos. Poult. Sci. 92, 303–9. doi:10.3382/ps.2012-02636

33. Sotherland, P.R., Spotila, J.R., Paganelli, C. V, 1987. Avian eggs: barriers to the exchange of heat and mass. J. Exp. Zool. Suppl. 1, 81.

34. Tazawa, H., Chiba, Y., Khandoker, A.H.H., Dzialowski, E.M.M., Burggren, W.W.W., 2004. Early development of thermoregulatory competence in chickens: Responses of heart rate and oxygen uptake to altered ambient temperatures. Avian Poult. Biol. Rev. 15, 166–176.

35. Tazawa, H., Mitsubayashi, H., Hirata, M., Höchel, J., Pearson, J.T., 1999. Cardiac rhythms in chick embryos during hatching. Comp. Biochem. Physiol. - A Mol. Integr. Physiol. 124, 511–521. doi:10.1016/S1095-6433(99)00144-0

36. Tong, Q., McGonnell, I. M., Romanini, C. E., Berckmans, D., Bergoug, H., Roulston, N., ... & Demmers, T. (2012). Effect of high levels of CO2 during the final 3 days of incubation on the timing of hatching in chick embryos. In *Infomation Technology, Automation and Precision Farming. International Conference of Agricultural Engineering-CIGR-AgEng 2012: Agriculture and Engineering for a Healthier Life, Valencia, Spain, 8-12 July 2012*. CIGR-EurAgEng.

37. Tong, Q., Romanini, C.E., Exadaktylos, V., Bahr, C., Berckmans, D., Bergoug, H., Eterradossi, N., Roulston, N., Verhelst, R., Mcgonnell, I.M., Demmers, T., 2013. Embryonic development and the physiological factors that coordinate hatching in domestic chickens. Poult. Sci. 92, 620–628.

38. Tullett, S.G., Deeming, D.C., 1982. The relationship between eggshell porosity and oxygen consumption of the embryo in the domestic fowl. Comp. Biochem. Physiol. -- Part A Physiol. 72, 529–533. doi:10.1016/0300-9629(82)90118-9

39. Tzschentke, B., Rumpf, M., 2011. Embryonic development of endothermy. Respir. Physiol. Neurobiol. doi:10.1016/j.resp.2011.06.004

40. Van Brecht, A., Hens, H., Lemaire, J.L., Aerts, J.M., Degraeve, P., Berckmans, D., 2005. Environment, well-being, and behavior - Quantification of the heat exchange of chicken eggs. Poult. Sci. 84, 353–361.

41. Van Brecht, a, Aerts, J.M., Degraeve, P., Berckmans, D., 2003. Quantification and control of the spatiotemporal gradients of air speed and air temperature in an incubator. Poult. Sci. 82, 1677–1687. doi:10.1093/ps/82.11.1677

42. Visschedijk, A.H., 1985. Gas exchange and hatchability of chicken eggs incubated at simulated high altitude. J. Appl. Physiol. 58, 416–418.

43. Vleck, C. M., D. Vleck, and D. F. Hoyt. 1980. Patterns of metabolism and growth in avian embryos. Am. Zool. 20:405–416.

44. Whittow, G.G.C., Tazawa, H., 1991. The early development of thermoregulation in birds. Physiol. Zool. 64, 1371–1390. doi:10.2307/30158220

45. Yalcin, S., Siegel, P., 2003. Exposure to cold or heat during incubation on developmental stability of broiler embryos. Poult. Sci. 82, 1388–1392. doi:10.1093/ps/82.9.1388

GENERAL CONCLUSIONS

Individual biological process:

The **biological process** discussed in this chapter was the thermoregulatory system of chicken embryos. Based on the relation between the micro-environmental air temperature (**input variable**) and the eggshell temperature (**output variable**) of individual eggs, we aimed at finding critical information about the embryo status.
Again, significant **inter-individual differences** were found.

Process models and feature generation:

Based on an **online input-output modelling** approach, it was possible to determine the time series of **steady state gain** (SSG) values during the incubation period. SSG was selected it this case since it could be related with the embryo status based on **available biological/physical knowledge** about the heat transfer processes. Therefore, the models were data-based mechanistic.

Individualised change detection:

Changes in the SSG time series could be used to **detect five different milestones in the development of individual embryos**.
This chapter confirms the three different approaches we defined before to obtain individualised monitoring systems:
1) Individualised change detection based on **serial baseline measurements and individual thresholds** (Milestone M1 and M2)
2) Individualised change detection based on **universal laws and insights** from control engineering, biology, etc. (Most clear example here was SSG = 1 for M1).
3) Individualised change detection based on (sub)**population statistics** (Histograms of all milestones and thresholds from ROC curve analyses for **predictions**).

Part 3
General Discussion

"The whole is more than the sum of its parts."
— Aristotle —

(From: Aristotle, Metaphysics, Book VIII, 1045a.8–10)

Depicted in figure 3.1 is the general scheme of the individualised monitoring approach, as initially proposed in the introduction. In the forthcoming parts of this section, we expand upon the various elements of figure 3.1, which underpin the discussion throughout. With the general scheme in mind, the following four main topics will be addressed:

1) The bio-process
2) The process model
3) The model-based features
4) Individual change detection

In the final paragraph of this section, we present a methodological approach for individualised change detection that can be used for individualised model-based monitoring of biological processes in a wide range of applications.

3.1 THE BIO-PROCESS

We herein consider the first box of figure 3.1: the individual bio-process. Table 3.1, on the other hand, is, essentially, an overview of all bio-processes (and their corresponding experiments) that were addressed in this PhD. Four different species were studied in connection with the different monitoring applications: rats (chapter I, IV, V), pigs (chapter II), humans (chapter III) and broiler embryos (chapter VI).

3.1.1 Measuring individual details of the process (variables, spatial and temporal scale)

Figure 3.2A depicts a simple schematic representation of a biological process. Depending on the relevant spatial level, this biological process could either be a group of cells (e.g. Chapter IV) or a whole organism (e.g. Chapter VI; Table 3.1). As

mentioned in the introduction, most bio-processes can be considered as input-output systems. Accordingly, the block diagram includes input variables, which are measured from the bio-process environment (environmental variables), and output variables, which represent the responses of the bio-process to its environmental inputs (bio-signals). Moreover, bio-processes are continuously subject to a wide range of perturbations in their (internal and external) micro-environment (e.g. temperature, medications, social contact etc.). The inputs and perturbations are environmental variables, but with regards to inputs, we consider variables that

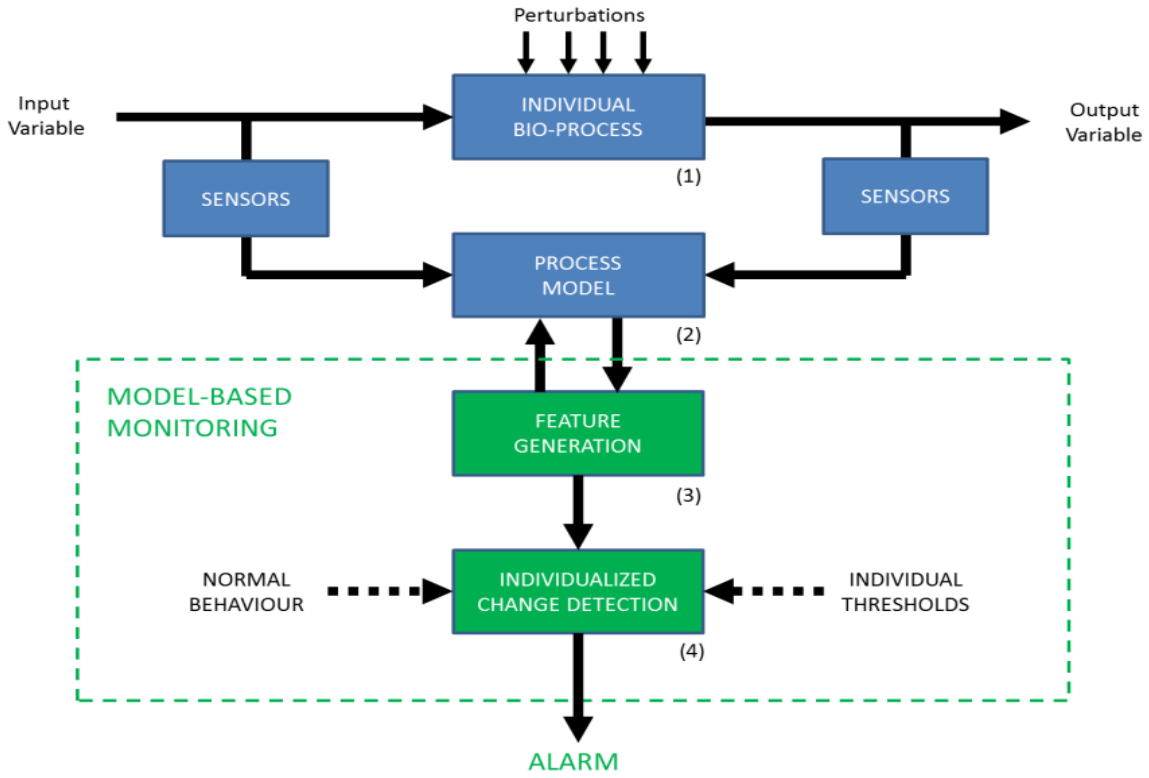

Figure 3.1 Block diagram representing the individualised model-based monitoring approach used in this PhD, including the following main blocks: (1) bio-process, (2) process model, (3) model-based features, (4) individual change detection.

are known or measured and might be actively changed during the monitoring, whereas the perturbations can be known or measured, but not controlled. For example, in chapter IV, we explain that by applying a drug (input variable) we could alter the measured brain cell responses (output variable). It can be assumed that temperature also has an effect on the measured brain cell response and, therefore, temperature could be considered as a perturbing variable. For each chapter of this PhD, the environmental variables and measured bio-responses are listed in table 3.1. In many cases, the input-output relation of the measured variables is known based on biological knowledge. If it's unclear as to whether a variable should be considered either an input or output variable, it is possible to use statistical approaches to determine causal relationships between variables (e.g. granger causality test, see e.g. Eichler, 2012).

Thus, for the analysis of a specific biological process, it is essential to have an overview of all relevant measurable variables that is based on available biological knowledge. In chapter V, we referred to starting from available biological insights when developing an individualised closed-loop deep brain stimulation system for rats. Since previous studies showed that theta oscillations in the hippocampus are highly related with locomotion, and that electrical stimulation in the mesencephalic reticular formation induces freezing, it was possible to develop a control system for suppression of locomotion.

Intuitively, one might assume that measuring more variables of the individual biological process automatically results in a more individualised and more accurate approach for monitoring, however, not all quantified individual information leads to an improvement in the performance of monitoring systems. Some variables might be irrelevant when monitoring a specific status of the biological process. Equally, some variables might strongly correlate with other measured variables, leading to redundant information. In such cases, the number of variables can be reduced by applying mathematical methods for dimensionality reduction (e.g. principal

component analyses, factor analysis or linear discriminant analysis; for more details on this topic see: Padmaja and Vishnuvardhan, 2016). In chapter III, the primary objective is the development of a model for accurate classification of infected patients based on heart rate characteristics and time series of cytokine. In this case, variables were included in the final model based on improvements of the discriminatory power (i.e. AUC). If the information extracted from an additional variable could not improve the classification results, the variable was removed, not to be included in the final classification model. The principal results of chapter III suggested that there was no significant additional value in adding cytokine time series information to the generated decision tree model based on heart rate characteristics. Thus, herein, another method for reducing the number of relevant variables was identified.

In some biological cases, the same physiological state can be characterised by different variables across different individuals. In other words, when detecting a change in state, one relevant variable found in individual A might be irrelevant in individual B, and vice-versa. We know from medicine that many diseases can lead to a number of signs and symptoms, which can vary from person to person. In many cases, a wide range of individual symptoms are involved, illustrating the interdependence of homeostatic mechanisms, whose perturbations lead to the individual manifestation of a disease (Zhou et al., 2014). For instance, the individual response of the body to an infection depends on many individual factors (e.g. susceptibility). This point is illustrated in figure 3.2, wherein it is shown that individual pigs can have different individual variables that reflect a change in infection state. Thus, for each pig the optimal individual variables should be selected. The individual selection of variables is one method of obtaining an individualised monitoring approach.

When all required variables are determined, it is also essential that the relevant temporal scale is known. In table 3.1, all used sampling frequencies of the measured variables are listed. Once again, we started from the available biological knowledge, since, for some biological processes, the sampling frequency can itself trigger the activation of physiological mechanisms that affect the time course of measured bio-responses and their underlying processes. In chapter IV, we show that the sampling frequency can influence the strength and time course of the synaptic plasticity responses. Similarly, in chapter II, we state that the number of blood samples affects the health status of the pigs, as extracting too much blood can result in unwanted health effects. However, from a modelling perspective, it should be noted that the sampling frequency should be high enough to prevent information loss (we expand upon this point in parts 3.2 The dynamic process model & 3.3 Model-based features).

To conclude, every physiological process is characterised by an exchange of mass, energy and/or information with its environment. Therefore, the individual state of the process can be assessed by measuring variables related to these exchanges. Ideally, we start from the available biological knowledge when selecting the relevant measurable (individual) variables for each biological process and their corresponding sampling frequencies. In addition to this, if possible, we define input-output relations between the selected variables.

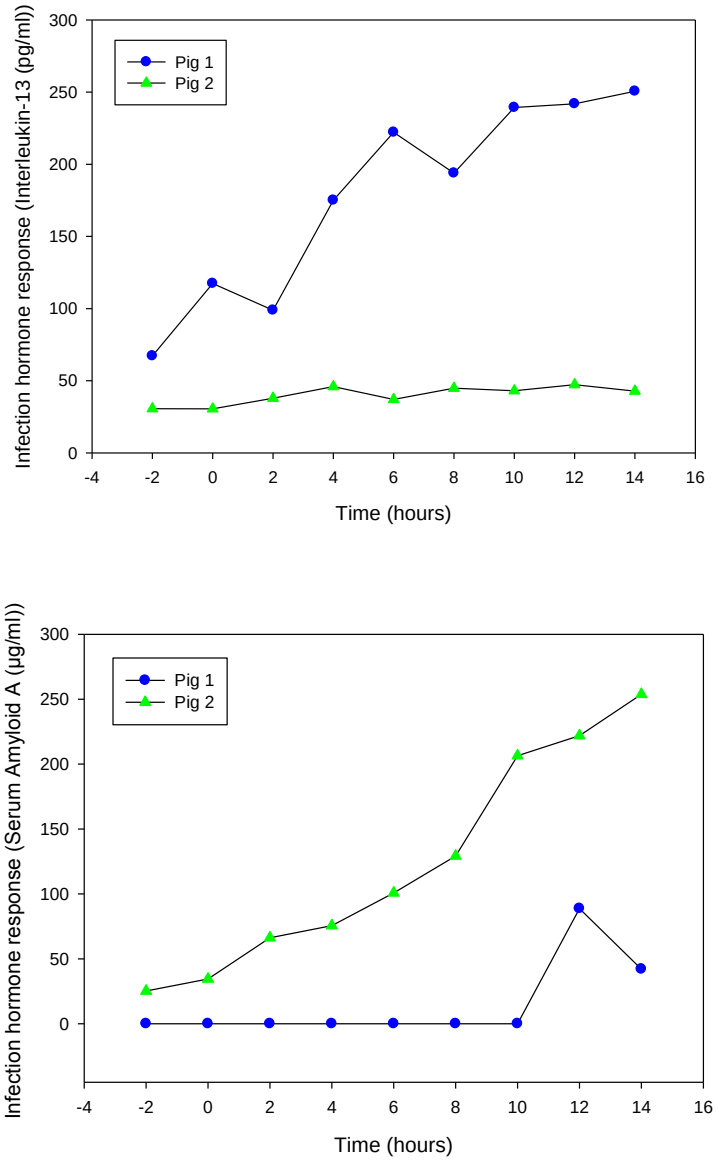

Figure 3.2 The infection response of the hormones IL-13 and SAA are depicted in relation to two different pigs (unpublished results). Time point 0 corresponds with the moment of infection (see methods section in Chapter II of Part 2). For Il-13, pig 1 shows a clear infection response, whereas no increase of IL-13 was detected for pig 2. For SAA, it was pig 2 that had the most pronounced response to infection. These results illustrate that each individual pig can have different individual variables which optimally respond to state changes (e.g. infection).

Table 3.1. Overview of the different bio-processes which are considered in the different chapters of this PhD

	Spatial level	Sampling Frequency	Environmental variables (inputs)	Measured bio-signals (output)	Species	Number of experiments
Chapter I	Organism scale	1/ day	Food availability	Food intake, Running wheel activity, Body weight	Rat	56
Chapter II	Organism scale	1/2 hrs	Endobronchial inoculation with bacteria (infection)	Blood hormone levels	Pig	30
Chapter III	Organism scale	1/ 10 min	Infection	Heart rate, Blood hormone levels	Human	39
Chapter IV	Cellular scale	1/ 5 min	Application of drug (e.g. DHPG)	fEPSP slope	Rat	55
Chapter V	Organism scale	10000/sec	Deep brain stimulation	Locomotion, Hippocampal theta oscillations	Rat	12
Chapter VI	Organism scale	1/min	Temperature of local egg environment	Eggshell temperature	Chicken embryo	74

3.1.2 Biological systems as control engineering components

Since we can consider biological systems as highly controlled systems, the individual bio-process can be interpreted from a control engineering point of view (see Figure 3.3). So as to ascertain system stability when subject to continuous perturbations, bio-processes are designed in a highly optimised way (See BOX 3.1). Therefore, measurements of the system architecture can also be relevant for the monitoring of biological processes. For example, when monitoring diseases in an individualised way, it might be necessary to obtain 'architectural' information of the biological process at different spatial levels (DNA profile, biopsy, CT scan of organ). Concepts of robustness, organisation and architecture (e.g. modularity) are essential to understanding complex networks (Doyle and Csete, 2011). Each biological system is composed of different components, which are the biological equivalents of engineering control systems, such as biological sensors, actuators, controllers and layers of feedback regulation (Csete and Doyle, 2002). Therefore, the first block diagram (figure 3.3A) could also be refined, as represented in figure

3.3B. In the block diagram, the biological controller (e.g. a brain region) calculates the required process input so that the process can be modified and, therein, homeostasis can be maintained. Typically, the controller determines the actuator action (e.g. pumping of the heart) needed to influence the process state (homeostatic variable). A biological sensor is needed to measure the actual state of the bio-process (e.g. eye, proprioceptor), which can then be compared with the desired state of the bio-process (i.e. target).
Together, these components ascertain robustness for uncertain environmental conditions. Robustness makes it possible for the complex biological system to preserve its functionalities against external and internal perturbations (Kitano, 2004; Stelling, 2004; Kitano, 2007). That said, biological systems can be robust in some environmental conditions, yet fragile in others (Doyle et al, 2011).

For example, in neuroscience, dopamine is part of a robust and flexible reward system, however, that same system is susceptible to hijacking by addiction. Within a fragile biological system, smart architecture can allow hiding and protecting these fragilities. For example, our skull protects our fragile brain from trauma and, similarly, the blood-brain barrier is very effective in protecting the brain from pathogens (Doyle et al, 2011).

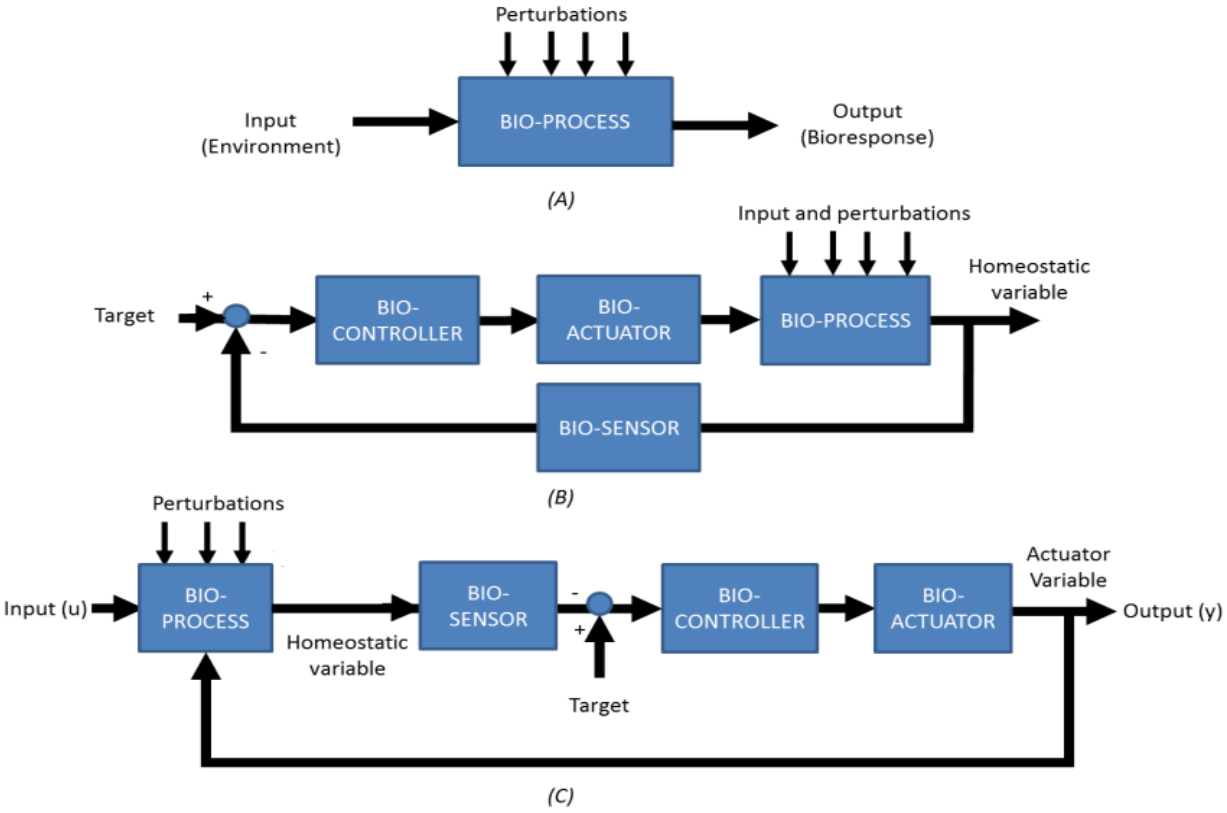

Figure 3.3 General block diagrams of biological processes. (A) Input-output representation of bio-process (B) Representation of controlled bio-process according to a general control system. (C) Input-output representation of a controlled bio-process with an environmental variable as input and an actuator variable as output.

BOX 3.1 Complex biological networks design

Every biological system can be considered as a complex network of many interacting individual dynamical systems (Strogatz, 2000). The field of complex systems science tries to decompose such **complex systems** into their main components and relates specific system architectures with typical dynamic system properties. Recent studies advocate that there are two **major architectural system features** which characterize such complex systems: i) the homo- or heterogeneity of the components and ii) their connectivity (Levin et al, 2000; Scheffer et al., 2012). The **homogeneity and connectivity of the components** determines the way such systems respond to changing conditions (Figure B.3.1; Scheffer et al., 2012). For example, many brain regions are characterised by a huge amount of similar, highly interconnected components (e.g. brain cells). When many individual neurons are connected, each of which having their own individual dynamics, a new, more complex system arises and dynamic system properties can originate such as, for example, synchrony. The dynamic properties of such networks can be a marker for disease (e.g. increased synchrony of brain activity in epilepsy, decreased synchrony in Parkinson's disease; Scheffer 2012; Stanley 2013) or health (EEG signals for detection of sleep stages; Bulckaert et al., 2010).

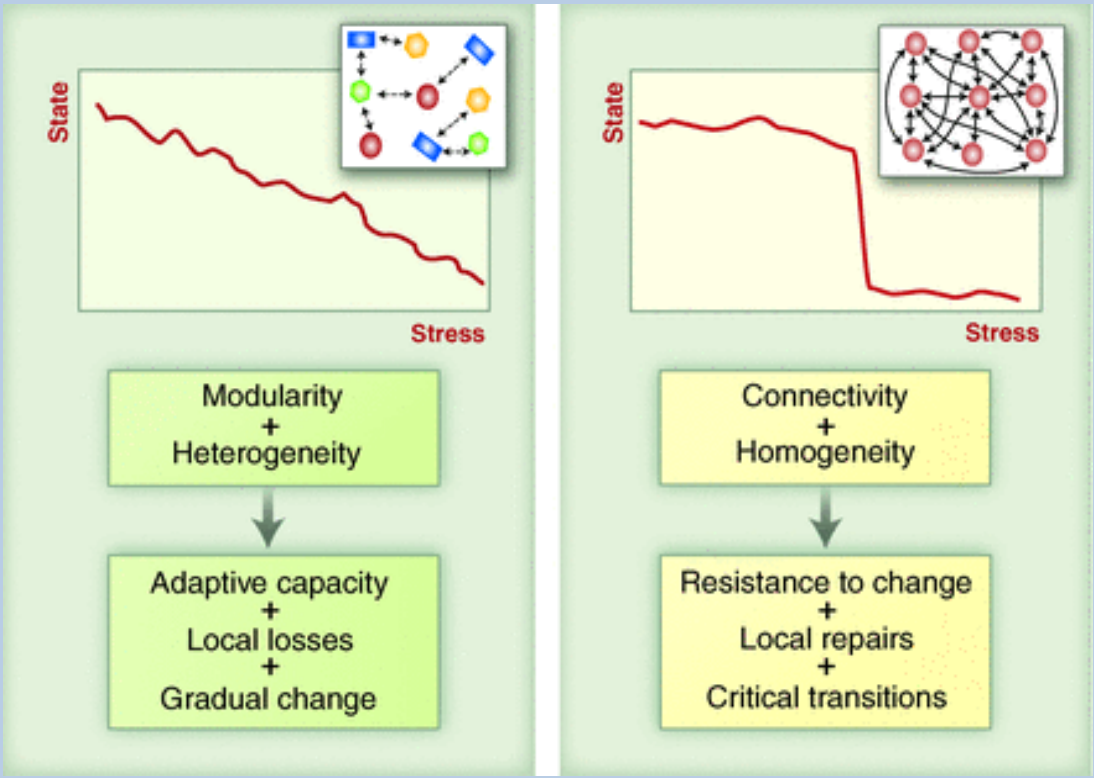

Figure B.3.1. Examples of architectural system characteristics related with system function (Scheffer et al, 2012)

Finally, the block diagram of Figure 3.3B can again be modulated to obtain an input-output system representation (Figure 3.3C), similar to those illustrated in Fig. 3.1 and Fig. 3.3A. Depending on the measured output variable, the scheme could have different configurations. In the represented configuration, the measured output variable is an actuator variable, but it could also be a homeostatic variable. Making this distinction is important, since a variable of a biological actuator has different properties compared with a homeostatic variable (Cannon, 1929; Li et al., 2014). Actuator variables typically show fast fluctuations (e.g. small time constants), since actuators should respond as quickly as possible to changing conditions, whereas homeostatic variables show less variations, because constancy is their key aspect of preserving healthy internal body conditions. A sensor should be able to react to fast fluctuations and with a minimal delay so as to ascertain fast responses in the controller component of the system (see e.g. Chapter V). In the following paragraphs, this approach is applied to the bio-processes considered in this PhD research.

In chapter I, body weight and food intake were two of the measured variables during the rat conditioning period of the activity-based anorexia rat model. Both variables are involved in the process of energy homeostasis, which is controlled by the central nervous system (Dhillon et al., 2006; Morton, et al; 2006). Food intake is known to be modified over time in order to regulate stability in the amount of body fuel stored as fat (e.g. body weight homeostasis; Morton, et al; 2006). In light of this, we can consider food intake as an actuator variable in that it is the result of food-seeking behaviour, whereas body weight can be considered as a homeostatic variable. It is expected that anorexia nervosa and obesity result from dysfunction of any, or several, of the components of this homeostatic control system.

In chapter II and III, the pro-inflammatory (and anti-inflammatory) cytokine response was described during infection conditions. Cytokines are released, at the cellular level, in response to invading pathogens. They can be considered as

actuator variables, which are regulated by the sympathetic/parasympathetic neural control of the infection response (Czura et al., 2005). In normal conditions of homeostasis, the inflammatory response reinstalls the body to healthy function following the clearance of the invading agents, and promotes appropriate tissue repair (Vodovodtz et al., 2006; Namas et al., 2012). On the other hand, a deregulated inflammatory response can lead to organ dysfunction or even death.

As explained in chapter IV, brain signals are measured at cellular level. Communication through brain cells is much faster compared with hormone signalling through the blood (e.g. less time delay in the system). Typically, the central nervous system, at organism scale, acts as controller of the many body systems (Chapter V). More specifically, in chapter IV, we looked at synaptic plasticity of the brain. Long-term potentiation (LTP) and long-term depression (LTD), two forms of synaptic plasticity, provide the basis for most learning and memory models. Neuronal circuits must be able to adapt their properties (read: to learn) in order to allow animals and humans to function in a robust way, within a dynamic environment, with many different types of perturbations (Desai, 2003). Several studies indicate that neural activity is itself dependent on homeostatic regulation for prohibiting neural circuits from becoming hyper- or hypoactive. There is evidence for the presence of "stabilizing mechanisms" operating at the level of neural circuits. These mechanisms prevent forms of plasticity, such as long-term potentiation (LTP) and long-term depression (LTD), drive neural activity towards runaway excitation or quiescence (e.g. "homeostatic synaptic plasticity") (Desai, 2003, Turrigiano et al., 2004). From this perspective, the postsynaptic neural activity can be considered a homeostatic variable, whereas variables related with the processes leading to LTD or LTP can be considered as actuator variables, which are controlled by these stabilizing mechanisms.

In chapter VI, we recorded our analysis of the individual eggshell temperature of embryos during incubation. The body temperature of homeothermic organisms can be considered as a homeostatic variable, which, for healthy conditions, is more or less stable between narrow boundaries (Grahn et al., 1997). However, the development of the thermoregulatory system initiates with non-specific and non-coordinated reactions without any adaptive effect (Youssef et al., 2014). Only later in the embryo development, the thermoregulatory system turns into a coordinated system with adaptive reactions. Afterwards the thermoregulatory system develops from an open loop system into a closed loop control system with feedback mechanisms to ascertain homeostasis (Tzschentke, 2010; Youssef et al., 2014). To obtain such internal thermal homeostasis, each individual organism (i.e. embryo) must be able to balance heat losses and heat gains.

In this section, we discussed the individual bio-process according to the general scheme (Figure 3.1). The featured examples show that the process of designing a model-based monitoring application can begin with combining biological knowledge of the individual bio-process (e.g. for defining homeostatic variables) with insights from control engineering (e.g. use of typical feedback control loop diagram; figure 3.3B and 3.3C).

3.2 THE DYNAMIC PROCESS MODEL

In the previous section, the considered bio-processes are discussed from a control engineering point of view. We show that bio-processes can be considered as input-output systems (figure 3.3A & 3.3C), and further indicate the need to distinguish between actuator and homeostatic bio-signals (outputs). Classical process change detection methods (e.g. Basseville and Nikiforov, 1993) are restricted to limit or trend checking of some directly measurable output variables. In order to

extract more process information, model-based methods of change detection were developed and subsequently used to extract (non-directly measurable) biological state information by using input and output signals and applying dynamic process models (see figure 3.1 and figure 3.4A; Isermann, 2005).

The chosen modelling approaches in this PhD can be linked with a general family of dynamic process models for modelling linear, dynamic, discrete-time, input-output relationships, as described by Box-Jenkins (BJ) (see figure 3.4B; Ljung, 1987; Box et al., 1994).

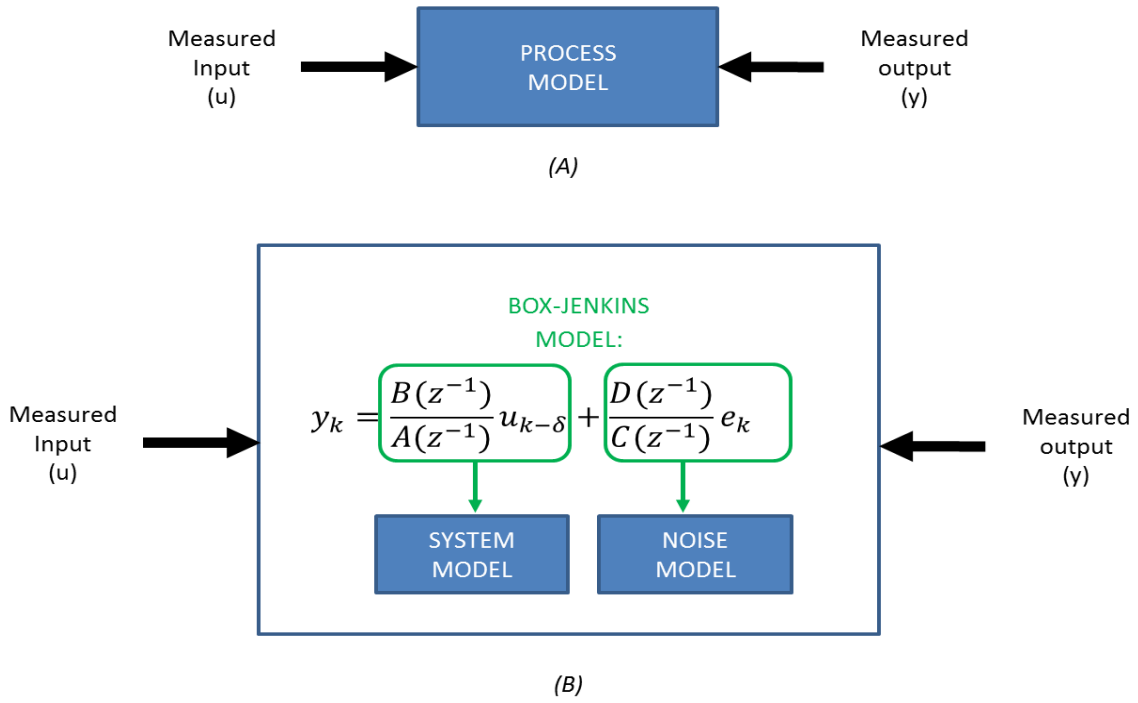

Figure 3.4 General block diagrams of a process model. (A) Input-output representation of process model; (B) Equation of Box-Jenkins model with system model and noise model.

As shown, the boxed equation on the left-hand side of figure 3.4B represents the system model; the right-hand sided boxed equation represents the noise model (defined according to Ljung et al, 1984; Box et al., 1994 and Young et al, 2011). The noise model represents the total uncertainty in the model, including measurement noise, modelling errors, and the effects of unmeasured (uncontrollable) inputs to the process (Ljung et al, 1987 and Young et al, 2011). Where *y(k)* and *u(k)* are the sampled values of the output(s) and input(s), respectively; k represents discrete time steps; δ is the time delay between system input and output; *e(k)* represents white noise, which is identically distributed and independent with zero mean value; and variance σ^2; $A(z^{-1})$, $B(z^{-1})$, $C(z^{-1})$ and $D(z^{-1})$ are the polynomials of model parameters (for more details on the Box-Jenkins model see e.g. Young, 2011). The polynomials are defined as follows:

$$A(z^{-1}) = 1 + a_1 z^{-1} + \cdots + a_n z^{-n}$$
$$B(z^{-1}) = b_0 + b_1 z^{-1} + \cdots + b_m z^{-m}$$
$$C(z^{-1}) = 1 + c_1 z^{-1} + \cdots + c_p z^{-p}$$
$$D(z^{-1}) = 1 + d_1 z^{-1} + \cdots + d_q z^{-q}$$

Every polynomial is a function of z^{-1}, a backward shift operator defined as $z^{-1}y_k = y_{k-1}$; a_i, b_i, c_i and d_i represent the model parameters; n, m, p and q represent the order of the polynomials *A, B, C* and *D.*

The most suitable models for a specific dataset can be selected based on three criteria: R_T^2, AIC and YIC. They can be used as statistical measures for goodness of fit, overparameterisation, and how well the model explains the data. Additionally, the available biological knowledge can assist in defining criteria for optimal model selection. In the methods section of chapter IV, a more elaborate explanation of these criteria is given.

The final stage of model synthesis should ideally be model validation. For example, the three criteria mentioned above can be used to validate the goodness of fit. Secondly, a validation by analysing the model residuals can be obtained by an autocorrelation test for the residuals and a cross-correlation test between the residuals and the inputs (Ljung, 1987). However, even the definition of validation is controversial and, often, the two approaches described above are not considered as model validation (Young, 2011; Clermont and Zenker, 2015). Nevertheless, one type of validation, known as 'predictive validation' is widely accepted. In that case, the predictive potential of the model is evaluated by verifying whether a model can accurately predict an outcome or a time course in data other than used in the earlier stages of model identification and parameter estimation (Aerts et al., 2003; Young, 2011; Clermont and Zenker, 2015). However, even a BJ model that is poorly specified from a biological system point of view may, in some cases, be practically perfect from a monitoring point of view (Clermont and Zenker, 2015).

In addition to the linear BJ models, there exists a wide range of non-linear models that could be used for data-based modelling (e.g. Hammerstein-Wiener models and non-linear ARX models, neural networks, etc.). However, in this PhD we focused on exploring the possibilities of linear model types (Table 3.2). BJ models allow the individual, time-varying and dynamic natures of bio-processes to be captured, as shown in Chapter IV. The input was the application of a drug (e.g. DHPG), and the output was the electrical response of the brain slices (e.g. fEPSP) (see also figure IV.1, in Chapter IV). It's been shown that linear models could describe significant non-linear phenomena in an accurate way (R_T^2 of all models > 0.82). Also, in chapters II, III and VI, linear models were successfully applied to quantify the biological responses (Table 3.2). Furthermore, in chapters II and III, we detailed using integrated random walk (IRW) models in the removal of trends in the data so as to obtain the model residuals. The use of these IRW models can be considered the

Table 3.2. Overview of different model types used in the PhD chapters.

	Model type	***Model equation(s)***	***System or Noise Model***
Chapter II	*Integrated Random Walk Model*	$y_k = y_{k-1} + s_{k-1}$ $s_k = s_{k-1} + e_k$	*Equivalent of BJ noise model*
Chapter III	*Integrated Random Walk Model*	$y_k = y_{k-1} + s_{k-1}$ $s_k = s_{k-1} + e_k$	*Equivalent of BJ noise model*
Chapter IV	*Output-Error Model*	$y_k = \frac{B(z^{-1})}{A(z^{-1})} . u_k + e_k$	*Equivalent of BJ system model*
Chapter VI	*Output-Error Model*	$y_k = \frac{B(z^{-1})}{A(z^{-1})} . u_k + e_k$	*Equivalent of BJ system model*

equivalent to determining the *BJ noise model* (Young et al, 2011). In chapters IV and VI, the *a*- and *b*- parameters of output error models were used to describe the individual relation between the input and output variable. Therefore, these models were considered as equivalents of the *BJ system model*. Each and every example presented in the preceding chapters showed that we can use compact linear models for monitoring individual non-linear bio-processes. These results support other studies that show we can use local linear approximations of non-linear systems to describe the local dynamics around equilibrium points (i.e. linear stability analysis; for more details: see May, 1974; Strogatz, 2001; Ives et al., 2012). Moreover, it is also possible to use linear modelling methods with time-varying parameters for monitoring non-linear biological processes (see for example Chowdhury, 2000 and section 3.4.4 further in the discussion).

The fact that we can use such compact BJ models to describe such bio-processes is, at first-sight, highly unexpected because bio-processes are, without any exception, very complex. However, as mentioned in section 3.1, bio-processes can be considered robustly controlled engineering systems (as mentioned in section 1: the bio-process; figure 3.3). In light of this, such systems often show relatively simple

responses (expressing the crucial dominant processes that ascertain healthy internal homeostatic or homeodynamic conditions) when exposed to perturbations, as illustrated by the given examples in this PhD. Consequently, these systems can be modelled successfully using compact models such as BJ models.

By describing individual relations between input and output variables with BJ models, individual models can be obtained for the specific biological process. However, some model characteristics can be fixed on group level. In chapter VI, for instance, first order models were used for all individuals (i.e. group level), but the parameter values reflected the inter- and intra-individual differences (i.e. individual level; figure VI.5). This approach is partially in line with the use of mixed-effect models for description of an individual bio-process response (e.g. individual pharmacokinetics; Davidian and Giltinan, 2003; Pillai et al., 2005). Mixed-effect models try to capture information at group/population level and more individual information, characterised as random effects (for more details: e.g. Davidian and Giltinan, 2003; Clermont and Zenker, 2015).

3.3 MODEL-BASED FEATURES

Once the suitable process model is identified for use with an individual bio-process, model-based features can be generated (as in figure 3.1). Based on such features, state changes in the system can be detected. In this PhD, three different model-based features were used for the developed model-based monitoring applications: model parameters, model order and model noise term (figure 3.5).

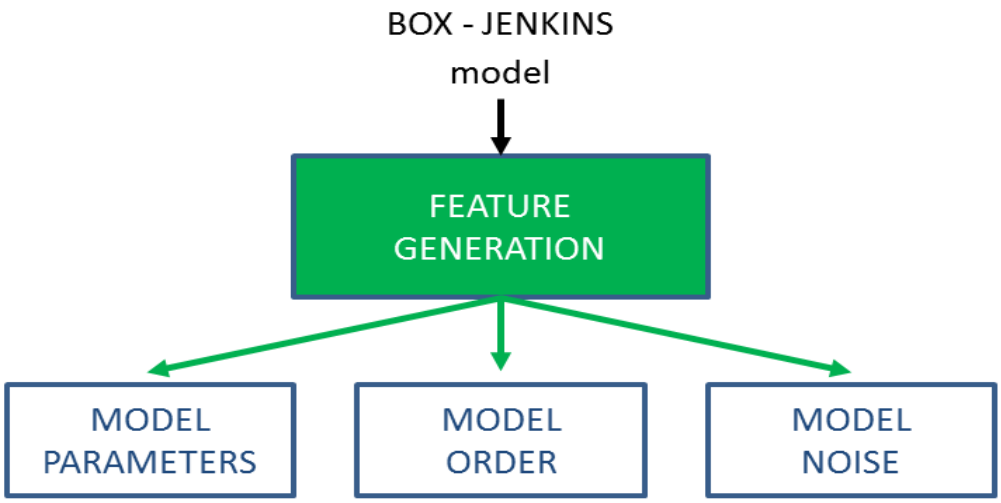

Figure 3.5 General block diagram of the feature generation with the three model-based features: model parameters, model order and model noise term.

3.3.1 Model parameters

In this PhD, we developed a monitor based on model parameter changes (as shown is Chapter VI)—or, more specifically, system model parameters (e.g. a_i and b_i of the general BJ model)—so as to detect individual system changes.

The most straightforward way to develop such a monitoring system would be to use the parameter values themselves as change detectors (e.g. Lefever et al., 2014). An alternative to the aforementioned method is the use of parameter derived metrics, such as the steady state gain (see figure 3.7; Lambrechts et al., 2014). In chapter VI, we cover the use of dynamic data-based transfer function models, which detect changes in embryo status during the incubation period. In these models, the local environmental temperature was used as input, and the eggshell temperature was used as output. Based on changes of the steady state gain values, we could detect the developmental milestones of the embryos.

Figure 3.6 shows the results of another study (unpublished results from internship at Control and Dynamical Systems, Caltech, Pasadena; supervisor: Prof. John Doyle), wherein the steady state gain could be used to detect physiological differences. In this study, the main objective was to explore whether heart rate responses to training intensity contain information which can be linked with physical fitness, in this case, during road cycling (in field conditions.). As can be seen in the figure below, a bad physical fitness (lactate threshold group 1) is related with a high steady state gain, and vice versa.

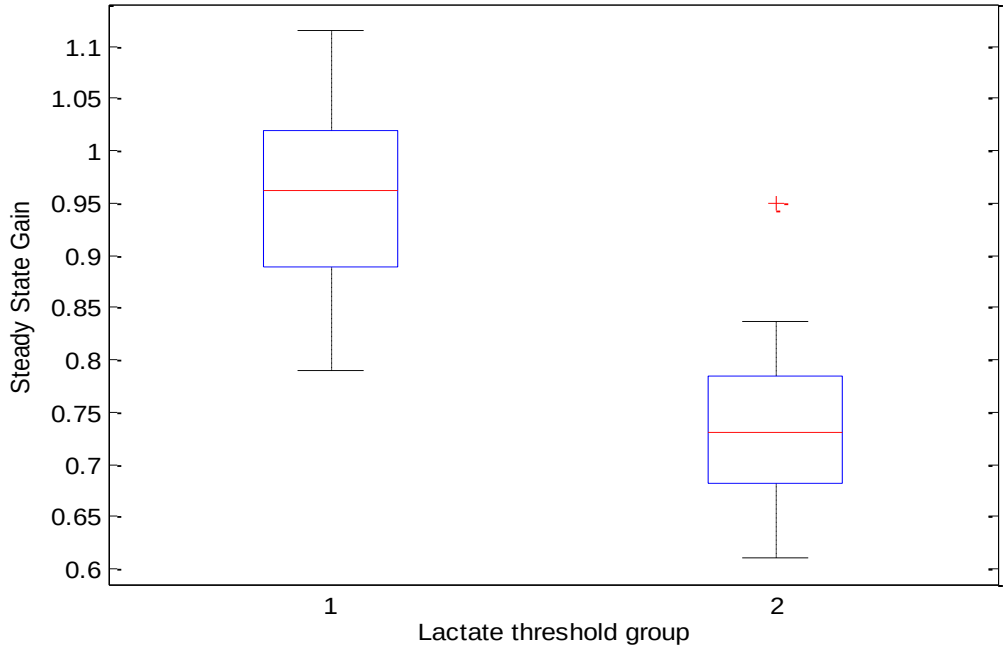

Figure 3.6. Boxplots showing the steady state gain on the y-axis and the lactate threshold group on the x-axis. Cyclists of group 1 (group with bad physical fitness) have a power level lower than 200 W at the lactate threshold. Cyclists of group 2 have a power higher than 200 W at the lactate thresholds and thus a better physical fitness. The SSG values of both groups are significantly different ($p < 0.01$).

The steady state gain can be calculated based on a function of the *a*- and the *b*-parameters (for more details on the definition and equations: see Methods section in chapter VI). Besides the steady state gain, it is also possible to use other parameter-derived metrics, such as the time constant (for definition and equation: see Eq. 2.7 in chapter IV; see figure 3.7). The time constant gives a measure of the dynamics of a considered biological system. In practical terms, assuming zero initial conditions, it is the time taken for the output to reach 63% of its steady-state value in response to a step input (see chapter IV). To be able to quantify the dynamics of a biological response with a model, the sampling rate should be high enough. Discrete measurements of continuous signals cause information loss and, therefore, only for an optimal sampling rate can the model parameters correctly represent the real underlying system. The sampling interval between two data points should be, maximally, half of the value of the time constant (Nyquist-Shannon sampling theorem; Nyquist, 1928). In the first section of the discussion, we saw that there can also be biological arguments for lowering the sampling rate (see 3.1 The Bio-process). In that case, it is essential to find an optimal balance between the modelling requirements and the biological requirements for the sampling rate.

However, the dynamics of an individual system can be analysed at different temporal scales. Therefore, the dynamic range of interest should be specified for each individual monitoring application. For example, if the person whose fitness we try to improve trains on a weekly basis, they will see gradual changes in their physical condition week-by-week. However, even in monitoring changes on a daily basis we notice many variables capable of impacting cardiovascular response, such as sleep pattern, reaction to environmental temperature, etc. Thus, for other monitoring applications much higher sampling rates would be indicated (e.g. heart rate monitor at intensive care).

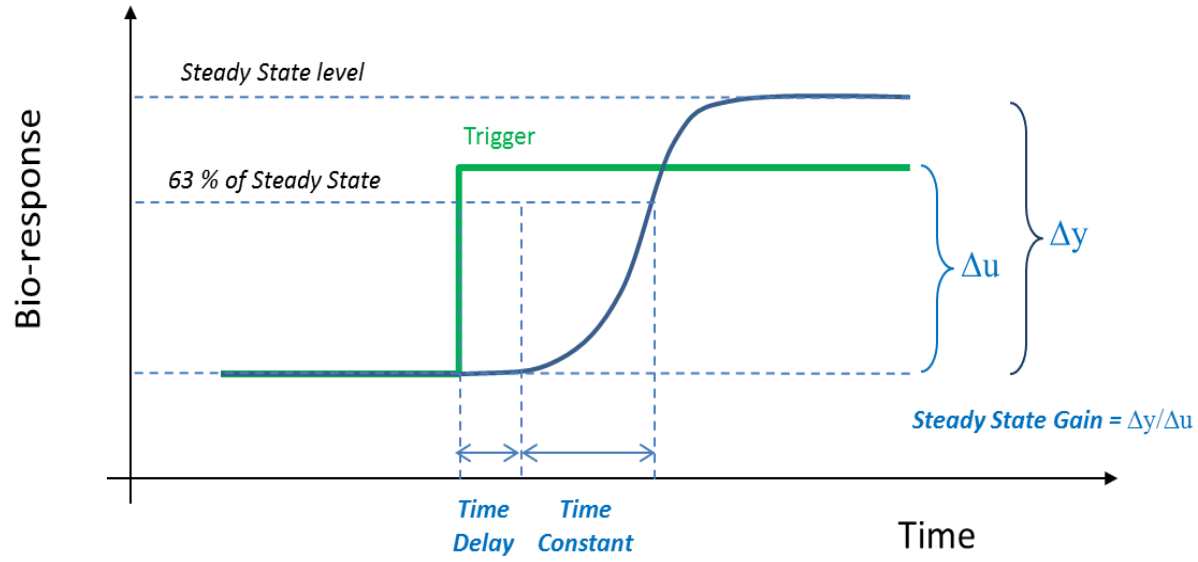

Figure 3.7 Visual representation of time constant and steady-state gain.

3.3.2 Model structure/order

An alternative method for quantifying individual model-based changes, as applied in this PhD, is to use the model order of the system model. As mentioned in the previous section (3.2 The dynamic process model), the number of *a*-parameters represents the order of the BJ model. In chapter IV, we found that we can determine the number of dominant underlying processes by defining the model order of the input-output models (see also Boonen, 2005). In that study, we investigated the underlying mechanisms of mGluR-dependent synaptic plasticity. A drug was applied (i.e. DHPG; input) to induce mGluR-dependent long-term depression (LTD) (i.e. fESPS; process output; see figure IV.1 in Chapter IV). Since we found a second order model as an optimal model, two major underlying processes were indicated by the modelling results. The second order models could be decomposed in two first order models, whereas each model corresponds with one of the two dominant processes. Based on these results, it is suggested to use several inhibitors or agonists of specific underlying pathways to link the obtained parameter values with specific

clusters of physiological pathways. It would be expected that blocking some of the underlying pathways could lead to a reduction in model order of the derived transfer function models. In an unpublished study, which was carried out to further explore the results described in chapter IV, we could confirm this hypothesis. In that study, insulin was used to induce long-term depression (LTD) responses. In baseline conditions (no inhibitor applied), an accurate second order model was obtained for the insulin dependent LTD responses (R_T^2= 96%), suggesting that two dominant processes underlie this type of synaptic plasticity. This result corresponds with other physiological studies, which suggest the presence of two main parallel signalling cascades: the extracellular signal-regulated kinase (ERK1/2) cascade and the phosphatidylinositol 3-kinase (PI3K)/Akt/mTOR cascade (see figure 3.8; Wada et al., 2005; van der Heide et al., 2006). Afterwards, the PI3K/Akt/mTOR pathway was inhibited at a downstream signalling complex constituted by Glycogen synthase kinase 3 (GSK-3β). Following the application of the GSK-3β inhibitor, we found a first order model. Thus, by application of this inhibitor, one of the two dominant processes were blocked (Figure 3.9). The results shown in figure 3.9, were based on LTD responses of young mice. Interestingly, we also found first order models without application of inhibitors in middle-aged mice. This could be explained by an alteration in the signalling pathway due to an age effect. Literature suggests GSK-3β plays a significant role in Alzheimer's disease (Hooper et al., 2008; Hernandez et al., 2009), therefore it could be assumed that there is a connection between GSK-3β regulation and ageing. Moreover, more recent data show that during ageing insulin-LTD changes its properties due to desensitization of the insulin-signalling pathway downstream of the insulin-receptor. A major role in this process play lipid changes in the membrane due to loss of cholesterol (Martín-Segura et al. submitted). Thus, this study shows how it is possible to obtain grey box models by linking the model

structure of data-based (black box) models with biological information from underlying pathways.

In other studies, similar approaches showed that model order can be used to monitor the state of a system. For example, Silva et al. (2011) used autoregressive models to quantify sound signals of pigs. Sick cough signals were characterised by third order models, whereas 'healthy' coughs were characterised by lower order models. This difference could be explained by the presence of mucus in the respiratory tract of sick animals.

In yet another study, Youssef et al. (2013) showed that differences in model order can be used to detect thermoregulatory state changes in organisms. More specifically, they developed dynamic models to describe the input-output relation of the incubation temperature (input) and the eggshell temperature (output) of broiler embryos during incubator-based embryo development. Interestingly, this study showed that a first-order model was optimal in describing the dynamic embryonic response of the egg shell temperature between days 9 and 13 of the embryonic development, whereas second order models were needed to describe this dynamic response after day 13 (day 14-19 of the embryonic development). Except for model parameters, the change in model order was attributed by the authors as a change in the complexity of the thermoregulatory system of the embryos.

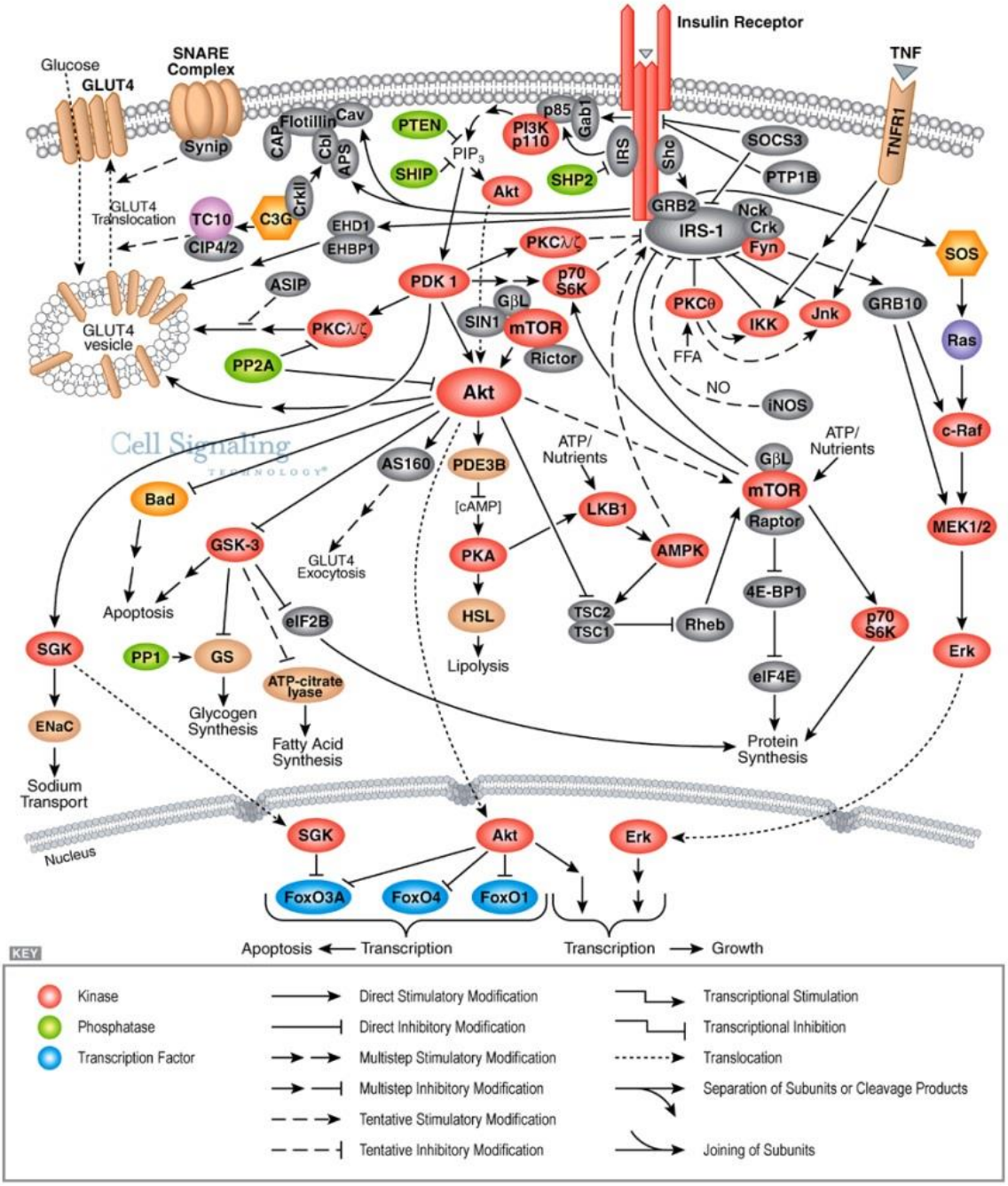

Figure 3.8 The insulin pathway (www.cellsignet.com)

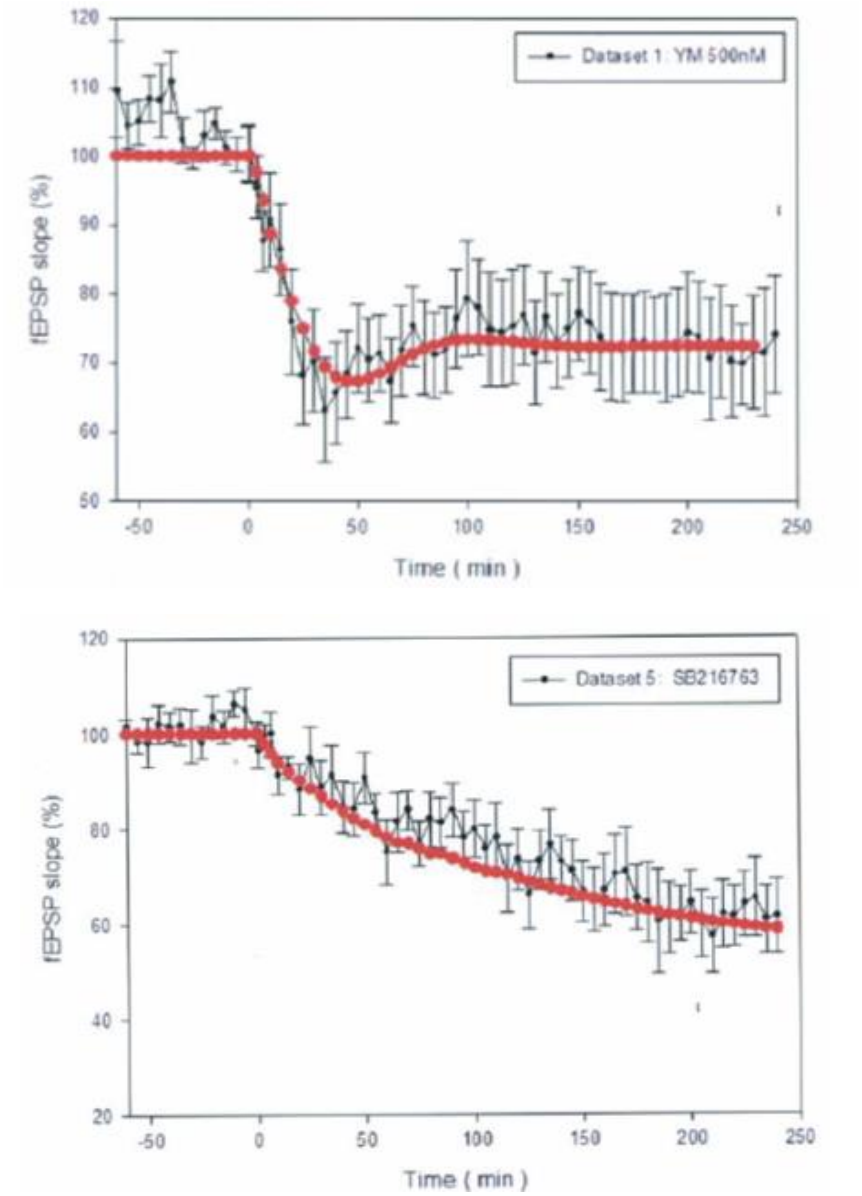

Figure 3.9 (A) Insulin-dependent LTD responses without application of inhibitor. For this response, a second order model was found (red). (B) Insulin responses with application of an inhibitor of one of the main underlying pathways. For this response, a first order model was found as optimal model (red).

3.3.3 Model noise

In addition to the model parameters and the model order of the system model, we demonstrated in this PhD that we can also use the noise term (as defined in Young, 2011; see noise model of the BJ model equation in section 3.2) for the development of an individualised monitoring system. Figure 3.10 shows an example of an input-output BJ model and how it can be used to decompose both the data in the system model component and the noise term component. Similarly, in chapter II, integrated random walk (IRW) models were shown to have been used in the removal of slow fluctuations (≈ system model) in the data (i.e. cytokine time series). The remaining residuals were used to determine the fast dynamics of the infection responses. Based on a quantification of these residuals (≈ noise model), we could correctly classify infection in pigs. More specifically, amplitude increases in the IRW model residuals of the cytokine time series showed that the residuals were correlated and thus, the time series of residuals cannot be interpreted as white noise (e.g. Scheffer et al., 2009). These amplitude increases were used as an indicator of the infection state in individual pigs. Recent studies suggested that increased variance in the pattern of fluctuations of the residuals can be an early indicator of approaching critical or non-critical transitions in complex dynamical systems (Scheffer et al., 2009; Kefi et al., 2013). Additionally, in chapter III, we covered a list of change indicators which can be used as early markers of transitions in time series (See also Dakos et al., 2012). So far, such time series approaches for quantification of early warning signs of changes in complex dynamical systems are, mostly, applied in ecological and climate studies. However, biological systems could be a particularly rich field of exploration for these methods (Scheffer, 2012; Trefois et al,. 2015). To the author's knowledge, it is the first time that these approaches are applied for quantification of measured cytokine responses to infection. Nevertheless, these methods also have a number of limitations (For more details see for example Dakos et al., 2015).

The BJ model is outstandingly complementary of the time series approaches from the emerging field of research, for it is uncovering early warning signs (EWS) in the proximity of critical or non-critical changes in complex dynamical systems (Scheffer et al., 2009; Kefi et al., 2013). Whereas the BJ model is typically used to analyse the output variable in response to an applied input variable (focus on the system model: input, u, output, y, and the corresponding model parameters in the polynomials A and B), the field of EWS analyses the system response on repeated small perturbations (focus on the noise model: model residuals, *e*, and its parameters reflected in C and D of the BJ model equation) (For further reading see e.g. Scheffer et al., 2009 and Kefi et al., 2013). Thus, removing the trends of a time series based on an integrated random walk, so as to obtain the residuals (fast dynamics), is equivalent to using the system BJ model based on input and output variables for the purpose of calculating the model residuals of the BJ model (See figure 3.10).

Therefore, for the general monitoring of bio-signals, we advocate a combination of both approaches (BJ model & EWS) into one framework. To the author's knowledge, it is the first time that both approaches are linked, which could lead to new insights in both scientific domains.

Based on the information in the previous paragraphs, we suggest three different model-based markers for individual state changes in organism: parameter changes, changes in model order and changes in model noise characteristics. For every monitoring application, we need to define the model-based feature of individual change for monitoring individual processes.

3.4 INDIVIDUALISED CHANGE DETECTION

3.4.1 Need for individualised change detection

In the previous section, we discussed how model-based features were used in this PhD to detect state changes of bioprocesses. However, we have also shown that there is need for individualised change detection. This means that we have to follow changes of model-based features per each individual bio-process.

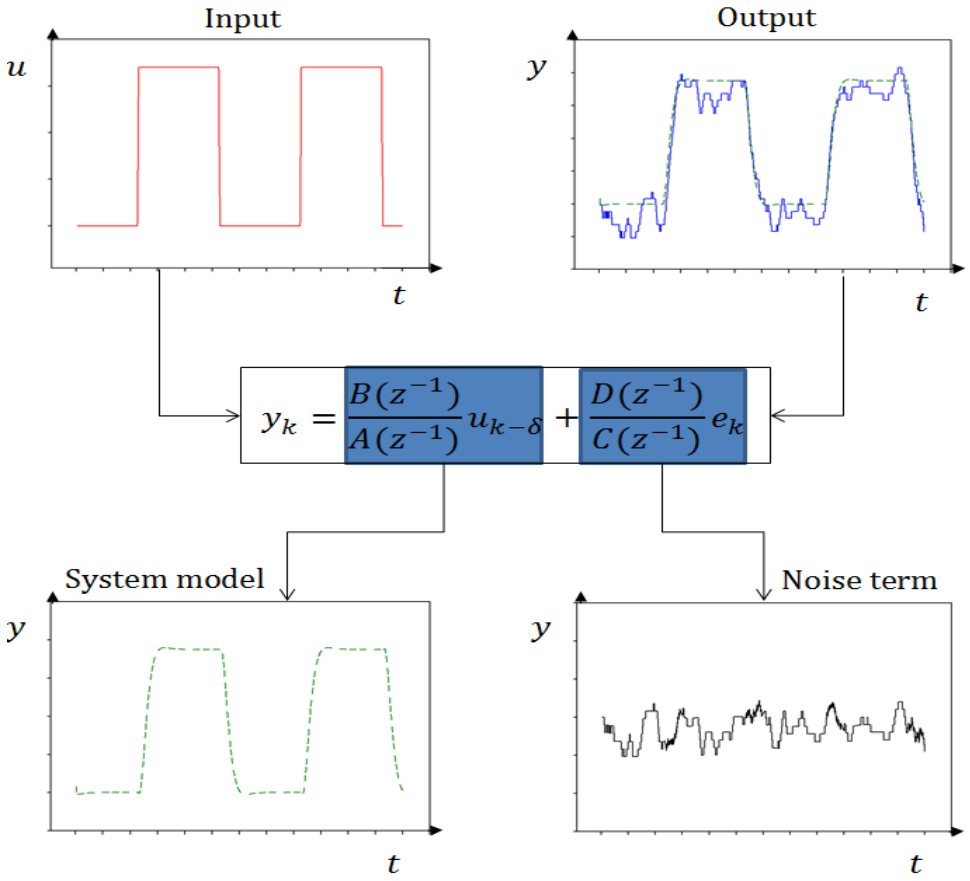

Figure 3.10 Graphical representation of an input (upper left) -output (upper right) BJ model. The BJ model can be used to split the output data into the BJ system model component (down left) and the BJ noise term (down right). For this example, we used data from an unpublished study (Results from internship at Control and Dynamical Systems, Caltech, Pasadena). The input variable is the power of a cyclist during a cycling test, whereas the output is the measured heart rate response.

In chapter I, food intake and activity of individual rodents were monitored during the conditioning period in an animal model for anorexia nervosa. All rats received the same conditioning procedure, but the measured responses were, in each individual, highly diverse (see figure I.3 chapter I). Such individual diversity of organisms was also shown in chapter II. Moreover, in chapter II, we state that all pigs received the same infection induction protocol, but each pig had a different blood cytokine time course and, thus, each pig responded in a different way (See figure II.3 chapter II). In chapter VI, we demonstrated that chicken embryos, when subject to the same environmental conditions, show substantial individual variation in the timing of their developmental milestones during the incubation (See figure VI.5 in chapter VI). Each of these examples emphasises that individual organisms are highly diverse. Such inter-individual variation (within the same species) is omnipresent in biological systems. Depending on factors such as stress and environment, individual biological systems can also differ significantly from one day to another. Thus, individual biological systems also reveal a time varying character, leading to intra-individual variations.

(Doyle, et al., 2011). However, the intra-individual variation is, typically, much smaller than the inter-individual variation (Fraser, 2009, see also figure 1.7).

As a consequence, due to the present inter- and intra-individual differences, monitoring of biological processes requires an individualised approach to capturing the individual state changes. However, dealing with the inter- and intra-individual variations remains one of the main obstacles in applying engineering approaches to biological systems (Doyle et al., 2011). In the forthcoming paragraphs, we propose several methods to obtaining an individualised approach for change detection (see figure 3.11). First, we will start with a general discussion on change detection methods. Following that, we will address each block within the figure below.

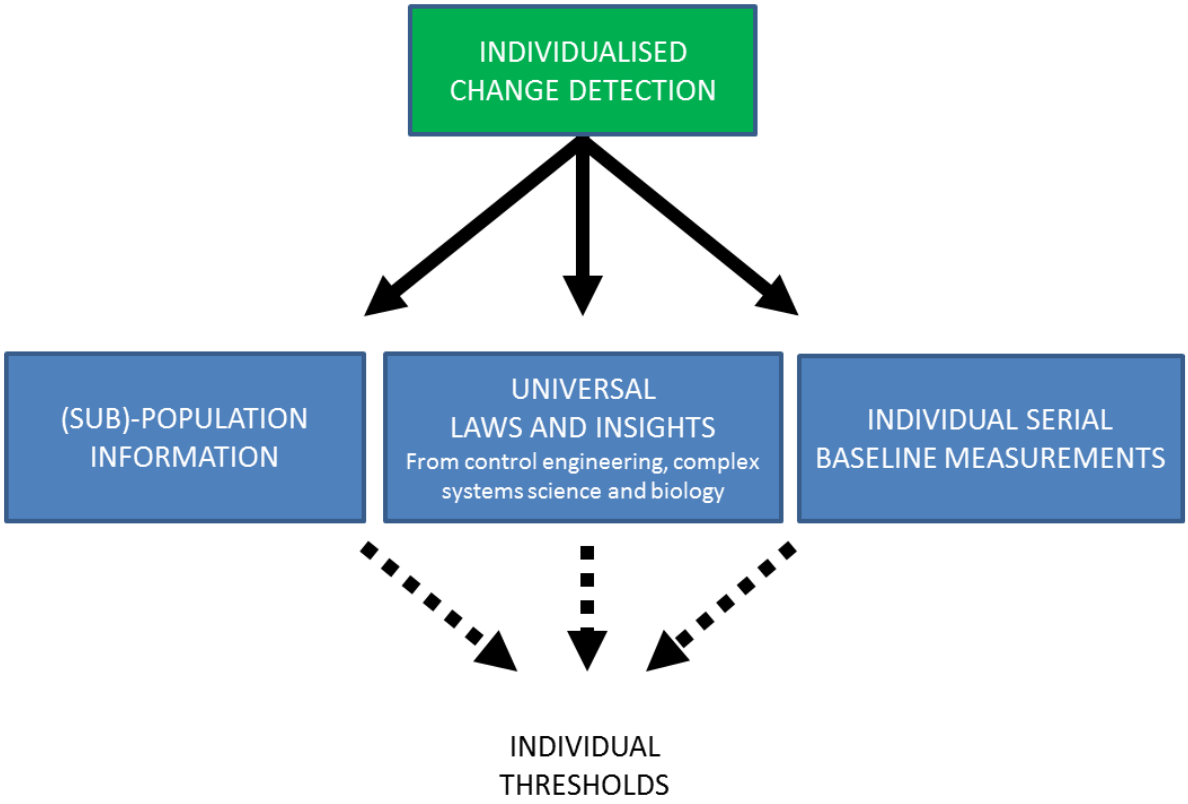

Figure 3.11 Proposed methods for individual change detection: i) Change detection based on sub-population information, ii) Change detection based on universal laws and insights from control engineering, complex systems science and biology, iii) Change detection based on individual serial baseline measurements. Each of these methods can be used to calculate individual monitoring thresholds.

3.4.2 Change detection and threshold methods

Introducing the field of change detection

In the field of change detection, there were two parallel directions of investigation: mathematical statistics and automatic control theory (Basseville and Nikiforov, 1993; Gustafson, 2000; Isermann, 2005). Well-known statistical approaches relating to these fields are control charts, Bayes-type algorithms and CUSUM-type algorithms (Basseville and Nikiforov, 1993; Shewhart, 1931; Page, 1954a). The next paragraph, a case of change detection is discussed based on a CUSUM-type algorithm.

Figure 3.12 gives an example of an unpublished study in which a CUSUM algorithm was used to automatically classify chicken embryo status in real-time, representing either a mortality or hatching situation. This application is particularly important for the immediate monitoring, management and control of incubation conditions used to improve the process outcomes. The time series of the individual egg temperature (Tegg) and the micro-environmental air temperature (Tair) were filtered using a median filter with a filtering window of 120 minutes. Afterwards, the Tair time series was subtracted from the Tegg time series resulting in a time series of temperature differences per individual egg. Page's cumulative sum test (CUSUM test) was applied to detect abrupt changes (e.g. temperature drops) in these times series' that related with embryo death or hatching (Page, 1954; Gustafsson, 2000). Below, the equation of this online change detection test is shown:

$$g_t = min(g_{t-1} + s_t - v_t, 0) \; with \; an \; alarm \; if \; g_t < h$$

where g_0 is 0; s_t is the temperature difference at time t; v_t is the drift parameter, which is defined here as the mean value of s_t (for the last 10 hours) minus the standard deviation of s_t (for the last 10 hours). In this case study, the value of

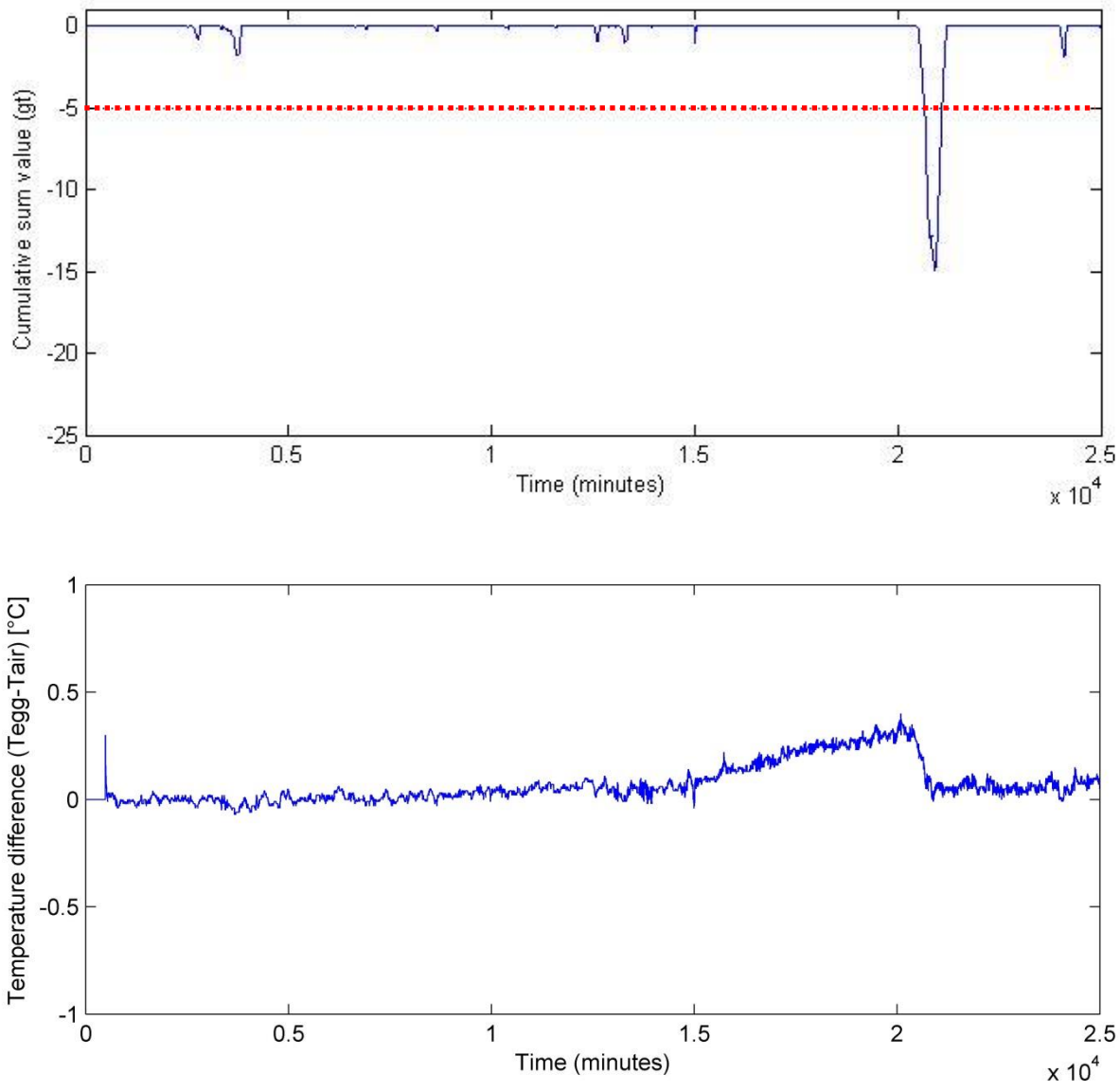

Figure 3.12 Illustration of CUSUM algorithm for detection of chicken embryo death during incubation. (Figure top) Example of a time series of temperature differences (Tegg- Tair) for on individual egg. (Figure bottom) CUSUM values according to the CUSUM equation. The red dotted line indicates the threshold value used for detection of embryo death.

threshold *h* is equal to 5. The upper plot of figure 3.12 shows an example of a time series of temperature differences of an individual egg. At time t=20715 min we can see a temperature drop, which is, in this case, related with the death of the embryo. The lower plot shows the corresponding CUSUM values according to the CUSUM equation. The CUSUM values cross the threshold line at the time of the drop.

In addition to the statistical change detection methods, change detection problems in the field of automatic control are referred to as model-based change (or fault) detection (Gustafson, 2000; Isermann, 2005). In the early 1970s, new investigations started to merge both research areas (mathematical statistics and automatic control theory). Basically, these studies started combining model-based approaches with change detection decision rules (or stopping rules) based on mathematical statistics.
In the framework of online monitoring, these stopping rules can usually be represented using the following form:

$$t_a = \inf\{n: g_n(y_1, \dots, y_n\} \geq \lambda$$

Here, λ is a threshold, and $(g_n)_{n\geq 1}$ is a family of functions of n coordinates. The alarm time t_a is the time at which the change is detected (Basseville and Nikiforov, 1993).
Ideally, for individualised monitoring purposes, the threshold is calculated based on characteristics of the individual bio-process so as to obtain an individual threshold (Figure 3.11).

There are five performance indexes for evaluating change detection algorithms: 1. Mean time between false alarms; 2. Probability of false detection; 3. Mean delay for detection; 4. Probability of non-detection; 5. Accuracy of the change time and magnitude estimates (Basseville and Nikiforov, 1993). Thus, it is important for each decision rule or threshold to determine the false positive rate (probability of false detection) and the false negative rate (probability of non-detection). The other

performance indexes are linked to the timing of detection relative to the timing of the event (change of state of biological process). For example, whereas chapters II and III focused on detection of infection, in chapter VI, we defined rules to predict the hatching of chicken embryos. In the former two chapters, we try to detect the event (i.e. infection) as soon as possible after its occurrence, as opposed to prediction methods, which allow us to plan interventions before the event or change is happening.

In chapter V, we developed a control system for locomotion suppression in rats. Here, we found that the system delay time (from receiving input to actual output: recording, detection, intervention) was less than 100 milliseconds. This result seemed acceptable in our model and comparable to other closed-loop neural stimulation systems. Moreover, the closed-loop DBS showed to be effective in suppressing locomotion.

Threshold methods

In this section, we focus on threshold methods that were used during the course of this PhD for detection of status changes in biological processes. First, all threshold methods used in the PhD are briefly addressed. Second, the three approaches for individualised change detection are presented in more detail.

Threshold methods tend to be based on the quantification of known patterns and differences of bio-signals that relate to a status change in a biological process.

In other cases, thresholds can be calculated based on deviations from normal signal behaviour, when no prior information on a specific status changes is available. Receiver Operating Curve (ROC) graphs have long been used in signal detection theory to depict the thresholds of classifiers (Metz, 1978; Fawcett, 2006). ROC curves rely on the existence of a gold standard that dichotomises all subjects of the dataset into the presence of status/condition or the absence of status/condition

(e.g. presence or absence of disease). A gold standard test can be referred to as the most reliable and accurate test available to determine the status of a biological process. For example, in chapter III, we used the CDC criteria for infections in the ICU setting as gold standard for determination of infection.

Based on ROC curves we can extract true positive, true negative, false positive and false negative rates (see performance indices for change detection above). However, ROC curve analysis is less suitable when we want to evaluate performance in terms of detection time relative to timing of event and response dynamics. Moreover, it is more complicated to use ROC curves for individual approaches.

In chapters I, II and III, AUC values of the ROC curves were calculated to quantify the discriminatory power of change indicators, but also to calculate thresholds (see chapter II).

For calculation of thresholds for multivariate analyses we used decision tree analysis (see for example chapter III). In comparison to alternative methods, this classification method has the advantage that it only has a limited number of assumptions. Other traditional methods are linear discriminant analysis and logistic regression (Varmuza et al., 2008). In addition, many other classification methods exist for the determination of thresholds, but those methods are beyond the scope of this PhD.

In the following sections, we discuss how to obtain individual thresholds based on sub-population information, generic laws/insights and individual baselines.

3.4.3 Change detection based on sub-population information

ROC curves are often used in medicine for the development of a diagnostic test for a disease or unhealthy condition. However, the clinical use of ROC curves is based on population measures (Attia, 2003). They measure the characteristics of a test over a

population, but how can we obtain results for an individual patient? How can we obtain correct results for subpopulations, such as for a 35-year-old female with diabetes—who will perform a sport exercise test? One way to get a more individualised approach is to use thresholds which are defined for subpopulations (Ellery et al., 2012). For example, the field of personalised medicine tries to identify information (e.g. disease susceptibility, specific treatment responses, disease etiology, development and prognosis) for and about (genetic) subpopulations (Epstein et al., 2010; Hoggatt, 2011; Evers et al., 2012). Thus, one option for obtaining more individual thresholds is to calculate ROC curves based on a dataset where only subjects corresponding with a specific list of common characteristics are included (i.e. sub-population).

As mentioned earlier, ROC curves are based on true positive and false positive rates. Other studies state that we should rather use likelihood ratios, since they do not vary in different population settings and can be used directly at the level of the individual patient. For example, they allow the quantification of the probability of a disease for any individual patient based on the Bayes' Theorem and the Bayes nomogram (for more details: see Attia, 2003; see also 3.4.6).

Another way to improve the general ROC curve approach is to use dynamic ROC curve analysis. Figure I.5 of chapter I, showed the evolution of the ROC AUC for different days of the conditioning period in the ABA model. Thus, more accurate and more individual thresholds were obtained, partly capturing the time-varying character.

Ideally, an individualised ROC curve should only be calculated based on measurements of the same individual. However, in that case, we need multiple measurements of the individual process under normal and change conditions, which is not always possible due to the invasive nature of the measurements or change conditions, for example.

3.4.4 Change detection based on universal laws and insights

In this section, we consider examples illustrating individualised change detection based on universal laws and insights from control engineering, complex systems science and biology.

In chapter VI, it was expected that the state of the embryo could be estimated by the relation between the input (local environmental temperature) and the output (eggshell temperature) variable. The steady state gain was selected as a model-based feature for the monitoring of eggs. In this application, the equation of SSG can be written as:

$$SSG = \frac{\Delta y}{\Delta u} = \frac{\Delta T_{Egg}}{\Delta T_{Local}} = \frac{\sum b_i}{1 + \sum a_i}$$

The decision to consider the steady state gain as a model-based feature was based upon a biological interpretation of this equation, since biological studies showed that chicken embryos have an endothermic phase and, afterwards, an exothermic phase. According to this equation, it would be expected that the SSG is smaller than 1 when the embryo is endothermic (e.g. the difference in T_{Egg} is smaller than the difference in T_{Local} or in other words the egg absorbs heat), and larger than 1 when it is exothermic (e.g. the difference in T_{Egg} is larger than the difference in T_{Local} or in other words the egg dissipates heat). By analysing the data we found an average SSG of 1 for all individuals, which confirmed the expected threshold value. Thus, it is shown how we can define threshold values based on insights from engineering and biology.

Additionally in chapter IV, we identify connections between the modelling approach and insights from biology (see 3.3 Model-based features). Based on a decreased

model order, it was possible to detect the inhibition of underlying physiological pathways. In this case, a specific model order can be used as a threshold for change detection. Both examples in chapters IV and VI show how we can combine insights from the modelling perspective with insights from biology to obtain data-based mechanistic models (DBM, for more details on the used DBM approaches: see e.g. Young, 1998) and individual threshold values.

In another study (Van Loon et al., 2012), we investigated whether real-time modelling techniques could be valuable when continuously evaluating individual critically ill patients and, equally so, in helping medical staff with estimation of prognosis. This preliminary study examined the possibilities of distinguishing survivors from non-survivors on the basis of the dynamics of daily measured variables.

A data set, containing 56 patients, was generated in the intensive care unit (ICU) of the university hospital of Leuven. We used daily measurements of three variables, namely: maximum body temperature (Tmax, °C), white blood cell count (WBC, 10^9/L) and blood urea concentration (Uconc, mg/dl). First order dynamic auto-regression (DAR) models were used to quantify the dynamics of the time series:

$$y_t = \frac{1}{A(z^{-1}, t)} e_t$$

In which $A(z^{-1}, t) = 1 + a_{1t} z^{-1}$ is a time variable parameter polynomial in the backward shift operator z^{-1}; y_t is the considered physiological variable; e_t is zero mean white noise.

ROC curve analysis was used to evaluate the performance of a diagnostic test based on the model parameter values. The best results were found for blood urea concentration with true negative fractions of 21/30 (70%), true positive fractions of 19/26 (73%) and an AUC of 0.78. Based on the ROC curve, it was possible to calculate optimal thresholds in the parameter values. Interestingly, the optimal

parameter value was nearly equal to -1 (≈ -1.0085), which is a boundary for model stability. To have a stable model, it is required that all poles of the transfer function lie inside the unit circle. For first order DAR models, the following criterion should be met for them to be stable (Box et al., 1994):

$$-1 < a_1 < 1$$

Figure 3.13 shows the time course of the measured urea concentration values and the calculated stability criterion for a surviving and non-surviving patient. The results indicate that critically ill patients' instabilities in the dynamics of time series' of urea concentration can be indicative of their clinical condition and outcome. There are studies that connect the proper workings of physiological systems with the stability of its dynamic response (Lipsitz, 2002). However, before the described methodology could be considered for future use as support to a physician in on-line monitoring and decision taking for individual patients, these findings need to be validated and subsequently confirmed in larger trials so as to evaluate the concept thoroughly. Moreover, at this stage, more information and evidence is needed to claim that the model instabilities are, in some way, linked with the stability of the involved physiological processes (e.g. are the physiological systems time invariant, linear, etc.?).

To conclude, this study showed another example of how general concepts from control engineering could, potentially, be combined with biological insights so as to define meaningful thresholds for monitoring applications.

As discussed in the Model-based features (3.3) section, several scientific fields (including complex systems science) suggest the existence of generic early-warning signs that may occur in a broad range of complex dynamical systems when a (non-)critical threshold is approaching (for further reading see e.g. Scheffer et al., 2009 and Kefi et al., 2013). The occurrences of autocorrelation tending to one or a variance increase (i.e. tends to infinity) are examples of early warning signs close to

a critical point. For example, an increase in signal fluctuations was used in chapter II for the detection of infection.

In conclusion, several examples (from chapters II, IV, VI and an unpublished study) were given to illustrate how theories and insights from control engineering, complex systems science and biology can be used to obtain thresholds values which, in turn, are used to monitor individual systems.

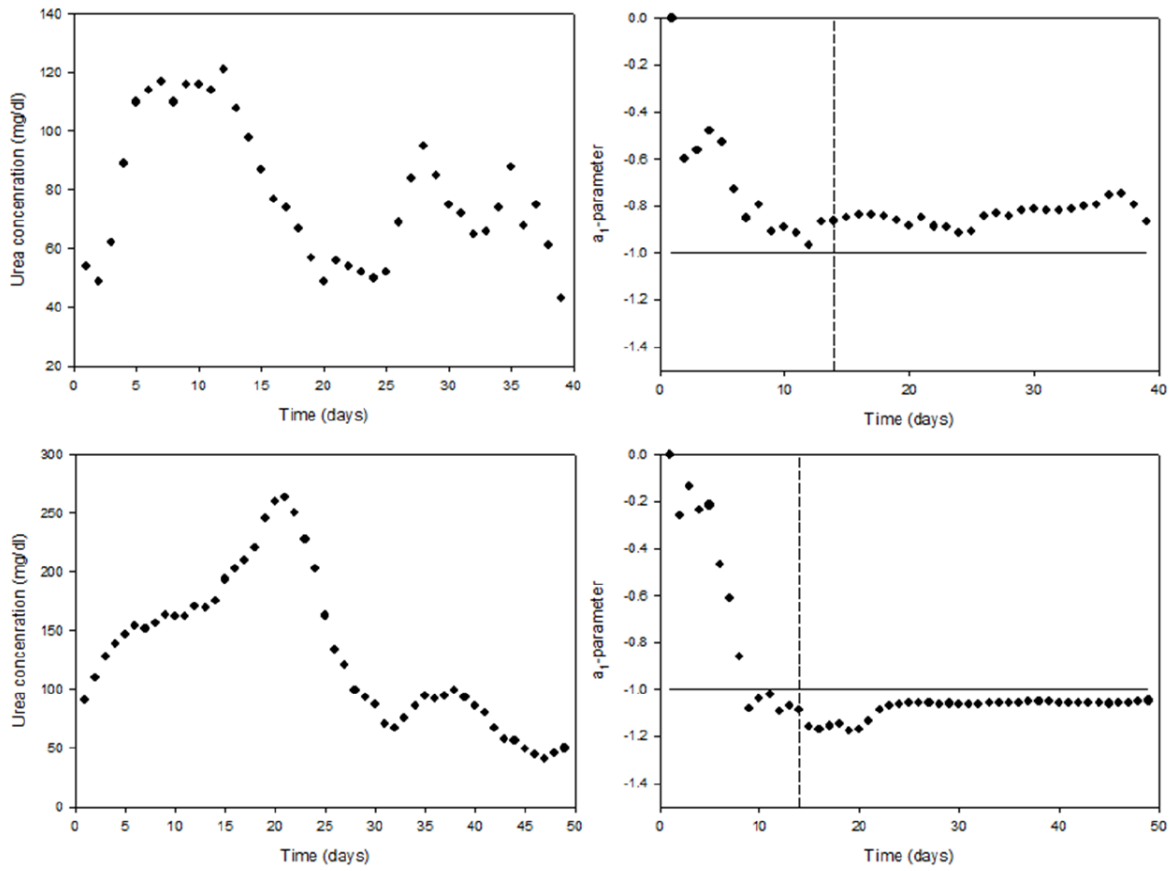

Figure 3.13 Top: Time courses of the daily measured blood urea concentration values (left) and the stability criterion ($-1 < a_1 < 1$) for a survivor (patient 3) (right). Bottom: Time courses of the daily measured urea concentration values (left) and the stability criterion ($-1 < a_1 < 1$) for a non-survivor (patient 12)(right). The vertical dashed line in the right graphs indicate the end of the period of the first 14 data points (days) that are needed for reliable parameter estimation. The horizontal line indicates the threshold of $a_1 = -1$.

3.4.5 Change detection based on baseline measurements

In the two previous approaches for change detection (sub-population information and general insights from different scientific domains), the determination of the more individualised threshold values is still partly population-based. Preferably, to detect an individual change, we can compare the values of the change indicators during 'new state conditions' with system behaviours under 'old state conditions'. In others words, change can only be detected when there is a deviation of 'normal system behaviour' (See Figure 3.1, Isermann, 2005). Very often, we use population baselines to define normal behaviour. For example, when we perform a classical blood analysis test, healthy levels for blood substances are defined by fixed population thresholds. The same holds for Body Mass Indexes (BMI). A BMI value higher than 25 is defined as overweight, whereas a BMI value lower than 20 is defined as underweight. However, such fixed thresholds do not work for all individuals. For example: athletes have a high muscle weight and low fat weight (Jeukendrup et al., 2010).

Therefore, it is crucial to be aware of the fact that every individual has its own normal state in a healthy condition. Thus, whenever possible, the evaluation of the current condition should be made against the value normally presented in that individual when in a healthy (or normal) state (Indrayan, 2012). In chapter II, we showed that it's impossible to use single IL-6 blood levels for detection of infection at pig group level. However, when we compared the static blood levels—14hrs after infection—with the individual baseline level of the same pig (2 hrs before infection), a higher discriminatory power was obtained. Even better results were obtained when we analysed the hormone dynamics at group level, but again, these results were improved by comparing the dynamics after infection with the dynamics during baseline conditions in the same individual, resulting in an individualised approach.

Thus, in comparison to population-based approaches, monitoring methods using individualised baselines can improve the discriminatory power. Therefore, the way forward in monitoring individuals is in using serial baseline measurements of normal (e.g. healthy) system behaviour to detect individual changes (Fraser et al 2009; Anderson et al., 2016).

In chapter VI, individual thresholds were defined to detect when an embryo goes from the endotherm to the exothermic phase. The thresholds were calculated based on the mean and standard deviation of the same variable in the same individual during baseline conditions. On population level, an average SSG of 1 was found, which corresponds with the expected value that correlated with the transition from being endothermic to being ectothermic (see 3.4.4). However, some embryos had baseline threshold values which were significantly different from 1, therefore stressing the need for an individualized approach (see figure VI.3 in chapter VI).
In chapter V, individual thresholds were determined for optimal detection of locomotion based on hippocampal theta oscillations. In this study, median and standard deviations of power spectral densities at specific theta frequencies were used for the calculation of the most accurate individual threshold values. The results showed different individual thresholds for the rat, confirming the need for baseline measurements of each individual.

In the previous part of the discussion (3.4 Individualised change detection), examples from the chapters showed the presence of inter- and intra-individual differences in the monitoring applications, indicating the need for an individualised approach in order to capture the individual state changes. In addition to the general, more traditional change detection methods (e.g. CUSUM algorithms), we presented three approaches for individualised change detection with individual thresholds: 1) Change detection based on (sub)-population information, 2) Change detection based on universal laws and insights from control engineering, complex systems science and biology and 3) Change detection based on individual serial baseline measurements, which can be considered is the most individualised way.

3.4.6 Change detection without thresholds

The previous sections focused on approaches to determine individual thresholds (e.g. chapter V and VI). From a monitoring point of view, the use of thresholds can directly contribute to the decision-making of the operator for planning interventions to change the state of the biological process (i.e. bio-process control). By defining fixed (population/individual) thresholds to dichotomise measurements of continuous bio-process variables, one can categorise individuals, for instance, as being hypertensive (i.e. continuous variable: blood pressure) or obese (i.e. continuous variable: BMI) and start appropriate treatments (Ragland, 1992; Altman and Royston, 2006). Using thresholds to force all individuals in two groups (e.g. ill vs. healthy) can simplify interpretation and presentation of results for monitoring biological processes. However, from the perspective of the biological system itself, it can be important to answer the question of whether the specific threshold actually exists in biological terms (Aldridge, 1986). Dichotomising continuous variables to obtain binary outcomes can lead to a significant loss of relevant bio-process information (Altman and Royston, 2006). It could be more suitable, for instance, to determine linear relations between continuous variables for monitoring the bio-process without defining threshold values (e.g. prediction of hatch time; figure VI.6 in chapter VI). While some changes of bio-processes are more critical switch-like transitions from one state to another (e.g. activation of a mGluR receptors; see chapter IV), other changes should rather be characterised as gradual transitions (see BOX 3.1; Scheffer et al., 2012). In the latter case, it can be more suitable to use continuous outcome variables for monitoring the gradual changes of the biological processes.

Another alternative for model-based monitoring purely on individual thresholds, is the use of a more probabilistic approach. This way one can move beyond binary statements about ‘change’ or ‘no change’ that are not considering uncertainties and variation under different circumstances (Leek et al., 2017). It can be an option, for example, to define risk factors and obtain prior and posterior probabilities of a specific state of biological processes (Attia, 2003; see also 3.4.3). Instead of assigning a specific state to a bio-process, the individual state of the bio-process could be

described by a multidimensional and multimodal probability distribution, using, for instance, a combination of a deterministic model and a Bayesian likelihood approach (for more details: see e.g. Zenker et al., 2006 and 2007). Such approaches would allow the operator of the specific monitoring application to quantify the uncertainty of the bio-process state (e.g. Meyfroidt et al., 2011) and could potentially contribute to the identification of additional bio-process characteristics that should be measured to decrease the uncertainty about the bio-process state (Zenker et al., 2007). In addition, there are many other examples of probabilistic approaches, but those methods are beyond the scope of this thesis.

3.4.7 Towards a methodological approach for individualised change detection

In this PhD, several aspects of the general monitoring scheme (cfr. Figure 3.1) were investigated. All the elements and methods handled in the discussion are summarised in one flow chart for individualised model-based monitoring of biological processes (Figure 4.1). The four main blocks of figure 3.1—the bio-process, the process model, feature generation and individualised change detection based on individual thresholds—are included. For each block, all the discussed elements and methods are listed. As indicated by the main results of this PhD, the researcher should start from all available biological knowledge at every step of this summarising scheme and aim to individualise the approach as much as possible. As shown by the results of each chapter, the presented approach could potentially be used in a wide range of applications stressing the generic power of the suggested model-based framework.

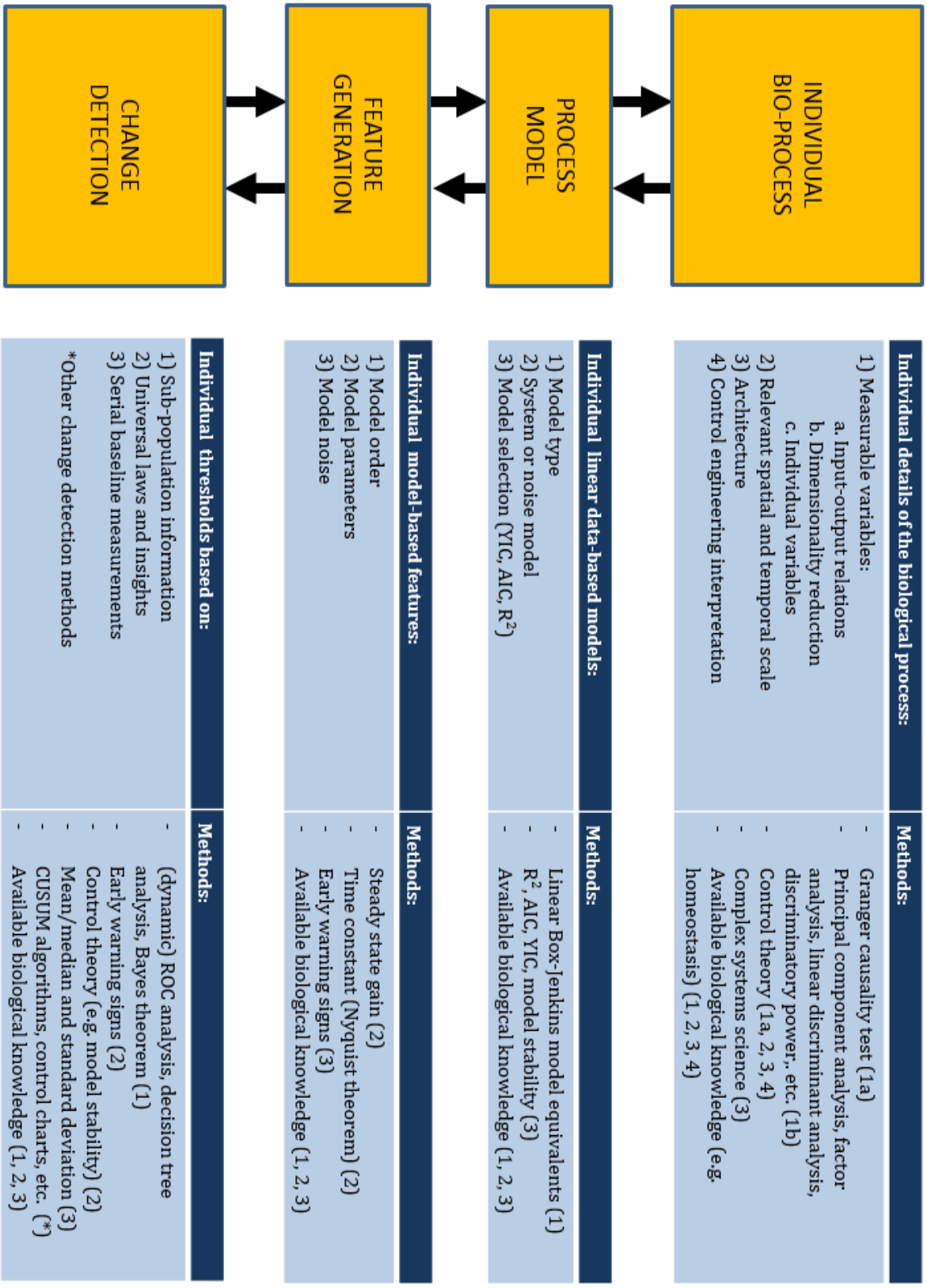

Figure 3.14 Flow chart with essential steps and methods for the design of a system for individualised model-based monitoring of bio-signals.

Part 4
Conclusions

"Imagination is more important than knowledge. Knowledge is limited.

Imagination encircles the world."

— Albert Einstein —

(From: "What Life Means to Einstein: An Interview by George Sylvester Viereck" The Saturday Evening Post (26 October 1929), p. 17.)

4.1 GENERAL CONCLUSIONS

Biological systems are continuously exposed to uncertain and variable conditions. In order to cope with these environmental uncertainties or disturbances, biological systems contain cleverly designed architectural components which allow them to remain stable, adapt to changing conditions (e.g. learning by brain plasticity, cfr. Chapter I) and grow (e.g. chicken embryo, cfr. Chapter V). To preserve homeostasis and stable internal conditions, biological systems contain components which can be compared with well-known control engineering components such as actuators (e.g. the heart), controllers (e.g. the central nervous system, cfr. Chapter IV), feedback loops, sensors, etc. Therefore, as the first step in the development of an individualised model-based monitoring system for bio-signals (i.e. developing monitoring systems "from biology to technology"), we suggested combining insights from biology and control engineering to interpret measured bio-signals (see general objective in 1.5).

Dealing with the inter- and intra-individual variations remains one of the main obstacles in applying engineering approaches to biological processes. In the introduction, we emphasised the need to start from the available biological knowledge of an individual bio-process in order to develop an effective individualised monitor. Moreover, only after this step has been taken can all the available information be interpreted from a control engineering perspective. The individual details of the biological process can be assessed at four different levels: measurable variables, relevant spatial and temporal scale and a control engineering interpretation (i.e. individual system structure, individual system dynamics, and individual bio-signals; figure 3.14). The results of the case studies showed that we could indeed define actuator and homeostatic variables for a range of different biological processes (see sub-objective 1; cfr. Table 3.1). Such results might indicate that we can unravel some of the mysteries of biological functioning by combining biological insights with insights from control engineering.

However, many biological processes are characterized by a number of non-linearities, which possibly complicate the design of monitors for bio-processes. In the second sub-objective, we suggested that we can use compact individual linear models (Box-Jenkins models) for the monitoring of such individual non-linear bio-processes. Based on these models, it was possible to describe the dynamics of the biological process and/or uncover information about the underlying mechanisms state by applying data-based mechanistic approaches for the specific case studies (see sub-objective 2; cfr. Chapter IV and VI). Several examples, spread across the various chapters, showed that we can use compact linear models for monitoring individual non-linear bio-processes (crf. Chapter II, III, IV and VI; figure 3.14). These models allow accurate descriptions of the dynamic, time-varying and individual character of bio-processes.

For every monitoring application, we need to define the optimal model-based indicator of individual change. Based on the results of the specific case studies, we suggest three different, general model-based markers for individual state changes in organisms: model parameters, changes in model order and changes in model noise term characteristics (figure 3.14). In addition, more than 20 other generic metrics from the fields of complex systems science, change detection and control engineering were identified that can be used while analysing individual time series. These features can be used for all individual bio-processes and were generated based on the specific individualised model-based monitoring applications of this PhD (See sub-objective 3; Chapter I-VI).

Due to the present inter- and intra-individual differences (cfr. Chapter I, II, III, V & VI), monitoring of biological processes requires individual thresholds to capture the individual state changes. Methods of online change detection are typically characterised by the use of threshold methods. Here, we combined insights from change detection and control engineering and developed a framework for individualised model-based monitoring with individual thresholds based on the specific case studies. Again, three possible approaches were proposed: 1) Individual thresholds based on (sub)-population information, 2) Individual thresholds based on

universal laws and insights from control engineering, complex systems science and biology and 3) Individual thresholds based on individual serial baseline measurements, which can be considered is the most individualised way (see sub-objective 4; figure 3.14).

The way forward in the monitoring of individuals is using serial baseline measurements of normal (e.g. healthy) system behaviour to detect individual changes (cfr. Chapter II). Such an individualized approach allows us to define individual thresholds (cfr. Chapter V and VI) purely based on data generated from the same individual process, leading to higher detection accuracies in comparison with population-based methods.

Overall, the presented approach could be used in a wide range of application domains (e.g. precision livestock farming, human health engineering, bio-technological processes,…), thus stressing the generic power of the suggested framework for individualized model-based monitoring of bio-processes based on individual thresholds. In the future, population-based threshold approaches should be combined with information at an individual level so as to optimise the performance of the monitoring systems (e.g. Chapter IV; e.g. mixed-effect models). Moreover, the list of used methods could be further expanded (e.g. non-linear models, more methods for multivariate analysis, validation methods, etc.). Finally, the individualised model-based monitoring approach could also be integrated in a broader framework, which, additionally, includes methods for defining individualised interventions and individualised control applications.

4.2 SPECIFIC CONCLUSIONS

This thesis has led to some innovative individualised monitoring applications based on the six specific case studies (i.e. Chapters I-VI; cell – embryo – animal – human):

Chapter I:

Individualised monitoring of activity and body weight in the activity-based anorexia rat model

The activity-based anorexia (ABA) rat model is characterised by many inter- and intra-individual differences. Based on the available biological knowledge, we were expecting food-anticipatory activities (FAA), a behavioural phenomenon frequently used to evaluate hyperactivity in the activity-based anorexia (ABA) model, to be directly proportional to, and the most discriminating predictor of percentage body weight loss. However, our study shows that postprandial activities (PPA) are more directly related to weight loss than FAA. The study showed the added value of using complete time series, which enable the researcher to obtain more individual information per animal and differentiate between different time periods relative to the scheduled moments of feeding.

In interpreting this case study from a control engineering perspective, we can consider anorexia nervosa as a dysfunction of the control system relating to energy homeostasis in the body. Hereby, food intake could be defined as an actuator variable and body weight as a homeostatic variable.

The results confirmed the presence of considerable inter- and intra-individual differences. Therefore, dynamic ROC curves were used to calculate dynamic thresholds for distinguishing between responders and non-responders (rats not susceptible to ABA). By recalculating the ROC curves for each day of the conditioning period the discriminatory power could be improved.

To conclude, the applied time-series approach can be used to identify the key factors leading to the inter-individual differences and to determine individualised dynamic thresholds capturing time-varying aspects leading to the intra-individual differences in the ABA model. By monitoring measurable variables related to the ABA model, we could determine a significant amount of individual variation, suggesting the need for individualised monitoring approaches.

Chapter II:

Individualised model-based monitoring of interleukin-6 for early detection of infection in pigs

The individual biological process of this case study was part of the immune system in pigs. The measured variable was interleukin-6, which is one of the cytokines that plays a key role in the infection response. The results indicated that IL-6 values of fixed time points show, after infection, a large individual variation in outbred animals. We hypothesised that model-based time series analyses of interleukin-6 (IL-6) at the individual level offers a method in detecting infection with pleuropneumonia in individual pigs. In applying model-based methods (Integrated Random Walk Models), we were able to quantify the dynamic properties of the Il-6 time series. We found that amplitude increases of IL-6 fluctuations in individual pigs should be used as an indicator of the infection state, rather than static IL-6 values, therefore showing the added value of IL-6 time series analyses of individual pigs. These results are a first step towards the development of objective individualised methods for model-based monitoring, early detection of sepsis and inflammation processes in pigs through the integration of animal response dynamics.

Based on all the methods used in this study, three important elements were suggested for obtaining an individualised monitoring approach:

1. Change detection based on (sub-)population information (e.g. thresholds from ROC curve analysis).
2. Change detection based universal laws and insights from control engineering, complex systems science and biology (e.g. early warning signs for critical transitions).
3. Change detection based on individual serial baseline measurements.

Chapter III:

Model-based monitoring of heart rate and blood cytokine time series for early detection of infections in critically ill patients

We applied 20 different generic metrics from the field of complex systems science, change detection, and control engineering, while analysing individual heart rate and blood cytokine time series for monitoring of infection in ICU patients. The main results suggest that two specific heart rate characteristics (i.e. the mean of the raw heart rate signals and the mean of the fast dynamics of the heart rate time series) are better markers for infection than information captured by the cytokine time series.

In this chapter, a compact linear model (Integrated Random Walk Model) was used before the feature extraction. The heart rate model showed that the best results were obtained by combining the raw heart rate signal and the fast dynamics of the heart rate time series. This result proves how model-based features can be an added value to monitors that purely focus on measured variables (e.g. ICU heart rate monitor only based on raw heart rate signal used in an).

Whereas ROC curve analysis was used to calculate the thresholds in the previous chapters, here we used decision tree analysis to obtain 'multivariate monitoring thresholds' for classification based on multiple variables. If more variables are measured, we obtain more individual information of the patient, potentially allowing for a more individualised approach. Ideally, future individualised monitors should implement dynamic analyses of different biomarkers for infection and their interactions, allowing the operator to determine the individual dynamic infection state of the patient.

In this study, the list of different metrics could be used for all individuals in order to distinguish infected from non-infected ICU patients. These methods could be added to the suggested approach for individualised model-based monitoring based on chapter II.

Chapter IV:

Model-based monitoring of mGluR-dependent synaptic plasticity in hippocampal brain slices of rats

Long-term synaptic modifications play a key role in the plasticity of behaviour, learning, and memory. To the author's knowledge, it is the first time that fEPSP slopes of mGluR-LTD responses are dynamically described using transfer function (TF) models. Starting from available biological information (optimal sampling frequency, hippocampal structure, etc.) all measurement procedures were determined.

Whereas the previous chapters focused mainly on the model noise of single-output models (integrated random walk models), this study aimed to quantify the model structure and time constants of the responses based on the input-output models. Accurate models were obtained, and the model structure suggested the presence of

two major underlying subprocesses. Based on the estimated times constants, links with existing pathways were suggested. Since the calculated models were data-based, and the fact that we could link the models with underlying physiology, the obtained models are data-based mechanistic models. Thus, although neural mechanisms are known to contain many nonlinearities, the linear models were able to describe the dynamics and uncover information about the underlying mechanisms without knowing all details of this form of synaptic plasticity.

This study suggests that the dynamic data-based modelling approach can be a valuable tool for reverse biological engineering of mGluR-dependent LTD responses. It is suggested that such system identification (SI) methods can aid in unravelling the complexities of synaptic function and its role in disease as also confirmed by the unpublished results of the insulin-LTD data (Figure 3.9).

Chapter V:

Individualised monitoring of hippocampal theta oscillations and individualised electrical stimulation in the mesencephalic reticular formation for real-time closed-loop suppression of locomotion in rat

Theta oscillations in the hippocampus (output variable) are highly related with locomotion, while electrical stimulation in the mesencephalic reticular formation (input variable) induces freezing. Starting from these two biological insights, we hypothesised that it is possible to develop a control system for suppression of locomotion in rodents. Since the closed-loop system was effective in suppressing the locomotion, this implicates less stimulation induced side effects, during clinical application, in comparison to that of open-loop stimulation.

In the case of closed-loop neuromodulation, the central nervous systems acts as controller of many body systems at organisms scale (e.g. control of movement). Furthermore, control of the central nervous system by DBS is a promising example of how control engineering concepts can be applied to adapt (pathological) behaviour of organisms.

By using individual baseline measurements, the control system could be individualised based on individual monitoring thresholds and individualised

stimulation parameters. As shown by the analyses, the threshold values and stimulation parameters were individually different, confirming the need for an individualised approach.

Chapter VI:

Individualised model-based monitoring of chicken embryo status during incubation based on eggshell temperature and micro-environmental air temperature

We hypothesise that we can develop a non-invasive individualised model-based monitoring approach which is able to detect or even predict online the individual progress of embryo development during the incubation of chicken eggs based on egg shell temperature and micro-environmental air temperature. We showed that we can detect, based on dynamic models of the local environmental air temperature and the individually measured eggshell temperature, 5 different milestones in the development of broiler embryos (milestone 1: transition from endothermic to exothermic status, milestone 2: plateau phase, milestone 3: internal pipping, milestone 4: external pipping and milestone 5: hatch). Moreover, links were suggested with physiological mechanisms and therefore the models can be considered as data-based mechanistic models. This individual monitoring approach could be an added value to give more insight to farmers, for individualised prediction of hatching and for other experimental designs and studies, where the developmental stage of the embryo is relevant.

Chapters I, II, IV and V present results of animal models for (medical) human applications. More specifically, chapter II shows how pigs are first used as animal models for the development of an early warning monitor for infection, whereas similar approaches are applied in chapter III to obtain a monitor for infection in intensive care units. In addition to the aforementioned step from biology to technology, this example illustrates how it is possible to make the step from animal to human health engineering.

Bibliography

This list contains all references from the introduction and discussion. References of chapters can be found at the end of each chapter.

1. Achten, J., & Jeukendrup, A. E. (2003). Heart rate monitoring. *Sports medicine*, *33*(7), 517-538.

2. Aerts, J. M., Van Buggenhout, S., Vranken, E., Lippens, M., Buyse, J., Decuypere, E., & Berckmans, D. (2003). Active control of the growth trajectory of broiler chickens based on online animal responses. *Poultry science*, *82*(12), 1853-1862.

3. Aldridge, W. N. (1986). The biological basis and measurement of thresholds. *Annual review of pharmacology and toxicology*, *26*(1), 39-58.

4. Altman, D. G., & Royston, P. (2006). The cost of dichotomising continuous variables. *Bmj*, *332*(7549), 1080.

5. Anderson L, Razavi M, Skates S, Anderson NG, Pearson TW. 2016. Squeezing more value from the analytes we have: personal baselines for multiple analytes in serial DBS. Bioanalysis 8:1539–42

6. Aydin, A., Bahr, C., Viazzi, S., Exadaktylos, V., Buyse, J., Berckmans, D. (2014). A novel method to automatically measure the feed intake of broiler chickens by sound technology. *Computers and Electronics in Agriculture, 101*, 17-23.

7. Attia, J. (2003). Moving beyond sensitivity and specificity: using likelihood ratios to help interpret diagnostic tests. *Issues*, 1.

8. Banhazi, T. M., Lehr, H., Black, J. L., Crabtree, H., Schofield, P., & Tscharke, M. (2012). Precision Livestock Farming: An international review of scientific and commercial aspects. *Int J Agric & Biol Eng*, *5*(3), 1-9.

9. Barabasi, A. L., & Oltvai, Z. N. (2004). Network biology: understanding the cell's functional organization. *Nature Reviews Genetics*, *5*(2), 101-113.

10. Baradez, M. O., & Marshall, D. (2011). The use of multidimensional image-based analysis to accurately monitor cell growth in 3D bioreactor culture. *PloS one*, *6*(10), e26104.

11. Basseville, M., & Nikiforov, I. V. (1993). *Detection of abrupt changes: theory and application* (Vol. 104). Englewood Cliffs: Prentice Hall.

12. Berckmans, D. (2006). Automatic on-line monitoring of animals by precision livestock farming. *Livestock production and society*, 51-54.

13. Berckmans, D., and Aerts, J.M. (2006). Integration of bio-response (Course), KU Leuven

14. Bites Romanini, C., Exadaktylos, V., Tong, Q., McGonnel, I., Demmers, T., Bergoug, H., Eterradossi, N., Roulston, N., Garain, P., Bahr, C., Berckmans, D. (2013). Monitoring the hatch time of individual chicken embryos. *Poultry Science, 92* (2), 303-309.

15. Boonen, C. On-line measurement and modelling of dynamic plant responses to variations of the microenvironment. 2005.

16. Bourgeois, W., Burgess, J. E., & Stuetz, R. M. (2001). On-line monitoring of wastewater quality: a review. *Journal of chemical technology and biotechnology*, *76*(4), 337-348.

17. Box, G. E., Jenkins, G. M. & Reinsel, G. C. (1994). *Time series analysis: forecasting and control.* Prentice-Hall International, New Jersey.

18. Bravi, A. (2014). *Variability monitoring for clinical applications* (Doctoral dissertation, University of Ottawa).

19. Bulckaert, A., Exadaktylos, V., De Bruyne, G., Haex, B., De Valck, E., Wuyts, J., ... & Berckmans, D. (2010). Heart rate-based nighttime awakening detection. *European journal of applied physiology*, *109*(2), 317-322.

20. Cannon, W. B. (1929). Vob. IX JULY, 1929 No. 3 ORGANIZATION FOR PHYSIOLOGICAL HOMEOSTASIS. *Physiological reviews*, *9*(3).

21. Cheng, B., Kuipers, H., Snyder, A. C., Keizer, H. A., Jeukendrup, A., & Hesselink, M. (1992). A new approach for the determination of ventilatory and lactate thresholds. *International journal of sports medicine*, *13*(7), 518-522.

22. Choi, J., Ahmed, B., & Gutierrez-Osuna, R. (2012). Development and evaluation of an ambulatory stress monitor based on wearable sensors.*Information Technology in Biomedicine, IEEE Transactions on*, *16*(2), 279-286.

23. Chowdhury, F. N. (2000). Input-output modeling of nonlinear systems with time-varying linear models. *IEEE Transactions on Automatic Control*, *45*(7), 1355-1358.

24. Clermont, G., & Zenker, S. (2015). The inverse problem in mathematical biology. *Mathematical biosciences*, *260*, 11-15.

25. Colijn, C., Jones, N., Johnston, I. G., Yaliraki, S., & Barahona, M. (2017). Toward Precision Healthcare: Context and Mathematical Challenges. *Frontiers in physiology*, *8*.

26. Csaszar, E., Chen, K., Caldwell, J., Chan, W., & Zandstra, P. W. (2014). Real-time monitoring and control of soluble signaling factors enables enhanced progenitor cell outputs from human cord blood stem cell cultures.*Biotechnology and bioengineering*, *111*(6), 1258-1264.

27. Csete, M. E., & Doyle, J. C. (2002). Reverse engineering of biological complexity. *science*, *295*(5560), 1664-1669.

28. Dakos, V., Carpenter, S. R., Brock, W. A., Ellison, A. M., Guttal, V., Ives, A. R., ... & Scheffer, M. (2012). Methods for detecting early warnings of critical transitions in time series illustrated using simulated ecological data. *PloS one*,*7*(7), e41010.

29. Dakos, V., Carpenter, S. R., van Nes, E. H., & Scheffer, M. (2015). Resilience indicators: prospects and limitations for early warnings of regime shifts. *Philosophical Transactions of the Royal Society of London B: Biological Sciences*, *370*(1659), 20130263.

30. Darwin, Charles; Wallace, Alfred Russel (1858), "On the Tendency of Species to form Varieties; and on the Perpetuation of Varieties and Species by Natural Means of Selection", *Zoological Journal of the Linnean Society* **3**: 46–50

31. Davidian, M., & Giltinan, D. M. (2003). Nonlinear models for repeated measurement data: an overview and update. *Journal of agricultural, biological, and environmental statistics*, *8*(4), 387-419.

32. Desai, N. S. (2003). Homeostatic plasticity in the CNS: synaptic and intrinsic forms. *Journal of Physiology-Paris*, *97*(4), 391-402.

33. Dhillon, H., Zigman, J. M., Ye, C., Lee, C. E., McGovern, R. A., Tang, V., ... & Lowell, B. B. (2006). Leptin directly activates SF1 neurons in the VMH, and this action by leptin is required for normal body-weight homeostasis. *Neuron*, *49*(2), 191-203

34. Dochain, D., Vanrolleghem, P. A., & Vanrolleghem, P. (2001). *Dynamical modelling and estimation in wastewater treatment processes*. IWA publishing.

35. Doryab, A., Min, J. K., Wiese, J., Zimmerman, J., & Hong, J. (2014, June). Detection of Behavior Change in People with Depression. In *Workshops at the Twenty-Eighth AAAI Conference on Artificial Intelligence*.

36. Doyle, J. C., & Csete, M. (2011). Architecture, constraints, and behavior.*Proceedings of the National Academy of Sciences*, *108*(Supplement 3), 15624-15630.

37. Drescher CW, Shah C, Thorpe J, O'Briant K, Anderson GL, et al. 2013. Longitudinal screening algorithm that incorporates change over time in CA125 levels identifies ovarian cancer earlier than a single-threshold rule. J. Clin. Oncol. 31:387–92

38. Ellery, T., & Hansen, N. (2012). Patient Subpopulations and Personalized Medicine. *Pharmaceutical Lifecycle Management: Making the Most of Each and Every Brand*, 131-139.

39. Epstein, R., & Teagarden, J. R. (2010). Comparative effectiveness and personalized medicine: evolving together or apart?. *Health Affairs*, *29*(10), 1783-1787

40. Evers, A. W., Rovers, M. M., Kremer, J. A., Veltman, J. A., Schalken, J. A., Bloem, B. R., & Van Gool, A. J. (2012). An integrated framework of personalized medicine: from individual genomes to participatory health care.*Croatian medical journal*, *53*(4), 301-303.

41. Exadaktylos, V., Silva, M., Berckmans, D. (2011). Real-time analysis of chicken embryo sounds to monitor different incubation stages. *Computers and Electronics in Agriculture, 75* (2), 321-326.

42. Exadaktylos, V., Jansen, F., Van der Krogt, J., Guarino, M., Berckmans, D. (2013). Real time monitoring of mental status of a horse to a negative stressor. In Berckmans, D. (Ed.), Vandermeulen, J. (Ed.), *Precision Livestock Farming '13*. ECPLF. Leuven, Belgium, 10-12 September 2013 (pp. 308-310).

43. Fairchild, K. D. & Aschner, J. L. HeRO monitoring to reduce mortality in NICU patients. Research and Reports in Neonatology 2, 65–76 (2012).

44. Eichler, M. (2012). Causal inference in time series analysis. *Causality: Statistical perspectives and applications*, 327-354.

45. Fawcett, T. (2006). An introduction to ROC analysis. *Pattern recognition letters*,*27*(8), 861-874.

46. F. J. Doyle III, B. W. Bequette, R. Middleton, B. Ogunnaike, B. Paden, R. S. Parker and M. Vidyasagar, "Control in Biological Systems", *The Impact of Control Technology*, 2011.

47. Fotiadis, D. I., Likas, A., & Protopappas, V. (2006). Intelligent patient monitoring. *Wiley Encyclopedia of Biomedical Engineering*.

48. Fraser, C. G. (2009). Reference change values: the way forward in monitoring. *Annals of clinical biochemistry*, *46*(3), 264-265.

49. Gardner, R. M., & Shabot, M. M. (2001). Patient-monitoring systems. In*Medical Informatics* (pp. 443-484). Springer New York.

50. Gavin, J., Myers, S. D., & Willems, M. E. T. (2013). Physiological responses at various lactate markers for running at 4 and 8 minute treadmill increments.*Sport Scientific and Practical Aspects: International Scientific Journal of Kinesiology*, *10*(1), 5-14.

51. Grahn, D., & Heller, H. C. (1997). The physiology of mammalian temperature homeostasis. In *SEMINAR HYPOTHERMIA IN TRAUMA DELIBERATE OR ACCIDENTAL* (Vol. 10).

52. Gustafsson, F., & Gustafsson, F. (2000). *Adaptive filtering and change detection*(Vol. 1). New York: Wiley.

53. Hernández, F., Barreda, E. G. D., Fuster-Matanzo, A., Goni-Oliver, P., Lucas, J. J., & Avila, J. (2009). The role of GSK3 in Alzheimer disease. *Brain research bulletin*, *80*(4), 248-250.

54. Hodgkin, A. L., & Huxley, A. F. (1952). A quantitative description of membrane current and its application to conduction and excitation in nerve. *The Journal of physiology*, *117*(4), 500-544.

55. Hoggatt, J. (2011). Personalized Medicine—Trends in Molecular Diagnosticsy.*Molecular diagnosis & therapy*, *15*(1), 53-55.

56. Hogben, L., 1930. *The Nature of Living Matter*, London: Kegan Paul, Trench, Trubner

57. Hooper, C., Killick, R., & Lovestone, S. (2008). The GSK3 hypothesis of Alzheimer's disease. *Journal of neurochemistry*, *104*(6), 1433-1439.

58. Indrayan, A. (2012). *Medical biostatistics*. CRC Press.

59. Leek, J., McShane, B., Gelman, A., Colquhoun, D. Nuijten, M. B., & Goodman, S. N. (2017). Five ways to fix statistics. *Nature*, *551*, 557-559.

60. Isermann, R. (2005). Model-based fault-detection and diagnosis–status and applications. *Annual Reviews in control*, *29*(1), 71-85.

61. Jansen, F., Van der Krogt, J., Van Loon, K., Quanten, S., Berckmans, D., Guarino, M., Avezzu, V. (2008). Quantification of negative mental status of a horse during physical activity*. The acute poorly performing sport horse.*. Conference on Equine Sports Medicine and Science. Utrecht, 9-13 july 2008.

62. Jeukendrup, A., & Gleeson, M. (2010). *Sport nutrition: an introduction to energy production and performance* (No. Ed. 2). Human Kinetics.

63. Junker, B. H., & Wang, H. Y. (2006). Bioprocess monitoring and computer control: key roots of the current PAT initiative. *Biotechnology and bioengineering*, *95*(2), 226-261.

64. Kashiha, M., Pluk, A., Bahr, C., Vranken, E., Berckmans, D. (2013). Development of an Early Warning System For a Broiler House Using Computer Vision. *Biosystems Engineering, 116* (1), 36-45.

65. Kashiha, M., Bahr, C., Ott, S., Moons, C., Niewold, T., Ödberg, F., Berckmans, D. (2014). Automatic Weight Estimation of Individual Pigs Using Image Analysis. *Computers and Electronics in Agriculture, 107*, 38-44.

66. Kashiha, M., Bahr, C., Ott, S., Moons, C., Niewold, T., Tuyttens, F., Berckmans, D. (2014). Automatic Monitoring of Pig Locomotion Using Image Analysis. *Livestock Science, 159*, 141-148.

67. Kéfi, S., Dakos, V., Scheffer, M., Van Nes, E. H., & Rietkerk, M. (2013). Early warning signals also precede non-catastrophic transitions. *Oikos*, *122*(5), 641-648.

68. Kitano, H. (2002). Systems biology: a brief overview. *Science*, *295*(5560), 1662-1664.

69. Kitano, H. (2004). Biological robustness. *Nature Reviews Genetics*, *5*(11), 826-837.

70. Kitano, H. (2007). Towards a theory of biological robustness. *Molecular systems biology*, *3*(1).

71. Kolb, B., & Whishaw, I. Q. (1998). Brain plasticity and behavior. *Annual review of psychology*, *49*(1), 43-64.

72. Komives, C., & Parker, R. S. (2003). Bioreactor state estimation and control.*Current Opinion in Biotechnology*, *14*(5), 468-474.

73. Kresnowati, M. T. A. P., Forde, G. M., & Chen, X. D. (2011). Model-based analysis and optimization of bioreactor for hematopoietic stem cell cultivation.*Bioprocess and biosystems engineering*, *34*(1), 81-93.

74. Lambrechts, T., Papantoniou, I., Sonnaert, M., Schrooten, J., Aerts, J. (2014). Model-based cell number quantification using online single-oxygen sensor data for tissue engineering perfusion bioreactors. *Biotechnology and Bioengineering, 111* (10), 1982-1992.

75. Lefever, J., Berckmans, D., & Aerts, J. M. (2014). Time-variant modelling of heart rate responses to exercise intensity during road cycling. *European journal of sport science*, *14*(sup1), S406-S412.

76. Leksrisompong, N., H. Romero-Sanchez, P. W. Plumstead, K. E. Brannan, and J. Brake. 2007. Broiler incubation. 1. Effect of elevated temperature during late incubation on body weight and organs of chicks. Poult. Sci. 86:2685–2691.

77. Lesko, L. J. (2007). Personalized medicine: elusive dream or imminent reality?.*Clinical Pharmacology & Therapeutics*, *81*(6), 807-816.

78. Li, N. (2012). *Robust Efficiency and Actuator Saturation Explain Healthy Heart Rate Control and Variability* (Doctoral dissertation, caltech).

79. Lipsitz, L. A. (2002). Dynamics of Stability: the Physiologic Basis of Functional Health and Frailty. *J Gerontol A-Biol*, 57, B115-B125.

80. Ljung, L. (1987). System identification: theory for the user. *Prentice-Hall, Englewood Cliffs, N.J.*,

81. Lourenço, N. D., Lopes, J. A., Almeida, C. F., Sarraguça, M. C., & Pinheiro, H. M. (2012). Bioreactor monitoring with spectroscopy and chemometrics: a review. *Analytical and bioanalytical chemistry*, *404*(4), 1211-1237.

82. Manning, J. S., & Jackson, W. C. (2015). Providing guideline-concordant assessment and monitoring for major depression in primary care. *The Journal of clinical psychiatry*, *76*(1), e3.

83. May, R. M. (1974). *Stability and complexity in model ecosystems* (Vol. 6). Princeton University Press.

84. Metz, C. E. (1978, October). Basic principles of ROC analysis. In *Seminars in nuclear medicine* (Vol. 8, No. 4, pp. 283-298). WB Saunders.

85. Meyfroidt, G., Güiza, F., Cottem, D., De Becker, W., Van Loon, K., Aerts, J. M., ... & Van den Berghe, G. (2011). Computerized prediction of intensive care unit discharge after cardiac surgery: development and validation of a Gaussian processes model. *BMC medical informatics and decision making*, *11*(1), 64.

86. Moorman, J. R. et al. Mortality Reduction by Heart Rate Characteristic Monitoring in Very Low Birth Weight Neonates: A Randomized Trial. The Journal of Pediatrics 159, 900–906.e1 (2011).

87. Mora, F. A., Passariello, G., Carrault, G., & Le Pichon, J. P. (1993). Intelligent patient monitoring and management systems: a review. *Engineering in Medicine and Biology Magazine, IEEE*, *12*(4), 23-33.

88. Morton, G. J., Cummings, D. E., Baskin, D. G., Barsh, G. S., & Schwartz, M. W. (2006). Central nervous system control of food intake and body weight. *Nature*, *443*(7109), 289-295.

89. Mossio, M., Montévil, M., & Longo, G. (2016). Theoretical principles for biology: organization. *Progress in biophysics and molecular biology*, *122*(1), 24-35.

90. Mukhopadhyay, S. (2015). Wearable Sensors for Human Activity Monitoring: A Review.

91. Namas, R., Zamora, R., Namas, R., An, G., Doyle, J., Dick, T. E., ... & Vodovotz, Y. (2012). Sepsis: something old, something new, and a systems view. *Journal of critical care*, *27*(3), 314-e1.

92. Newman, M. E. (2003). The structure and function of complex networks. *SIAM review*, *45*(2), 167-256

93. Nichelmann, M., & Tzschentke, B. (2003). Efficiency of thermoregulatory control elements in precocial poultry embryos. *Avian and Poultry Biology Reviews*, *14*(1), 1-19.

94. Nuyts, K., Exadaktylos, V., Berckmans, D. (2013). On-line monitoring of human-horse relationship. In Berckmans, D. (Ed.), Vandermeulen, J. (Ed.), *Precision Livestock Farming '13*. ECPLF. Leuven, Belgium, 10-12 September 2013 (pp. 299-307).

95. Nyquist, H. (1928). Certain topics in telegraph transmission theory. AIEEE Transactions, 47,617-644.

96. Oczak, M., Ismayilova, G., Costa, A., Viazzi, S., Sonoda, L., Fels, M., Bahr, C., Hartung, J., Guarino, M., Berckmans, D., Vranken, E. (2013). Analysis of aggressive behaviours of pigs by automatic video recordings. *Computers and Electronics in Agriculture, 99*, 209-217.

97. Padmaja, D. L., & Vishnuvardhan, B. (2016, February). Comparative study of feature subset selection methods for dimensionality reduction on scientific data. In *Advanced Computing (IACC), 2016 IEEE 6th International Conference on* (pp. 31-34). IEEE.

98. Page, E. S. (1954). Continuous inspection schemes. *Biometrika*, *41*(1/2), 100-115.

99. P. C. Young. Recursive Estimation and Time Series Analysis:An Introduction for the Student and Practitioner. Springer, 2011.

100. Pillai, G. C., Mentré, F., & Steimer, J. L. (2005). Non-linear mixed effects modeling–from methodology and software development to driving implementation in drug development science. *Journal of pharmacokinetics and pharmacodynamics*, *32*(2), 161-183.

101. Plasqui, G., Bonomi, A., & Westerterp, K. R. (2013). Daily physical activity assessment with accelerometers: new insights and validation studies. *obesity reviews*, *14*(6), 451-462.

102. Premkumar, K. (2004). *The massage connection: anatomy and physiology*. Lippincott Williams & Wilkins.

103. Proulx, S. R., Promislow, D. E., & Phillips, P. C. (2005). Network thinking in ecology and evolution. *Trends in Ecology & Evolution*, *20*(6), 345-353.

104. Psychlopedia, (2017). Action potential; Retrieved from: https://psychlopedia.wikispaces.com/action+potential

105. Quanten, S., De Valck, E., Cluydts, R., AERTS, J., & Berckmans, D. (2006). Individualized and time-variant model for the functional link between thermoregulation and sleep onset. *Journal of sleep research*, *15*(2), 183-198.

106. Ragland, D. R. (1992). Dichotomizing continuous outcome variables: dependence of the magnitude of association and statistical power on the cutpoint. *Epidemiology*, 434-440.

107. Raven, P. H., Johnson, G. B., Losos, J. B., & Singer, S. R. (2005). Biology, 7 t h edn.

108. Bites Romanini, C. E., Exadaktylos, V., Tong, Q., Demmers, T., McGonnell, I. M., Bergoug, H., ... & Berckmans, D. (2013, September). Monitoring of eggshell temperature to detect hatching time and its thermodynamic relations. In *Precision Livestock Farming 2013* (pp. 862-869).

109. Salahuddin, L., Cho, J., Jeong, M. G., & Kim, D. (2007, August). Ultra short term analysis of heart rate variability for monitoring mental stress in mobile settings. In *Engineering in Medicine and Biology Society, 2007. EMBS 2007. 29th Annual International Conference of the IEEE* (pp. 4656-4659). IEEE.

110. Scheffer, M., Carpenter, S. R., Lenton, T. M., Bascompte, J., Brock, W., Dakos, V., ... & Vandermeer, J. (2012). Anticipating critical transitions.*Science*, *338*(6105), 344-348.

111. Ives, A. R., & Dakos, V. (2012). Detecting dynamical changes in nonlinear time series using locally linear state-space models. *Ecosphere*, *3*(6), art58.

112. Schlageter-Tello, A., Bokkers, E., Groot Koerkamp, P., Van Hertem, T., Viazzi, S., Bites Romanini, C., Halachmi, I., Bahr, C., Berckmans, D., Lokhorst, K. (2014). Manual and automatic locomotion scoring systems in dairy cows: A review. *Preventive Veterinary Medicine, 116* (1-2), 12-25.

113. Schork, N. J. (2015). Personalized medicine: time for one-person trials. *Nature*, *520*(7549), 609-611.

114. Schork, N. J., & Goetz, L. H. (2017). Single Subject (N-of-1) Studies in Translational Nutrition Research. *Annual Review of Nutrition*, *37*(1).

115. Shewhart, W. A. (1931). *Economic control of quality of manufactured product*. ASQ Quality Press.

116. Silva, M. (2011). Bio-acoustics as a measure for status of living organisms.

117. Smets, E., Joosen, P., Taelman, J., Exadaktylos, V., & Berckmans, D. (2013). Monitoring the mental status of football players. In *Proceedings of the International Congress on Sports Science Research and Technology Support*(pp. 206-213).

118. Stanley, G. B. (2013). Reading and writing the neural code. *Nature neuroscience*, *16*(3), 259-263.

119. Stelling, J., Sauer, U., Szallasi, Z., Doyle III, F. J., & Doyle, J. (2004). Robustness of cellular functions. *Cell*, *118*(6), 675-685.

120. Strogatz, S. H. (2001). Exploring complex networks. *Nature*, *410*(6825), 268-276.

121. Scheffer, M., Bascompte, J., Brock, W. A., Brovkin, V., Carpenter, S. R., Dakos, V., ... & Sugihara, G. (2009). Early-warning signals for critical transitions. *Nature*, *461*(7260), 53-59.

122. Strogatz, S. H. (2001). *Nonlinear dynamics and chaos: with applications to physics, biology and chemistry*. Perseus publishing.

123. Tait, A., McNay, L., Gumley, A., & O'Grady, M. (2002). The development and implementation of an individualised early signs monitoring system in the prediction of relapse in schizophrenia. *Journal of mental health*, *11*(2), 141-153.

124. Tarassenko, L. BIOSIGNTM : multi-parameter monitoring for early warning of patient deterioration. in 2005, 71–76 (IEE, 2005).

125. Thompson, P. M., Cannon, T. D., Narr, K. L., Van Erp, T., Poutanen, V. P., Huttunen, M., ... & Toga, A. W. (2001). Genetic influences on brain structure.*Nature neuroscience*, *4*(12), 1253-1258.

126. Topalović, M., Vrancken, I., Piette, D., Exadaktylos, V., Berckmans, D., Claes, S., & Aerts, J. M. Monitoring emotions of depressive patients using wearable sensors. International Conference on Biomedical and Health Informatics - BHI 2017. Orlando, 16 - 19 February 2017.

127. Torous, J., Friedman, R., & Keshavan, M. (2014). Smartphone ownership and interest in mobile applications to monitor symptoms of mental health conditions. *JMIR mHealth and uHealth*, *2*(1).

128. Trefois, C., Antony, P. M., Goncalves, J., Skupin, A., & Balling, R. (2015). Critical transitions in chronic disease: transferring concepts from ecology to systems medicine. *Current opinion in biotechnology*, *34*, 48-55.

129. Turrigiano, G. G., & Nelson, S. B. (2004). Homeostatic plasticity in the developing nervous system. *Nature Reviews Neuroscience*, *5*(2), 97-107.

130. Tzschentke, B. (2008). Monitoring the development of thermoregulation in poultry embryos and its influence by incubation temperature. *Computers and electronics in agriculture*, *64*(1), 61-71.

131. Uhlhaas, P. J., & Singer, W. (2006). Neural synchrony in brain disorders: relevance for cognitive dysfunctions and pathophysiology. *Neuron*, *52*(1), 155-168.

132. Ündey, C., Ertunç, S., Mistretta, T., & Looze, B. (2010). Applied advanced process analytics in biopharmaceutical manufacturing: Challenges and prospects in real-time monitoring and control. *Journal of Process Control*, *20*(9), 1009-1018.

133. Van den Kerkhof, P., Gins, G., Vanlaer, J., & Van Impe, J. F. (2012). Dynamic model-based fault diagnosis for (bio) chemical batch processes. *Computers & Chemical Engineering*, *40*, 12-21.

134. Vandermeulen, J., Bahr, C., Tullo, E., Fontana, I., Ott, S., Kashiha, M., Guarino, M., Moons, C., Tuyttens, F., Niewold, T., Berckmans, D. (2015). Discerning pig screams in production environments. *PLoS One*.

135. Van Hertem, T., Viazzi, S., Steensels, M., Maltz, E., Antler, A., Alchanatis, V., Schlageter Tello, A., Lokhorst, K., Bites Romanini, C., Bahr, C., Berckmans, D., Halachmi, I. (2014). Automatic lameness detection based on consecutive 3D-video recordings. *Biosystems Engineering, 119*, 108-116.

136. van Impe, J. F., Vanrolleghem, P. A., & Iserentant, D. M. (Eds.). (2013).*Advanced instrumentation, data interpretation, and control of biotechnological processes*. Springer Science & Business Media.

137. Vanlaer, J. (2013). Analysis of Statistical Process Monitoring for (Bio) chemical Batch Processes (Analyse van statistische procesopvolging voor (bio) chemische batchprocessen).

138. Van Loon, K., Meyfroidt, G., Van den Berghe, G., Berckmans, D., & Aerts, J. M. (2009). Application of multivariate autoregressive models for individualized evaluation of dynamics of ICU patients.

139. Vanrolleghem, P. A., & Lee, D. S. (2003). On-line monitoring equipment for wastewater treatment processes: state of the art. *Water Science & Technology*, *47*(2), 1-34.

140. Varmuza, K., & Filzmoser, P. (2008). *Introduction to multivariate statistical analysis in chemometrics*. CRC press.

141. Viazzi, S., Bahr, C., Schlageter-Tello, A., Van Hertem, T., Bites Romanini, C., Pluk, A., Halachmi, I., Lokhorst, C., Berckmans, D. (2013). Analysis of individual classification of lameness using automatic measurement of back posture in dairy cattle. *Journal of Dairy Science, 96* (1), art.nr. 10.3168/jds.2012-5806, 257-266.

142. Viazzi, S., Van Hoestenberghe, S., Goddeeris, B., Berckmans, D. (2014). Automatic mass estimation of Jade perch Scortum barcoo by computer vision. *Aquacultural Engineering*, art.nr. AQUE1781.

143. Vodovotz, Y., Chow, C. C., Bartels, J., Lagoa, C., Prince, J. M., Levy, R. M., ... & Clermont, G. (2006). In silico models of acute inflammation in animals.*Shock*, *26*(3), 235-244.

144. Wathes, C. M., Aland, A., & Madec, F. (2009). Precision livestock farming for animal health, welfare and production. *Sustainable Animal Production: The Challenges and Potential Developments for Professional Farming. A. Aland and F. Madec, ed. Wageningen Academic Publishers, Wageningen, the Netherlands*, 411-419.

145. Wilson, Robert A. and Barker, Matthew, "The Biological Notion of Individual", *The Stanford Encyclopedia of Philosophy* (Spring 2014 Edition), Edward N. Zalta (ed.), URL = <http://plato.stanford.edu/archives/spr2014/entries/biology-individual/>.

146. Woodrow, K. M., Friedman, G. D., Siegelaub, A. B., & Collen, M. F. (1972). Pain tolerance: differences according to age, sex and race. *Psychosomatic Medicine*, *34*(6), 548-556.

147. Yang, C. C., & Hsu, Y. L. (2010). A review of accelerometry-based wearable motion detectors for physical activity monitoring. *Sensors*, *10*(8), 7772-7788.

148. Young, P. C. (2011). *Recursive estimation and time-series analysis: An introduction for the student and practitioner*. Springer Science & Business Media.

149. Young, P. (1998). Data-based mechanistic modelling of environmental, ecological, economic and engineering systems. *Environmental Modelling & Software*, *13*(2), 105-122.

150. Youssef, A., Exadaktylos, V., & Berckmans, D. (2014). Modelling and quantification of the thermoregulatory responses of the developing avian embryo: Electrical analogies of a physiological system. *Journal of thermal biology*, *44*, 14-19.

151. Youssef Ali Amer, A., Viazzi, S., Exadaktylos, V., Berckmans, D. (2014). Non-contact, motion-tolerant measurements of chicken (Gallus gallus) embryo heart rate (HR) using video imaging and signal processing. *Biosystems Engineering*, *125*, 9-16.

152. Youssef Ali, A. (2014). Model-Based Control of Micro-Environment with Real-Time Feedback of Bioresponses. *status: accepted 2014*.

153. Yung, A. R., McGorry, P. D., McFarlane, C. A., Jackson, H. J., Patton, G. C., & Rakkar, A. (2014). Monitoring and care of young people at incipient risk of psychosis.

154. Zenker, S., Rubin, J., & Clermont, G. (2006). Towards a model-based medicine: integration of probabilistic inference with mechanistic knowledge. *Journal of Critical Care*, *21*(4), 350.

155. Zenker, S., Clermont, G., & Pinsky, M. R. (2007). Using mathematical models to improve the utility of quantitative ICU data. *Intensive Care Medicine*, 479-492.

156. Zhou, X., Menche, J., Barabási, A. L., & Sharma, A. (2014). Human symptoms–disease network. *Nature communications*, *5*, 4212.

Curriculum vitae

Tim Tambuyzer was born in Lier, Belgium. He finished his bachelor and master studies in Bioscience Engineering at KU Leuven in 2010. Afterwards, Tim joined the research group M3-BIORES as a research and teaching assistant. In 2013, he won the best paper award at the International Conference on Bio-inspired Systems and Signal Processing (BIOSIGNALS, Barcelona, 11-14 Feb, 2013). Tim was a member of the department council from 2013 to 2015. In August 2015, Tim travelled as visiting researcher (1,5 month) to Caltech University, which is one of the world-wide leaders in (control) engineering (Control and dynamical systems, Caltech, Pasadena, LA; Supervisor: Prof. John C. Doyle). Starting from November 2015, he combined his work at KU Leuven (part-time) with a position as program leader of nutrition research at UCLL. One of the main topics at UCLL was malnutrition monitoring. Tim has published 7 peer reviewed journal publications, 3 under review journal articles and 8 articles in international conference proceedings. Based on his experience until now, his main interests are: individualised model-based monitoring, medical applications, neuro-engineering.

Publications

Articles in peer reviewed international journal publications

Published

Tambuyzer, T., Ahmed, T., Taylor, C. J., Berckmans, D., Balschun, D., & Aerts, J. M. (2013). System identification of mGluR-dependent long-term depression. *Neural computation*, *25*(3), 650-670.

Tambuyzer, T., De Waele, T., Chiers, K., Berckmans, D., Goddeeris, B. M., & Aerts, J. M. (2014). Interleukin-6 dynamics as a basis for an early-warning monitor for sepsis and inflammation in individual pigs. *Research in veterinary science*, *96*(3), 460-463.

Wu, H., Van Kuyck, K., Tambuyzer, T., Luyten, L., Aerts, J. M., & Nuttin, B. (2014). Rethinking food anticipatory activity in the activity-based anorexia rat model. *Scientific reports*, *4*.

Wu, H., Ghekiere, H., Beeckmans, D., Tambuyzer, T., Van Kuyck, K., Aerts, J. M., & Nuttin, B. (2015). Conceptualization and validation of an open-source closed-loop deep brain stimulation system in rat. *Scientific reports*, *4*, srep09921.

Tambuyzer, T., Guiza, F., Boonen, E., Meersseman, P., Vervenne, H., Hansen, T. K., ... & Meyfroidt, G. (2016). Heart rate time series characteristics for early detection of infections in critically ill patients. *Journal of clinical monitoring and computing*, *31*(2), 407-415.

Wu, H.*, Tambuyzer, T*., Nica, I.*, Deprez, M., van Kuyck, K., Aerts, J. M., ... & Nuttin, B. (2016). Field Potential Oscillations in the Bed Nucleus of the Stria Terminalis Correlate with Compulsion in a Rat Model of Obsessive-Compulsive Disorder. *Journal of Neuroscience*, *36*(39), 10050-10059.
Shared first authors

Luyck, K., Tambuyzer, T., Deprez, M., Rangarajan, J., Nuttin, B., & Luyten, L. (2017). Electrical stimulation of the bed nucleus of the stria terminalis reduces anxiety in a rat model. *Translational psychiatry*, *7*(2), e1033.

Submitted/Full drafts ready for submission

Deprez, M., Luyck, K., Luyten, L, Tambuyzer, T., Nuttin, B., Mc Laughlin, M., (2017). An evaluation of the effect of pulse-shape on grey and white matter stimulation in the rat brain. (under review in Scientific Reports).

Tambuyzer, T.*, Romanini, C. E. B.*, Tong, Q., Demmers, T., McGonnell, I. M., Roulston, N., Bergoug, H., Guinebretiere, M., Eterradossi, N., Bahr, C., Exadaktylos, V., Aerts, J.-M., Berckmans, D. (2017). Individualised model-based monitoring of chicken embryo status during incubation based on eggshell temperature. (in preparation for submission to Biosystems engineering).
Shared first authors

Tambuyzer, T.*, Romanini, C. E. B.*, Tong, Q., Demmers, T., McGonnell, I. M., Roulston, N., Bergoug, H., Guinebretiere, M., Eterradossi, N., Bahr, C., Exadaktylos, V., Aerts, J.-M., Berckmans, D. (2017). Individualised change detection of embryo status based on eggshell temperature to monitor embryo death. (in preparation for submission to Poultry Science).
Shared first authors

Tambuyzer, T.*, Hemmings, W.*, Deprez, M., Bauweleers, K., van Kuyck, K., Aerts, J.-M, Nuttin, B. (2017). A Novel Method to Measure Compulsivity in the Schedule-Induced Polydipsia in Rats, a Model for Obsessive-Compulsive Disorder (in preparation for submission to Frontiers in Behavioural Neuroscience).
Shared first authors

Articles in international conference proceedings

Tambuyzer T., De Waele T., Meyfroidt G., Van den Berghe G., Goddeeris B., Berckmans D., Aerts J. (2011). ALGORITHMS OF BIOMARKERS FOR MONITORING INFECTION/INFLAMMATION PROCESSES IN PIGS. Proceedings of the XVth ISAH Congress 2011. XVth International Congress on Animal Hygiene 2011. Vienna, Austria, 3-7 July 2011 (pp. 1-4).

Tambuyzer T., Ahmed T., Berckmans D., Balschun D., Aerts J. (2011). Reverse engineering of metabotropic glutamate receptor-dependent long-term depression in the hippocampus. Annual Computational Neuroscience Meeting CNS*2011. KTH Royal Institute of Technology, Stockholm, 23-28 July 2011.

Van Loon K., Meyfroidt G., Tambuyzer T., Van den Berghe G., Berckmans D., Aerts J. (2012). DYNAMIC AUTOREGRESSIVE MODELLING OF CRITICAL CARE PATIENTS AS A BASIS FOR HEALTH MONITORING. BIOSIGNALS. Vilamoura, Portugal, 2012.

H Wu K., van Kuyck K., Ceyssens F., Tambuyzer T., Aerts J., Nuttin B. (2012). Behavior Analysis of a Rat model of Obsessive-Compulsive Disorder Treated with High Frequency Electrical Stimulation in the Bed Nucleus of Stria Terminalis. . Congress ESSFN. Cascais, 26-29 September 2012.

Tambuyzer T., Wu H., Cortebeeck S., Cosemans N., Loveniers M., Verhaegen M., Berckmans D., van Kuyck K., Aerts J. (2012). New criteria for detection of compulsive behaviour in SIP model based on an automated video analysis system. International Journal of Psychophysiology: vol. 85 (3). World congress of psychophysiology. Pisa, Italy, 13-17 Sep 2012, 368.

Tambuyzer T., De Waele T., Goddeeris B., Berckmans D., Aerts J. (2012). Time-varying Interleukin-6 characteristics for early detection of disease outcome. International Workshop on Biosignal Interpretation. Como, Italy.

Bulckaert A., Vandekerckhove M., Tambuyzer T., De Valck E., Haex B., Verbraecken J., Berckmans D., Exadaktylos V. (2012). Emotional heart rate component and frontal alpha asymmetry during REM sleep. International Journal of Psychophysiology: vol. 85 (3). World congress of psychophysiology. Pisa, Italy, 13-17 Sep 2012, 368.

Tambuyzer T., Ahmed T., Taylor C., Balschun D., Aerts J. (2013). Dynamic Data-based Modelling of Synaptic Plasticity: mGluR-dependent Long-term Depression. 2013 - Proceedings of the International Conference on Bio-inspired Systems and Signal Processing. BIOSIGNALS. Barcelona, 11-14 Feb 2013 (pp. 48-53).